Ocean and climate variability in the North Atlantic from seasonal to decadal timescales

Juliette Mignot

UNIVERSITE PIERRE ET MARIE CURIE
École doctorale des Sciences de la Terre et de l'Univers

MEMOIRE D'HABILITATION A DIRIGER LES RECHERCHES
Spécialité : Océanographie Physique

présenté par
Juliette Mignot

Sujet du mémoire :

Ocean and climate variability in the North Atlantic from seasonal to decadal timescales

July 13, 2016

Résumé

Le climat, défini ici comme l'état du système incluant l'océan, l'atmosphère, la surface terrestre et la cryosphère, varie sur des échelles de temps journalières à millénnaires. Ces variations résultent de la nature chaotique des interactions entre ces composantes, ainsi que des processus en jeu au sein de chacune d'entre elles. Le climat varie également sous l'influence de facteurs externes, tels que les variations de l'irradiance solaire ou de la composition chimique de l'atmosphère et les éruptions volcaniques.

Les variations climatiques à l'échelle de temps saisonnière sont très énergétiques et influencent les échelles de temps interannuelles à décennales. Ces dernières intéressent particulièrement les décisionnaires, mais sont mélangées aux effets du changement climatique global tel qu'observé jusqu'à aujourd'hui. Améliorer le niveau de compréhension de la variabilité climatique aux échelles de temps saisonnières à décennales est essentiel pour évaluer l'intervalle possible des fluctuations climatiques futures, leur prévisibilité éventuelle ainsi que de comprendre l'impact des changements climatiques induits par l'homme. A ces échelles de temps, l'océan joue un rôle majeur, de part son inertie thermique. Le secteur Atlantique est le théâtre d'une variabilité, et donc d'une prévisibilité décennales particuliérement fortes, en partie du fait de la circulation méridienne de retournement (AMOC). Les mécanismes de variabilité interne, le rôle relatif des bassins subpolaires et tropicaux et des autres bassins océaniques, le rôle du forçage externe, et les conséquences de ces phénoménes pour la prévisibilité sont des questions encore ouvertes et font l'objet d'intenses recherches.

Je synthétise ici ma contribution à ces questions, depuis le début de ma thèse en 2000. Dans l'Atlantique tropical et subtropical, j'ai exploré plusieurs aspects des mécanismes de variabilité saisonnières à l'aide d'observations. Néanmoins, étant donné le manque de séries d'observations océaniques longues et fiables sur des grandes échelles spatiales, mon travail de recherche a été principalement basé sur l'utilisation de modèles de climat, ainsi que des méthodes d'analyses statistiques et plus conceptuelles. Je me suis en particulier intéressée au rôle de la circulation océanique et de la salinité de surface dans la variabilité interne du système climatique en Atlantique Nord, et à l'impact des éruptions volcaniques et d'anomalies d'eau douce sur cette variabilité. Ces dernières années, cette expertise et le contexte international m'ont amenée à travailler sur la question de la prévisibilité climatique à l'échelle de temps décennale et à réflechir à la possibilité de livrer des prévisions avec les outils que les climatologues et océanographes ont actuellement en main.

Je présente pour finir quelques pistes de recherche que j'envisage pour les prochaines années. Elles se placent essentiellement dans la continuité de mes efforts menés jusqu'ici pour la compréhension de la variabilité océanique et climatique à l'échelle de temps décennale. Les modèles de climat devraient rester à la base de mon travail de recherche, ainsi que le rôle de l'océan dans les variations climatiques interannuelles à décennales depuis les 1000 dernières années jusqu'au prochain siècle environ. Je souhaite poursuivre l'évolution de mon travail vers une utilisation plus intégrée des modèles de climat avec les observations existantes. L'idée est de progressehttp://www.pb18.fr/r dans la compréhension des évènements récents ou passés afin de mieux appréhender ceux du futur. Un autre aspect prospectif de mon travail concerne l'Atlantique tropical nord-est et le climat des régions adjacentes. Le système d'upwelling sénégalo-mauritanien et la mousson ouest africaine en sont les points focaux.

Summary

The climate, here considered as the state of the system including the ocean, the atmosphere, the land and the cryosphere, varies at timescales ranging from days to millennia. These variations result from the chaotic nature of interactions between these components, as well as processes within each component. It also varies through the influence of external factors, such as modulations of the solar irradiance, volcanic eruptions, or externally-induced changes of the composition of the atmosphere. Seasonal variations cause regular patterns of variability in the oceans, and they may help to understand the basic dynamics of the system. They are furthermore very energetic and influence modulations of the climate at interannual to decadal timescales. The latter are of particular relevance in the context of global climate change, first because global warming evolves on a similar timescale, and second because impacts of this variability on society and environment are the most useful for decision-makers. Improved understanding of this variability is essential for assessing the likely range of future climate fluctuations and the extent to which they may be predictable, as well as understanding the potential impact of human-induced climate change. At these timescales, the ocean plays a major role for climate modulations through its thermal inertia. The Atlantic sector, in particular, displays particularly strong decadal variability, and thus predictability, probably largely because of the Atlantic Meridional Overturning Circulation (AMOC). Mechanisms of internal variability, the relative role of subpolar and tropical basins, of remote oceanic basins, the role of external forcing, and consequences in terms of predictability are still largely open questions and the focus of intense research.

I report here my contribution to these topics since the beginning of my phD in 2000. I have been exploring some aspects of the seasonal variability using observations of the tropical and subtropical Atlantic mainly. Given the lack of sufficiently long and trustable data sets on large spatial scales my research has nevertheless been primarily based on the use of climate models, as well as statistical and conceptual approaches. I have been specifically interested in the role of the oceanic circulation and the sea surface salinity for the internal climate variability in the Atlantic basin, as well as in the impact of volcanic eruptions and anomalous inputs of freshwater into the ocean on this variability. In the more recent years, this expertise and the international context brought me to think on the climate predictability at the decadal timescales and on possibilities for oceanographers and climate scientists to deliver predictions given the tools they have in hands.

I also present several research perspectives which I would like to explore. They are basically envisioned as a continuity to my previous research for the understanding of the ocean and climate variability at the interannual to decadal timescales. Climate models should remain at the basis of my work, as well as studying climate variations from roughly the last 1000 years up to the coming century. I wish to pursue the evolution of my work towards an integrated use of climate models using existing observed data sets over these timescales. The idea is to better understand past observed or reconstructed climate events in order to better apprehend the futur ones. Another prospective aspect of my work is dedicated to oceanography in the northeastern tropical Atlantic and climate of the surrounding regions. The southern part of the canarian upwelling and the west-african monsoon will be a the heart of these studies.

Foreword

This report does not intend to be a textbook nor an exhaustive review. I propose here a consistent story of my view of the seasonal to decadal climate variability in the tropical and North Atlantic as derived from the studies I have been leading, supervising or co-achieving so far. In order to highlight my contributions, I have pointed in bold publications in which I was a co-author, but I have tried to discuss them as much as possible in the light of other earlier, contemporaneous or subsequent studies. I hope that this manuscript may be useful to some students or other researchers. At least it has been a useful and interesting exercise to me.

English or French. This has been a tough question. Science is in english, and writing a text which I consider interesting scientifically in a language that could not be understood by a large proportion of my colleagues and collaborators appeared poorly useful to me. On the other hand, I am aware that a reference document written in french can be very useful and much appreciated by the young students. I know that in particular from my experience in collaborating with students in Africa (Senegal, Benin). I hope that the latter will forgive me not to provide them such document, and perhaps will use this report as an opportunity to be less afraid of written english.

Geographically, my scientific life began in Paris (during my phD, at the LODYC -now LOCEAN- under the supervision of Claude Frankignoul) and then took me to Potsdam (Germany, PIK, with Stefan Rahmstorf), back to Paris (LOCEAN), and to Bern (Switzerland, Bern University, Climate and environmental physics laboratory, KUP, hosted by Thomas Stocker) in the recent years, all this with regular stays in Dakar (Senegal, at the LPAOSF, Université Cheikh Anta Diop). I am indebted to colleagues, administrative staff and students from all these places for the work presented here.

Contents

Chapter 1

Scientific context

Climate can be defined very generally as a bio-chemical-physical system with different components, active mechanisms within each component and interactions between components. The main components of the Earth system are the atmosphere, ocean, land surface, snow and ice at the surface of both oceans and land, and biota near the interfaces of atmosphere, ocean and land. Main natural mechanisms within each components include for example turbulent and radiative transfer, the planetary-scale circulation of the atmosphere and ocean, photochemical processes, and biogeochemical cycles of trace gases and nutrients. The major interactions between the components of the climate system are given by the exchanges of energy, momentum, water and trace constituents. Within this vast and fascinating context, my research focuses on the ocean, and its interactions with the other physical components of the system, in particular the atmosphere and the sea ice.

Climate may also be defined with respect to weather: the latter describes atmospheric conditions, such as rainfall, temperature and wind speed, at a particular place and time. Weather forecasts describe what is expected in the near (few days) future, given the current conditions. Climate, on the other hand, is what one may expect on average beyond this horizon, the "normal" state, or attractor, of the system defined above. Climate can thus be understood as the mean state, and typical deviations from this mean, of relevant quantities over a sufficiently long period to establish robust statistics. The World Meteorological Organization (WMO) advises to consider periods of typically30 years. Climate variability is then defined as variations in the mean state and other statistics of the system on all temporal and spatial scales, beyond individual weather events. These deviations are usually named anomalies.

Climate variability may be due to natural internal processes, such as the chaotic nature of fluid motions and interactions between the components of the climate system. This defines the internal variability. At interannual to multidecadal timescales, internal climate variability is typically organised into large-scale patterns, called modes of variability, the most mediatic one being the El Niño-Southern Oscillation. This internal variability comes in addition to variations due to factors that are external to the system defined above. These can be natural such as solar activity and volcanism, and anthropogenic, such as emissions of greenhouse gases and sulfate aerosols. In the context of recent climate change, it is important to understand both the internal and forced variability, as well as to understand the role of natural and anthropogenic external forcing in past and future changes. The temporary

deceleration of the global surface temperature increase observed in the early 2000s (e.g. Kirtman et al., 2013), so-called temperature hiatus, is a nice illustration of this problem. As can be inferred from the abundant literature proposing explanations for this "warming pause" (e.g. Kosaka and Xie, 2013; Trenberth and Fasullo, 2013; Meehl et al., 2014; England et al., 2014; Watanabe et al., 2014; Karl et al., 2015; Nieves et al., 2015, among many others), there is a debate in the community on the relative importance of internal (role of El Niño-Southern Oscillation, of the North Pacific vs the North Atlantic basins, of basin scale heat uptake) vs. externally-paced variability (possible role of aerosol forcing, volcanic eruptions, solar forcing), or even an interaction between the two. **A better understanding of climate variability at interannual to decadal timescales and climate response to external forcing is needed to better understand, and possibly predict, such events**.

The hiatus example also highlights the fact that observations at the climatic space and time scales are crucial, but still sparse and insufficient. Sampling errors have indeed first led to exaggerate this pause in the global warming (Cowtan and Way, 2014). Furthermore, while the role of ocean heat uptake has been proposed quite early as a physically plausible explanation for the hiatus, it has rapidly become evident that the latter is still largely under-observed and thus quite uncertain (e.g. Trenberth et al., 2014). In this context, modelling approaches are an important complementary tool. A wide diversity of "models" are used in climate studies, from statistical models to box models and general circulation models (GCMs). The latter are based on the primitive equations of the motion of fluid dynamics. Coupled atmosphere-ocean general circulation models (AOGCMs) have been developed specifically for climate studies from the seasonal to multicentennial time scales. Although not a model developer myself, my research is largely based on AOGCMs, and I have been involved in the development and validation of several of them **(Montoya et al., 2005; Marti et al., 2010; Dufresne et al., 2013; Lehner et al., 2015)**. I hope that the following will illustrate the use that can be made of such models, but also their biases and limitations.

Traditionally, climate models simulations are used to reproduce a statistical evolution of the climate: either under control (constant) external conditions or forced by boundary conditions such as the increase of atmospheric CO_2 concentration, typical interplay between the climate components can be studied. Evolution of these interactions with evolving external conditions may also be analysed. These statistics can be compared with an observed climatic sequence, but the exact timing of observed events has no reason to be reproduce in such climate simulations, which are not phased on observations. A rather novel use of climate models is to assimilate available historical observations in a numerical model of the ocean and/or the atmosphere dynamics or, in other words, constrain climate simulations with observations. Resulting data sets, so-called reanalysis, have the advantage of providing complete spatial and temporal coverage which, furthermore, obey the equations of motions. As I began my research career, such reanalysis only existed for the atmosphere. Since then, **ocean reanalysis have widely developed (see for example http://www.clivar.org/clivar-panels/gsop) and this has been, in my view, a major change for oceanographers**. On a personal point of view, this evolution has greatly contributed to drive me progressively from pure mechanistic studies based on climate models to a more observation-orientated investigation of the recent and future climate variability. To date, nevertheless, ocean reanalysis performed with different models, different observation data sets and different procedures to constrain the former by the latter yield very different variability (e.g. Munoz et al., 2011;

Karspeck et al., 2015; Shi et al., 2015). Beyond improving observation networks and climate models physics, more work is thus needed on the best way to perform these reanalysis and understand their interplay with numerical models which are themselves biased.

Regionally, my research has been mostly restricted to the North and tropical Atlantic ocean and surrounding regions. Why the Atlantic ocean? One answer is obviously that it is the closest ocean to Europe, and thus probably the one, if any, most directly influencing our climate. Furthermore, **the Atlantic Ocean is caracterized by a specific and unique feature: a zonally averaged northward heat transport at all latitudes north of 30°N**, while general considerations of the Earth energy budget would rather predict a poleward redistribution of heat by the ocean and the atmosphere. This specificity is linked to the Atlantic meridional overturning circulation (AMOC). Conceptually, this large-scale circulation can be divided in four branches. In the upper branch, water is moving poleward in the upper ocean. The second branch involves descent into the deep ocean in high latitude deep convection regions. Southward movement in the deep ocean comprises the third branch. Upward movement through stratification in low latitudes and/or wind-driven upwelling in the Southern Ocean closes the circuit. None of these branches has trivial dynamics. As I began my phD, the large scale oceanic circulation spanning the world's deep oceans was named the thermohaline circulation, after the main mechanism from which it originates. Yet, several seminal papers came out during my early career (among which Kuhlbrodt et al., 2007), inviting for a reconsideration of this name. Indeed, this large-scale circulation, which has attracted a lot of attention from oceanographers and climatologists because of its large spatial and temporal scale, and its potential impact on the climate, is of course a much more complex feature than a conveyor belt (Broecker, 1991) pulled by a single deep convection process in the high latitudes. Firstly, deep convection itself is partly forced, or at least favoured by wind forcing (e.g. Lazier et al., 2001). Secondly Lozier (2010) nicely reviewed the numerous studies leading the deconstruct the paradigm view according to which "the ocean's meridional overturning circulation operates like a conveyor belt, transporting cold continuous stream of deep waters spreading waters equatorward at depth and warm waters poleward at the surface". The vital role of eddies and wind fields in establishing the structure and variability of the ocean's overturning and the lack of continuity of the different branches of this large-scale circulation (e.g. Brambilla and Talley, 2006) imply to revisit the concept of "thermohaline circulation". Therefore, in recent years, the term "AMOC", based on the mathematical definition of the stream function, has been preferred to describe this circulation. Understanding the dynamics of the AMOC, its different branches and representations, its variability and predictability has been at the heart of my research interests.

Nevertheless, thermohaline contrasts, in particular in the North Atlantic, remain crucial to explain variations of the structure and intensity of this large scale circulation. Density variations are in particular involved in the descending branch, and salinity in particular has been found to be closely linked to oceanic deep convection (e.g. Gelderloos et al., 2012). More generally, oceanic salinity has massive impacts on the ocean circulation and the global climate. It is important for the formation of water masses and it may modulate certain modes of variability such as ENSO (e.g. Singh et al., 2011; Hasson et al., 2014). Surface salinity has been proposed by Yu (2011) to be used as a rain gauge for the global water cycle and may thus be used as an indicator to detect human influence on the latter (Durack et al., 2012; Terray et al., 2012) , and even a predictor for the Sahel monsoon (Li et al., 2016). It has

also been shown ton influence the global ocean heat uptake in response to global warming (Smith et al., 2014). Salinity dynamics and variability in the ocean has nevertheless attracted much less attention than the temperature. One of the reason is probably that its influence on climate is more indirect than temperature, which influences air-sea heat fluxes thereby feeding back on the atmosphere. The fact that it is much more difficult to observe, both in situ and from space, may also have delayed our understanding of the relevance of this parameter for climate. Observation from space required relatively long technological developments but recent success might change the situation in the coming years (Boutin et al., 2016). Salinity dynamics, variability and link to the AMOC has been another focus of my studies, as detailed below.

In climate models, an AMOC intensification is generally associated with an anomalous warming of the North Atlantic surface, most importantly in the subpolar regions. Given the difficulty to observe the AMOC, this link can not yet be clearly verified from observations. Yet, the latter show a basin-wide mode of SST variation in the North Atlantic, named the Atlantic Multidecadal Variability (or Oscillation, although its oscillatory behaviour has not really been confirmed), which resembles that predicted by the models. The observed AMV has regional and global climate associations. At midlatitudes, links have been found with the North American and European summer climate (e.g. Sutton and Hodson, 2005). Several impacts have also been found in the tropics, such as on the northeast Brazilian and African Sahel rainfall (Folland et al., 1986; Rowell, 2003; Wang et al., 2012), the Atlantic warm pool (e.g. Wang and Zhang, 2013) and Atlantic hurricanes (Goldenberg et al., 2001). AMV warming or cooling also translates into tropical North Atlantic SST anomalies (Wang and Zhang, 2013). The tropical Atlantic also plays a specific role for decadal variability through the influence of the salty subtropical Atlantic and the fresh equatorial band, which the upper branch of the AMOC crosses on its way northward. This basin thus has a strong interplay with the North Atlantic variability, probably both influencing it and feeling its effects. My interest for the tropical Atlantic climate interest has essentially taken the form of collaborations with the Laboratoire de Physique de l'Atmosphere et de l'Ocean Simeon Fongang (LPAOSF) at the University of Dakar (Senegal).

Chapter 2

Seasonal variability

Seasonal variability is primarily due to intra-year changes in solar input. This causes changes in such features as the position of the intertropical convergence zone (ITCZ), paths of mid-latitude storm tracks, monsoon circulation, and changes in the temperature and humidity of the air that comes into close contact with the ocean. While typical residence time for water in the atmosphere is on the order of 7 days (Bengtsson, 2010), ocean circulation processes can have time scales of years to decades. The seasonal time scale sits at the boundary between these scales. It makes a contribution to exchanges between atmosphere and ocean at least as far as the upper oceanic layer (mixed layer depth) is concerned. I present here an overview of three aspects of the seasonal variability in the ocean I have been working on.

2.1 Barrier layers

In the climate system, ocean and atmosphere interact by exchanging momentum, heat and freshwater. In the ocean, these exchanges take place in the upper mixed layer. As its name indicates, this layer is well mixed and thus roughly vertically uniform in temperature and salinity. Although temperature generally dominates the density changes in tropical oceans, both temperature and salinity can locally control the stratification, hence the mixed layer depth (MLD). The tropical Atlantic is characterised by very strong river discharges. The Amazon and the Congo rivers in particular account by themselves for almost 20% of the global amount of rivers discharges. Added to intense precipitations under the Inter-Tropical Convergence Zone, this makes the tropical Atlantic an area of intense spatial heterogeneities of the sea surface salinity (SSS) with potentially important temporal variations (e.g. Dessier and Donguy, 1994; Delcroix et al., 2005) and an important impact on the vertical stratification. In several areas of the tropical Atlantic basin, the sharp vertical salinity gradient in the upper ocean indeed limits depth of the mixed layer, while the temperature is homogeneous or even warmer than in surface down to much higher depths (Fig. 2.1). In this case, the isothermal layer found below the mixed layer is called a barrier layer, as it prevents exchanges between the warm mixed layer and the cold ocean interior (Lukas and Lindstrom, 1991; Godfrey and Lindstrom, 1989). By modifying air-sea interactions, the barrier layers can have important climatic effects (e.g. Masson et al., 2005; Foltz and McPhaden, 2009; Grodsky et al., 2012; Balaguru, 2011).

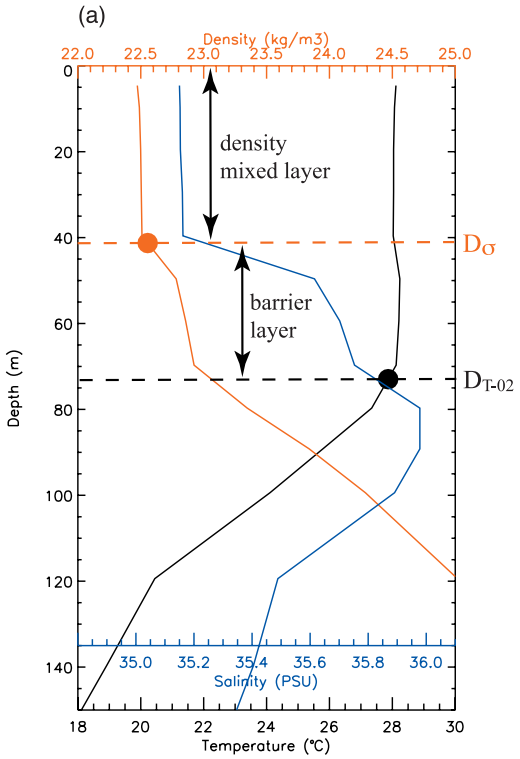

Figure 2.1: Example of hydrographic profile in the ocean where salinity controls the depth of the mixed layer. Temperature (black), salinity (blue), and density (red) profiles are measured from an Argo float on 31 January 2002 in the southeastern Arabian Sea (67.3°E, 7.4°N). The red solid dot shows the depth where the depth of the layer homogeneous in density, thereby defining D_σ. The black solid dot shows the depth of homogeneous temperature, thus defining D_{T-02}. D_σ and D_{T-02} limit the barrier layer (BL) (see text for details). From ***de Boyer Montégut et al. (2007)***

The barrier layer thickness is thus defined as:

$$BL = D_\sigma - D_{T*-02}, with D_{T*-02} < D_\sigma < 0 \tag{2.1}$$

D_{T*-02} is the depth where the temperature has decreased by 0.2 °C as compared to the temperature at the reference depth of 10m. The 0.2 °C threshold is based on the current precision of most common temperature sensors. D_σ is the depth where the potential density, here referred to as σ_θ (potential density − reference density), has increased from the reference depth by a threshold Δ_σ equivalent to the density difference for the same temperature change at constant salinity:

$$\Delta_\sigma = \sigma_\theta(T* - 0.2, S*, P_0) - \sigma_\theta(T*, S*, P_0) \tag{2.2}$$

with $T*$ and $S*$ are the temperature and salinity at the reference depth $10m$ and P_0 is the pressure at the ocean surface. D_σ corresponds to the top of the thermocline.

Making use of recently compiled vertical profiles of temperature and salinity, we proposed in 2007 a novel climatology of this phenomenon **(de Boyer Montégut et al., 2007)**. Its main novelty as

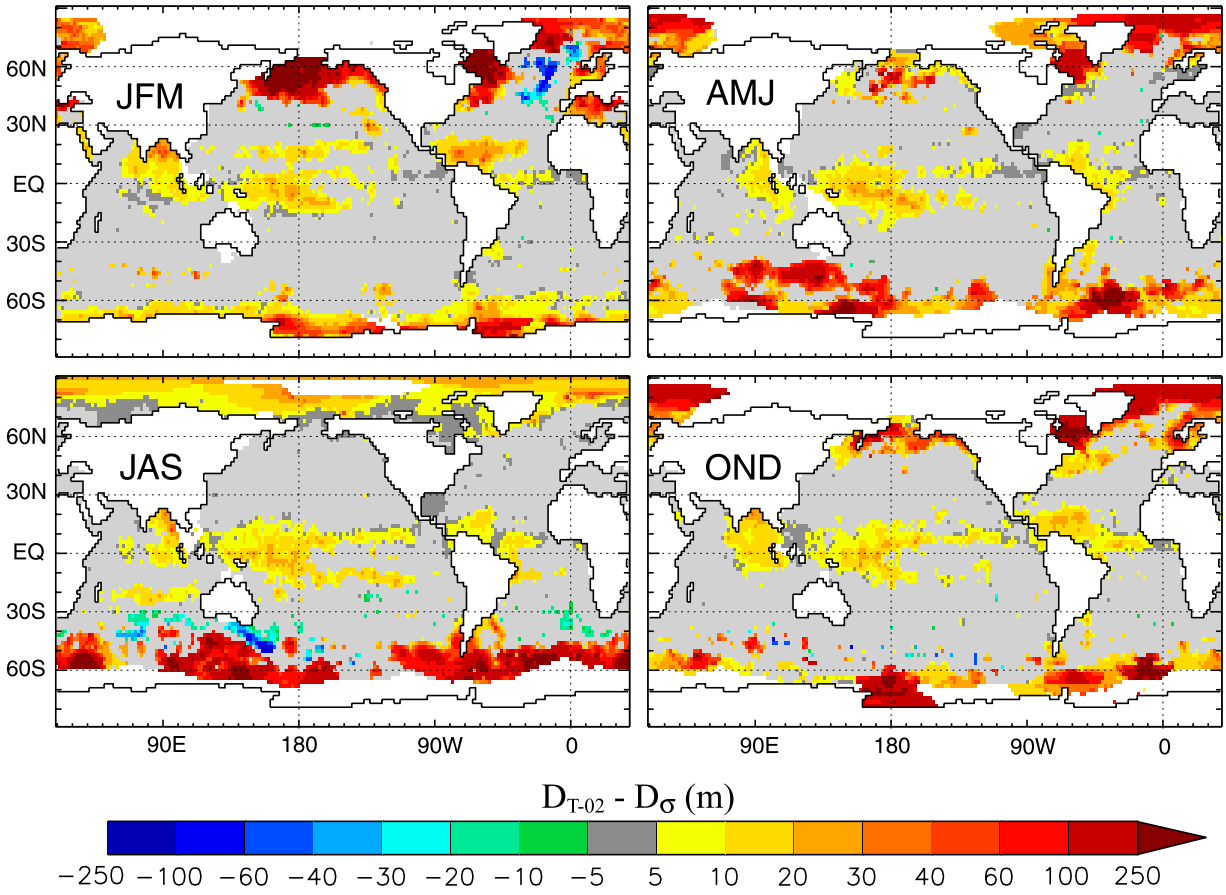

Figure 2.2: Seasonal maps of the difference between D_{T-02} and D_σ as compiled from individual profiles by ***de Boyer Montégut et al. (2007)****. Panels represent seasonal averages over January to March (JFM), April to June (AMJ), July to September (JAS), and October to December (OND). Positive values correspond to barrier layer thickness (BLT), while negative values corresponds to compensated layer thickness. Grid points where the layer thickness is less than 10% of the maximal depth (D_{T-02} or D_σ)are shown in light grey. White areas represent grid points with no observation or only 1 month observation during the season.*

compared to previous global and large-scale studies is that it is based on profile-wise computations. This results in more realistic and detailed structures than already gridded profiles, since no merging by smoothing or interpolation is applied. From this new data set, three types of BL regions could be identified (Fig. 2.2): regions of seasonal BLs in the northern subpart basins, regions of quasi-permanent BLs in the equatorial and western tropical Atlantic and Pacific, the Bay of Bengal, the eastern equatorial Indian Ocean, the Labrador Sea, and parts of the Arctic and Southern Ocean and finally regions where BLs are typically never detected between 25°N and 45°N latitude in each basin. Away from the deep tropics, the analysis revealed strong similarities between the two hemispheres and the three oceans regarding BL seasonality and formation mechanisms. The latter involves various mechanisms such as intense precipitations, oceanic circulation, wind seasonality, and river runoff, in relation with the specific geography and climatology of each basin. In the deep tropical Atlantic (Fig. 2.3), in partic-

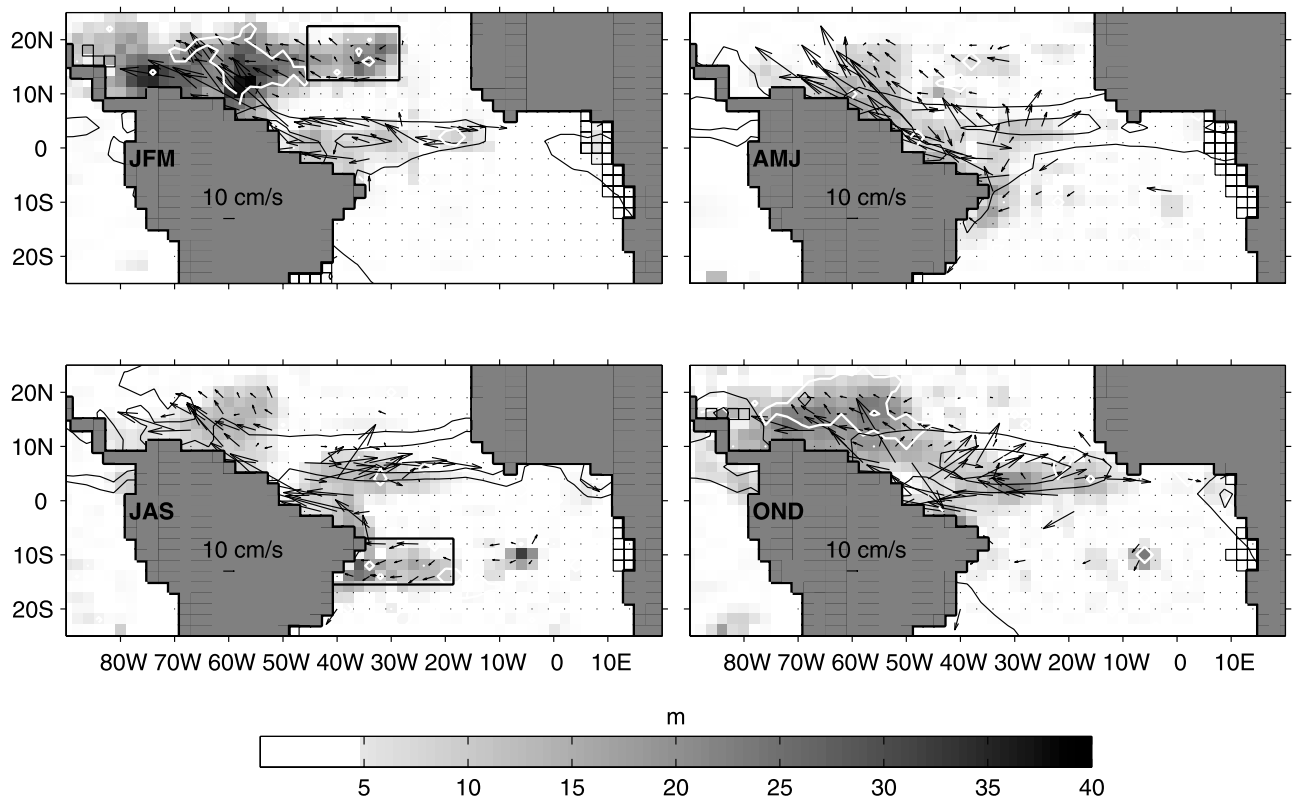

Figure 2.3: Grey scale gives seasonal BL thickness in the tropical Atlantic basin from the climatology of ***de Boyer Montégut et al. (2007)****. Grid points with no data during at least 1 month of the season are shown contoured in black. Arrows denote drifter-derived seasonal near-surface currents from Lumpkin and Garraffo (2005). For clarity, the currents have been smoothed using a three-point hanning window over both dimensions, and only one vector out of three is shown, and only at areas where the BL is thicker than 5 m. Black contours are 4 mm/d and 8 mm/d precipitation contours from the Xie and Arkins (1997) data set. From* ***Mignot et al. (2007)***

ular, intense precipitations under the ITCZ, large runoff from the Amazon river and the seasonality of the oceanic circulation are the main drivers of a complex BL system, with a clear seasonal cycle. Thick BLs are also detected in winter on the equatorial flank of each of the subtropical salinity maxima, as highlighted one year before by Sato et al. (2006) for example based on the profiles obtained by ARGO floats from January 2000 to June 2005. Here the intense surface freshening resulting from poleward Ekman advection of the fresh equatorial surface waters combined with the presence of subsurface salty waters lead to a strong, robust and permanent salinity stratification. In winter, the surface waters are additionally cooled by surface heat loss, so that temperature stratification is reduced. This induces BLs of up to 20 (in the South Atlantic and Indian oceans) and 30 (in the North and South Pacific and the North Atlantic) meters thick during the local winter season on the equatorial flank of the subtropical salinity maxima. In summer, the thermocline shoals under the effect of atmospheric heating and coincides again with the top of the pycnocline.

Given the sparsity of observations, in particular in subsurface, oceanic models are an important tool to deepen our understanding of barrier layers formation, persistency, climatic impact and life cycle.

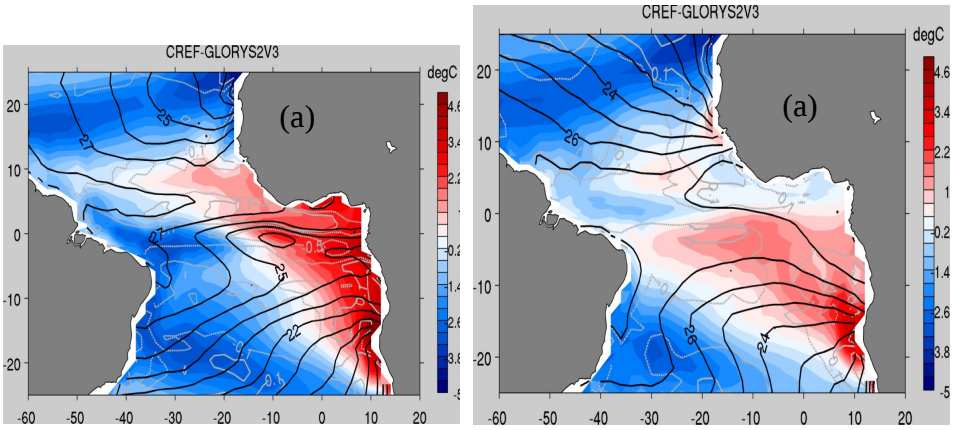

Figure 2.4: Sea surface temperature bias in the IPSL-CM5A-LR climate model ***Dufresne et al. (2013)*** *with respect to the oceanic reanalysis GLORYS2V3 (Ferry et al., 2012) averaged over January-February-March (left) and June-July-August (right) over the period 1993-2005. The black contours show the GLORYS climatology and the grey contour show the difference between the GLORYS reanalysis and the ERSST data set (Smith et al., 2008), giving an estimate for the uncertainty of SST observations and reanalysis. From* ***Sylla (2015)***

.

By comparing the mean state in three general circulation climate models with oceanic reanalysis, we firstly established a link between the representation of barrier layers and the SST bias in the eastern tropical Atlantic (illustrated for the IPSL-CM5A-LR model, which will be presented in more details below, in Fig. 2.4), thereby highlighting the role of sea surface salinity for the amplification of the precipitation and wind stress biases in forced atmospheric models **(Breugem et al., 2008)**. In the western tropical Atlantic now, Fig. 2.3 shows that the warm pool is the location for particularly thick BLs, which are also associated to important temperature maxima in subsurface. This means that the vertical temperature gradient is reversed as compared to what is expected from simple hydrostatic consideration. In this case, the salinity assures the vertical stability, even though its influence on density is relatively weak in warm tropical waters. Thus, this indicate that the salinity stratification is particularly strong. Based on climatological output of a general circulation ocean model, we showed that its development consists of two phases **(Mignot et al., 2012)**. In summer, the BL is relatively shallow and thin but subsurface temperature maxima are intense. The latter develop as a result of the specific seasonality of the freshwater discharge in this area, which limits the mixed layer to a very thin depth while the intense radiative heat flux penetrates significantly below, thereby heating the subsurface waters protected from air-sea interactions and inducing a barrier layer between the mixed layer and the ocean interior. In winter, the BL development is the same as the one described above at similar latitudes and during the same season on the equatorial flank of each of the subtropical salinity maxima.

Building on all these analysis, we have developed a simple linear equation linking the BL development to time evolution of temperature and salinity stratification to prognose the BL thickness. This conceptual model is based on the case of a water column with subsurface heat fluxes negligible in the

vicinity of D_{T*-02}, a simplified temporal equation for D_{T*-02} is:

$$\partial_t D_{T*-02} = (\partial_z T)^{-1} \mid_{D_{T*-02}} \times \partial_t SST \tag{2.3}$$

where the vertical temperature gradient is computed at the depth D_{T*-02}. Equation (2.3) shows that, in such an idealised water column, and in particular with a standard upward temperature gradient in the thermocline ($\partial_z T < 0$), D_{T*-02} shoals (respectively deepens) by construction when the SST warms up (resp. cools down). A similar equation can be derived for the evolution of the pycnocline depth D_σ and the halocline $D_{S*\pm\Delta S}$ and introducing the vertical density ratio $R_z = \frac{\alpha_T \partial_z T}{\beta_S \partial_z S}$, one can finally write:

$$\partial_t BL = \frac{1}{1 - R_z}(\partial_t D_{T*-02} - \partial_t D_{S*\pm\Delta S}) \tag{2.4}$$

This equation indicates that the BL development depends on the evolution of the distance between the top of the thermocline and of the halocline respectively. Hence one can verify that a BL tends to develop if $D_{T*-0.2}$ deepens faster than $D_{S*+\Delta S}$, since the latter will limit the deepening trend of D_σ. Fig 2.5 shows a sketch of the main types of idealised stable vertical profiles of temperature and salinity below the MLD, as in Liu et al. (2009). The simplest, and most common, case of vertical stratification in the upper ocean corresponds to an upward temperature gradient below the thermocline and a downward salinity gradient below the halocline. In this case, $R_z < 0$ at the base of the thermocline. For $R_z << -1$, the temperature gradient largely dominates the salinity in terms of its effect on the density gradient, and $1/(1 - R_z)$ tends towards zero and damps BL development in Eq. (2.4). In other words, D_σ varies almost like $D_{T*-0.2}$, at the expense of BL development. For R_z close to zero and negative, the salinity gradient now dominates the temperature one, and BL varies in unity with changes in $D_{S*+\Delta S} - D_{T*-0.2}$. Such a profile corresponds mainly to weak temperature and strong salinity gradients. In this case, the BL develops essentially because $D_{T*-0.2}$ deepens easily while D_σ varies almost like $D_{S*+\Delta S}$, that is little since the halocline is strong. For $0 < R_z <= 1$, a temperature inversion prevails and density is compensated by a salinity increase. However, Eq. (2.4) do not hold since D_{T*-02} is not present in such an idealised profile. Another equation for the development of a CL should be derived. Note nevertheless that the temperature decreases at greater depth and a thick BL could be defined, as discussed in de Boyer Montégut et al. (2007). For $R_z >= 1$, the temperature profile is stable and compensated. Equation (2.4) functions as for the latter regime: $D_{T*-0.2} > D_{S*+\Delta S} > D_\sigma$ and $(1 - R_z)^{-1}$ reach high negative values, and a small deepening of $D_{T*-0.2}$ is, as expected, highly favorable to the development of a CL. Finally, for R_z much larger than 1, profiles are not compensated and the density gradient is controlled by the temperature gradient.

Fig. 2.6 shows the values of R_z averaged over the northwestern tropical Atlantic (top) and in the central Atlantic and Pacific basins (middle and bottom respectively) in forced oceanic GCM simulation with a horizontal resolution of 0.5° and 10m thickness in the upper 120m. This figure shows that $-1 << R_z < 0$ in summer in the North Atlantic warm pool and Eq. 2.4 confirms that such a situation is favorable to the development of a BL (Fig. 2.5). In the central Pacific and Atlantic basins (Fig. 2.6 middle and bottom), on the contrary, in summer, the halocline is relatively deep while the thermocline is stable or tends to shoal, due to intense surface warming. Hence R_z is strongly negative, and this limits BL formation. In autumn, the rapid weakening of $\partial T/\partial z$ due to surface cooling reduces (in absolute

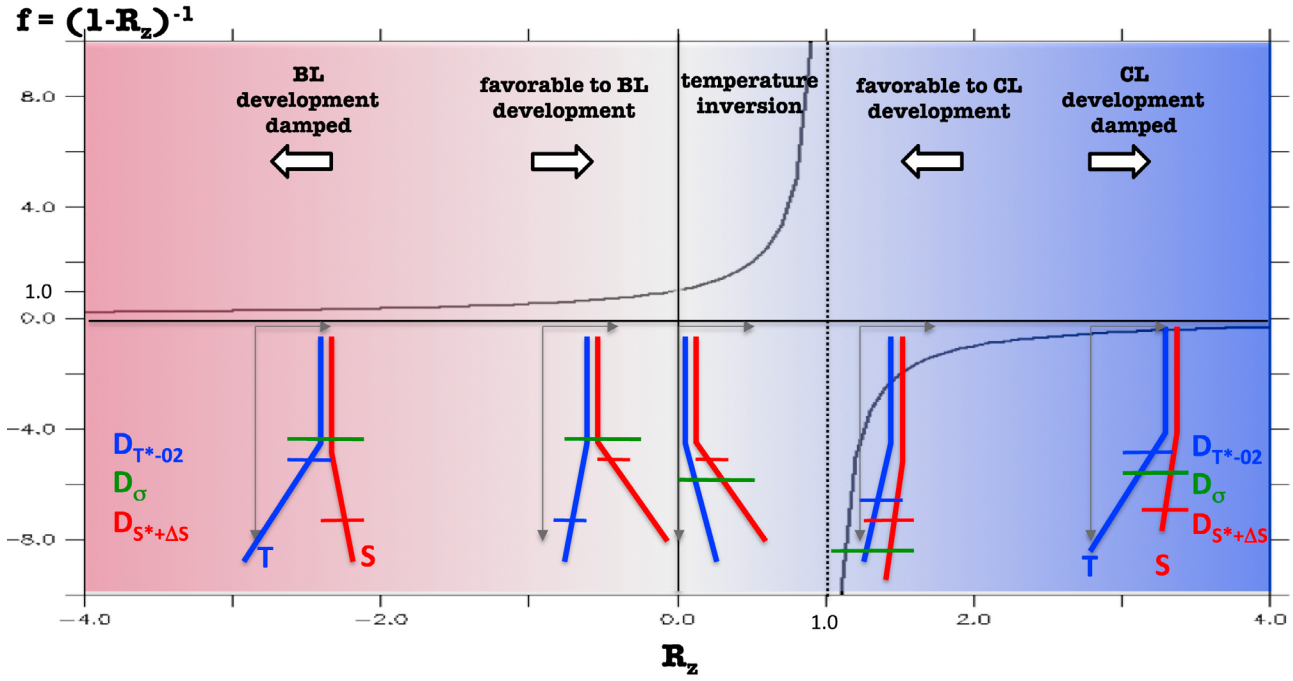

Figure 2.5: Schematic of the different stratification regimes described after **??** *and link to BL development conditions proposed by* ***(Mignot et al., 2012)****. The profile graphics illustrate typical temperature (in blue), salinity (in red) profiles as a function of* R_z*. Horizontal lines on the profiles sketch the* D_{T*-02} *(in blue),* $D_{S*+\Delta S}$ *(in red) and* D_σ *(in green) (see text for definitions). The background graphics shows the function* $f = (1 - R_z)^{-1}$*, which is the modulating factor in equations 2.4.*

values) R_z in all three regions. $D_{T*-0.2}$ deepens slightly faster than $D_{S*+\Delta S}$, and consequently the BL thickens. This holds both in the western tropical Atlantic and in the central basins (Fig. 2.6). Despite strong assumptions, the simple linear prognostic model for BL development thus constitutes a good framework to discuss BL developments, and compare the behaviour in different basins or seasons. Numerous improvements are yet needed, such as the inclusion of subsurface heat fluxes and thereby the representation of subsurface temperature inversions.

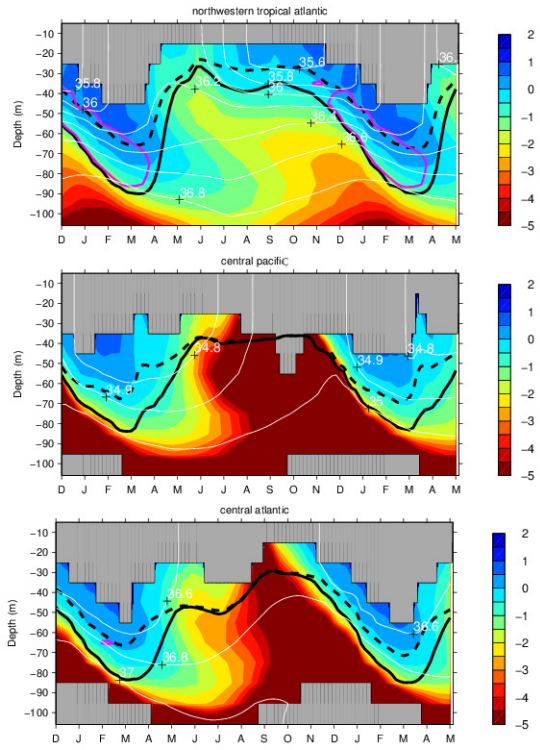

Figure 2.6: Vertical density ratio $R_z = \frac{\alpha_T \partial_z T}{\beta_S \partial_z S}$ *averaged over the western tropical north Atlantic (top) and over the central Pacific area (middle) and central Atlantic area (bottom). Areas where* $\partial_z S = 0$ *are shown in grey. The thick black lines show the depth* D_{T*-02} *(solid) and the MLD (dashed) diagnosed from the model data averaged over the same area. The magenta contour shows areas where a temperature inversion has been detected. From* ***Mignot et al. (2012)****.*

2.2 Seasonal salinity budget in the tropical Atlantic

In order to better understand the dynamics of the barrier layer and of the mixed layer in the tropical Atlantic, linked to atmospheric fluxes as well as horizontal and vertical ocean dynamics, budgets of the seasonal salinity variations are needed. Yet, because of the lack of SSS direct observations, early efforts to characterise these variations have been confined to local regions of the tropical Atlantic, or have failed to fully close the salinity budget (e.g. Dessier and Donguy, 1994; Reverdin et al., 1997; Foltz and McPhaden, 2008; Tzortzi et al., 2013; Da-Allada et al., 2013; D'Addezio and Bingham, 2014). We have proposed a full analysis of the physical processes controlling the mixed layer salinity (MLS) seasonal budget in the tropical Atlantic ocean using the regional configuration of an ocean general circulation model **(Camara et al., 2015)**. Central result of this analysis is that the MLS seasonal cycle as found to be generally weak as compared to individual physical processes entering in the salt budget, because of strong compensations between the physical drivers of this variability. Three main regions could be defined (Fig. 2.7): (i) evaporative regions, located in particular on the equatorward flanks of the subtropical SSS maxima, where poleward Ekman transport mainly contributes to supply freshwater originating from ITCZ regions, while vertical diffusion of salt within the mixed layer adds

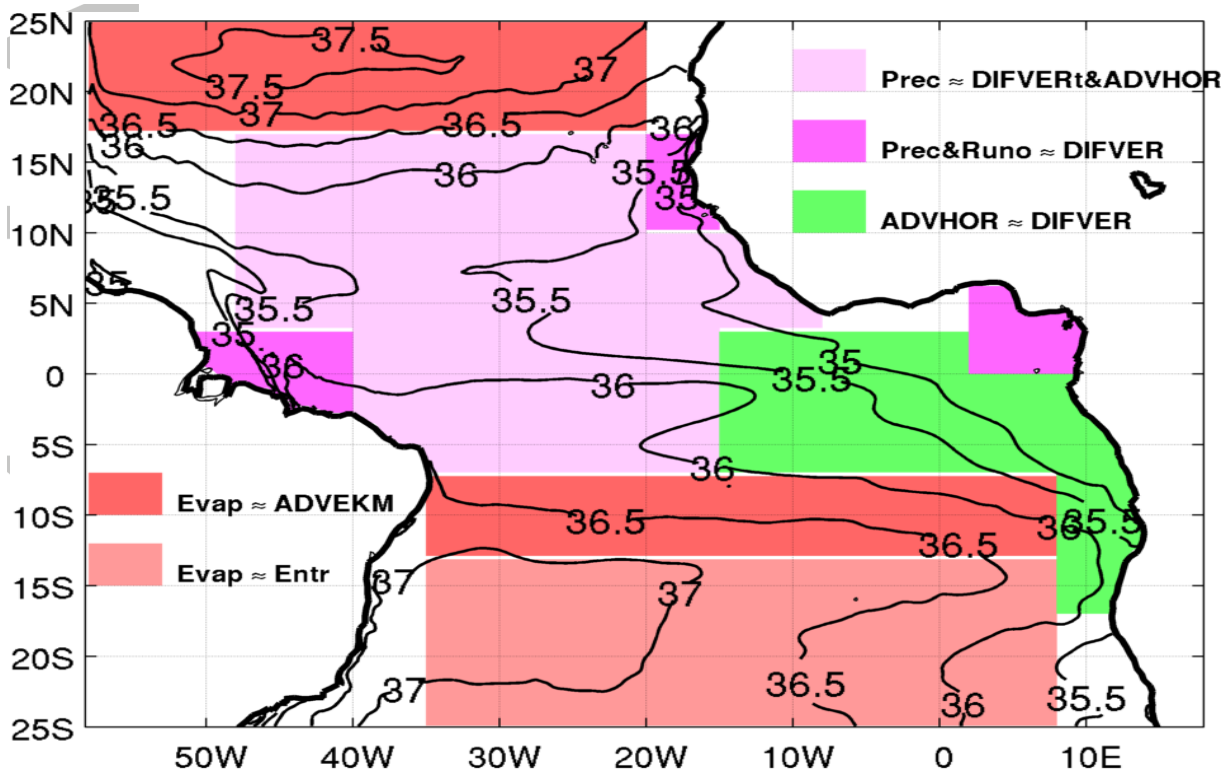

Figure 2.7: Summary of the main compensating processes influencing the seasonal variability of the mixed layer salinity as derived from ***Camara et al. (2015)****. Compensation between the effect of: evaporation and Ekman advection (red color), evaporation and entrainment (red light), precipitation + runoff and vertical diffusion (magenta), precipitation and vertical diffusion (magenta light), horizontal advection and vertical diffusion (green). Contours show the annual mean salinity in the mixed layer, in psu.*

on the effect of evaporation to counteract this freshening. All these terms are phase-locked through the effect of the wind. Each of these individual terms were shown to be quite strong but the resulting salinity variability is much weaker. (ii) Under the seasonal march of the ITCZ and in coastal areas affected by river (7° S:15° N), the upper ocean freshening by precipitations and/or runoff is attenuated by vertical salinity diffusion. (iii) In the eastern equatorial regions, finally, the seasonal cycle of wind forced surface currents advect freshwaters which are mixed with subsurface saline water because of the strong vertical turbulent diffusion. In all these regions, in the model, the vertical diffusion makes an important contribution to the MLS budget by providing, in general, an upwelling flux of salinity except poleward of the southern SSS maxima. It is generally due to vertical salinity gradient and mixing due to wind stress. Furthermore, in the equator where the vertical shear, associated to surface horizontal currents, is developed, the diffusion depends also on the sheared flow stability. This study reveals a complex interplay between atmospheric and oceanic salinity flux at seasonal scale, which results in the lack of a direct relationship between freshwater flux and MLS. A direct relationship between freshwater forcing and MLS is indeed rather found at longer time scales (inter annual to decadal) (Durack et al., 2012; Terray et al., 2012; Vinogradova and Ponte, 2013, e.g.). Nevertheless, details in the processes highlighted in this study would require validation with salinity observations.

In my view, one of the most important and interesting result of this study is the importance of the vertical salinity diffusion at the base of the mixed layer in most regions of the tropical Atlantic, in spite of a generally weak seasonal cycle of the salinity. This result may have important consequences for our understanding of the transmission of signals within the ocean interior, vertical dynamic inducing strong flux exchange between the upper and interior ocean. Implications in terms of density and spiciness injection in the ocean interior is ongoing work.

2.3 The Atlantic Meridional Overturning Circulation

As introduced above, the AMOC is a key component of the global oceanic circulation. Johns and Baringer (2011) estimates that the AMOC contributes to 90% of ocean meridional heat transport at 26.5°N. Measuring the AMOC is nevertheless challenging, as it requires observations that cover a complete basin. Thus, historically the observational record has been quite limited and most studies based on the AMOC variability and impact on the climate are based on models. Fig. 2.8 shows the zonally averaged oceanic circulation in the Atlantic in 5 simulations performed with different configurations of the NEMO oceanic model: ORCA2-coupled corresponds to the control simulation of the IPSL-CM5A-LR climate model, using NEMO on a ORCA2 grid (nominal resolution of 2°) **(Dufresne et al., 2013)**; ORCA1-coupled corresponds to the control simulation of the CNRM-CM5 climate model, using NEMO on a ORCA1-grid (nominal resolution of 1°) (Voldoire et al., 2012). ORCA2-forced and ORCA1-forced are oceanic simulations using the ORCA2 and ORCA1 grids respectively using the same CORE2 forcing protocol (Griffies et al., 2009). ORCA025-forced uses a higher resolution (nominal resolution of 0.25°) and the DFS4 forcing set (Brodeau et al., 2010). Beyond shallow circulation cells in the tropics and the subtropics mostly forced by the wind, these figures highlights a northward flow in the upper layer, sinking at high latitudes, and returning southward at depth as North Atlantic Deep Water (NADW). This figure also highlights strong differences among models, both in terms of spatial structure and maximum value and motivates for observational estimates of the AMOC This is the motivation for the RAPID project, which continuously monitors of the AMOC at 26.5°N since 2004 (see Cunningham et al. (2007); Kanzow et al. (2007) for early results, and McCarthy et al. (2015) for a recent review). Analysis of the first 4 years of data by Kanzow et al. (2010) showed that the AMOC at 26.5N had a mean strength of 18.7 Sv. The now 10 years of data have highlighted the intense variability of the AMOC at all time scales (Cunningham et al., 2007; Kanzow et al., 2010; McCarthy et al., 2012; Smeed et al., 2014). The seasonal cycle, in particular, was shown to have a peak-to-peak amplitude of roughly 6.7 Sv. Contrarily to the accepted view based on numerical models (e.g. Böning et al., 2001), this seasonality is not dominated by the northward Ekman transport variability. Fluctuations of the geostrophic mid-ocean and Gulf Stream transports are rather significantly larger. Similar conclusions were reached regarding inter annual timescales (compare McCarthy et al. (2012) and Böning et al. (2001)), the meridional heat transport (Johns and Baringer, 2011; Msadek et al., 2013) and also in the southern ocean (e.g. Dong et al., 2011, 2014). These differences between numerical models and observations suggest that the AMOC and MHT in models may respond to forcing differently than in the real ocean. It is crucial to evaluate and diagnose what causes these differences in order to improve numerical models.

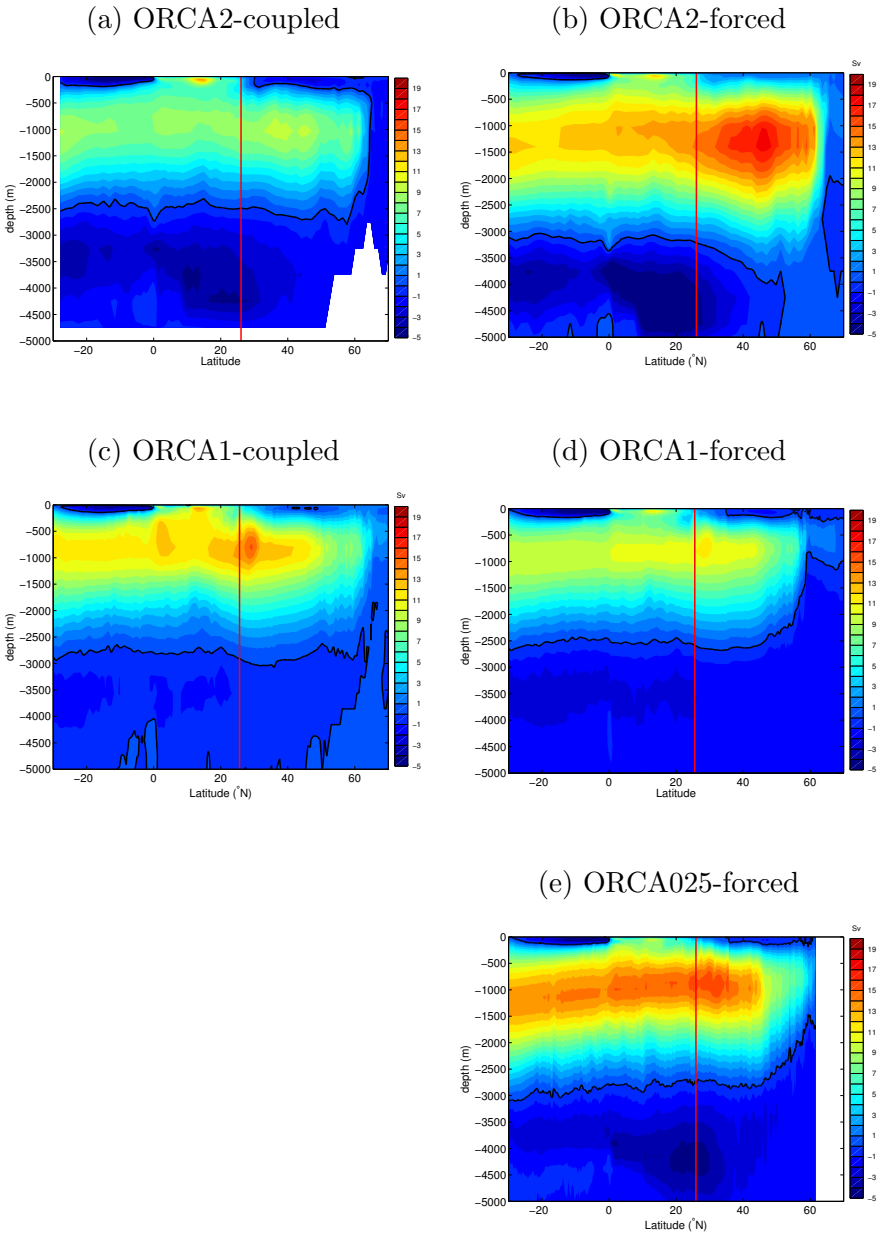

Figure 2.8: Mean Atlantic meridional overturning streamfunction (AMOC, Sv) as a function of latitude and depth, in (a) ORCA2-coupled (IPSL-CM5A-LR climate model), (b) ORCA2-forced (CNRM-CM5 climate model), (c) ORCA1-coupled, (d) ORCA1-forced and (e) ORCA025-forced simulation. Red line marks the 26.5°N (RAPID) section and black contour marks the zero value of the stream function.

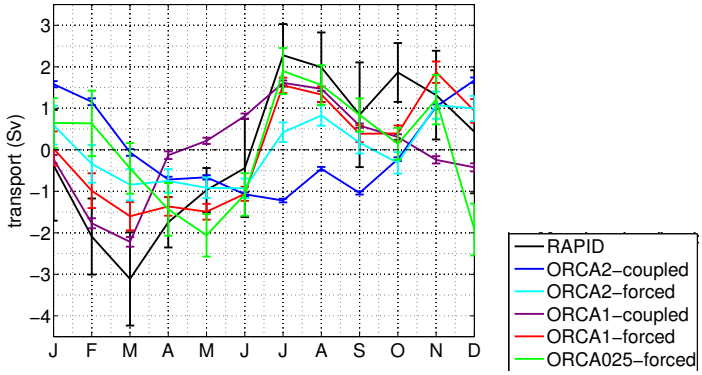

Figure 2.9: Seasonal anomaly of AMOC, with standard error for RAPID array (black), ORCA2-coupled (blue), ORCA2-forced (light blue), ORCA1-coupled (purple), ORCA1-forced (red) and ORCA025-forced (green). R. Waldman, pers.com.

The origin of the observed AMOC seasonal variability is furthermore only partly understood. It is generally linked to the seasonal variability in the wind stress curl along the African coast (Kanzow et al., 2010; Chidichimo et al., 2010; Sinha et al., 2013) but the most recent data show that a clear seasonal cycle is not evident in the sixth year of measurements and dramatic changes are apparent in the AMOC during the winter of 2009/10 (McCarthy et al., 2012) and the following (Blaker et al., 2014).

Fig. 2.9 show the AMOC seasonal cycle at 26.5°N, in the five same coupled and forced simulations as above, together with observational estimates from the RAPID reconstruction (in black). As for the mean AMOC structure, the representation of the AMOC seasonal cycle in oceanic models show significant differences with what can be inferred from the RAPID data. Biases are due to all three components of the AMOC as decomposed in the RAPID array: the upper Ekman transport, the interior geostrophic transport, and transport associated to the western boundary. The latter is not fully represented in coarse resolution simulations (ORCA2 and ORCA1 here) where the Bermuda Islands are missing. The channel part of this current (Florida Current) is thus missing and only the Antilles Current, which generally follows the dynamics of the return western boundary current in the Sverdrup theory, ensures the full return current. As a result, the dynamics of the western boundary current is different in coarse resolution models and in observations, and so is its seasonal cycle. The high resolution model illustrates that the Florida Current an the Antilles Current have very different dynamics but discrepancy with data remain. The representation of the Ekman transport is of course directly sensitive to the momentum forcing and it can thus be significantly biased in coupled mode. The interior geostrophic component finally also shows large discrepancies as compared to data in terms of vertical and zonal structures.

Lessons from this analysis may be used for early models validation and impacts on atmospheric and oceanic large scale biases on the AMOC representation. Recently, Mercier et al. (2015) noted that also at sub polar latitudes, the seasonal cycle of the zonally averaged stream function amounts about 5 Sv, same order of magnitude as the interannual to decadal variability. Given the relevance of subpolar variations of the AMOC for climate, better understanding its dynamics and its representation

in climate models is crucial. The seasonal variability constitutes in my view an interesting framework for such goal.

Chapter 3

Internal variability at interannual to decadal timescales

Climate variations also occur beyond the seasonal and intra-seasonal timescale. Here, I propose to investigate the variability of sea surface salinity and AMOC on timescales spanning from several months to several years.

3.1 Sea surface salinity

3.1.1 The stochastic modelling framework

Let us consider a slab mixed-layer model where the temperature T, the salinity S, and the horizontal current u are constant within a mixed layer of depth h. The vertically integrated temperature and salinity equations can be written

$$h\frac{dT}{dt} + (T - T^-)\Gamma(w_e)w_e - \kappa h\nabla^2 T - \frac{Q}{\rho C_p} = 0 \tag{3.1}$$

and

$$h\frac{dS}{dt} + (S - S^-)\Gamma(w_e)w_e - \kappa h\nabla^2 S - S(E - P) = 0 \tag{3.2}$$

where Γ is the Heaviside function, w_e the entrainement velocity, κ the horizontal mixing coefficient, Q the surface heat flux (positive downward), E the evaporation, and P the precipitation rate. ρ is the water density and C_p its specific heat. The fluxes at the mixed layer base have been neglected for simplicity, although **Camara et al. (2015)** have shown their importance for the salinity in the tropical Atlantic for example at seasonal timescales. If the mixed layer is deepening, there is entrainement of water from below the mixed layer (denoted by the minus index), whereas if it is shoaling, there is detrainement and fluid is left behind without changing the SST or the SSS.

Each field can be decomposed into a seasonally varying mean (denoted by an overline) and an anomaly (denoted by a prime). To a good approximation, the equation for large-scale SST anomalies

can be written (Frankignoul, 1985)

$$\frac{dT'}{dt} \approx \frac{(U'_E + U'_G).\nabla(\overline{T} + T')}{\overline{h}} - \frac{h'}{\overline{h}}\partial_t\overline{T} - \frac{(\Gamma(w_e)w_e(T - T^-))'}{\overline{h}} + \frac{Q'}{\rho C_p \overline{h}} + \kappa\nabla^2 T' \tag{3.3}$$

Similarly, the SSS anomaly equation is

$$\frac{dS'}{dt} \approx \frac{(U'_E + U'_G).\nabla(\overline{S} + S')}{\overline{h}} - \frac{h'}{\overline{h}}\partial_t\overline{S} - \frac{(\Gamma(w_e)w_e(S - S^-))'}{\overline{h}} + \frac{\overline{S}(E' - P')}{\overline{h}} + \kappa\nabla^2 S' \tag{3.4}$$

Here $d/dt = \partial_t + \overline{u}.\nabla$ is the time derivative following the mean current and the transport in the mixed layer (hereafter noted U) has been decomposed into an Ekman component U_E and a geostrophic one U_G, with the former obeying

$$U_E = \frac{\tau \wedge n}{\rho f} \tag{3.5}$$

where τ is the surface wind stress, f the coriolis parameter, and n the vertical unit vector.

At extratropical latitudes, the atmospheric forcing is dominated by the day-to-day changes in the weather and has a primarily white spectrum at low frequencies. Because of its small mechanical inertia, the oceanic mixed layer responds rapidly and h' also has a white spectrum at low frequencies (Alexander and Penland, 1996). Except for the geostrophic contribution, the forcing terms in (3.3) and (3.4) are thus well-represented by white noise on monthly and longer time scales. They create growing anomalies whose amplitude is limited by dissipation and feedback processes (Hasselmann, 1976; Frankignoul and Hasselmann, 1977). For small anomalies, the latter are well represented by linearising the (in part hidden) T' or S' dependence of the right-hand side of (3.3) and (3.4), respectively. Neglecting geostrophic variability, the equations can then be written

$$\frac{dT'}{dt} = F'_T - \lambda_T T' \tag{3.6}$$

and

$$\frac{dS'}{dt} = F'_S - \lambda_S S' \tag{3.7}$$

where F' represents the stochastic forcing terms (the part that is solely controlled by the intrinsic dynamics of the atmosphere), λ a scale-dependent feedback factor (positive when the feedback is negative), and the T and S indices denote temperature and salinity, respectively.
In regions of small mean current, however, one has $\frac{d}{dt} \approx \partial_t$ and, if the seasonal modulation is neglected, (3.6) and (3.7) represent first order Markov processes with frequency spectrum and auto-covariance function respectively given by

$$F_{XX}(\omega) = \frac{F_{F_X F_X}(0)}{\omega^2 + \lambda_X^2} \tag{3.8}$$

$$R_{XX}(\tau) = \frac{\pi}{\lambda_X} F_{F_X F_X}(0) e^{-\lambda_X |\tau|} \tag{3.9}$$

where X holds for T' or S' and $F_{F_X F_X}(0)$ is the white noise level of the forcing. This expression clearly shows that λ^{-1} represents the decay time of X.

Away from strong currents, observed SST and SSS anomalies are well represented by (3.8) and (3.9)

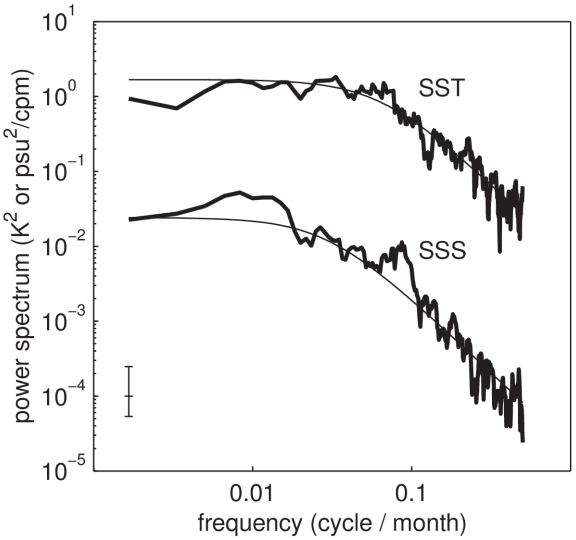

Figure 3.1: Power spectrum (estimated with the multi-taper method) of SSS and SST anomalies at 37° N-32° W (western subtropical North Atlantic) in the ECHAM4/OPA8 coupled model. The error bar gives the 95% confidence interval. The smooth curve represents the fit by the red noise spectrum in Eq. (3.8). Figure from ***Mignot and Frankignoul (2003)***

(Frankignoul, 1985; Hall and Manabe, 1997). This also holds in coupled models at most grid points, as illustrated in Fig. 3.1. The characteristic time scale of the SSS anomalies is longer because the surface heat flux damps existing SST anomalies, but not SSS anomalies. This is also reflected in the cross-correlation functions between the freshwater flux and SSS anomalies: There is thus no correlation between the two variables when SSS leads by a month or more; the correlation is large at zero lag because of the small atmospheric persistence and the use of monthly averages, and it slowly decays when the ocean lags by more than one month. This differs from the cross-correlation between SST and heat flux anomalies is negative when SST leads, reflecting the negative heat flux feedback. Fig. 3.2 shows that in a typical climate simulation using a coarse resolution coupled model of the CMIP3 generation (Bergen Climate Model Furevik et al. 2003) typical values for λ_S^{-1} are 4-8 months in the westerlies and 8-15 months in the subtropics. For comparison, the SST anomaly persistence is typically 2 months, with smaller values off Africa and near the equator, and a 5 month peak in the western part of the subtropical gyre. **Frankignoul et al. (2002)** have shown that in regions of small currents, the difference in SSS and SST anomaly persistence can give a reasonable estimate of the strength of the heat flux feedback.This longer persistence of SSS anomalies in the ocean has implications for its dynamics which are described below.

3.1.2 Sea surface salinity response to the atmospheric variability

Atmospheric variability is the major source of variability at inter annual timescale at the ocean surface. Anomalous Ekman advection is found to be as important as the freshwater flux in generating SSS anomalies, in contrast to sea surface temperature (SST) anomalies which are primarily caused by surface heat flux fluctuations. Anomalous Ekman advection also primarily controls the response of SSS anomalies to the dominant patterns of atmospheric variability, at least in the North Atlantic sector: Fig.

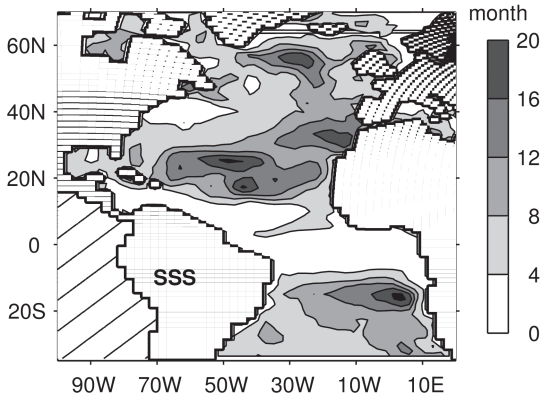

Figure 3.2: Local SSS anomaly persistence (in months) in the Bergen climate model (BCM), computed from the decreasing time of the SSS autocorrelation function at each grid point. Figure from ***Mignot and Frankignoul (2004)***

3.3 shows that in a simulation performed with the ECHAM4/OPA8 climate model, the North Atlantic Oscillation, leading mode of atmospheric variability in the Atlantic sector at inter annual timescale, and particularly prominent in winter, generates SSS anomalies much more by Ekman advection than by freshwater exchanges. Similar results were found in the Bergen Climate Model (BCM, **Mignot and Frankignoul 2004**) This differs again from SST anomalies, which are more much more directly forced by anomalous atmospheric fluxes. The reason for this difference may lie in the sharper SSS gradients as compared to SST gradients, which are damped by atmospheric feedback. As geostrophic currents mostly vary at low frequency, anomalous geostrophic advection becomes comparable to or dominates the direct atmospheric forcing over most of the basin at periods larger than about 2 years. Again anomalous geostrophic currents have a efficient effect on salinity variability because of the longer characteristic timescales of salinity anomalies. This results confirm in state-of-the-art general circulation climate models Spall (1993) and Hall and Manabe (1997) earlier conceptual studies.

Once created, salinity anomalies persist for a longer time and may be advected by mean currents quite efficiently. We have highlighted advective pathways in the subpolar North Atlantic in the BCM simulation using lagrangian tracers released off Newfoundland, where sea surface salinity variability was found to be particularly high **(Mignot and Frankignoul, 2004)**. But Such propagations around the sub polar gyre have been identified in the past, in particular related to the Great Salinity anomalies (GSA) (Belkin et al., 1998; Belkin, 2004; Sundby and Drinkwater, 2007). For instance, a salinity anomaly was first identified in the Nordic Seas in 1968, and then detected in the Labrador Sea around 1971. This anomaly was monitored along its propagation within the subpolar gyre during the following 7 years, and it reached the eastern part of the Nordic Seas in 1978 (Belkin et al., 1998). Analysing a 115 year long record of sea surface temperature and salinity in the North Atlantic supbolar gyre area, Reverdin (2010) also identified a clear influence of advection on salinity records in the sub polar gyre. His findings also confirmed the longer autocorrelation of salinity time series as compared to temperature. He also found that inter annual salinity variations are significantly (at the 95% level) negatively correlated with the NAO when the NAO leads by 2-3 years, while this is not the case anymore for temperature. Note that advective pathways originating in the tropics have also been

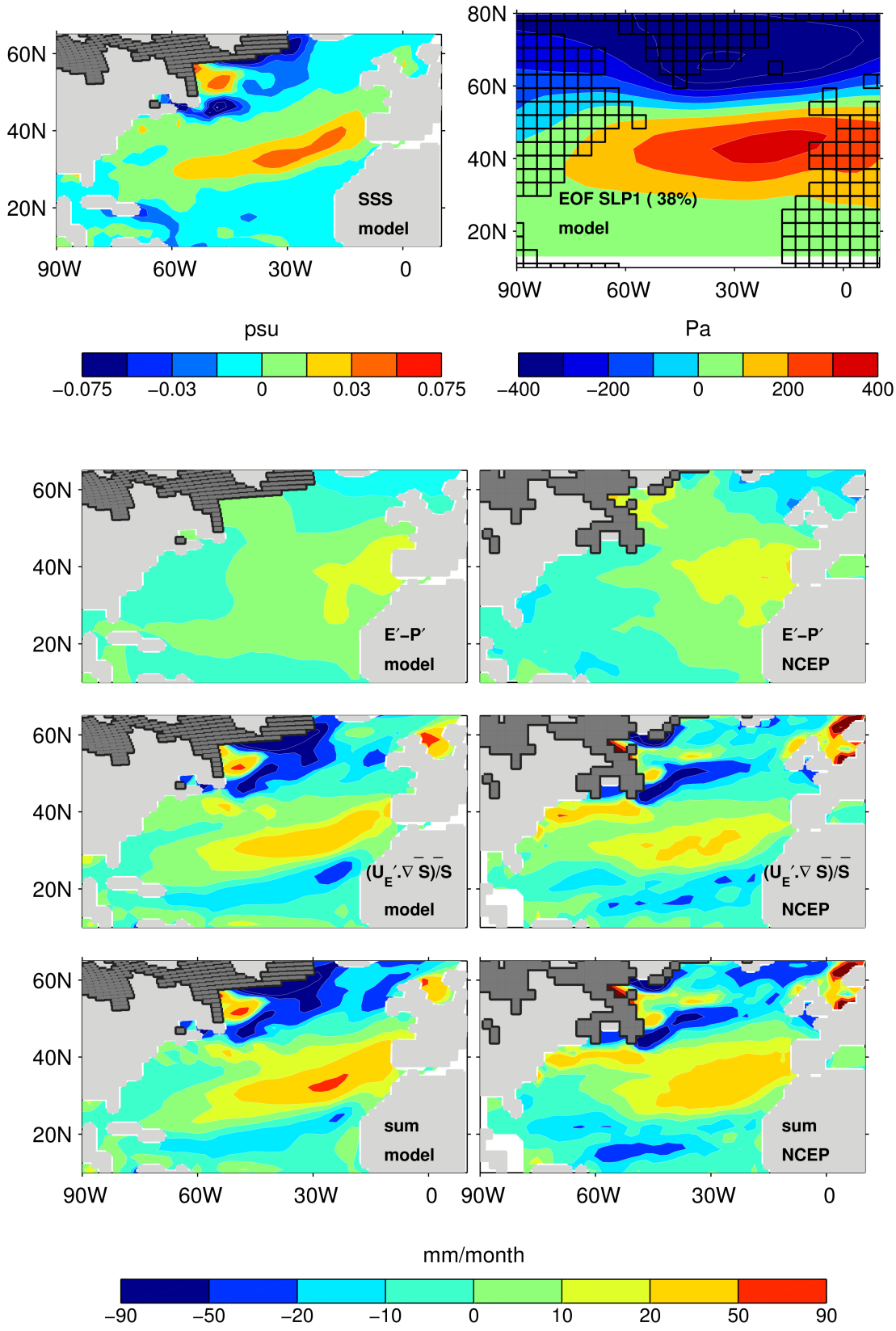

Figure 3.3: Top: projection of SSS (left) on the PC of the model NAO one month earlier (right) in a control simulation of the ECHAM4/OPA8 climate model. Bottom panels: in-phase projection of various forcing terms on the NAO for the coupled model (left) and NCEP reanalysis (Kalnay and Others, 1996) (right). From ***Mignot and Frankignoul (2003)****.*

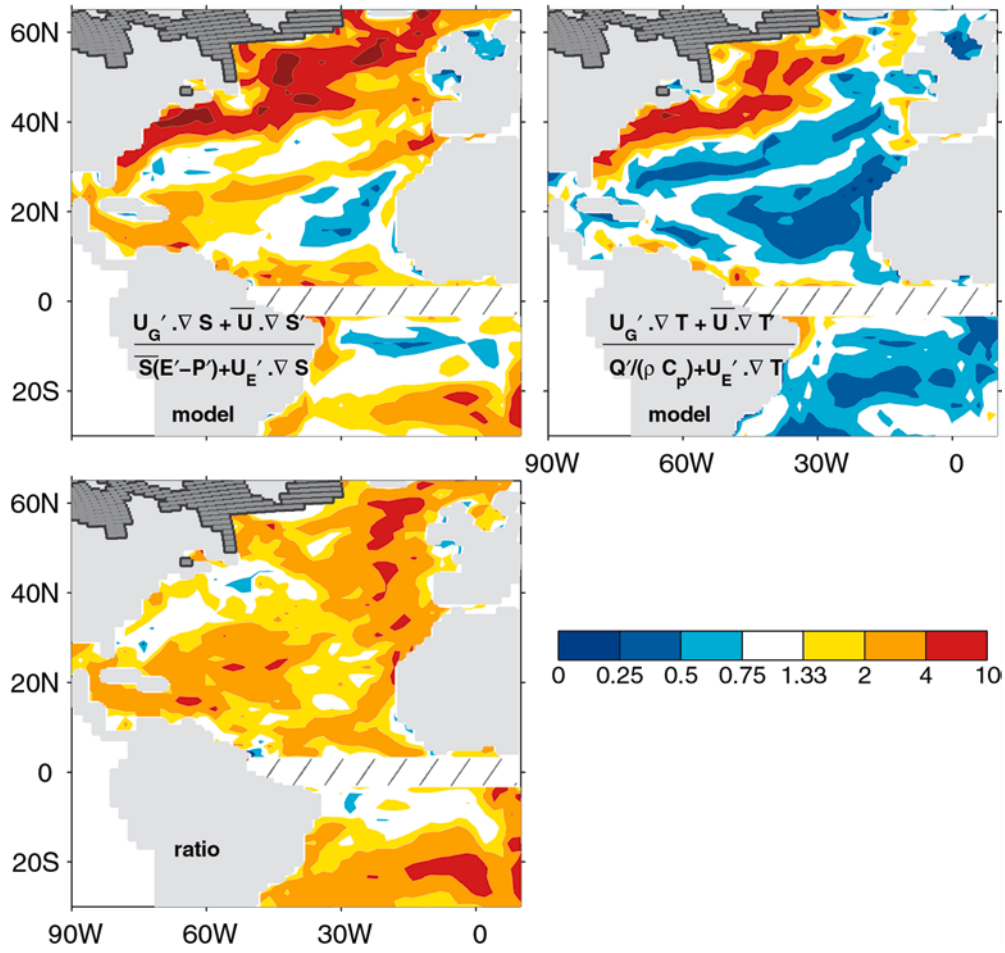

Figure 3.4: Top left: ratio between the standard deviation of the sum of anomalous geostrophic advection of salt and the mean advection of SSS anomalies and that of the sum of freshwater flux and anomalous Ekman advection of salt in the ECHAM4/OPA8 control simulation ***(Mignot and Frankignoul, 2003)****. Frequencies higher than 2 cycles/year have been filtered out. Top right: as left but for SST. Bottom: ratio between the top left and top right panels.*

identified **(Mignot and Frankignoul, 2004, 2005)**. Fig. 3.4 proposes a last illustration of the stronger importance of geotropic anomalous advection as well as advection by the mean currents for SS than for SST: except along the Gulf Stream and the North Atlantic current, the relative importance of advection at low frequencies is smaller for the SST anomalies, the ratio typically ranging between 2 and 4 in the subtropics and the eastern North Atlantic.

3.1.3 Salinity pathways towards the high latitudes and water mass transformations

The previous results have important potential climatic consequences as salinity anomalies may thus be advected over large distances. Sea surface salinity anomalies created in the tropical Atlantic can thereby be advected all along the high latitudes, as has been identified in several climate models **(Mignot and Frankignoul, 2004, 2005; Goelzer et al., 2006)**. More specifically, they first propagate along the

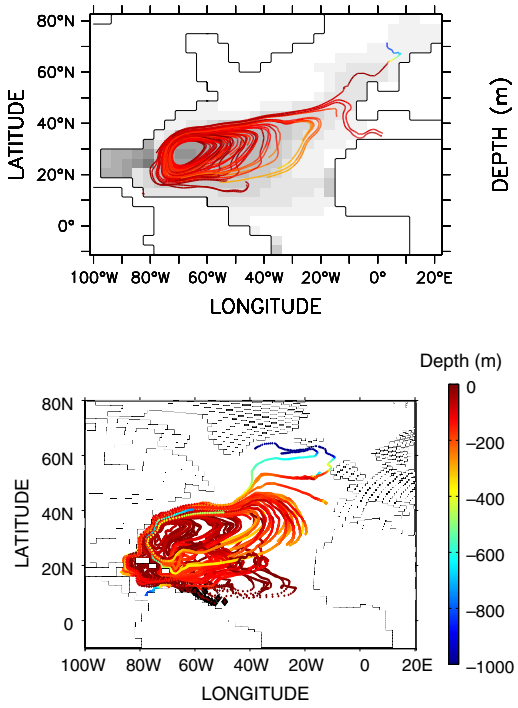

Figure 3.5: Particle trajectories after 20 years of control integration in CLIMBER-3α ***(Goelzer et al., 2006)*** *(top) and in the Bergen Climate Model* ***(Mignot and Frankignoul, 2005)*** *(bottom). The color code represented the trajectory depth in meters. The grey shading in the upper panel illustrated the concentration of Eulerian tracers after 20 years in the CLIMBER-3α simulation.*

subtropical gyre, where they subduct. In the ocean interior, part of the anomaly is advected along the North Atlantic current, eventually reaching the Irminger and Labrador Seas after about 20 to 30 years in the BCM **(Mignot and Frankignoul, 2005)** and in the coarser resolution model of intermediate complexity CLIMBER-3α model **(Goelzer et al., 2006)** (Fig. 3.5). Once in the high latitudes, the salinity anomalies may influence the stability of the water column and thus convection and the AMOC.

Another view of this propagation of tropical Atlantic anomalies towards the northern North Atlantic is proposed in Fig. 3.6. In this study performed with the IPSL-CM4-v2 climate model **(Marti et al., 2010)**, a constant and uniform negative freshwater flux of 0.4 Sv was applied between 15°N and 15°N during 50 years in a six-members ensemble. The initial perturbation does not reach below the mixed layer, as seen on the $\sigma = 27kg.m^{-3}$ isopycnal, which is located at 100 to 300m depth equatorward of $30°N$ (Fig. 3.6a). Panels b and c show that by the sixth year, the salinity anomaly has began to penetrate in the ocean interior, which is primarily ventilated from the area of maximum salinity, where the isopycnal outcrops (e.g. Laurian et al., 2006). The northern subtropics are thus ventilated from the North, after the anomaly has propagated near surface[1]. After about 10 years, after circulating in the subtropical gyre, the anomalies return to the western boundary in an area of deep winter mixed layer, as illustrated for $\sigma = 27.4kg/m^3$ (500 to 700m depth between 35°N and 55°N) in panels d-f.

[1]Note that because of an anomalous freshwater tongue coming from the Labrador Sea, the isopycnal $\sigma = 27kg/m^3$ outcrops south of Newfoundland in the model (grey areas). This is not realistic but does not drastically affect the results.

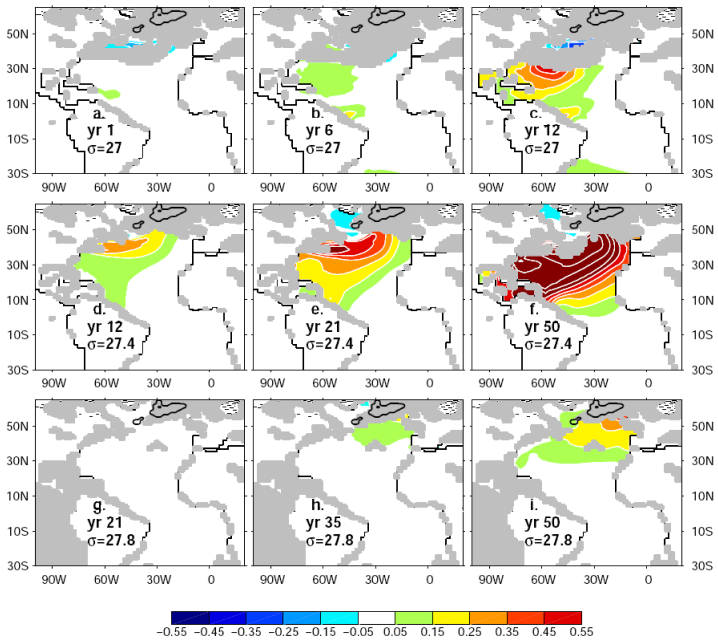

Figure 3.6: Anomalous salinity (in psu) at different time (indicated in years in each panel) after the beginning of a salinity perturbation imposed continuously in the tropical Atlantic in the IPSL-CM4-v2 climate model ***(Mignot and Frankignoul, 2010)****. Anomalies are displayed on three isopycnals (indicated in* $kg.m^{-3}$*). The black thick contours hows the areas of deep convection in the control run. To account for the intermittent character of deep convection, it was defined by a criterion on mixed layer depth variability, namely where the standard deviation of mixed layer in March exceeds 350m. The grey shading indicates regions of the isopycnal outcrop.*

This allows the anomalies to reach deeper isopycnals, and follow their route northward toward the deep convection region. They reach the latter after about 20 years. The increase of density associated to these anomalies favours deep water formation, as can be seen from a deepening of mixed layer depths (not shown). Finally, panels g-i illustrate the propagation of anomalous salinity on the isopycnal $\sigma = 27.8kg/m^3$. This isopycnal is found around 700m at high latitude and below 1000m in the Tropics and subtropics. It is thus too deep to be ventilated in the subtropical gyre and the mixing region off Newfoundland. As a result, the isopycnal is hardly perturbed by salinity during the first two decades of forcing (panel g). Anomalous salinity appears on this layer from the high northern latitudes around year 25, corresponding to water masses that sank during deep convection. Then, they progressively invade the Atlantic basin via the deep southward western boundary current (panel h-i).

At the time of this work, this description was based on much more detailed dedicated works based on data climatologies (e.g. Qiu and Huang, 1995) and high resolution ocean models (e.g. Laurian et al., 2006, 2009). We emphasise that since then, the recent ARGO data set has allowed a comprehensive description of the subduction and ventilation mechanisms at the center of the gyre Kolodziejczyk et al. (2014); Qu et al. (2016) and advances were also gained from high level model computations (Qu et al., 2013).

On their way northward, subtropical water masses carried by the North Atlantic Current are furthermore transformed into subpolar mode water, which is the dominant water mass above the

permanent pycnocline in the eastern subpolar region, by heat loss and freshwater input from the atmosphere. The water mass transformation is also an important step of the salinity anomalies travel from the subtropics to the high latitudes. Several processes may lead to WMT, including mixing, entrainment of denser water into the mixed layer and diapycnal mixing, but WMT at high northern latitudes is dominated by air-sea exchanges (Nurser et al., 1999). Walin (1982) thereafter proposed a diagnostic based on buoyancy forcing. Comparison of three 500-yrs long control climate simulations (Fig. 3.7) illustrates that the thermal contribution dominates the WMT in the eastern subpolar region in all three models, both in terms of mean state and variability. Hence densification of the northward flowing water occurs in this part of the basin **(Langehaug et al., 2012)**

As can be seen from this paragraph, all of my studies on this topic were based on model data. Indeed, until recently, very few data were available at the basin scale for analysis of the salinity inter annual variability (Reverdin et al., 1997, 2007; Reverdin, 2010). Recently, several novel data sets may allow much more in depth analysis of the upper ocean salinity from observations: Soil Moisture and Ocean Salinity (SMOS) satellite mission launched in 2009 provides microwave measurements of two-dimensional salinity fields of the surface ocean at a less than 100 km resolution (e.g. Font et al., 2013), unmatched by existing in situ networks. Promising signals have already been detected in different tropical oceanic basins (Durand et al., 2013; Hasson et al., 2014; Hernandez et al., 2014; Kolodziejczyk et al., 2015). Although promising, this data set is still rather short (Tzortzi et al., 2013) and until now, much focus has been put at investigating mesoscale structures revealed by SMOS in areas of high thermohaline contrasts such as the Gulf Stream region (Reul et al., 2014) or the Amazon plume (Grodsky et al., 2014). Recent studies promisingly suggest that interannual variability is robust represented in SMOS salinity measurements (Boutin et al., 2016). Compilation of ARGO floats bat CORIOLIS (Gaillard et al., 2009) is also promising, in particular as it also includes subsurface information (e.g. Kolodziejczyk et al., 2014). In the near future, I would like to focus more on this type of data. Reanalysed salinity data sets are yet still largely divergent (Shi et al., 2015), including in terms of sea surface data as illustrated in **(Mignot et al., 2015)**.

3.1.4 Implications for longer term variability

Two major implications can be deduced from sea surface salinity properties described in details above. Firstly, since it can integrate fluxes over time, sea surface salinity may record surface hydrology and its response to global climate. Several studies have thereby shown there are trends in ocean salinity consistent with surface warming, an amplification of the hydrological cycle, and model-estimated evaporation and precipitation fields (Boyer et al., 2005; Hosoda et al., 2009; Durack and Wijffels, 2010; Helm et al., 2010; Durack et al., 2012). For example, using a finger-print-based detection and attribution analysis of the CMIP5 models, Pierce et al. (2012) found that recent upper ocean salinity changes are inconsistent with the effects of natural climate variability while it is rather consistent with changes expected due to human forcing of the climate system. The linear trend of SSS in the subtropical North Atlantic has been linked to the recent amplification of hydrological cycle (e.g. Held et al., 2006) and the global warming effect on the Earth's freshwater cycle (e.g. Durack and Wijffels, 2010).

For these reasons, large scale variations of the salinity at decadal timescales are particularly scru-

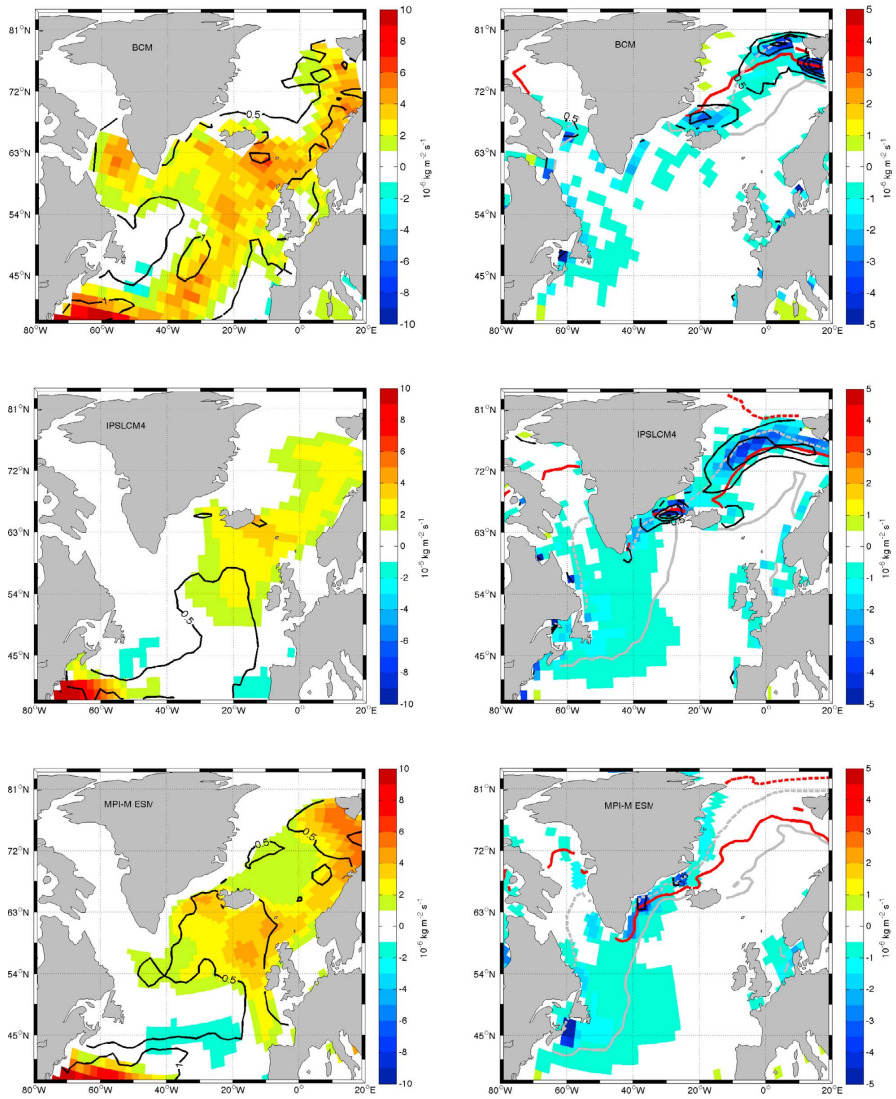

Figure 3.7: (left) Mean thermal (FT) and (right) haline (FS) contribution to the density flux into the ocean over 500 years for the three climate models (names indicated on the figures), given in $10^6 kg.m^{-2}.s^{-1}$. *Positive values indicate densification. Model names are indicated in the upper left corner of the figures. Note the different scales on the color bars between FT and FS, and that ice melting/freezing is not taken into account in the FS for MPI-M ESM. One standard deviation of the interannual variability of FT and FS are shown by black contours with intervals of 0.5. The red solid (dashed) lines indicate maximum (minimum) sea ice extent in September. The lines are drawn where the sea ice percentage is zero. Likewise for the gray lines, but for March. See* ***Langehaug et al. (2012)*** *for details.*

tinised. During the first half of the twentieth century, a large-scale decline of salinity in the high latitude North Atlantic Ocean was observed (Dickson et al., 1988, 2002; Curry et al., 2003; Curry and Mauritzen, 2005; Peterson et al., 2006)). Yet, from the 1990s onward, these tendencies tended to reverse Hakkinen and Rhines (2004); Yashayaev (2007). A difficulty in identifying long-term signals using only data from the last few decades is that trends are aliased by large-scale modes of decadal and multi-decadal variability (Stott et al., 2008; Terray et al., 2012; Skliris et al., 2014).

Secondly, sea surface salinity anomalies can play an active role on the oceanic circulation as they persist longer and may thus potentially be transported by the oceanic circulation, and in turn influence it. In the Bergen climate model, such mechanism has been shown to explain an influence of the tropical Pacific on the AMOC with a time lag of about 40 yr, via the anomalous precipitation in the tropical Atlantic associated with ENSO events **(Mignot and Frankignoul, 2005)**. In most coupled models, decadal to multi-decadal AMOC fluctuations indeed involve salinity changes in the regions of dense water formation (see section 3.2.2). In these simulations, salinity exerts a direct influence on ocean circulation: positive salinity anomalies increase density in subpolar gyre interior, intensify deep convection, and enhance the AMOC (while negative salinity anomalies exert analogous anomalies of opposite sign). Models nevertheless differ in how these salinity anomalies are built (see e.g. Menary et al., 2015, for a review), and the effective link between salinity and the oceanic circulation has been suggested to depend on timescales (Deshayes et al., 2014). I describe below my view of AMOC variability (section 3.2) and the sensitivity of the AMOC to externally-induced anomalous freshwater fluxes will be discussed in section 4.2.

3.2 Ocean circulation variability in the subpolar North Atlantic

3.2.1 The atmospheric dynamical forcing

Through its influence on the deep convection, the atmosphere in general, and the NAO in particular may induce AMOC variability at inter annual to decadal timescales, as shown in coupled (Timmermann et al., 1998; Delworth and Greatbatch, 2000; Eden and Willebrand, 2001; Born and Mignot, 2012) and forced models (Gulev et al., 2003; Böning et al., 2006). These modes of variability will be discussed further down. Firstly, let's discuss the direct effect of the atmosphere variability on the AMOC through wind forcing and thus momentum input into the ocean. Fig. 3.8 (left) illustrates for example that the monthly AMOC anomaly that covaries with the NAO is very significant and is essentially due to Ekman pumping. During a positive NAO phase, the Ekman pumping is anomalously negative between 32° and 55°N as a consequence of the convergence of the Ekman currents due to the intensification of the westerlies and the trade winds, and anomalously positive elsewhere. The horizontal circulation is maximum at the surface and almost constant beneath the mixed layer, suggesting a barotropic response to the wind forcing, as in Eden and Willebrand (2001). The barotropic response persists little, about 1 month at extratropical latitudes and up to 4 months in the subtropics, with a weak southward propagation (not shown). When the AMOC follows the NAO by 1 yr (middle), the AMOC response is composed of two cells that are almost opposite to the ones in phase. A large positive cell that is weak at the surface and maximum between 1000 and 2000 m is centered at 50°N

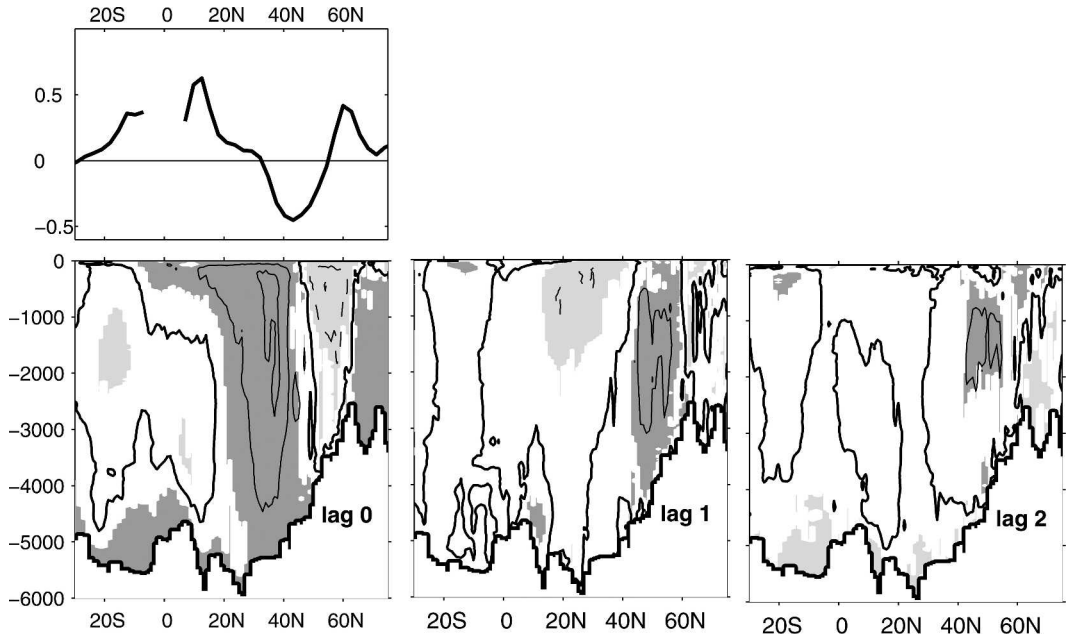

Figure 3.8: (top left) In-phase regression of the zonal mean Ekman pumping anomalies on the normalised time series of annual NAO anomalies in a control simulation of the Bergen Climate Model ***(Mignot and Frankignoul, 2005)****. Note that the Ekman pumping is not defined near the equator. (bottom left) Same for the AMOC annual anomalies. The contour interval is 0.2 Sv. Light (dark) shaded areas are negative (positive) and significant at the 10% level. (bottom middle and left) Same with a lag (in years), the NAO leads for positive lags.*

and persists up to lag 3. A weak negative cell is located farther south around 20°N, with a maximum near 500m, but significance is lost by lag 2. This pattern resembles the baroclinic response to the NAO winds found by Eden and Willebrand (2001), except that it only appears after 3 yr in their model. Note that the associated horizontal currents (not shown) resemble the gyre variability discussed by (Curry and McCartney, 2001; Marshall et al., 2001). No significant signal is found when the AMOC leads.

Similar AMOC adjustment is expected after any pattern of overlying atmosphere variability, simply through an imprint of momentum into the system. We have for example also investigated the links between the atmospheric southern annular mode (SAM), the Southern Ocean, and the Atlantic meridional overturning circulation (AMOC) at interannual to multidecadal time scales in a 500-yr control integration of the IPSL-CM4 climate model **(Marini et al., 2011)**. In phase with a positive SAM, the global meridional overturning circulation is modified in the Southern Hemisphere, reflecting again the local forced barotropic response. Yet, this fast-developing anomalous circulation is significant but not relevant in terms of anomalous heat transport and long-term climatic effects. Decadal modes of variability, where the ocean integrates the stochastic atmospheric forcing, are more relevant for climatic studies and one aspect will be described below (section 3.2.4).

3.2.2 AMOC and deep convection

The deep and bottom water masses in the North Atlantic are mainly formed in the Greenland-Iceland-Norwegian (GIN) Sea, the Labrador Sea, and the Irminger Sea: deep convection in the northern North Atlantic has been observed in the center of the Labrador Sea (Clarke and Gascard, 1983; Pickart et al., 2002), in the Irminger Sea (Bacon et al., 2003; Pickart et al., 2003b) and in the Nordic Seas (Schott et al., 1993). In the IPSL family models, with which I worked quite intensively, the cold model bias leads to an excess of sea ice cover in the Labrador Sea in winter and thus a lack of deep convection there **(Marti et al., 2010; Dufresne et al., 2013)**. This has often been attributed to a low resolution of the oceanic model. Yet, in the Bergen Climate Model which I used earlier on **(Mignot and Frankignoul, 2004)**, deep convection in the Labrador Sea does occur in spite of a nominal resolution of 2.4° (Furevik et al., 2003), very similar to what is used in IPSLCM4 and IPSLCM5 model versions. Furthermore, forced versions of the NEMO ocean model using the same horizontal resolution as in the two coupled model do show a realistic distribution of maximum mixed layer depth (Griffies et al., 2009). In the IPSLCM4 model, this bias has been attributed to a cold and fresh bias in the North Atlantic, due to an excess of precipitation on evaporation over the North Atlantic (Swingedouw et al., 2006) and a poleward shift of the atmospheric jet streams **(Marti et al., 2010)**.

The relative influence of sea surface temperature and salinity on the sea surface density anomalies in the deep convection areas in also subject to large uncertainties. Several models, in particular the IPSL family, show that anomalous mixing is triggered by sea surface salinity anomalies **(e.g. Escudier et al., 2013)**. Yet, temperature generally dominates when density is averaged over the whole convection site or the subpolar gyre **(Born and Mignot, 2012)**. Furthermore, the impact of salinity is likely to be timescale dependent (Deshayes et al., 2013).

In all climate simulations, deep convection is in fine primarily forced by atmospheric patterns that induce anomalous cooling and salting over the area. The impact of the North Atlantic Oscillation on deep convection is illustrated in Fig. 3.9 for the Bergen Climate model. It shows that in this model, a positive phase of the NAO enhances deep convection in the Labrador Sea but it reduces it in the GIN Seas and vice versa, consistently with observations (Dickson et al., 1996). Deep convection in the Irminger Sea might also occur during positive NAO phases in the observations (Pickart et al., 2003a) but in it is to the case in this model, presumably because of the limited spatial resolution. In IPSL-CM4, Msadek and Frankignoul (2008) have shown that it is rather changes in the East Atlantic Pattern (EAP), the second mode of atmospheric variability in the North Atlantic region, which induce anomalous advection of salinity due to changes in the subpolar gyre south of Iceland. The North Atlantic Oscillation is the dominant mode, but it plays a secondary role on deep convection fluctuations. In IPSL-CM5A-LR, the NAO is also not the primary driver of deep convection anomalies, which are rather forced by anomalous northerly winds along the eastern coast of Greenland **(Escudier et al., 2013)**.

In climate models, the maximum value of the AMOC and its interannual variations is generally closely related to deep convection (HadCM3 Hawkins and Sutton (2007), CCSM3 Danabasoglu (2008); Kwon and Frankignoul (2014), GFDL-CM2.1 Zhang et al. (2011), ECHO-G **Ortega et al. (2011b)**, IPSL-CM5A-LR **Escudier et al. (2013)**, CNRM-CM5 (Thomas et al., 2015)). An acceleration of the

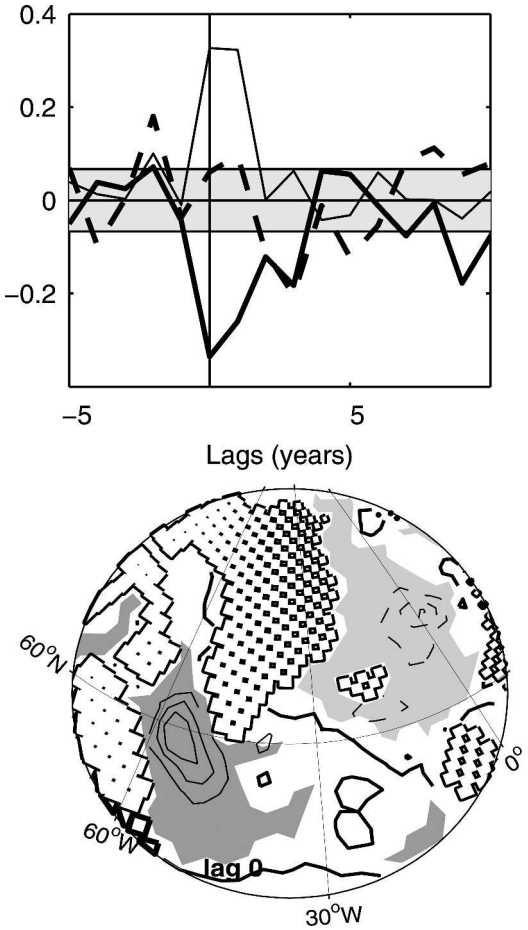

Figure 3.9: (top) Cross correlation between the annual NAO time series and the mixed layer depth averaged over the areas of deep convection during the winter season (Jan-Apr) in the Bergen Climate Model. The NAO leads at positive lags. The thin line refers to the Labrador Sea, the dashed line to the Irminger Sea, and the thick line to the GIN Seas. The gray area limits the 10% significant domain. (bottom) Regression of the annual mixed layer depth on the normalised annual NAO time series. The contour interval is 10 m. The thick contour denotes zero. Light (dark) shaded areas are negative (positive) and significant at the 10% level. From ***Mignot and Frankignoul (2005)****.*

AMOC roughly 2 to 10 years after the intensification in deep convection is usually detected in climate models. Fig. 3.10 illustrates that roughly 6 years before a basin-scale AMOC intensification, anomalies associated to enhanced deep convection at seen in the northern North Atlantic. In the following years, the latter expands and indeed covers the whole North Atlantic basin at lag 0. Later, the anomalous intensification weakens and vanishes towards de southern hemisphere. This timescale depends again on climate models: a delay of 2-3 years have been reported by Eden and Willebrand (2001) in a forced ocean general circulation model, 3-5 years by Msadek and Frankignoul (2008) in IPSL-CM4-v2 and Danabasoglu (2008); Kwon and Frankignoul (2012) in the CCSM3 climate model, 9 years by Escudier et al. (2013) in IPSL-CM5A-LR and 12 years by Jungclaus et al. (2005) in the ECHAM5-MPIOM. The time lag between convection in the North Atlantic and the AMOC down to 35°N has been explained by advection of density anomalies by the deep western boundary currents or in the interior in a few

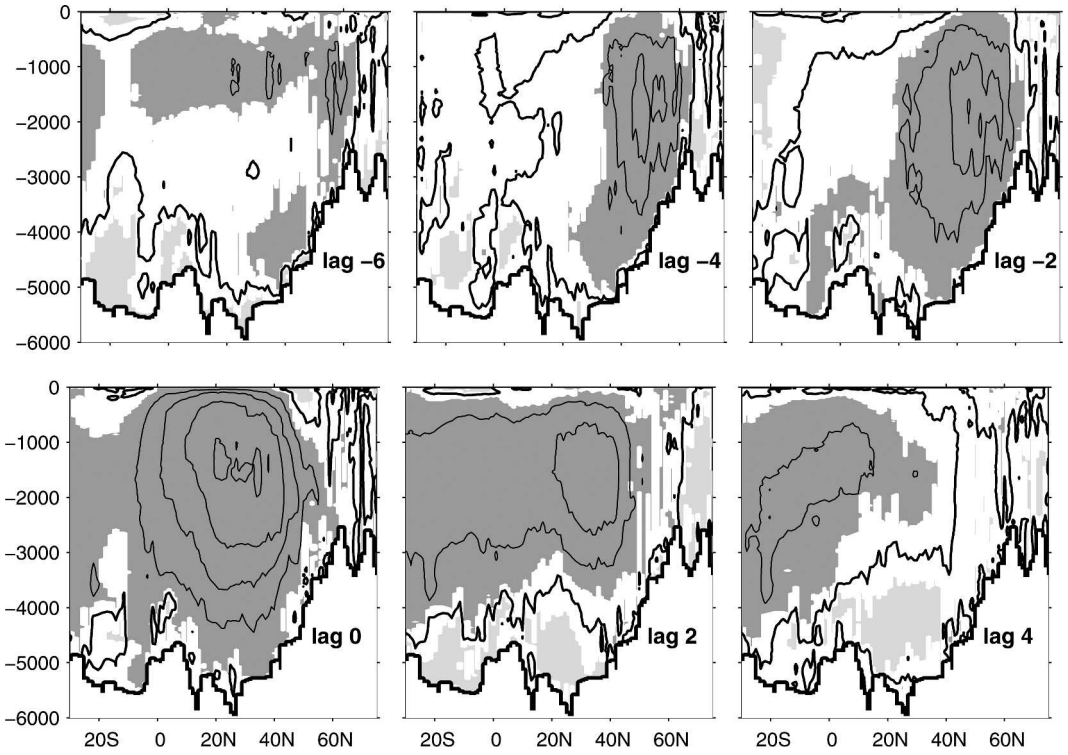

Figure 3.10: Regression of the AMOC on the time evolution of its maximum in the Bergen Climate Model. AMOC leads at negative lags (in years). The contour interval is 0.2 Sv, continuous for positive and dashed for negative values. The thick contour denotes zero. Light (dark) shaded areas are negative (positive) and significant at the 10% level. Figure from ***Mignot and Frankignoul (2005)****.*

years (Zhang, 2010). Further south, the AMOC adjustment is thought to be achieved through Kelvin and Rossby waves generation.

The direct link of deep convection intensity and the AMOC strength is yet debated in observations (Koltermann et al., 1999; Straneo, 2006; Pickart and Spall, 2007). Mauritzen and Hakkinen (1999); Straneo (2006) indeed emphasised that the rate of dense water formation and the AMOC are not linearly related because of the distinction between diapycnal and vertical mass flux, and the role of the boundary currents. Idealised studies furthermore emphasise the role of eddies to link the small scale convective plumes to the larger scale export of water masses at depth (e.g. Deshayes et al., 2009). On the other hand, measurements by Rhein et al. (2015) suggest a continuous advection Labrador Sea Water towards the Southern Hemisphere by the Deep Western Boundary Current. Robson et al. (2014) exploit the link found in a climate model between the AMOC and convection in the Labrador Sea to infer predictions of the AMOC in the coming years. Bower et al. (2009) suggest that most of the subtropical exchange in the North Atlantic occurs along interior pathways and Dengler et al. (2004) suggest that the DWBC breaks up into eddies at 11¡S. . One of the main limitation of climate models lies in their coarse resolution. Mesoscale eddies and boundary processes have indeed been shown to be important for AMOC, and in particular in deep convection areas (Chanut et al., 2008; Fox-Kemper et al., 2008). At this resolution, many oceanic processes, such as the effect of mesoscale eddies and boundary layer processes are not explicitly resolved (see Griffies et al., 2009, for a review). Several studies show that

the representation of the oceanic circulation in models is improved with the resolution (Tréguier et al., 2005; Spence et al., 2012; Talandier et al., 2014), with important consequences for AMOC variability and impacts on climate (Hodson and Sutton, 2012; Delworth and Zeng, 2012; Kirtman et al., 2012). In the coming years improved computing efficiency and improved computer will allow eddy permitting if not eddy resolving ocean models incorporated in coupled climate models. Evaluating the robustness of the previous results in these new generation of climate models will definitely challenge our current understanding of the AMOC variability and link with deep convection.

3.2.3 The subpolar gyre

Another mathematical view of the circulation in the North Atlantic consists in averaging the circulation vertically rather than zonally, leading to a description of the barotropic circulation. In this view, the extra-equatorial North Atlantic is characterised by a double gyre circulation: an anticyclonic gyre at the subtropical latitudes and a cyclonic gyre at sub polar latitudes. The role of the former in the northward pathway of water masses in the Atlantic has been discussed in section 3.1.3. The subpolar gyre (SPG) was found, in climate models, to redistribute freshwater anomalies in the North Atlantic and Nordic Seas (Hátún et al., 2005; Wu and Wood, 2008) and to advect salinity anomalies into the Labrador Sea convection region (Delworth et al., 1993). As for the AMOC, the SPG shows enhanced inter annual to multidecadal variability. In climate models though, it is in general associated with decadal variability, while multidecadal variability rather involves cross-hemispheric anomalous transports: see Yoshimori et al. (2009) for an early review and Menary et al. (2015) for a more recent one. Its intensity is also closely linked to deep water formation, as illustrated in Fig. 3.11 in the IPSL-CM4 climate model: enhanced deep convection in the gyre's center leads to a stronger cyclonic circulation. This picture pleads for an importance of the density structure on the gyre transport, as emphasised in many studies (Mellor et al., 1982; Greatbatch et al., 1991; Myers et al., 1996; Penduff et al., 2000; Eden and Jung, 2001). Levermann and Born (2007) have proposed a conceptual analysis of the buoyancy driven gyre circulation in terms of a combination of positive and negative feedback mechanisms. First, a stronger SPG transports more saline subtropical water into the subpolar North Atlantic (salt feedback). This increases the density gradient between the center and the relatively light exterior of the gyre. Sea surface elevation drops through pressure adjustments in the water column and the geostrophic response strengthens the gyre. Secondly, isopycnal mixing is intensified owing to the enhanced isopycnal outcropping associated to a stronger SPG. This results in a cooling of the SPG center, thereby an increase of its density and therewith of its strength (temperature feedback). These feedback mechanisms were shown to be at play in the IPSL-CM4 climate model **(Born and Mignot, 2012)**.

Yet, both observational and model studies also suggest that surface wind stress has a strong influence on the SPG strength and variability (Curry et al., 1998; Böning et al., 2006; Häkkinen et al., 2011; Moffa-Sanchez et al., 2014). This mechanism has gained credit in the years 2000s, when several studies have linked the strong warming of the North Atlantic SPG observed in the mid-1990s to the NAO abrupt short between 1995 and 1996 (Bersch, 2002; Flatau et al., 2003; Hakkinen and Rhines, 2004; Bersch et al., 2007; Lozier et al., 2008; Sarafanov et al., 2008). As discussed above, the direct

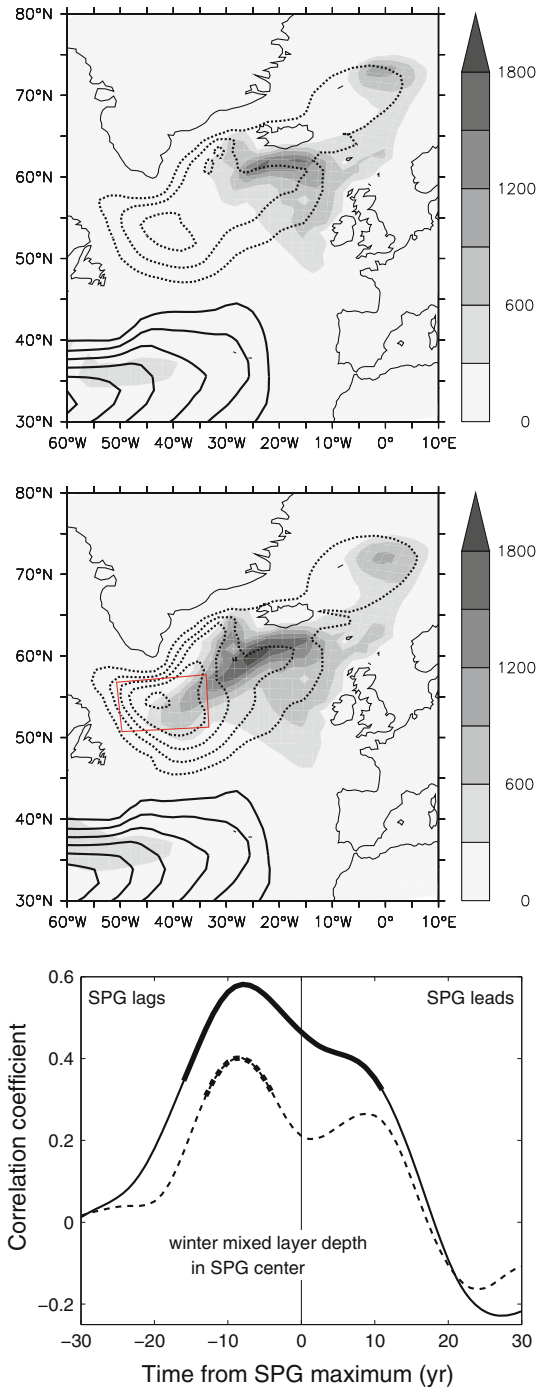

Figure 3.11: (Upper) Composite of the depth-integrated streamfunction for anomalies of the SPG intensity weaker than 1.5 standard deviations (contours, spacing 5 Sv, negative dashed) and composite mixed layer depth leading by 8 years (shading, in m), from a control simulation of the IPSL-CM4 climate model ***(Born and Mignot, 2012)****. Middle As before but for anomalies of the SPG intensity stronger than 1.5 standard deviations. Red box shows SPG center region used subsequently. Lower Correlation of winter mixed layer depth in the SPG center (red box) with the normalised anomalies of the SPG intensity, 15-year (solid) and 5-year running averages (dashed). Correlations significant at the 95% level are shown as bold lines.*

impact of the NAO on surface temperature and salinity has been confirmed from direct measurements (Reverdin, 2010) and simulations (Herbaut and Houssais, 2009). Häkkinen (2001) rather call for the role of the second leading mode of atmospheric variability in the region, namely the East Atlantic Pattern. Indeed, they suggest that the wind-stress curl anomalies associated to this model projects best on the mean position of the gyres and these are more likely to modulate the strength of the horizontal circulation. Eden and Jung (2001) attempts to reconcile the role of wind forcing and buoyancy forcing by suggesting that the wind forcing is the dominant player for the suppler gyre variability at inter annual timescales while buoyancy may be more important at decadal timescales. Another view to advance on the current understanding of the sub polar gyre variability is to consider separately the western and eastern sub polar regions. Such a decomposition is motivated that deep connection occurs only in the western suppler gyre (Labrador and Irminger Seas) while the Reykjanes Ridge constitutes an important breaking point in terms of water masses in the region (Thierry et al., 2008). Using such decomposition, Barrier et al. (2015) found an important role for oceanic convergence of heat to explain temperature anomalies in the western part, and a more direct role of the atmospheric wind in the east. This result has important implications in terms of predictability.

Although AMOC and the sub polar gyre (SPG) are two complementary views of the oceanic circulation in the North Atlantic, and variations on the SPG are tightly linked with changes in the deep overturning circulation, their interplay has often been overlooked in the literature.The SPG modulates inter hemispheric heat transport, it even dominates the meridional heat transport at subpolar latitudes (Rhein et al., 2011). It also determines the amount of heat advected into the Nordic Seas and eventually in the Arctic ocean (Holliday et al., 2008), with consequences for the sea ice cover (Lehner et al., 2013). Further south, the SPG was also found to influence the frequency of Atlantic hurricanes as well as their predictability with a lead time of several years (Dunstone et al., 2011). As for the AMOC, this large scale circulation pattern is difficult to measure. Its total volume transport is estimated around 37-42 Sv (Bacon, 1997; Read, 2001; Fischer et al., 2004, 2010; Xu et al., 2013). Some reconstructions of its variability are based on satellite altimetry (Hakkinen and Rhines, 2004) or combinations of satellite data and interpolated tide gauge measurements (Hamlington et al., 2011). Yet, most studies investigating its variability and link to climate are thus based on numerical models, in spite difficulties to represent it even at high resolution (Tréguier et al., 2005). Recent advances at $1/12°$ suggest an important role of oceanic mesoscale eddies (Marzocchi et al., 2015). Ocean reanalysis, combining model forced with (subsets of) similar observational data sets and hydrographic (sometimes also satellite) oceanic data propose reconstructions but the absolute circulation strength and its standard deviation differ considerably between datasets (Fig. 3.12). A coherent picture is partly recovered by a simple conceptual model solely forced by reanalysed surface air temperatures **(Born et al., 2015)**. This confirms that surface heat flux indeed plays a leading role for this type of variability, as has been suggested in previous studies. The results further suggest that large variations in the SPG correspond to the crossing of a bifurcation point that is predicted from idealised experiments and an analytical solution of the model used herein.

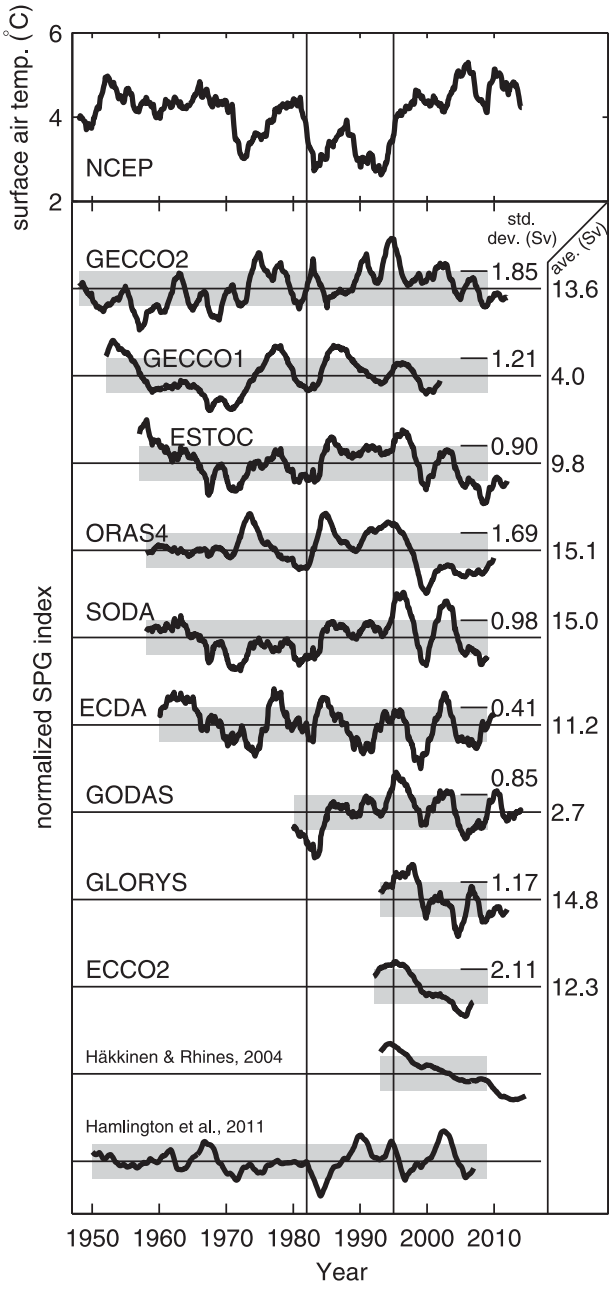

Figure 3.12: Western subpolar gyre intensity for a range of reanalysis products and two indices based on sea surface height, normalised to a standard deviation of one. (top) The NCEP air temperature used to force the box model. All curves have been deseasonalised and smoothed with a 2-yr running average. Average circulation strength and one standard deviation are shown on the right side where appropriate. Vertical lines mark the beginning of years 1982 and 1995. From ***Born et al. (2015)***

3.2.4 A 20-yr mode of variability in the northern North Atlantic?

As already discussed, the AMOC is known to have strong variability at decadal to multidecadal timescales, and to represent an important component of the climate system variability at these timescales through its role in redistributing the heat received from the Sun at the surface of the globe The CMIP3 and CMIP5 multi-models show the most energetic variability on the multidecadal timescale band, both with respect to the AMO and AMOC, but with a large model spread in both amplitude and frequency (**Ba et al. 2014** Zhang and Wang 2013; Cheng et al. 2013). Understanding the preferential timescales of variability in the North Atlantic, usually associated with the Atlantic meridional overturning circulation (AMOC), is yet essential for the prospects for decadal prediction. However, the wide variety of mechanisms proposed from the analysis of climate simulations, potentially dependent on the models themselves, has stimulated the debate of which processes take place in reality. As indicated above, the most general view for AMOC variability relates to deep convection, and variability is thus in this case associated to some advection mechanism to bring anomalies in the area of convection.

Evidence for 20 yr variability in subpolar North Atlantic arises from several sources of observations (Divine and Dick, 2006; Frankcombe et al., 2010; Sicre et al., 2008; Chylek et al., 2011). Several climate models also exhibit this timescale, as reviewed by Menary et al. (2015), while some studies suggest that the climate models underestimate the spectral peak in the 70-80yrs range and overestimate the ones in the 10-20 year range (Ruiz-Barradas et al., 2013). The 20-year timescale describes variability generally confined to the subpolar gyre, with feedbacks to other regions in the Arctic and/or subtropical North Atlantic usually involving longer timescales (Jungclaus et al., 2005; Vellinga and Wu, 2004; Menary et al., 2011). Yet, these mechanisms are strongly model-dependent and difficult to reconcile. One common aspect identified in several models is the modulation of the AMOC and North Atlantic Current strength by changes in upper ocean density anomalies at the western margin of the basin, an important region for the thermal wind relation (Tulloch and Marshall, 2012). The source region of these anomalies can however vary from one model to another, depending, for example, on the location of the main regions of convection. Bi-decadal variability is also found in idealised oceanic configurations forced by constant surface fluxes, suggesting that this timescale may arise from spontaneous oscillatory behaviour in the ocean (Huck et al., 1999; Arzel et al., 2007). The diversity of bi-decadal variability mechanisms in the subpolar North Atlantic in different climate models is well illustrated by simply looking at the different generations of the IPSL climate models. 20-year variability was identified in two generations of the IPSL climate model:

In IPSL-CM4 (144 x 96 horizontal atmospheric grid points with 19 vertical levels, coupled to the NEMO ocean module on the ORCA2 grid, see **Dufresne et al. (2013)** for details), the subpolar gyre shows irregular oscillations of decadal time scale with most spectral power between 15 and 20 years. **Born et al. (2012)** found that positive and negative feedback mechanisms act successively on the circulation leading to an internal oscillation. This involves periodically enhanced deep convection in the subpolar gyre center and intermittently enhanced air-sea thermal coupling. As a result, anomalies of the large-scale atmospheric circulation can be transferred to the ocean on its intrinsic time scale, exciting the oscillator stochastically. In this case, the SPG plays an active role, responds to atmospheric stochastic forcing at a timescale set by thermal and haline feedbacks as in Levermann

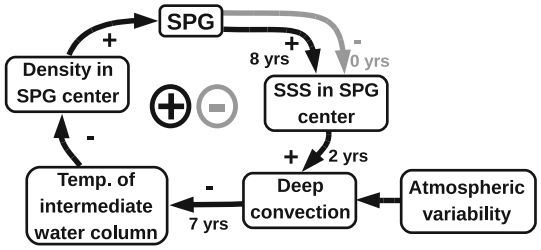

Figure 3.13: Summary of the mechanisms controlling the oscillation cycle in the IPSL-CM4 control simulation, as found in ***Born et al. (2012)****. A primary feedback loop strengthens the SPG through the advection of sea surface salinity (SSS) anomalies, deep convection and cooling of the intermediate water column. However, salt advection is delayed and the immediate result of stronger advection is the removal of salt from the key region. This causes the end of the present cycle in a secondary, negative feedback loop. Thus, advection both ends the present oscillation cycle through the removal of surface salt and initialises the next cycle by renewed positive transport with a delay. Atmospheric variability is transmitted to the ocean preferentially during times of increased convection. Thus, the ocean oscillator determines the time scale of air-sea interaction.*

and Born (2007). The mechanisms controlling the oscillation cycle in this case are summarised in Fig. 3.13. Interestingly, Msadek and Frankignoul (2008) did not find such a significant 20-year cycle in this version of the model with a lower atmospheric resolution (96 x 71 grid points, with 19 vertical levels). More fundamentally, Msadek and Frankignoul (2008) reported much less variability in the subpolar area and focused on the AMOC variability. One major difference between their model version and the subsequent ones is that in the earliest model version with coarsest atmospheric resolution, only two deep convection regions could be defined, one in the Nordic Seas and one in the Irminger basin south of Iceland. In the model versions studied by **Born et al. (2012)**, strong variability of convection is found in an additional region located further west, in the center of the SPG, at the entrance of the Labrador Sea. We speculate that this explains partly the different variability found in the different versions of the model.

In the most recent version of the model (IPSL-CM5A-LR), the largest deep convection region is also located south of Greenland, at then entrance of (but not in) the Labrador Sea. Variability at 20-year timescale is particularly energetic in this configuration, as evidenced by **Escudier et al. (2013)**, with important climatic consequences (Fig. 3.14). Figure 3.15 shows a simplified schematic of the mechanism responsible for one half of this cycle. For example, starting from a positive temperature and salinity anomaly in the Labrador Sea, the surface mean currents along the subpolar gyre advect these anomalies of same sign east- ward. The anomalous salty surface waters favour deep convection south of Greenland and Iceland along their path, thereby inducing an AMOC intensification after 9 years, and they eventually reach the Nordic Seas. There, the associated positive temperature anomaly associated with the salinity anomaly induces sea ice melting and an anomalous cyclonic circulation over the Nordic Seas, which strengthens the East Greenland Current (EGC), and in turn creates negative temperature and salinity anomalies in the Labrador Sea. This process lasts 10 years, and the second phase of the cycle begins. In this mechanism, the SPG was not found to play an active role, except for transporting temperature and salinity anomalies. Air-sea coupling is also fundamental for

this mechanism.

Several authors have suggested that the 20-year variability arises from the ocean only, either due to the interaction between the Gulf StreamÐNorth Atlantic Current and the equatorward deep return flow (Kwon and Frankignoul, 2014), or to large scale baroclinic instability in the ocean and westward propagation of the subsurface temperature anomalies across the North Atlantic basin, referred as subsurface basin mode (e.g. Colin de Verdière and Huck, 1999; Huck et al., 1999; te Raa and Dijkstra, 2002)), and in particular 20 years in the linearised version of OPA (Sévellec and Fedorov, 2013).This mode is related to the westward propagation of subsurface temperature anomalies across the North Atlantic basin and its timescale seems to be intrinsically related with the zonal size of the basin (Sévellec and Huck, 2015). Its link with the AMOC is explained by a thermal-wind driven interplay between the zonal and meridional overturning circulations (te Raa and Dijkstra, 2002). This mechanism is also referred to as "thermal Rossby mode", because temperature anomalies propagate westwards across the mean temperature gradient, in the same way that Rossby waves do across the background potential vorticity gradient field. There exist evidence of a similar westward propagation in North Atlantic observations of sea-level height (Tulloch et al., 2009; Vianna and Menezes, 2013, e.g.), subsurface (Frankcombe et al., 2008), and sea surface temperature (Feng and Dijkstra, 2014), with comparable basin-crossing times as for the subsurface basin mode. It has only been detected in more comprehensive models (Frankcombe et al., 2008, 2009). Despite this consistency between observations, modelling and theory, it is still under debate whether this interdecadal AMOC variability is excited by the atmosphere or maintained by pure ocean dynamics. Whereas Colin de Verdière and Huck (1999) and Sévellec and Huck (2015) suggest that it can be internally forced by large-scale baroclinic instabilities, (Sévellec et al., 2009) advocate for the need of an external energy source, either a local wind forcing or a buoyancy exchange (e.g. heat or freshwater fluxes). Furthermore, the development of this mode in coupled models had not been described in coupled models except for the study of Tulloch and Marshall (2012) using both CCSM3 and GFDL climate Model version 2.1. A question that arise is also to understand whether this mode is compatible with the convection-driven AMOC mechanisms described above. Are both modes developing independently, and interact constructively or destructively over time? Otherwise, is one driving the other? Or are both coupled to each other?

In the IPSL-CM5A-LR climate model, the two modes have been shown to coexist, as illustrated in Fig. 3.16. In essence, the whole cycle develops as follows: upper ocean positive salinity anomalies are advected by the subpolar gyre from the Labrador Sea into the sinking regions south of Iceland (in 5 years), where they enhance deep convection and a negative thermal anomaly is formed from the surface down to 2000 m. This induces a geostrophic response, characterised by a cyclonic flow that propagates westwards in the subsurface as a result of its interaction with the mean meridional density gradient. As the anomalies reach the eastern Greenland coast 2 years after, the associated cyclonic flow leads at the surface to an intensification of the EGC. This effect on the EGC comes on top of the weak feedback mechanism with sea ice and SLP anomalies in the Nordic Seas already described in **Escudier et al. (2013)**, and contributes to synchronise the two multidecadal modes. At depth, density anomalies continue their westward propagation until they reach the Canadian coast 6 years after, propagating southward along the western boundary current, and establishing a strong zonal gradient that triggers a northward thermal wind response, thus strengthen- ing the AMOC. Phase reversal in the upper

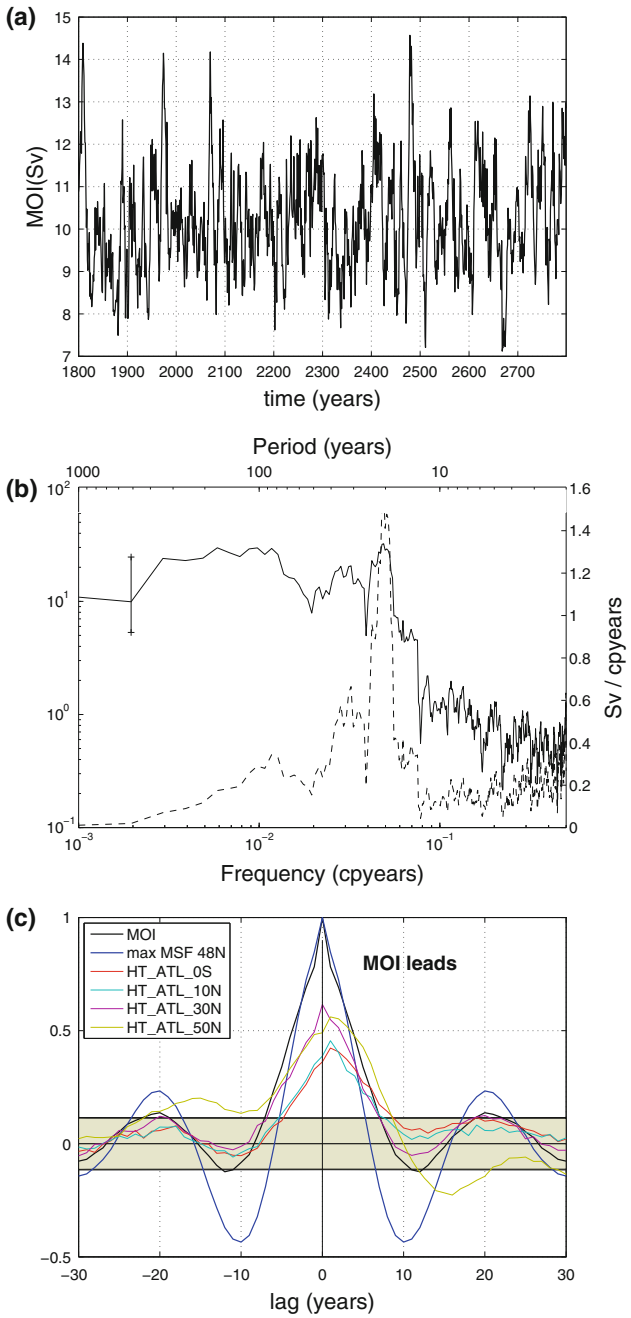

Figure 3.14: a Time evolution of the intensity of the AMOC (defined as the maximum of the meridional stream function over the North Atlantic, named meridional overturning index MOI) in the control simulation of the IPSL-CM5A-LR climate model. b Spectrum of MOI, in log-log units (solid line) and in log-linear units (variance preserving spectrum: dashed line). The spectrum was calculated by the multi-taper method using four tapers. The vertical line indicates the 95 % confidence interval. c Autocorrelation of MOI (thick black), the maximum of meridional stream function at 48°N (thick blue) and cross correlations of the MOI with the poleward oceanic heat transport taken at different latitudes (color lines). The grey shading indicates 95% confidence interval for zero correlation. This level can in fact vary for each correlation curve of the figure because of different effective numbers of degrees of freedom (Bretherton et al., 1999). Nevertheless, here, it is very similar for all the correlations shown in the figure. From ***Escudier et al. (2013)***

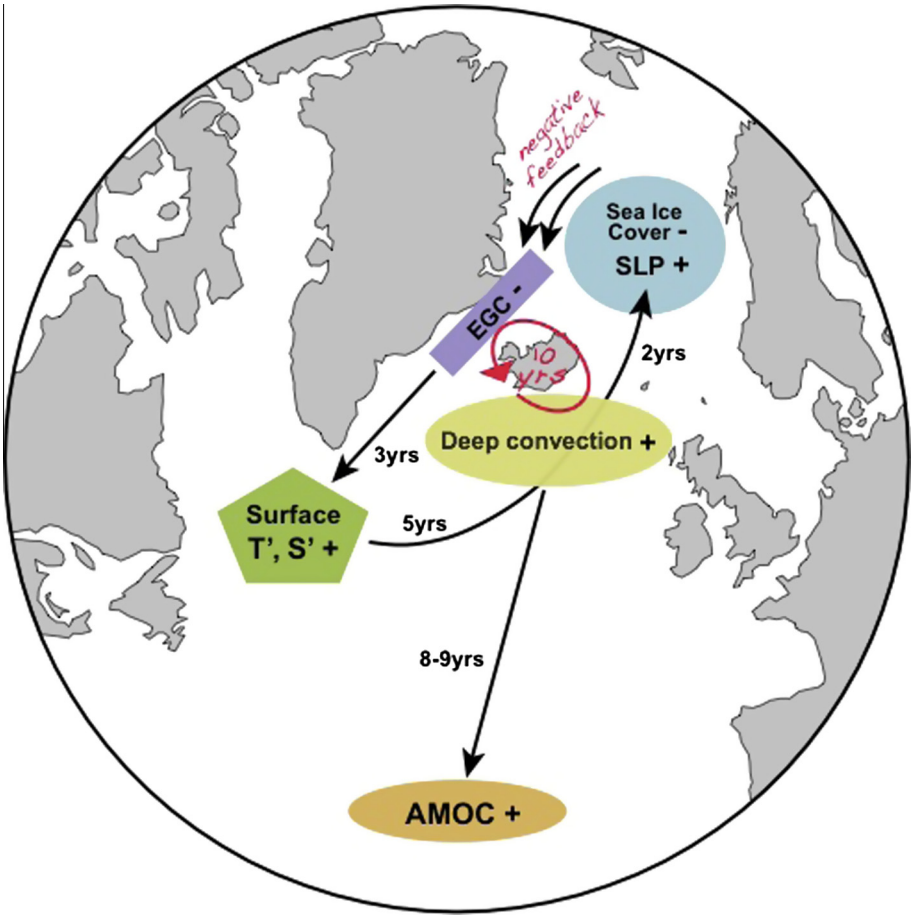

Figure 3.15: Schematic view of the mechanism identified in ***Escudier et al. (2013)*** *to explain the AMOC bi-decadal variability in the IPSL-CM5A-LR control climate simulation. We represent the North Atlantic basin and show the appearance of temperature and salinity anomalies in the Labrador Sea (T' and S' in the green pentagon). Estimated time lags are indicated all along their advection in the subpolar and Nordic Seas, affecting the convection sites along their path. In the Nordic Seas is represented the melting of sea ice and the anomalous low pressure system that modifies the wind stress. This in turn intensifies the EGC, leading to tracers anomalies of the opposite sign around 10 years after their inception. From* ***Escudier et al. (2013)****.*

ocean is related to the EGC, and its export of fresh waters from the Arctic into the subpolar gyre, building up large anomalies in the Labrador Sea 3 years after (10 years if we count from the beginning of the cycle). Accordingly, the phase reversal in the deeper ocean appears when these negative salinity anomalies reach the vicinity of Iceland 5 years later, and debilitate deep convection. Note that at this stage, surface waters over the region are gradually warming, in response to the increase in northward heat transport that follows the strengthened AMOC phase. This suggests that the AMOC plays a preconditioning role in the phase reversal of convection.

This whole mechanism is described in Fig. 3.17. In my view, the specific interplay between the surface **(Escudier et al., 2013)** and the subsurface **(Sévellec and Fedorov, 2013)** bi-decadal variability model found in IPSL-CM5A-LR **(Ortega et al., 2015)** explains the prominent bi-decadal variability in this model. And this interplay is partly due to the biased location of the subpolar con-

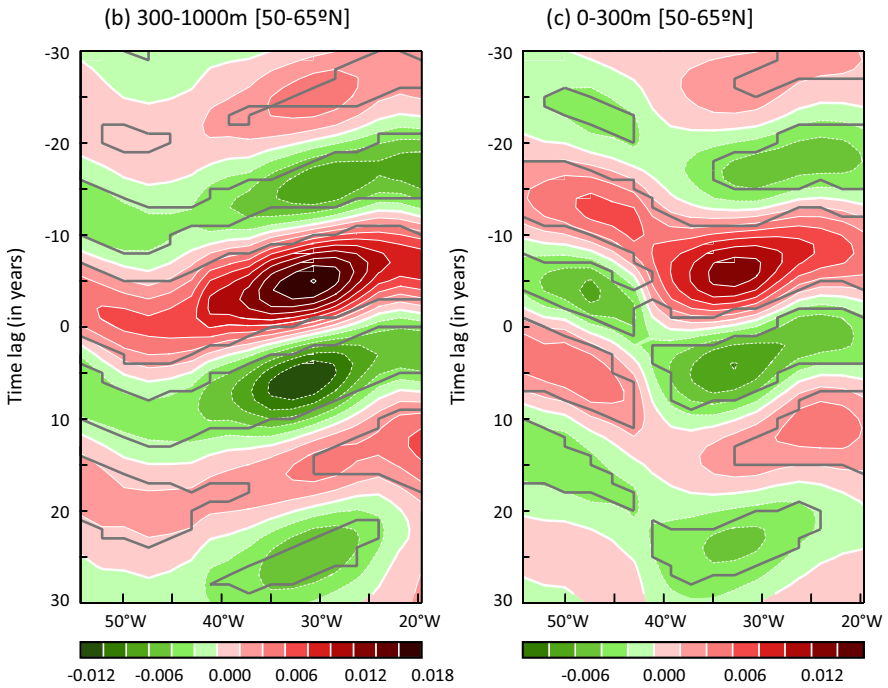

Figure 3.16: Hovmoeller plot (Time lag vs. Longitude) of the regression (in kg/m3) between the standardised MOI computed at 48°N and the meridionally averaged density anomalies at: (b) 300-1000m in 50-65°N and (c) 0-300m in 50-65°N in the IPSL-CM5A-LR climate model (From ***Ortega et al. 2015****). Significant values at the 95% confidence level are enclosed by the thick gray contours. This figure illustrates the eastward propagation of density anomalies in the upper layer, following the mechanism described in* ***Escudier et al. (2013)*** *and the westward propagate in the subsurface layer, following Sévellec and Huck (e.g. 2015). .*

vection sites: the most active subpolar convection site is located south of Iceland rather than in the Labrador Sea, so that it can interact constructively with the subsurface mechanism as described above (Fig. 3.17). This study is thus a promising step towards the reconciliation of the various mechanisms of decadal variability which have been proposed in independent studies, but the question of the maintenance of the internal oceanic mode in more realistic conditions thus remains partly open. In a version of the same model including higher atmospheric resolution (IPSL-CM5A-MR 144x142 horizontal grid points, 19 vertical levels), the second AMOC EOF has maximum amplitude between 45 and 50°N, and a dominant timescale of 20 years (Wen et al., 2015). Correspondingly, the NAO has a small, but significant 20 years variability, suggesting that it responds to the AMOC.The air-sea coupling in the MR model thus may enhance the low frequency variability of AMOC, but it did not appear to play a substantial role to generate it. Similar interplay between the upper ocean advection and westward propagation Rossby wave at depth was found in this model, possibly contributing to the generation of the 20-year variability of AMOC. However, the specific mechanism is different from that proposed for the LR model. Further studies are needed, while the importance of westward propagation of SST to generate decadal variability in the North Atlantic has recently been shown to be general in the CMIP5 database (Muir and Fedorov, 2016).

All mechanisms and analysis presented above are at least partly based on model simulations.

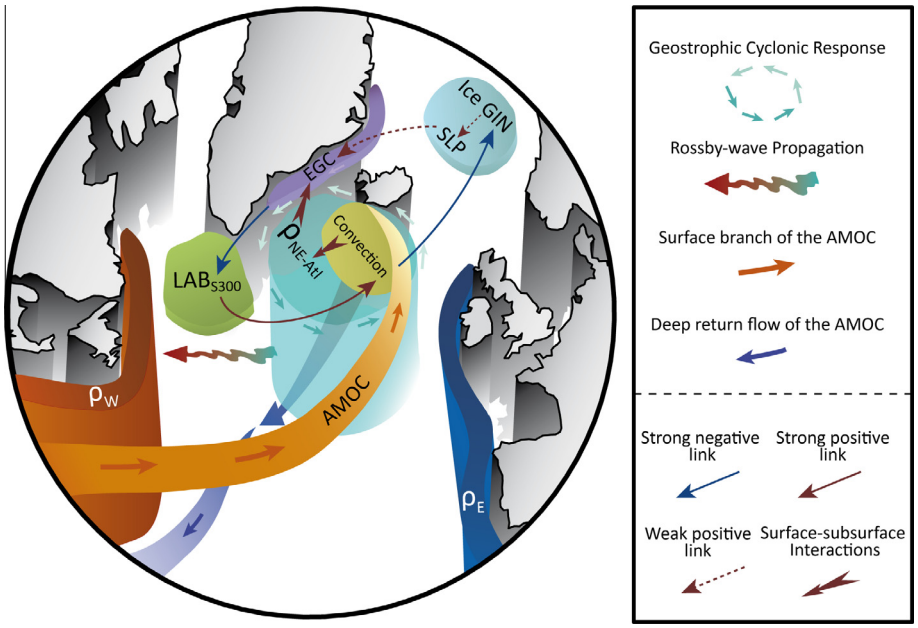

Figure 3.17: Schematic of the variables and interactions involved in the North Atlantic 20-year cycle in IPSL-CM5A-LR, from ***Ortega et al. (2015)****.*

Because of the scarcity of historical transoceanic measurements and despite the recent progress in the development of observational networks, only a few observation-based estimates of the MOC variability in the North Atlantic are indeed currently available. The RAPID array, presented above (section 2.3), is pioneering in this respect, and the now more than 10 years of data have highlighted significant interannual variability of the AMOC at 26.5°N (McCarthy et al., 2015). Nevertheless, studies indicating that the AMOC is not coherent between the subtropical and subpolar gyres on interannual timescales (Bingham et al., 2007) have led to proposals for array-based observing systems at other latitudes, including the subpolar North Atlantic (OSNAP), (Send et al., 2011) and the South Atlantic at 34°S (SAMOC) (Lozier, 2010). Additionally, several arrays in the western basin monitor the deep western boundary current (DWBC), including Line W off the coast of New England (Toole et al., 2011) and the MOVE array at 16°N (Kanzow et al., 2006). Repeated hydrographic sections at key locations of the sub polar North Atlantic also provide important information on the AMOC intensity and inter annual variations (Mercier et al., 2015). Maintenance of such long term observation systems is crucial for climate studies in order to build up long time series and backup model studies.

Chapter 4

The influence of external forcings

As explained in the introduction, climate variability results from internal variability as well as external factors. In the previous section, we have described several aspects of the internal variability at play in the North Atlantic. "External" factors are so-called as they are not explicitly represented in the classical view of the climate system. In climate models, typically, their effect is prescribed. External forcing impact the climate, as well as variability of the ocean circulation (e.g. Hofer et al., 2010). I give below an overview of my work related to an external forcing factor of natural origin (volcanic eruption, 4.1) and one of anthropic origin (freshwater, 4.2)

4.1 Volcanoes

Volcanic eruptions eject large amount of materials into the atmosphere. In particular, the sulphur dioxide gas released in the stratosphere leads to aerosol formation that reflects part of the incoming solar radiation, thus affecting the climate. The volcanic eruptions primarily impact the global radiative budget of the Earth, leading to a global temperature drop, as described in the introduction and first noticed by Lamb (1970). Although this direct effect of volcanic eruptions on the Earth has been known since long, estimating their impact on the climate system has recently gained attention with the debate on the origin of the hiatus. It has indeed been suggested that the slower warming observed since 1998 than previously observed could be at least partly attributed to the effect of relatively weak but cumulative recent volcanic eruptions (Santer et al., 2014). Furthermore, in spite of few recent studies suggesting a climate impact of high latitude volcanic eruptions (e.g. Pausata et al., 2015), climate models and their analysis classically concentrate on the tropical large explosive eruptions. Tropical eruptions are indeed selected because their impacts are thought to be global due to the rapid spread of the aerosol by the stratospheric tropical circulation.

My work so far has also focused only on the marge tropical eruptions. Relatively few studies have focused on their impact on the oceans. Among the few, we have shown in **Mignot et al. (2011)** that the thermal response of the ocean consists of a fast tropical cooling due to the radiative forcing by the volcanic eruptions, followed by a penetration of this cooling in the subtropical ocean interior one to five years after the eruption, and propagation of the anomalies toward the high latitudes (Fig. 4.1). This study was based on a simulation performed with the IPSL-CM4 model, including the external forcing

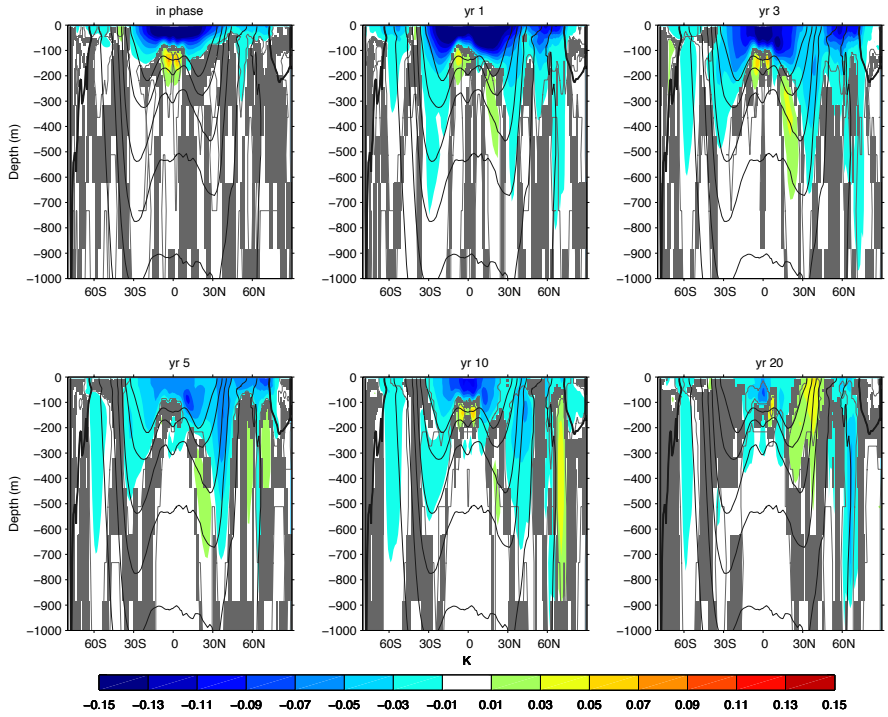

Figure 4.1: Composites of anomalous zonally averaged oceanic temperature response at different time lags (in years) after volcanic eruptions of more than $2.8 W.m^{-2}$ *radiative impact (AOD more than* 1.5*) in the IPSL-CM4 transient simulation of the last millennium* ***Mignot et al. (2011)****. Shaded areas are not significant at the 20 % level. Grey contours indicate anomalies significant at the 5 % level. Dark contours show the zonal mean global temperature (contour interval is 3° C).*

reconstructed from the last 1000 years (so-called last millennium). Indeed, over this period of time, volcanic eruptions are more numerous so that the sampling of events is more adequate than the sole historical period to produce robust statistics and minimise the pollution of the signal by the natural variability. Because of such heterogeneous spatial pattern and possible feedbacks on several elements of the climate system, these volcanic eruptions not only induce a general cooling of the surface climate of the Earth by altering the incoming solar radiation, they may also affect the climate system variability. As being a SST-based index, the AMO is of course strongly affected by the radiative effect of volcanic eruptions. Fig. 4.2 illustrates this volcanic effect using two simulations of the last millennium performed with the IPSL-CM4 climate model, the one described above including all the forcing, and one forced with the sole variations of the total solar irradiance (Servonnat et al., 2010). The correlation between the modelled AMO and the AMO reconstruction from Gray (2004) is of 0.18 (not significant at the 90% level) when only solar variations are accounted for; it reaches 0.45 (significant at the 95% level) when volcanic eruptions are also included as a forcing. Similar effect on volcanoes on the AMO was illustrated in another climate model by Zanchettin et al. (2012a).This evidences the crucial role played by volcanoes for pacing the climate variability, in particular from its direct impact on the earth surface temperature.

The oceanic circulation also responds to volcanic eruptions. It first adjusts rapidly to low latitude anomalous wind stress induced by the strong cooling, and this feature was seen in several climate

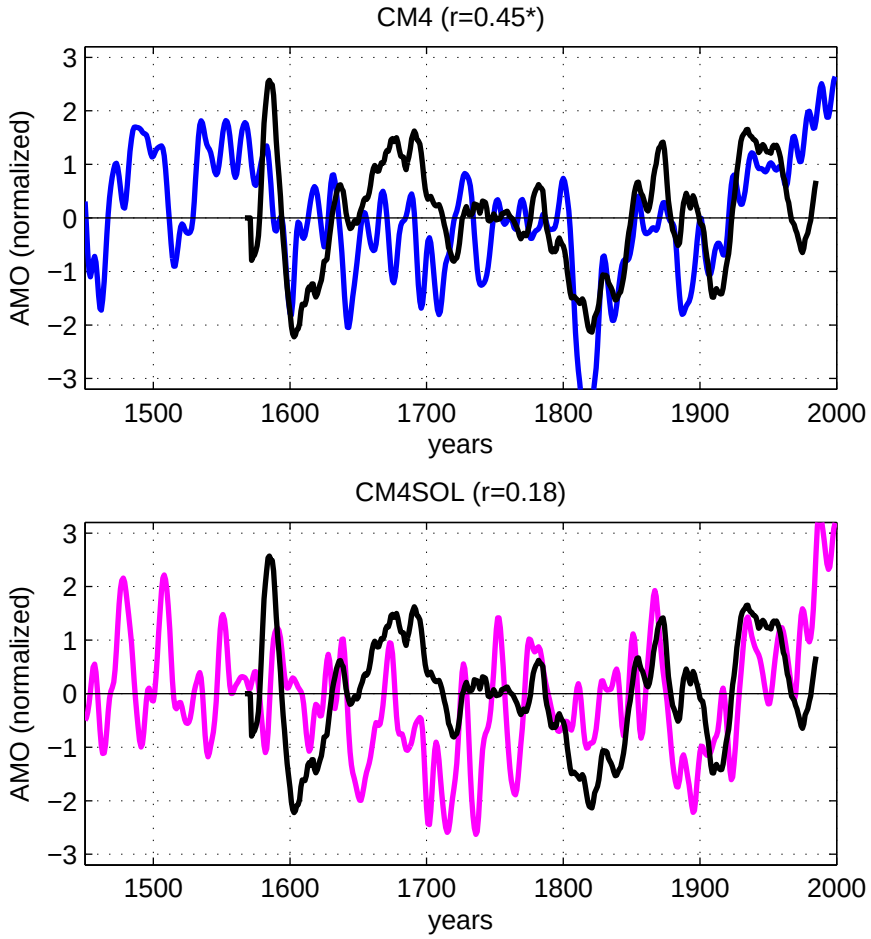

Figure 4.2: AMO evolution from the reconstruction of Gray (2004) in black and in two IPSL-CM4 simulations including before 1850 a) solar and volcanic forcing ***(Mignot et al., 2011)*** *and b) only solar forcing (Servonnat et al., 2010). From 1850 onwards, both simulations contains all observed forcing, including greenhouse gas concentrations large increase. In the simulations, AMO is computed as the SST average between 0 and 60° N in the Atlantic low-pass filtered with a 10-years cut off frequency.*

models in the Atlantic (IPSL-CM4: Mignot et al. (2011), MPI-ESM Zanchettin et al. (2012b), IPSL-CM5A-LR: not shown). The anomalous wind stress is itself associated to the well-documented polar vortex adjustment after volcanic eruptions which imprints on the surface NAO (Robock, 2000). This fast-developing anomalous circulation is similar to the fast dynamical adjustment of AMOC to atmospheric anomalies described in section sec:atmAMOC. It is significant but not relevant in terms of anomalous heat transport and long-term climatic effects. Unfortunately, response of the AMOC at longer timescales is less robust. In the IPSL-CM4 model, it was shown to significantly intensify 5 to 10 years after the eruptions of the period post-1400 A.D.. This response follows a deepening of the mixed layer depth due to the global cooling imposed by the volcanoes. It is consistent with the AMOC response to volcanic eruptions seen in several other studies (Stenchikov et al. 2009; Zanchettin et al. 2012b, **Ortega et al. 2011a**, Ding et al. 2014, **Swingedouw et al. 2015**), but mechanisms differ among studies: Stenchikov et al. (2009) and **Ortega et al. (2011a)** invoked a thermohaline mechanism after the cooling of the ocean induced by the direct radiative forcing of the volcanic eruption, while Zanchettin et al. (2012b) and **Mignot et al. (2011)** found a delayed response to atmospheric perturbations. Other studies propose even more complicated mechanisms. For instance, using the HadCM3 climate model, Iwi et al. (2012) reported an AMOC intensification after a Krakatau-like eruption through the runoff reduction towards the Arctic basin, but they also found that this effect was not seen after a weaker Pinatubo-like eruption, thereby illustrating a strong sensitivity to the magnitude of the eruption. Effectively, in response to the stronger eruptions occurring between 1100 and 1300, **Mignot et al. (2011)** found that the cooling is such that the sea ice extent dramatically increases in the model and caps the deep convection region. This yields on the contrary a reduction of the AMOC 10 to 12 years after the eruption. I found a similar dual response in the last millennium simulation performed with the subsequent version of the IPSL model (IPSL-CM5A-LR, Fig. 4.3). This highlights possible non linear responses of the climate to volcanic eruptions and may constitute a step towards understanding the diversity of response of the AMOC to the volcanic eruptions of the historical period in the CMIP5 experiments (e.g. Ding et al., 2014): depending on the mean state bias of each models, in particular in terms of sea ice cover, the response may be triggered towards one or the other type. It may be emphasised here that proxy-evidence for such profound and long-lasting effects on the sea ice extension have been found by **Sicre et al. (2013)**, consistently with the model results. The importance of the amplitude of the volcanoes has been further highlighted by **Swingedouw et al. (2015)**: Fig. 4.4 shows that depending on the magnitude of the eruption, different areas of the northern North Atlantic may be affected, thereby possibly leading to opposite anomalies of the oceanic deep convection.

We have highlighted above the diversity of deep convection and AMOC responses to volcanic eruptions. Differences in models physics, models internal variability, models implementation of the volcanic forcing, magnitude of the eruption, season of the eruption may be invalid to explain this diversities. Nevertheless, Fig. 4.5 suggests that for similar internal variability and similar eruptions, the model response in terms of AMOC may be more consistent than what can be inferred from the literature review of independent studies looking at the AMOC response using different techniques. This figure indeed shows that in the sub-ensemble of CMIP5 simulations selected because of their approximately bi-decadal dominant variability timescale in the North Atlantic (discussed in section 3.2.4 for example)

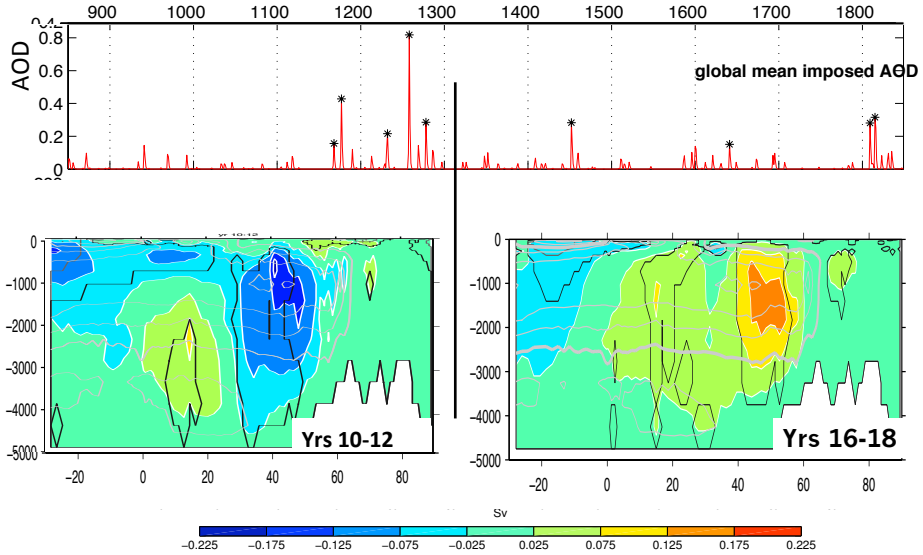

Figure 4.3: Top: time series of imposed optical depth of volcanic aerosols in the IPSL-CMR-LR transient simulation of the last millennium (details on the simulation in ***Sicre et al. (2013)****). Bottom left: Composites of anomalous Atlantic meridional streamfunction 10 to 12 years after the selected (stars on the top panel) volcanic eruptions which occurred before 1400 A.D. Positive (negative) values correspond to a clockwise (counter-clockwise) circulation in. Black and day grey contours mark significant areas at the 95 % and 80 % level, respectively, according to the Monte Carlo permutation test. Light grey contours show the annual mean Atlantic meridional circulation in the control simulation (contour interval is 3 Sv, thick contour corresponding to the zero contour.) Bottom right: same for the lag 16-18 years and selected eruptions which occurred after 1400 A.D.*

the variability is phased over the historical period, and this phasing is consistent with the impact of the Agung volcanic eruption on the subpolar North Atlantic. Note that we had first identified this pacing effect in the IPSL-CM5A-LR climate model **(Swingedouw et al., 2015)**.

In this context, and although the link between AMOC and AMO is relevant for climate studies, it is difficult to unravel the radiative and dynamic impact of volcanic eruptions on temperatures. In particular, it may be useful to quantify the impact of AMOC response to volcanic eruptions on the AMO, so as to investigate if and how AMO proxies can be used to reconstruct past variations of the AMOC. Fig. 4.6 illustrates that the AMO-AMOC typical relationship found in control conditions (black curve), where the AMOC leads the AMOC by 6-7 years, is strongly modified where external forcings are superimposed: in the IPSL-CM4 last millennium simulation, no significant correlation is found when the AMO lags the AMOC by a few yr ($r < 0.2$), as shown in Fig. 4.6, but there is a small anti-correlation ($r = 0.25$) at zero-lag or when the AMO leads. This might reflect the simultaneous radiative cooling together with the rapid dynamical adjustment of the AMOC after volcanic eruptions

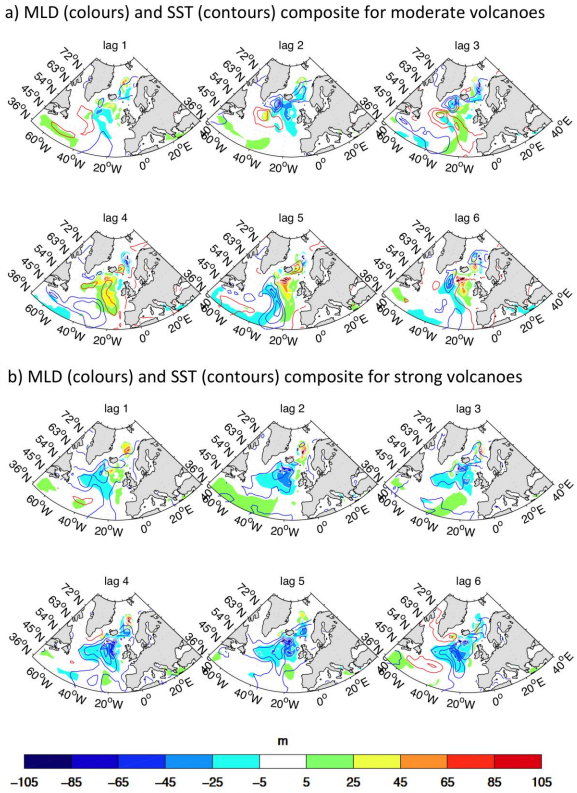

Figure 4.4: Composite over moderate (lower than 1.5 Agung) and strong (larger than 1.5 Agung) volcanic eruptions of the mixed layer depth (MLD) in colour and SST in contours computed within the last millennium simulation of the IPSL-CM5A-LR climate model. Fig from ***Swingedouw et al. (2015)***

described above. It illustrates that the perturbation of the AMO by the volcanic radiative forcing leads to a strong deterioration of the AMO-AMOC link, as also found by Otterå et al. (2010). It also implies that the AMO may not be used as a proxy of the AMOC variations. In order to remove the external forcing effects from the AMO and try the recover the dynamical link between AMO and AMOC identified in the control simulation, we have used a linear inverse model (LIM), following Marini and Frankignoul (2013). The first LIM modes of the last millennium simulation are shown in Fig. 4.7. The first mode (Mod1) is non-oscillatory with a decay time of 5 yr, and it corresponds to a global cooling, more pronounced in the Tropics. Its time series shows strong peaks at the time of volcanic eruptions, and its correlation with the global AOD is r = 0.7 ($p<0.05$). This mode thus largely represents the radiative cooling associated with the volcanic eruptions. The oscillatory mode 2/3 has a period of 26 yr with strong positive anomalies in the North Atlantic and in the North Pacific. Mode 4/5 shows strong ENSO-like SST anomalies in the tropical Pacific, with a period of 2.9 yr, similarly to mode 6/7 (not shown). Except for Mod1, the first 7 modes strongly ressemble the modes of CTRL (not shown), suggesting that LIM is efficient at isolating the radiative forcing signal from the intrinsic oceanic ones, as in Marini and Frankignoul (2013). To remove the radiative impact of volcanic activity from the AMO, we subtract Mod1 from the SST field, and compute a new AMO index (AMO-Ext). This new AMO signal largely resembles the AMO pattern from the control simulation (not shown), and a posi-

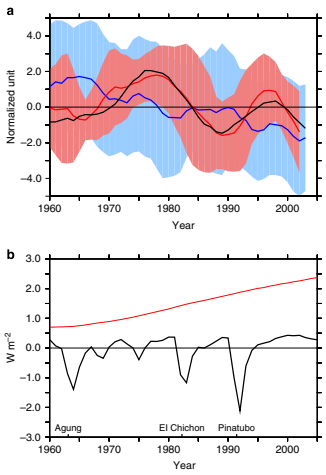

Figure 4.5: Simulated AMOC changes and radiative external forcing ***(Swingedouw et al., 2015)****. (a) Variations of the AMOC maximum at 48°N over the period 1960-2005 for the ensemble of five historical simulations performed with the IPSL-CM5A-LR model (black); for a subset of eight CMIP5 models, excluding the IPSL-CM5A-LR simulation, which also exhibit variability in the 10Ð30 years spectral band, in red, see Methods, Supplementary Table 1 and Supplementary Fig. 1 in* ***(Swingedouw et al., 2015)*** *for details); for the ensemble mean of the 10 other CMIP5 historical simulations (in blue). The standard deviation (s.d.) of the two CMIP5 ensembles is shown with the red and blue envelopes. All the AMOC indices have been normalised with the s.d. of the detrended time series over the period 1850Ð2005. (b) External radiative forcing (in W.m^{-2}) computed in the IPSL-CM5A-LR historical simulation. The black curve is the natural forcing including solar and volcanic eruptions and the red curve represents the anthropogenic forcing including greenhouse gas changes and the anthropogenic aerosols effects. A 5-year running mean has been applied to all time series from a.*

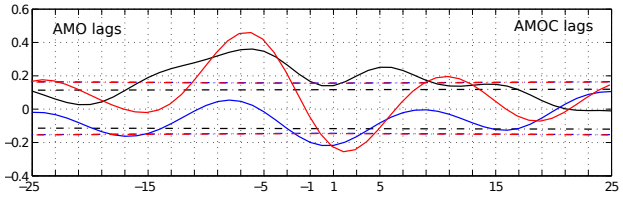

Figure 4.6: Correlation of the AMOC with the traditional AMO (blue curve, defined as the SST average over the North Atlantic 0 and 60°N, lowpass filtered with a cutoff-period of Tc = 10yr) and with the AMO where the external forcing has been removed using a linear inverse model (e.g. Marini et al., 2011), ie AMO-Ext (red curve), in the last millennium simulation of the IPSL-CM4 model (as in Fig. 4.1 and 4.2), and with the traditional AMO in the control simulation performed with the same model (black curve).

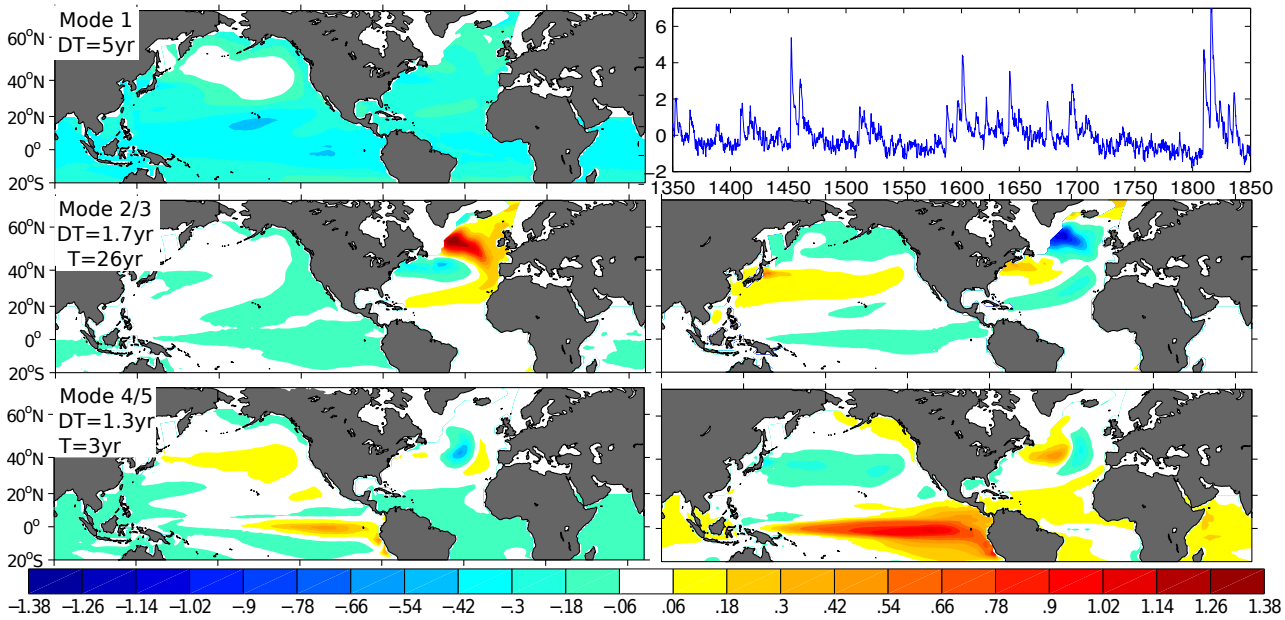

Figure 4.7: Normal modes (in K) of the linear inverse model in the IPSL-CM4 transient simulation of the last millennium. Mode 1 and its associated time series are shown on the top, modes 2/3, 4/5 and 6/7 in the second, third and fourth rows respectively.

tive AMO-Ext phase is found 6 to 7 yr after an AMOC acceleration (r reaching 0.5 in MILL, vs r = 0.36 in CTRL, Fig. 4.6). A significant negative correlation is also found when the AMOC lags by a few years, reflecting that the strong cooling following volcanic eruptions favours deep convection and thus enhances the AMOC, as described above. This unpublished work done by C. Marini in collaboration with C. Frankignoul illustrates possible research directions for better identifying the impact of volcanic eruptions on the climate dynamics and making progress in terms of proxy records interpretation. Note nevertheless that results obtained in the IPSL-CM4 transient simulation may have been particularly significant because of an overestimated radiative impact of volcanic eruptions in this model. The LIM analysis performed with the IPSL-CM5A-LR transient simulation of the last millennium were not as clear (not shown).

Another example where dynamical impact of volcanic eruptions has to be cautiously distinguished form the radiative impact on SSTs in the question of the link between eruptions and ENSO. Observations (Tung and Zhou, 2010) and proxies (e.g. Brad Adams et al., 2003; McGregor et al., 2010; Li et al., 2013) both suggest that tropical volcanic eruptions favour the warm (El Niño) phase of ENSO within two years after the eruption. Modelling studies have however so far reached no consensus on either the sign or the physical mechanism of ENSO response to volcanism (Driscoll et al., 2012; Ohba et al., 2013; Maher et al., 2015). By using the subtile diagnostic of relative SST anomalies and dedicated sensitivity experiments, **Khodri et al. (2016)** show that an El Niño is likely to occur within two years after volcanic eruptions in historical simulations from the Fifth Coupled Model Inter-comparison Project (CMIP5), and that the triggering mechanism implies anomalous westerlies due to the low heat capacity of land which promotes a faster cooling of the Indonesian Maritime continent than of the

surrounding ocean after the eruption.

4.2 Freshwater forcing

So-called hosing experiments, where freshwater may be distributed over broad or narrow regions of the North Atlantic in numerical models in order to investigate the sensitivity of the AMOC to freshwater flux, have been widely used to study the stability of the AMOC and its impact on climate (e.g. Stocker and Wright, 1991; Manabe and Stouffer, 1995; Rahmstorf, 1996; Fanning and Weaver, 1997; Schiller et al., 1997; Rind et al., 2001; Rahmstorf et al., 2005; Stouffer et al., 2006; Jackson et al., 2015; Yu et al., 2015, to cite a few). These idealised experiments are motivated by the necessity to understand past abrupt changes of the ocean circulation, as well as its response to future climate change. A large discharge of freshwater into the North Atlantic during glacial time and deglaciation is indeed believed to be responsible for major shifts in the ocean circulation recorded by various paleoclimate proxies (e.g. Bond et al., 1992; McManus et al., 2004). Concerning future climate change, model simulations suggest that global warming would intensify the freshwater input into the North Atlantic, as a consequence of an intensification of northward atmospheric moisture transport, increase of river discharge into the Arctic ocean and melting of the Greenland ice sheet (Church and Others, 2001). Recent observations give consistent indications (Peterson and Holmes, 2002; Dickson et al., 2002). The melting of Greenland ice Sheet was long thought to be very small, but recent measurements suggest an acceleration of the melting rate (Bamber et al., 2012). Rahmstorf et al. (2015) has argued that some effects of this freshwater input on the subpolar North Atlantic oceanic circulation might already be seen today. Up to now, only very few studies have been able to investigate these effects with a dynamic ice sheet model interactively coupled to a climate model (Gierz et al., 2015, is one of the few). Most other studies investigate these effects for past or future climates using a prescribed anomalous freshwater flux in the northern North Atlantic.

In most hosing experiments, anomalous freshwater flux has been applied to the North Atlantic and, in spite of differences in models, areas and magnitudes of the applied freshwater flux, a number of robust features of the models response emerged. In particular, it has been shown that a sufficiently large anomalous freshwater flux (typically 0.1 to 1 Sv, this value being strongly model-dependent) can shut down the AMOC completely on decadal to centennial timescales (e.g. Rahmstorf et al., 2005; Stouffer et al., 2006). This leads to a strong surface oceanic and atmospheric cooling in the North Atlantic realm (order of 10 K) and a pronounced cooling over most of the northern hemisphere. Yet, using more realistic anomalous forcing, some of these studies suggest that AMOC strength is sensitive to Greenland melting (Fichefet et al., 2003), while others do not (Jungclaus and Keenlyside, 2006; Ridley et al., 2005). Fig. 4.8 illustrates this model-sensitivity, in a protocol where five coupled climate models and one ocean-only model were used to evaluate the impact of 0.1 Sv (1 Sv = 106 m3/s) of freshwater equally distributed around the coast of Greenland during the historical era 1965-2004 **(e.g. Swingedouw et al., 2013b)**. In these experiments, the additional freshwater was shown to spread along the main currents of the subpolar gyre. Part of the anomaly crosses the Atlantic eastward and enters into the Canary Current constituting a freshwater leakage tapping the sub- polar gyre system. The multi-model set up allowed to show that the AMOC weakening is smaller if the leakage is larger.

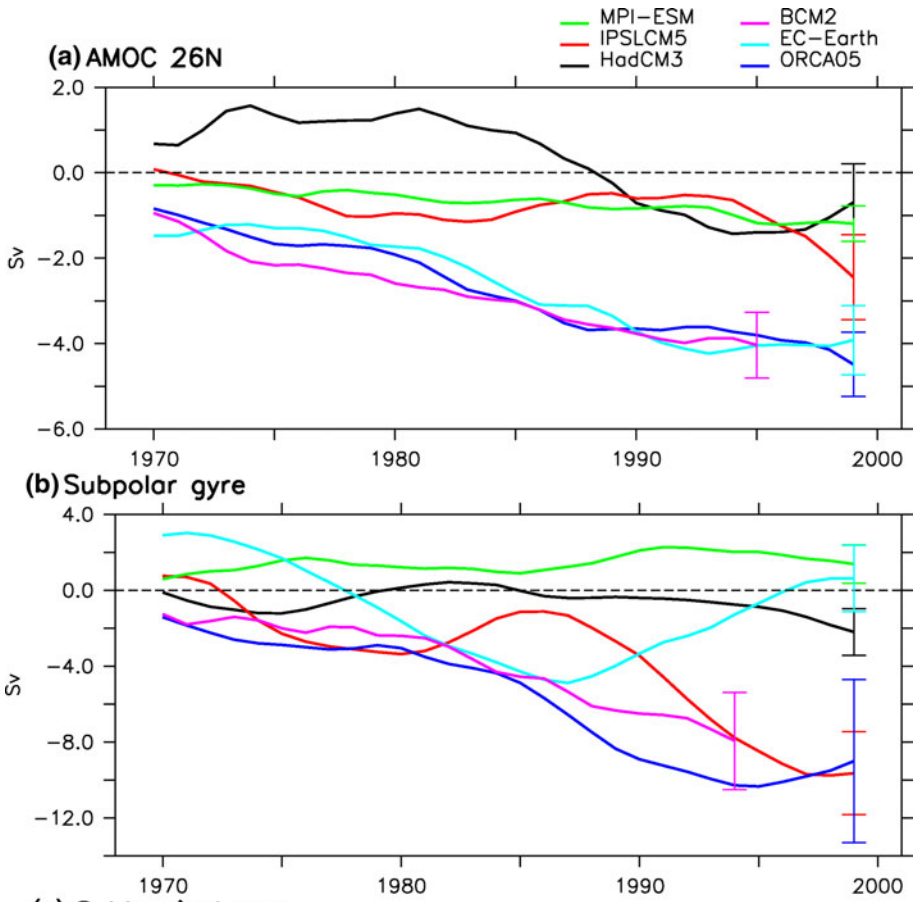

Figure 4.8: Time evolution of two oceanic circulation indices (differences between hosing and control simulations) in response to an anomalous freshwater input of 0.1 Sv equally distributed around the coast of Greenland in 5 coupled models and 1 forced model (HadCM3 is in black, IPSLCM5 is in red, MPI- ESM is in green, ORCA05 (forced configuration) is in blue, EC-Earth is in magenta, BCM2 is in cyan.). a Atlantic meridional stream function maximum at 26°N, b absolute value of the minimum (ie maximal transport due to convention of rotation orientation) of the barotropic stream function in the Atlantic subpolar gyre. A 10-year smoothing has been applied to all the time series. The error bars at the end of each time series represent two standard deviations computed in the control simulations. Figure from ***Swingedouw et al. (2013b)****.*

We have argued that the magnitude of the freshwater leakage is related to the asymmetry between the subpolar-subtropical gyres in the control simulations, which may ultimately be a primary cause for the diversity of AMOC responses to the hosing in the multi-model ensemble. This hypothesis remains to be more deeply investigated.

Using the coupled climate model of intermediate complexity CLIMBER3α, I investigated more specifically the sensitivity of the AMOC to the freshwater input location: we compared experiments where a surface freshwater perturbation was applied either in the high latitudes of the North Atlantic (over the deep convection sites) or in the Atlantic mid-latitudes. We found that although both experiments lead to a rapid shut-down of deep water formation and the AMOC (Fig. 4.9, first 100 years) and to a surface cooling in the North Atlantic (Fig. 4.10, top panels), they induce radically different sub-

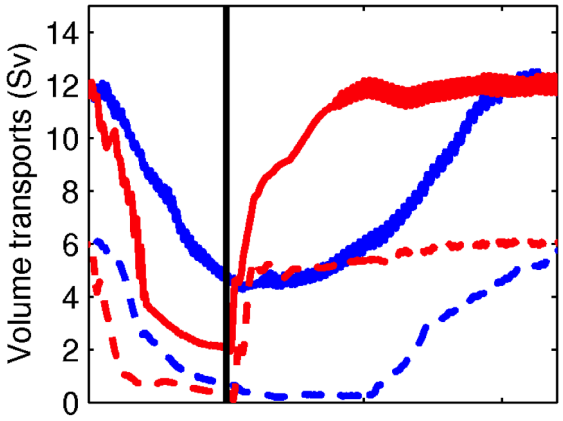

Figure 4.9: Time series of the maximum overturning circulation (solid) and overflow over the GreenlandÐScotland ridge (dashed) annual averages in two experiments where additional anomalous freshwater was imposed in a control simulation of the climate model of intermediate complexity CLIMBER-3α model ***(Mignot et al., 2006)****. In S-2050N, the anomalous freshwater input was applied in the North Atlantic between 20°N and 50°N (cold case, blue) and in S-5080N, it was applied in the North Atlantic between 50°N and 80°N (warm case, red), respectively. The perturbation (equivalent to a freshwater flux of 0.35 Sv) was applied during 100 yr (black vertical line) before being removed.*

surface temperature anomalies (Fig. 4.10, bottom panels). This difference was to shown to be linked to the possibility for intermediate depth ventilation to take place or not. When anomalous freshwater is imposed directly on the convection sites (experiment called S-5080N here), ventilation is completely capped and thus suppressed. The subsurface waters in the North Atlantic are then completely isolated from the cold atmosphere in the northern NorthAtlantic and only the subtropical ventilation is active. Propagation of warm water masses at intermediate depth into the northern North Atlantic leads to robust warm subsurface anomalies and the development of a strong vertical temperature inversion in the Nordic Seas (warm case). When anomalous freshwater input is imposed further away from the convection areas, namely at subtropical latitudes (experiment S-2050N here), intermediate depth ventilation at subpolar latitudes can remain active and subsurface waters are cooled by contact with the atmosphere (cold case). These two cases have been reported separately in previous studies, without being specifically explicited: Manabe and Stouffer (1997) and Rind et al. (2001) for example reported a subsurface cooling in response to the shut-down of the AMOC while Rühlemann et al. (2004) and Knutti et al. (2004) observed a warming. Our study sheds light on understanding these differences: the sign of the anomaly depends on whether intermediate ventilation continues or is shut down completely under freshwater perturbation and the magnitude and region of water hosing required to completely shut down intermediate water formation is model dependent. Note that a subsurface warming was also found in **Swingedouw et al. (2013b)**'s multimode study, showing that the mechanism of subsurface advection of Atlantic water towards the Nordic Seas, when a freshwater perturbation is released uniformly across the entire North Atlantic is robust across models in a refined experiment mimicking Greenland Ice Sheet melting.

We also showed that the subsurface temperature structure has crucial implications for the recovery of the AMOC once the freshwater perturbation is removed (Fig. 4.9). In experiments where the

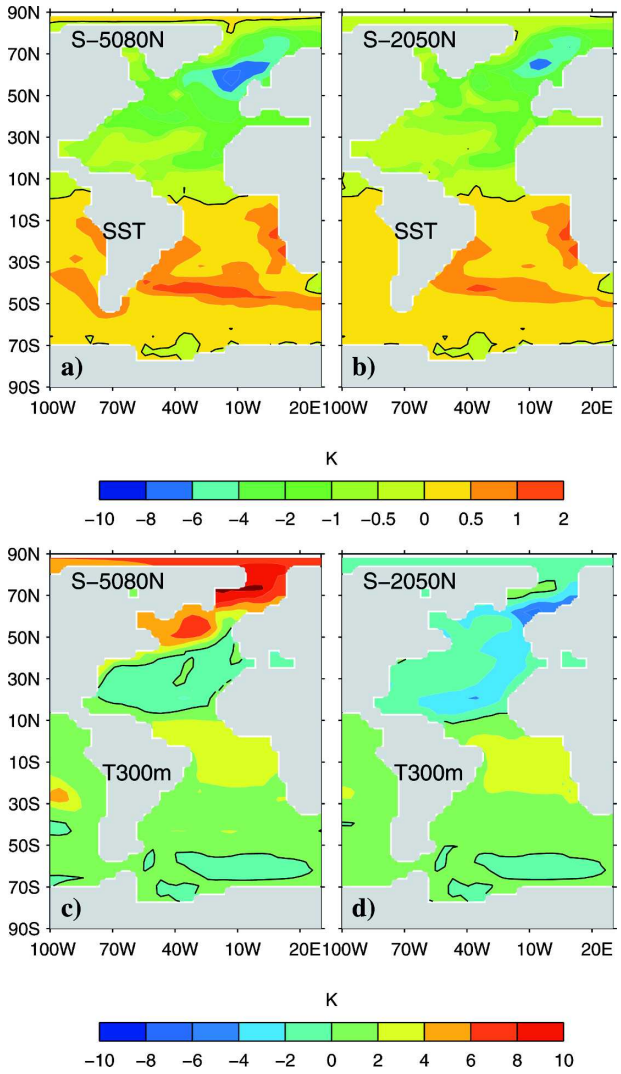

Figure 4.10: Sea surface temperature anomaly in the Atlantic after 100 yr of anomalous forcing as compared to the control run in experiments where (a) where the freshwater anomaly has been imposed over the sub polar latitudes (50°N-80°N, S-5080N, warm case) and (b) the freshwater anomaly has been imposed over the subtropical latitudes (20°N-50°N, S-2050N, cold case), respectively in the CLIMBER3α climate model (same experiments as in Fig. 4.9). The black contour lines represent 0 K. (c), (d) Same as (a), (b), but for the temperature at 300-m depth. From ***Mignot et al. (2006)****.*

AMOC was perturbed in mid-latitudes, and where subsurface cold anomalies were maintained by intermediate depth ventilation, the AMOC recovery is gradual, typically occurring over a century. In this case, it is the weak and shallow residual circulation associated with this ventilation that progressively evacuates the freshwater and brings at the same time relatively salty tropical waters to the north. When a warm reservoir has developed in subsurface, on the contrary, the recovery occurs on decadal timescales. Indeed, SSS rises rapidly and, with the help of wind-driven upwelling, the water column can be easily destabilised. This gives rise to intense flushes of deep water formation that evacuate the warm subsurface anomaly very quickly through air-sea interactions and erode the surface fresh anomaly. These initial flushes allow a rapid increase of the subsurface northward density gradient.

A sustainable AMOC and permanent deep water formation in the North Atlantic thus occur within another decade. Additional experiments where the freshwater input was applied for a longer period even showed an AMOC overshoot of its initial value during the recovery. This resembles the dynamics of the Dansgaard-Oeschger warm events recorded during the last glacial cycle in Greenland and other locations (Dansgaard et al., 1993), and corroborates the results of simulations of Dansgaard-Oeschger events obtained with two-dimensional ocean models (Winton, 1997; Ganopolski and Rahmstorf, 2001). Interestingly, a pronounced warming of the subsurface water masses during cold (stadial) conditions in the Nordic Seas was reported by Rasmussen and Thomsen (2004), though the interpretation of benthic isotopes remains ambiguous. Additional simulations, especially using glacial climate conditions, would be needed to corroborate applicability of our results to the mechanism of Dansgaard-Oeschger events.

The sensitivity of the AMOC to an anomalous freshwater input at high latitudes indeed also depends on the background state. **Swingedouw et al. (2009)** have indeed compared pairs of IPSL-CM4 simulations of several climatic states [last interglacial, Last Glacial Maximum (LGM), mid-Holocene, preindustrial, and future (2 x CO2)] where an anomalous freshwater input computed interactively according to a surface heat flux budget over the ice sheets is applied. This study has shown that, in agreement with the literature, the AMOC is more sensitive to freshwater input under LGM conditions than under warmer climates. In a complementary study, we have suggested the existence of a freshwater threshold for which the AMOC collapses: three glacial simulations obtained with the IPSL-CM4-v2 coupled general circulation model and differing by successive 0.1 Sv freshwater perturbations in the North Atlantic yielded AMOC strengths of 18, 15 and 2 Sv respectively **Kageyama et al. (2009)**. These different AMOC states have with very different global climatic impacts, which may explain the wide amplitude of variations variations as recorded by paleorecords from distant locations on the globe during the last glacial period. Unfortunately, in none of the above to studies we tested the presence of subsurface warm waters in the subpolar North Atlantic. Using a climate model of intermediate complexity with glacial boundary conditions, Flückiger et al. (2006) found a strong subsurface cooling for a freshwater perturbation of 0.2 Sv (as compared to an on-state with the same freshwater flux), and a subsurface warming for a large freshwater flux (0.4 Sv). This differs from our results, where the sign of the subsurface anomaly does not depend on the strength of freshwater forcing but it confirms that subsurface warming may occur under LGM conditions thereby giving credit to applicability of our results to understand past climatic events.

Finally, regarding the future climate, **Swingedouw et al. (2014)** found a moderate additional decrease of the AMOC at 26°N of 1.1 ± 0.6 Sv after 40 years of 0.1 Sv hosing between 2050 and 2089 (FutHos) as compared to the experiments with no additional hosing (FutCon). The rationale for this additional freshwater flux imposed in addition of the increase of atmospheric greenhouse gases concentration is to account for the projected Greenland ice sheet melting discussed above. The impact of the anomalous freshwater input is reduced compared to identical hosing simulations under recent historical climate conditions performed on the same ensemble of models **(Swingedouw et al., 2013b)**. This reduced sensitivity in future climate is first explained by a tendency of decoupling is detected between the surface and the deep ocean caused by an increased thermal stratification in the North Atlantic under the effect of global warming. This induces a shoal- ing of ocean deep ventilation through con-

vection hence ventilating only intermediate levels. The second important effect concerns the so-called Canary Current freshwater leakage discussed above. This leakage is increasing in a warming climate, which is a consequence of decreasing gyres asymmetry (Fig. 4.11) due to changes in Ekman pumping. We suggest that these modifications are related with the northward shift of the jet stream in a warmer world. For these two reasons the AMOC is less susceptible to freshwater perturbations (near the deep water formation sides) in the North Atlantic as compared to the recent historical climate conditions.

This sensitivity of the AMOC to freshwater flux in the high latitudes is also dependent on the vertical mixing parametrisation. Classical conceptual views to the thermohaline circulation, considering the AMOC as a narrow sinking in high latitudes and a broad upwelling in low latitudes (thus omitting the southern ocean and other basins), state that it should increase with (i) equator-to-pole surface density differences, which favours the northern branch towards the North, and (ii) with vertical diffusivity at low latitudes which drives the upwelling of deep water and thus possibly the return branch of the AMOC. The overturning strength ψ classically obeys (e.g. Welander, 1986):

$$\Psi \approx \Delta\rho^{1/3}\kappa^{2/3} \tag{4.1}$$

where $\Delta\rho$ is the equator-to-pole surface (or midlatitude surface-to-depth, as the two are equal in classical oceanographic configurations) density difference and κ is the vertical diffusivity. If κ is fixed in the ocean interior, as it is the case in most ocean general circulation model, including NEMO up to now, the AMOC strength obviously increases with density difference. On the contrary, it decreases if $\Delta\rho$ is artificially weakened through anomalous freshwater input at high latitudes, as in the case of the freshwater hosing experiments discussed above. Yet, since more turbulent kinetic energy is naturally required to displace water across a strong vertical density gradient, the vertical diffusivity of the ocean interior is in reality probably influenced by stratification. Thus, κ is expected to decrease when $\Delta\rho$ increases. Depending on the scaling law of κ with $\Delta\rho$, the AMOC may thus finally increase or decrease with decreasing $\Delta\rho$. Nilsson and Walin (2001) used a two-layer model to show that under plausible parameterisations of κ as a function of stratification, freshwater forcing could act as a "booster of thermohaline circulation". These results were confirmed in an idealised setup for an OGCM (Nilsson et al., 2003). Nevertheless, we didn't find such freshwater-boosted regime in the global coupled climate model of intermediate complexity CLIMBER-3α **(Montoya et al., 2005)**. The vertical diffusivity was parameterised as $\kappa \approx N^{-\alpha}$, where N is the local buoyancy frequency and the parameter α is a measure of the sensitivity of the vertical diffusivity to changes in stratification. In this model, the overturning was found to be reduced by the anomalous freshwater flux, independent of the choice of α. For high values of α (larger than a threshold value found to be between 0.5 and 1), a sharp increase in the sensitivity of the AMOC to anomalous freshwater flux, in the sense of a reduction, was even found. Indeed, in this case, the anomalous increase of stratification at high latitudes and the associated reduction of deep water convection, not accounted for the in scaling, was found to dominate the decrease of stratification at high latitudes (and associated equator-to-pole density gradient). The overturning thus significantly weakens **(Marzeion et al., 2007)**. More work is needed to better understand the possible effects of a more realistic parametrisation of vertical diffusivity

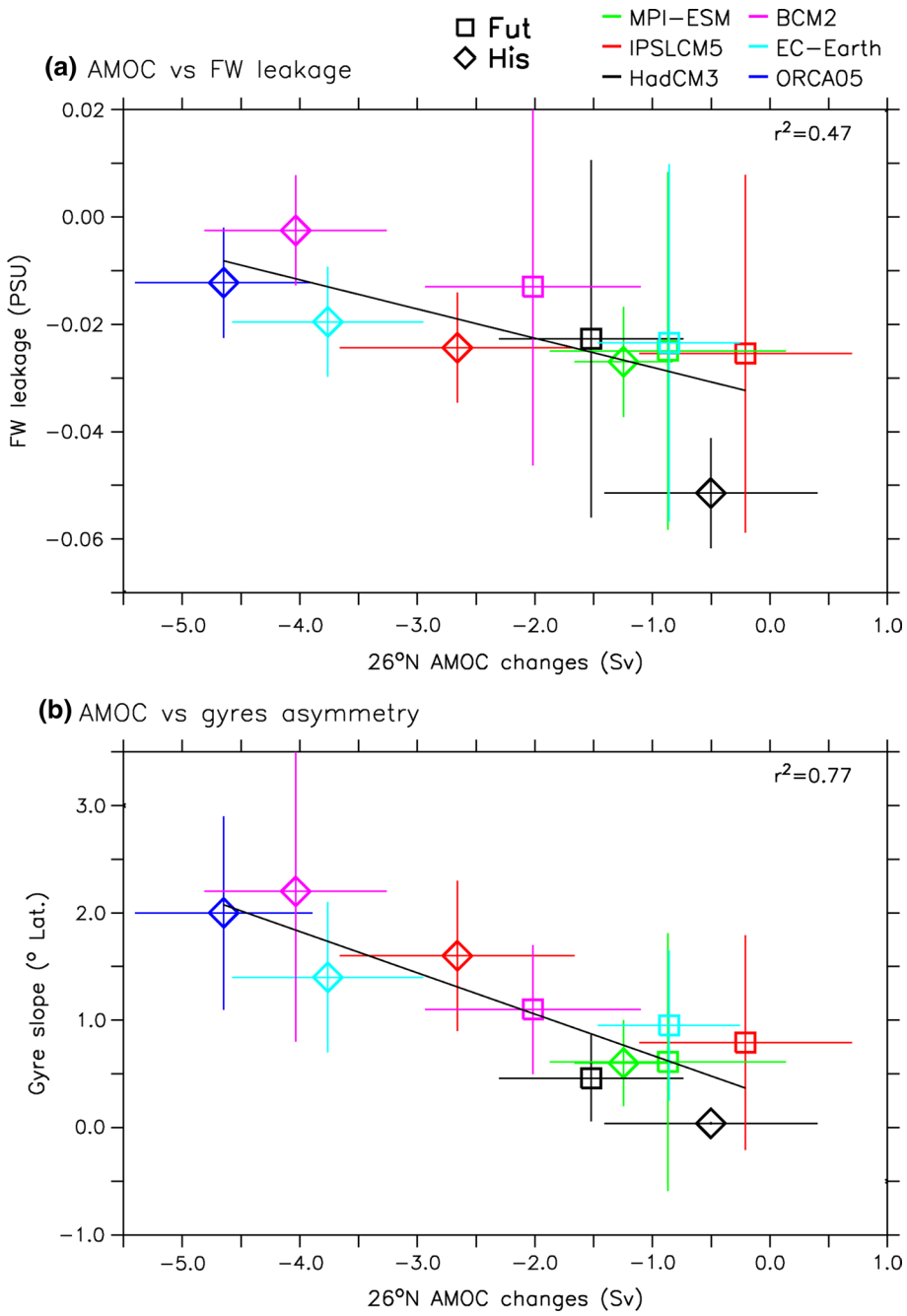

Figure 4.11: a AMOC changes versus "freshwater leakage" (FW leakage) averaged over the 4th decade of anomalous freshwater input of 0.1 Sv applied uniformly around the Greenland coast in the same 5 coupled models as in Fig. 4.8. The AMOC changes are defined as the difference between the melt water impact in control and future climate conditions for the AMOC maximum at 26°N (horizontal squares). The diamonds are the simulations points from ***(Swingedouw et al., 2013b)*** *(difference between hosing and control experiments under historical forcing). FW leakage is defined as the averaged salinity anomaly over the region 20°S-50°N, 50°W-20°E up to 1,000 m depth for the 4th decade. The black lines are a least squares linear regression made with the 11 couples of simulations (r2 = 0.47, p < 0.05). b Same as a but for the AMOC changes at 26¡N versus the slope of the gyres (r2 = 0.77, p < 0.01) computed from a linear regression of the zero line of the barotropic stream function between 45° W-15° W and 40° N-50° N expressed in degrees of latitude for 10° of longitude. The x and y error bars at the end of each time series represent two standard deviations computed in the control simulations.. From* ***Swingedouw et al. (2014)****.*

in ocean general circulation models. Interestingly, this point is currently being developed and tested in the NEMO model: de Lavergne et al. (2016) have recently shown that accounting for for reduced mixing efficiencies in regions of weak stratification or energetic turbulence strongly limits the ability internal mixing to drive abyssal Antarctic Bottom Water upwelling. A parametrisation where internal mixing is proportional to the available energy, that is N^{-2} will be implemented in the version of the IPSL-CM climate model in preparation for CMIP6.

Chapter 5

Predictability and predictions

In contrast to both weather and seasonal forecasts, "decadal prediction", which encompasses predictions on annual, multi-annual to decadal timescales, is still an emerging topic. The possibility of making skilful forecasts on these timescales, and the ability to do so, is investigated by means of predictability studies as well as retrospective predictions (hindcasts) made using the latest generation of climate models. The ocean is assumed to be among the most predictable component of the climate system on the decadal timescale due to its large thermal inertia. Indeed, as illustrated in the previous chapters, it plays a key role in climatic variability at these timescales. However, we saw that there is no clear consensus on the timescale and the mechanism of climatic variability, and there is also still no clear understanding of the predictability limits associated to the ocean. Using several techniques and several models, Branstator and Teng (2010, 2012); Branstator et al. (2012) have estimated that information from the ocean heat content in the upper 300m initial conditions may persist for about one decade. Beyond this limit, initial conditions have no remaining impact and this may be the upper limit for climate predictions. It is important to note that predictions at decadal timescales differ from the traditional climate projections primarily through the initialisation step, where models' variability is constrained towards direct observations of the climate system or to estimations via reanalyses. Thereby, decadal predictions aim at reproducing the observed fluctuations whereas climatic projections only aim at estimating the response of the climate system to external forcings. Even if the ocean provides most predictability at decadal timescales, the extent to which predictability of oceanic variables (such as AMOC or upper oceanic heat content) can be leveraged for prediction of meteorological variables over land is not clear at all. As discussed above, this is fundamentally a consequence of much weaker air-sea coupling in middle latitudes as compared to the tropics. Nevertheless, decadal variations of SST in this region (AMO) are thought to influence important climatic features, including rainfall over the African Sahel, India and Brazil, Atlantic hurricanes and summer climate over Europe and America (Pohlmann et al., 2004; Sutton and Hodson, 2005; Zhang and Delworth, 2006; Knight et al., 2006; Dunstone et al., 2011, e.g.). As there is evidence from climate models that the AMO is linked to the Atlantic Meridional Overturning Circulation (AMOC) (Knight et al., 2005), the AMOC has therefore been considered as a key target for the study of decadal potential predictability (Delworth and Mann, 2000; Curry et al., 2003; Latif et al., 2004; Collins et al., 2006, e.g.).

5.1 Predictability

Predictability of a physical or mathematical system may be defined as the rate at which the trajectories of initially close states separate, or the rate of displacement and broadening of initial states probability distribution (Branstator and Teng, 2010). Predictability is typically estimated from model experiments, although it may then depend on the model on which it is based and do not necessarily fully represent the behaviour of the physical climate system. Predictability studies, used with care, can nevertheless give an indication as to where, under what circumstances, and the level of confidence with which it may be possible to predict various climate parameters on timescales from seasons to decades.

Using a 1000-year control run of the IPSL-CM5A-LR climate model, we have analysed the prognostic potential predictability (PPP) of the AMOC through ensembles of simulations with perturbed initial conditions **(Persechino et al., 2013)** (Fig. 5.1). Based on a measure of the ensemble spread, the modelled AMOC has an average predictive skill of 8 years, consistently with other studies (Griffies, 1997; Pohlmann et al., 2004; Collins et al., 2006; Hawkins and Sutton, 2008; Msadek et al., 2010), with some degree of dependence on the AMOC initial state (see also Hermanson and Sutton, 2010; Msadek et al., 2010). Diagnostic and prognostic potential predictability clearly bring out the same regions exhibiting the highest predictive skill. Generally, surface temperature has the highest skill up to 2 decades in the far North Atlantic ocean. There are also weak signals over a few oceanic areas in the tropics and subtropics. Predictability over land is restricted to the coastal areas bordering oceanic predictable regions. Potential predictability at interannual and longer timescales is largely absent for precipitation in spite of weak signals identified mainly in the Nordic Seas. Regions of weak signals show some dependence on AMOC initial state. All the identified regions are closely linked to decadal AMOC fluctuations suggesting that the potential predictability of climate arises from the mechanisms controlling these fluctuations. Evidence for dependence on AMOC initial state also suggests that studying skills from case studies may prove more useful to understand predictability mechanisms than computing average skill from numerous start dates.

These model experiments are referred to as a perfect model framework for several reasons. One of them is that as already indicated, the observed climate variability results from internal interactions between the climate components, with a major role of the ocean at decadal timescales, superposed to forced external variations induced by the increase of greenhouse gases in the atmosphere and/or other sources of external forcing such as volcanic eruptions. Future evolution of the latter is not predictable (as far as volcanic eruptions are concerned for example) or based on scenarios (as for the greenhouse gases and aerosols) which contain some uncertainty. They are not included in the protocol shown above. Another reason is that these experiments assume perfect knowledge of ocean initial conditions while in reality, this knowledge is limited by the data availability and possibility to start (initialise) the model from the observed state. Within the fifth international coupled model intercomparison project (CMIP5), the scientific community has conducted, for the first time, a coordinated ensemble of simulations for decadal predictions. The aim of this initiative was to estimate the predictability of the climate modulations, in particular at regional scales. One underlying hypothesis for this exercise was that oceanic observations were now sufficiently long and precise to reconstruct climate decadal variabil-

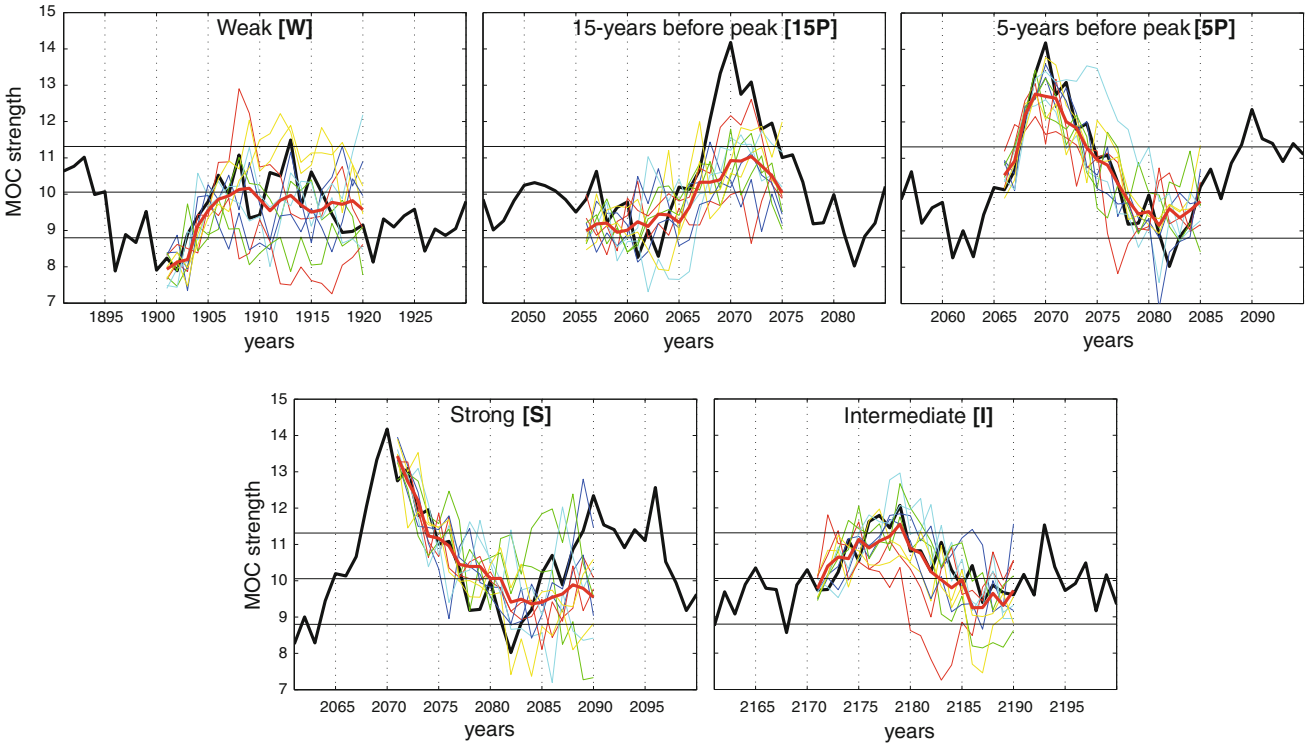

Figure 5.1: 'Plumes' of maximum-annual mean AMOC from ensembles of the IPSL-CM5A-LR in which the initial conditions have been perturbed (from ***(Persechino et al., 2013)****). Five ensembles are shown starting from different dates in the control simulation. The individual ensemble members, generated by applying at each grid point an anomaly randomly chosen between* $-0.05°C$ *and* $+0.05°C$ *to the SST field passed to the atmosphere at the first time step, are shown as coloured lines, the ensemble mean as the red thick line, and the control run as the thick black line. The middle horizontal black line is the mean AMOC, and both upper and lower horizontal black lines show standard deviations highlighting the range of variability of the AMOC.*

ity and that climate models were sufficiently accurate to realistically represent variability mechanisms and be compatible with observations. Although this exercise has been very instructive in general, and for us at IPSL in particular, main results in terms of prediction skill may suggest that these assumptions were over optimistic. Main results from this exercise show that surface air temperature at the global scale have considerable prediction skill for a number of years, but mainly provided from the externally forced component after the first few years (Doblas-Reyes et al., 2013), Kirtman et al. (2013). In general, prediction skill over land is very weak, and oceanic variables show the creates prediction skill beyond the externally forced variations. I present below the work we have been developing at IPSL on this topic. Building on **Cassou and Mignot (2013)**, one can define four necessary steps in order to perform predictions: (1) the initialisation of the model, (2) the generation of the ensemble, (3) the model integration, taking into account the external forcing, and (4) debiasing the model. This work was performed within the MEDDEM-GICC EPIDOM project and the EUFP7 SPECS project, for both of which I coordinated IPSL activities.

5.2 Model initialisation

As reviewed by **Meehl et al. (2014)** and Kirtman et al. (2013), initialisation techniques are numerous, including assimilation of surface information only (e.g. Keenlyside et al. 2008; Merryfield et al. 2010, **Swingedouw et al. 2013a; Ray et al. 2015**), restoring to 3-dimensional data (e.g. Voldoire et al., 2014; Bombardi et al., 2014), forcing of the ocean model with atmospheric observations (Matei et al., 2012; Yeager et al., 2012), partial coupling techniques (Thoma et al., 2015), and more sophisticated alternatives based on fully coupled data assimilation schemes (Zhang, 2007; Sugiura et al., 2009; Karspeck et al., 2014). This diversity of approaches to reconstruct an initial state is due to a combination of factors: the lack of quality multi-decadal three-dimensional ocean observations, the presence of climate model errors and drift, the impact of external forcing, the large range of space and time scales involved, to name the main ones. As a consequence, defining the most effective initialisation strategy is a challenge and none has yet been identified as 'the best'. It is indeed still difficult to distinguish whether one specific method clearly yields enhanced skill, as few studies have focused on comparing different techniques with a single climate model. Using perfect model approaches, Dunstone and Smith (2010) and Zhang et al. (2010) found, rather unsurprisingly, an improvement in skill when subsurface information is used as part of the initialisation. Nevertheless, given the uncertainty in ocean reanalysis below the surface (e.g. **Ray et al. 2015**, Karspeck et al. 2015) (Fig. 5.2), several studies also focused on prediction skill using only information from the sea surface (e.g. Keenlyside et al., 2008; Merryfield et al., 2010). Recently for example, Counillon et al. (2014) tested the accuracy of an ensemble Kalman filter SST assimilation skill for predictions: they show that although for specific hydrographic properties, more observations should be assimilated in addition to SST, the system does demonstrate decadal predictability for Atlantic overturning and sub-polar gyre circulations, as well as heat content in the Nordic Seas. Surface initialisation has been the claimed approach at IPSL.

In order to validate this approach, we first returned to perfect model studies **(Servonnat et al., 2014)**. We considered a target period of the long control simulation of the IPSL-CM5A-LR climate model; SST and SSS data from this target are used to nudge a simulation starting from a completely independent start date, in the aim of reproducing the target climate sequence. Advantages of such approaches is limit model-observations inconsistencies, thereby optimise the effect of the nudging, and to have a perfect knowledge of the target, in terms of AMOC in particular, thereby allowing a precise assessment of what has been reconstructed and not. Our experiments showed that in the tropics, nudging the SST is enough to reconstruct the tropical atmosphere circulation and the associated dynamical and thermodynamical impacts on the underlying ocean (Fig. 5.3, left). The joint SST + SSS nudging applied over the whole ocean is nevertheless the most efficient approach in general. At mid to high latitudes, in particular, it ensures that the right water masses are formed at the right surface density, the subsequent circulation, subduction and deep convection further transporting them at depth (Fig. 5.3, right). Kumar et al. (2014) and **Ray et al. (2015)** confirmed in historical conditions that SST nudging is efficient in reconstructing the observed subsurface variability in the equatorial Pacific.

Regarding mid to high latitudes and the important role of SSS nudging, this is more difficult to apply in historical conditions. Indeed, as indicated earlier in this document, SSS observations are still rare and relatively uncertain, in particular at the global sale. Tests performed up to now using SSS re-

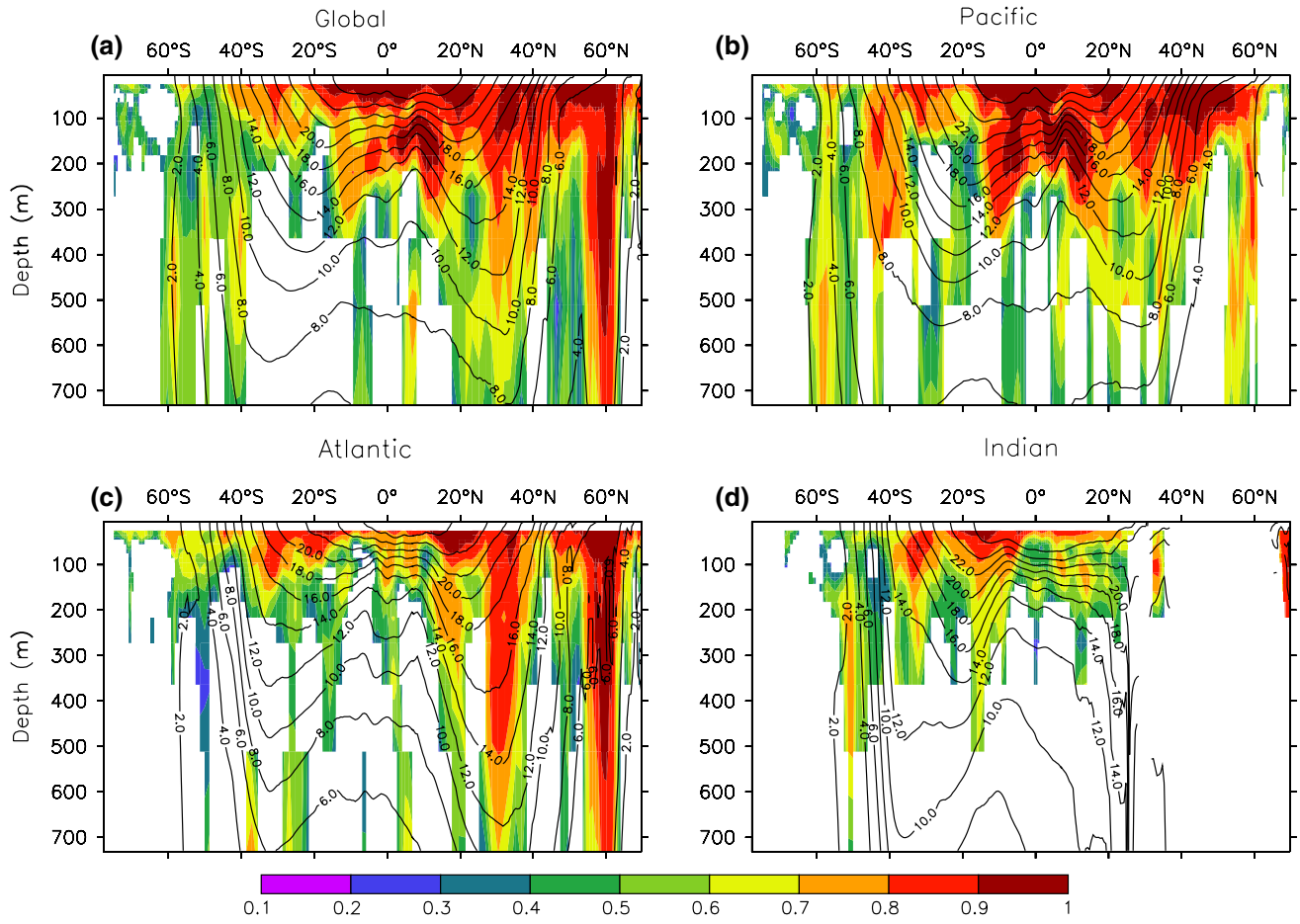

Figure 5.2: In-phase correlation between SODA (Giese and Ray, 2011) and ORAS4 (Balmaseda et al., 2013) reanalysis for annual mean over the period 1958-2001 for zonally-averaged temperature for a global, b Pacific, c Atlantic, and d Indian Ocean. Correlations significant at the 90 % level are shown. Isotherms of SODA overlaid in black. From ***Ray et al. (2015)***

analysis data sets have not been conclusive. The use of regional SSS data sets, to constrain specifically the North Atlantic for example, or the use of statistical properties between SST and SSS anomalies in the North Atlantic in order to constrain the water masses formation location is among our next ideas to be tested. In the meantime, we focus on SST nudging away from sea ice areas. **Swingedouw et al. (2013a)** have shown that such system has skill in reproducing the Atlantic Meridional Overturning Circulation (AMOC) variability (Fig. 5.4). In fact, this skill partly arises from the effect of external forcing, identified as volcanic eruptions, which contribute to phase the AMOC variability by resetting the 20-year internal variability model described above **(Escudier et al., 2013; Ortega et al., 2015)** (Fig. 5.4 panels (e) and (d)). The nudged simulations nevertheless better reproduce this second maximum than the historical simulations. This is due to the initialisation of a cooling of the convection sites in the 1980s under the effect of a persistent North Atlantic oscillation (NAO) positive phase, a feature not captured in the historical simulations. In terms of oceanic temperature, SST nudging has proven to allow significant reconstruction of the subsurface in specific regions, namely region of subduction in the subtropical Atlantic, below the thermocline in the equatorial Pacific and, in some

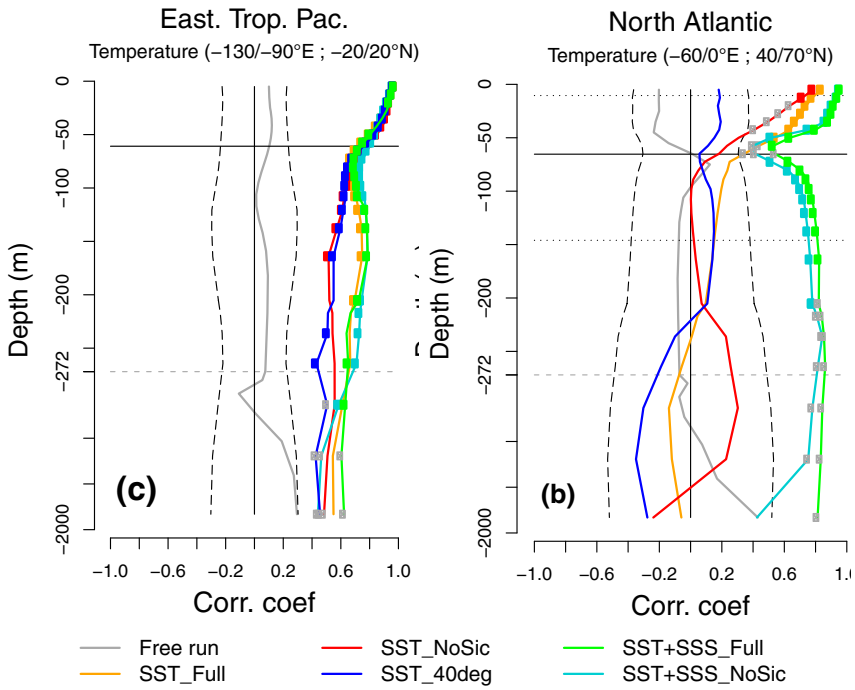

Figure 5.3: Correlation between the nudged simulations (colour solid lines, see legend for the colour code), the portion of the free control run starting from the same conditions as the nudged run (grey solid line) and the target (portion of the control run from which SST and/or SSS data are used for the nudging and which the nudged run aims at reproducing). Correlations are shown for temperature (upper row) and salinity (lower row), and for the areas indicated at the top of each panel, as a function of depth. The dashed vertical lines show the 99 % significance level for the correlation (Student t test taking into account the effective length of the time series). The coloured circles indicate the depths for which the correlation is significant (outside the dashed interval) and the Fisher F test not rejected (at 99 %). The grey squares highlight when the correlation is not different from the correlation between the free run and the target (test of difference between two Pearson correlation coefficients based on the Fisher transform, at 99 %). The horizontal solid lines show the mean depth of the 20° C isotherm and the dashed horizontal lines the mean JFM and JJA depth of the 20° C isotherm. The horizontal grey dashed line at -272 m indicates a change in the vertical scale. All experiments are based on the IPSL-CM5A-LR climate model ***(Servonnat et al., 2014)****.*

cases, in the North Atlantic deep convection regions (Fig. 5.5 shows the global correlations, see **Ray et al. 2015** for basins separation.

Surface nudging is probably not the technique that allows decadal predictions to start from the closest state to observations as possible. Nevertheless, in our view, it is perhaps one of the technique that allows to bring the model most smoothly towards a state not too far from the observations and still relatively consistent dynamically. Our prediction experiments suggest that it yields some prediction skill beyond the effect of external forcing, indicating that it allows initialisation of some part of the system (section 5.4). Note however that in all the studies discussed above, we used a fixed restoring coefficient of $40 W/m^{-2}$. While measurements of the oceanic heat flux feedback estimate to be close to this value (Frankignoul and Kestenare, 2002) many nudging studies have instead considered substantially larger restoring terms (6 to 60 times larger (e.g. Luo et al., 2005; Pohlmann and

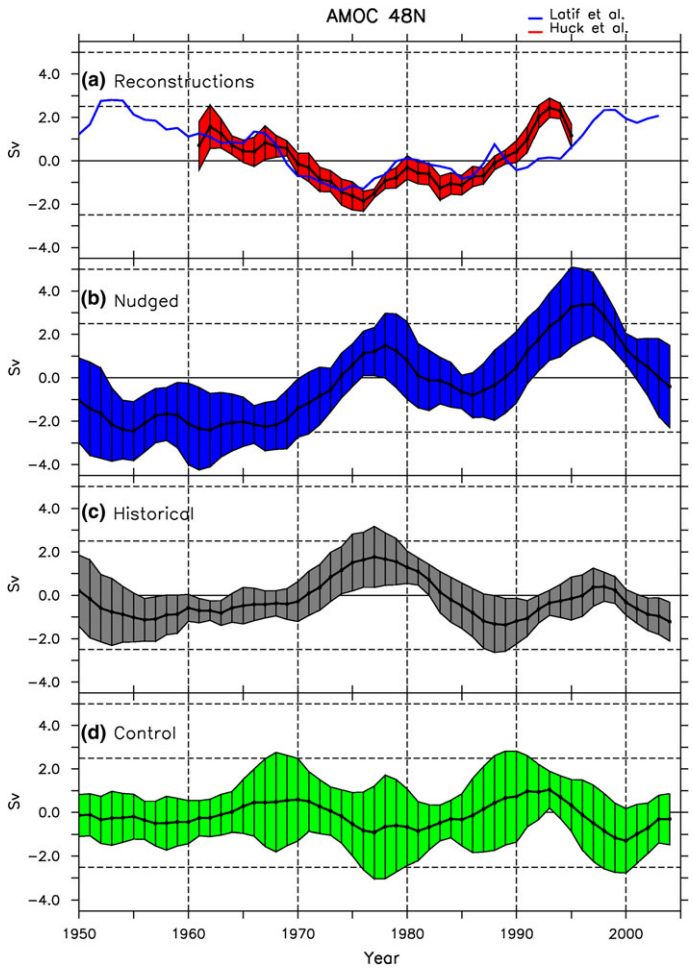

Figure 5.4: AMOC indices defined as the maximum of the meridional overturning stream function in the Atlantic at 48°N. a Reconstructions from Huck et al. (2008) in red and Latif et al. (2004) in blue, b mean and standard deviation (STD) of five-member ensemble of IPSL-CM5-LR simulations nudged towards anomalous observed SST over the period 1948- 2005, c mean and STD of historical simulations without any initialisation method, d mean and STD of control simulations without any initialisation and external forcing. A 3-year running mean has been applied to all the data. From ***Swingedouw et al. (2013a)***

Jungclaus, 2009; Dunstone and Smith, 2010) in order to constrain the simulated temperatures more closely to observations. However, the drawback of using un-physically large restoring values is the risk of applying overly high restoring heat fluxes in regions with strong model biases, which can tamper with key high-??frequency ocean-??atmosphere interactions (C. Cassou, pers. comm.). In our case, strong restoring terms lead to a drift of the AMOC towards unrealistically strong intensity because of a breakdown of the thermal negative feedback of the AMOC (not shown). In the future, we wish to investigate other techniques such as the use of a spatially variable restoring coefficient, promising in a perfect model world (Ortega et al, in prep.), the use of SSS restoring, making use of the recent data sets, nudging of the atmospheric circulation. We have submitted several projects to achieve these tests.

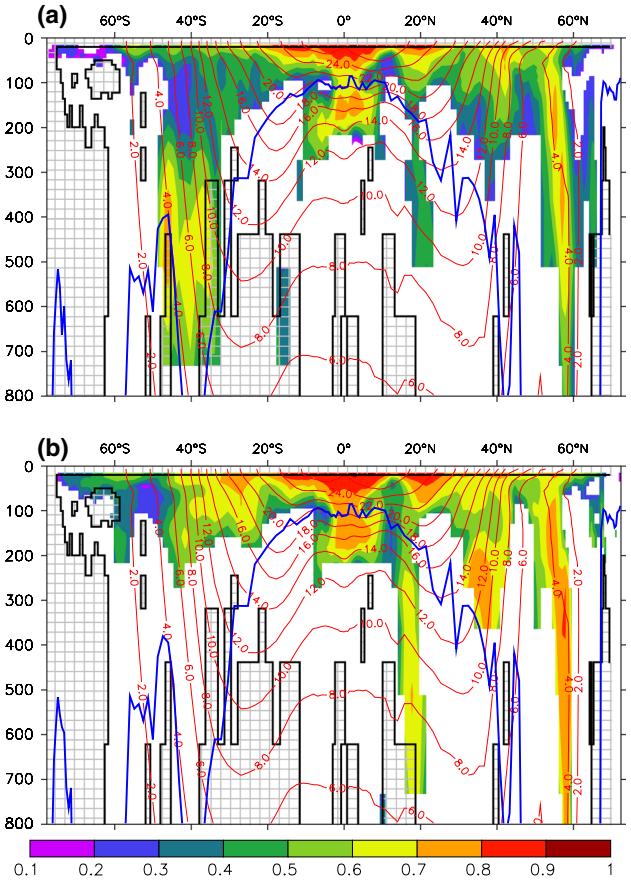

Figure 5.5: Correlation (significant at the 90% level) of globally averaged zonal subsurface temperature (monthly anomalies) between a a simulation where SST are nudged towards the observed ERSST data set using the IPSL-CM5A-LR climate model (one member from the five shown in Fig. 5.4 panel b) and SODA 2.2.4 for the period 1949-2005; and b the same nudged simulation and ORAS4 for the period 1958Ð2005. Black contour the boundary of 90 % significant correlation among reanalyses, the hatched side shows significant disagreement (and includes land points as well). The bold blue line is the maximum depth of mixed layer. Isotherms from the nudged simulations are in red contours. From ***Ray et al. (2015)***

5.3 Ensemble generation

As for seasonal predictions, the issue of initial condition uncertainties and chaotic evolution of the system is dealt with by performing an ensemble of predictions. In principle, the way the ensemble is generated should reflect the initial state uncertainties. It may impact its future evolution, and therefore the predicted state and its reliability. Several techniques among the wide range of methods explored in seasonal prediction (Stockdale et al., 1998; Stan and Kirtman, 2008) have been used so far. Common methods used for near-term predictions consist in adding random perturbations or perturbation patterns assessed by singular vectors, to the atmospheric state (Griffies 1997; Pohlmann et al. 2004; Collins et al. 2006, **Swingedouw et al. 2013a; Persechino et al. 2013**, Hazeleger et al. 2013b). Yet, as they do not take into account oceanic uncertainties, these techniques, which are optimised for the short-term variability, may give only an upper limit of predictability at interannual to decadal

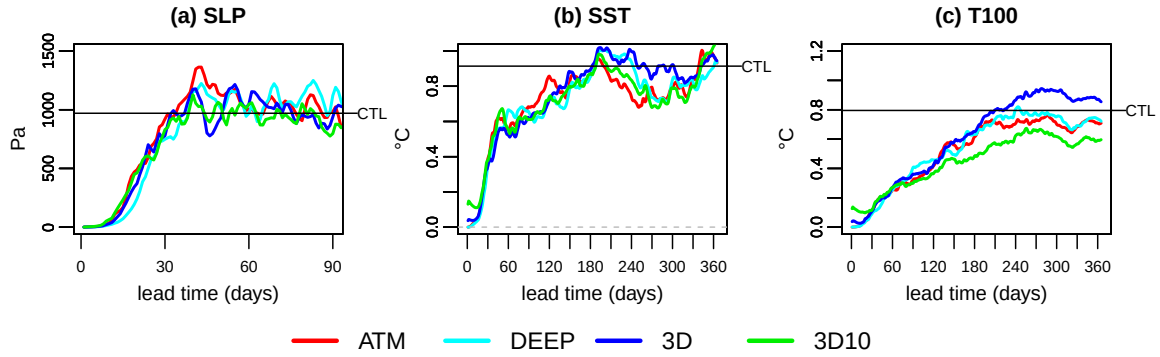

Figure 5.6: Daily time series of the Euclidean distance between a perturbed and an unperturbed (CTL) simulations of the IPSL-CM5A-LR model for the SLP (a), SST (b), and T100 (c) ***(Germe et al., 2016)****. Perturbation at the initial time steps has been applied as an anomalous white noise to the SST field passed to the atmosphere in ATM (as in Fig. 5.1), to the 3-dimensional oceanic temperature in 3D, to the oceanic temperature only below 2000m in DEEP and to the full 3D temperature but with a magnitude multiplied by 10 in 3D10. The SST is taken as the ocean temperature in the first depth level, which is 10 m thick. The black thin line corresponds to the natural variability of the temperature anomalies, assessed as sqrt(2) times the Euclidean norm of the CTL daily STD field once the seasonal cycle removed. The sqrt(2) factor is explained by the variance of the difference between two time series of the same variance being twice the variance of the time series.*

timescales. They may thus yield under-dispersed predictions, which might therefore be poorly reliable. In this case, the predictions do not explore the full range of possible states. In more recent studies, several techniques, such as using lagged atmospheric and oceanic states (Smith et al., 2007; Baehr and Piontek, 2014), different oceanic reanalysis datasets (Du et al., 2012; Pohlmann et al., 2013; Müller et al., 2014), fast-growing perturbation patterns assessed by a breeding technique (Ham et al., 2014; Baehr and Piontek, 2014) or anomaly transforms (Romanova and Hense, 2015), have been proposed to take into account oceanic uncertainties. Unfortunately, very few analyses focused on the divergence of the ensemble in itself to give insight on the impact of using one method or another. As one of the few, **Germe et al. (2016)** has investigated the impact of accounting for oceanic initial state uncertainties versus the classical approach accounting for atmospheric state uncertainties on the predictability of the climate system in a perfect model framework. It is found that a perturbation mimicking random oceanic uncertainties have the same impact as an atmospheric-only perturbation on the future evolution of the ensemble after the first three months, even if they are initially only located in the deep ocean (Fig. 5.6). This is due to the fast (1 month) perturbation of the atmospheric component regardless of the initial ensemble generation strategy. The divergence of the ensemble upper-ocean characteristics is then mainly induced by ocean-atmosphere interactions. While the seasonally varying mixed layer depth allows the penetration of the different signals in the thermocline in the mid-high latitudes, the rapid adjustment of the thermocline to wind anomalies followed by Kelvin and Rossby waves dominates the growth of the ensemble spread in the tropics. These mechanisms result in similar ensemble distribution characteristics for the four ensembles design strategy at the interannual timescale.

As a second step, we propose to test the effect of linear optimal perturbations, computed to opti-

mally modify an oceanic metric (such as the AMOC or the oceanic heat content over a certain depth and a certain area). The perturbations are diagnosed from adjoint linear oceanic models and we are testing their effect in climate models for the first time. Hawkins and Sutton (2011) have proposed another method to compute the optimal perturbation patterns, using a large ensemble of simulations performed with the coupled climate model. Their preliminary tests confirm that the dispersion increases in regions where the perturbation was largest. However, the effect on predictability was not clear (E. Hawkins pers.com.). Preliminary results with the IPSL-CM5A-LR model show that the linear optimal perturbations computed from the oceanic model has the expected effect in the coupled model but with a much weaker sensitivity (A. Germe, pers. com.). On other words, a much larger perturbation has to be applied in the coupled model to have the same effect on the AMOC for example than in the forced model. Reasons and implications of this result are still under investigation.

5.4 Debiasing and estimating the prediction skill

As explained above the strategy at IPSL has been to use only surface data for the model initialisation. Given the lack of SSS observations, we have concentrated on SST only until now. In such conditions, it appeared almost necessary to initialise the model only towards observed SST anomalies, as opposed to full field. Indeed, when the salinity is not constrained, correcting the model's biases in temperature only yields uncontrolled feedback effects at the sea ice edge, leading the model into a thermohaline catastrophe (not shown). Magnusson et al. (2012); Hazeleger et al. (2013a); Smith et al. (2013) have shown that at decadal time scales, it is difficult to determine whether full field or anomaly initialisation is more skilful than the other. We are nevertheless aware that initialising the model using only observed SST anomalies may induce inconsistencies such as imposing variability away from the model's associated mean structures (think of the shifted Gulf Stream for example). Still, we believe it may have interesting advantages in terms of physical consistency of the system, and we have tested it for decadal predictions, where consistencies between the model and the initial conditions is expected to be crucial (e.g. Liu et al., 2016)

Eventually, after initialisation (section 5.2) and ensemble generation (section 5.3) ensemble simulations are launched from the initialised simulation and run under the sole influence of external forcing. As detailed in **Cassou and Mignot (2013)**, the model unavoidably adjusts at the beginning of this hindcast phase, drifting from a constrained state close to observations towards its free attractive state. Although it is clear that this drift is stronger when the model is initialised towards the observed full state as opposed to observations, drift in the latter case must down be overseen. Imposing observed anomalies on a biased mean state necessarily induces an adjustment of the oceanic circulation (think again of frontal zone like the Gulf Stream area). Beyond statistical predictability issues linked to skill score estimations, the dynamical study of model drift and associated bias adjustment gives some clues to understand the model behaviours and provide some guidance for model improvements (Vannière et al., 2014; Voldoire et al., 2014; Hawkins et al., 2014; Sanchez-Gomez et al., 2015). We didn't explicitly analysed the drift of the model in the hind casts performed with the IPSL model and initialised towards SST anomalies. Nevertheless, we took it into account by computing the predicted anomalies with respect to a mean state which depends itself on the lead time **(Mignot et al., 2015)**.

Fig. 5.7 shows the anomaly correlation coefficient of the non-initialised and initialised 3-members prediction ensembles computed grid-point-wise against the initialised (nudged) simulation for detrended SST for the lead times 1, 2-5 and 6-9 years. The forecasting skill against the nudged simulation indeed gives an idea of the upper limit of possible skill in the system, while the one computed against observation data sets measures the actual skill against a particular reconstruction of reality. It can be viewed as an upper limit of possible skill in the system. The actual prediction skill, computed as anomaly correlation coefficient against observations, if of course the one expected by possible end-users. However, for most oceanic variables, it is still subject to some uncertainty in the reference observed state. The added-value of initialisation for the first lead time is clearly illustrated on the top panel of Fig. 5.7: for a lead time of 1 year, SST is skilfully predicted over all oceanic regions in the initialised hindcasts, in clear contrast to initialised hindcasts. The remaining skill seen in Fig. 5.7 (top left) may be due to non linear effects of the external forcing. For longer lead times (Fig. 5.7 right panels), fewer regions remain skilfully predicted in the initialised runs. The subpolar North Atlantic, the extratropical North Pacific, the northern Indian Ocean and the western tropical Pacific, as well as localised areas of the Southern Ocean stand out and generally outperform predictability obtained with non-initialised hindcasts (left panels) Actual prediction skill (verified against observational or reanalysis data) is overall more limited and less robust. Even so, large actual skill is found in the extratropical North Atlantic for SST and in the tropical to subtropical North Pacific for upper-ocean heat content (not shown). Note that in spite of a relatively weak actual prediction score of SST in the tropical Pacific (1 year), because of large interannual variations, the net primary productivity was found to have a predictive skill of 3 years **(Séférian et al., 2014)**. The higher predictability of NPP was attributed to the poleward advection of nutrient anomalies (nitrate and iron), which sustain fluctuations in phytoplankton productivity over several years. These results open previously unidentified perspectives to the development of science-based management approaches to marine resources relying on integrated physical-biogeochemical forecasting systems.

The joint analysis of two systems of decadal forecast performed with the same climate model (IPSL-CM5A-LR) and the same initialisation strategy (nudging towards SST anomalies) has enabled us to address carefully some issues related to the impact of increasing the number of hindcast start dates and ensemble size. One of the systems comprises yearly start dates between 1961 and 2013, with 3 members for each hindcast (named DEC3). The other system uses one start date every 5 years (the ones imposed by the CMIP5 protocol) with 9 members for each start date (named DEC9). Fig. 5.8 shows the correlation skill of the global mean temperature in each of these systems (left and right panels respectively) against various benchmarks (see caption for more details). Noting that the start dates used in DEC9 (following the CMIP5 protocol) are in phase or slightly leading the eruptions which occurred over the last 50 years (Mt Agung in 1963, El Chichon in 1982, Mt Pinatubo in 1991), one can see that for the forecast range 2-5 years for example, two start dates (1982-1985 and 1992-1995) are very strongly influenced by the eruptions (given that the radiative forcing of an eruption typically lasts 3 years, Robock e.g. 2000). This highly contrasts with the forecast range 4-7 years, which is, for each start date, only impacted by the last year of the volcanic radiative (see also Figure 10 in Germe et al. (2014)). As a result, the main source of predictability for global SST is partly lost for the forecast range 4-7 years and the correlation skill drops in DEC9 (right panel). Impact of the main

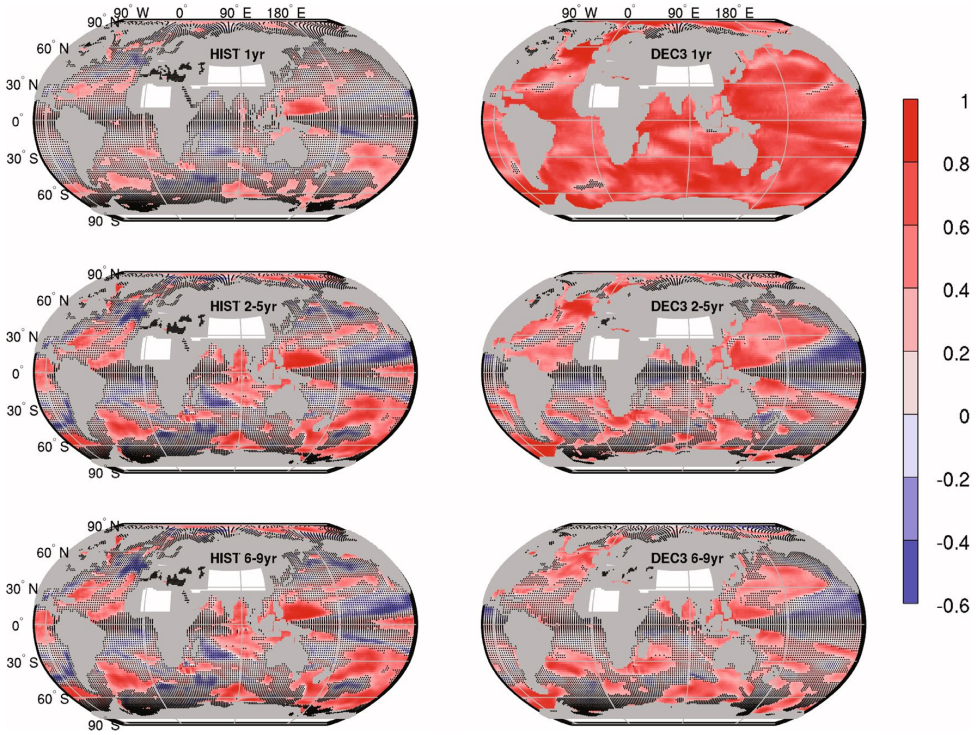

Figure 5.7: Ensemble mean (3 members) of the anomaly correlation coefficient of detrended SST in the non initialised hindcasts (HIST, left) and hindcasts initialised with nudging towards SST anomalies (DEC right) against the nudged simulation, for a lead time of 1 year (top), 2Đ5 years (middle) and 6Đ9 years (bottom). All simulations are based on the IPSL-CM5A-LR climate model, ensembles are generated using a stochastic perturbation (as in Fig. 5.1 and 5.6). Non-significant correlations at the 90% confidence level are marked with black dots. From ***Mignot et al. (2015)***

volcanic eruptions in the last 60 years falls again in the time window of the predictions at lead times 6-9 years, thereby contributing to enhance the correlation skill again. Such specific sampling issue does not occur in DEC3 (left panel), illustrating the high impact of the number of starting dates on the skill scores. Complementary analysis have shown that 3 members (the minimum size of ensembles requested for CMIP5) is clearly not enough to produce reliable predictions, as the ensemble mean is then not accurately estimated, so that the RMSE is large and much stronger than the intrinsic spread. The CMIP6 protocol promotes to perform hindcasts with start dates at least every second year and at least 10 members. This sounds like an expensive set up, and this may filter out some groups (perhaps including IPSL) that can't afford such cost. However, such set up is definitely needed to produce much more robust statistics.

One other important outcome of our analysis of the prediction skill of our system is precisely the difficulty to assess the actual skill, because of data uncertainty. For SST, ACC and RMSE measured from one observational dataset (ERSST) and two reanalysis (ORAS4 and SODA) led in general to similar conclusions in terms of predictability horizon, but with different values for the ACC and the RMSE. For the salinity and the ocean heat content, EN3, ORAS4 and SODA could also lead to different predictability horizons (Fig. 5.9). Clearly, oceanic observations are not yet sufficiently robust to

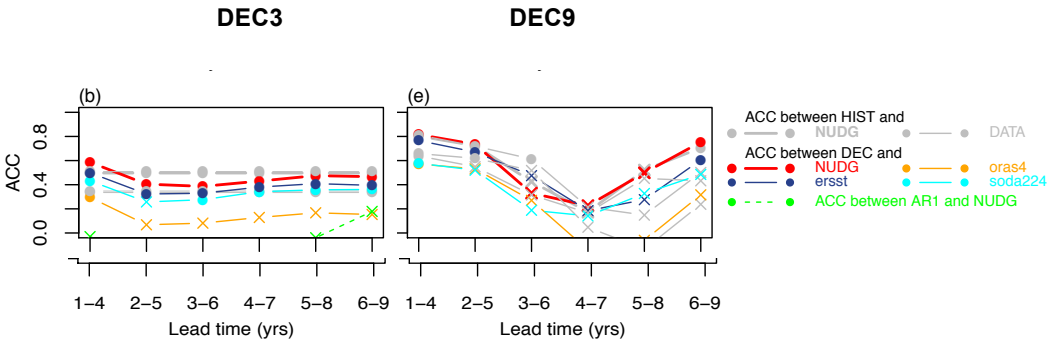

Figure 5.8: Correlation of the ensemble mean time series of the global mean SST with the nudged simulation (thick red and grey lines respectively, for the initialised (DEC, red) and non-initialised (HIST, thick grey) forecast ensembles), along the forecast time for 4-year averages. These correlations give an idea of the ability of the prediction system to reproduce the variability of the nudged simulation, for different prediction horizons ***(Mignot et al., 2015)****. The figure also shows the correlation of DEC with ERSST (dark blue), ORAS4 (orange) and SODA (light blue) in thin lines, together with their counterparts for the HIST ensemble (grey thin lines, different data sets not identified with colours). Left panel: decadal prediction system using 3 members and yearly start dates (named DEC3). Right panel: decadal prediction system using 9 members and start dates every 5 years (named DEC9).*

give a quantitative assessment of prediction skill.

Results from our analysis overall confirm that predictions at the decadal timescale is a promising but still academic type of research. Indeed, it concentrates the difficulties in both modelling (impact/estimation of coupled model drifts and biases on variability and predictive skill, etc.) and observations that are crucial for the initialisation step (scarcity of the observations, assimilation techniques, etc.). The level of knowledge is such that it appears to be premature to use the actual decadal forecasts for impacts studies for the next one or two decades lead-time, while process-oriented approaches are needed to better understand the decadal variability and its interaction with the on-going external forcings, before being able to enhance in fine the level of predictability.

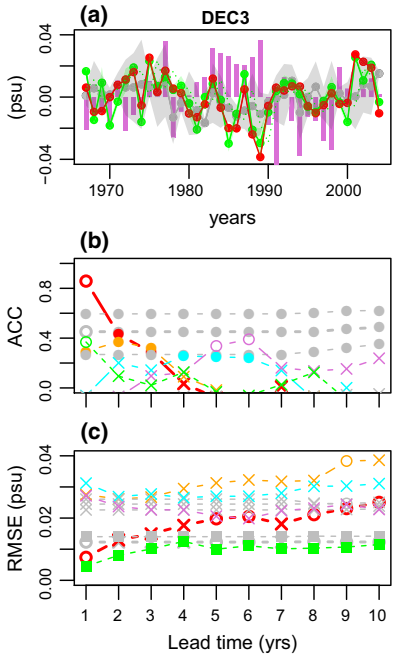

Figure 5.9: a Time series of the detrended ensemble mean forecast anomalies averaged over the forecast years 2-5 [green, DEC3] and the accompanying non-initialised (grey) experiments of the sea surface salinity averaged over the tropical band (20°S-20°N). The green and grey shadings respectively show the spread of the forecasts. The red line shows the time series from the nudged experiment. The observational time series from the ERSST dataset are represented with dark blue vertical bars, where a 4-year running mean has been applied for consistency with the time averaging of the predictions. The time axis corresponds to the first year of the forecast period (i.e. year 2 of each forecast). b Correlation of the ensemble mean with the NUDG reference (thick red and grey lines respectively, for the DEC and HIST forecast ensembles), along the forecast time for 4-year averages. The figure also shows the correlation of DEC with ERSST (dark blue), ORAS4 (orange) and SODA (light blue) in thin lines, together with their counterparts for the HIST ensemble (grey thin linesÕ, different data sets not identified with colours). Significant correlations according to a one-sided 90% confidence level with a t-distribution are represented with a circle, non significant ones with a cross. The number of degrees of freedom has been computed taking into account the autocorrelation of the time series, which are different for each forecast time. A filled circle indicates significant correlations but not passing a two-sided t test for the differences between the DEC and HIST correlations. c RMSE of the ensemble mean along the forecast time for 4-year forecast averages are plotted with solid lines. Circles are used where the DEC skill is significantly better than the HIST skill with 90% confidence using a two-sided F test. Dashed lines represent the ensemble spread estimated as the standard deviation of the anomalies around the multi-model ensemble mean. Green line is for the spread of the initialised hindcasts [DEC3 (c)], grey dashed lines for the non-initialised ones. From ***(Mignot et al., 2015)***

Chapter 6

What's next?

6.1 Internal oceanic and climate variability at decadal timescales

As illustrated through these research results, the ocean is thus a central element of the climate system, and a crucial regulator of the climate system (see e.g. Stocker, 2015). Several questions yet remain regarding its role in mechanisms of climate variability, in particular in the Atlantic. These questions are, in a way, even more pressing after the decadal prediction exercise: the highest skill for the unforced decadal predictability has been confirmed to arise mostly from the large inertia and predictability of the Atlantic Meridional Overturning Circulation, but what are the drivers of this circulation's variations, and what are their consequences for climate? What is the exact link between the AMOC and deep convection, and between AMOC and vertical mixing in the ocean interior are for example crucial questions that may control the AMOC dynamics on the first order. How different, or not, are the AMOC (zonally integrated streamfunction) and the subpolar gyre (vertically integrated streamfunction) which are, in fine two mathematical constructions. What is the role of the western "transition" zone near the boundary between the subtropical and the subpolar gyre, of buoyancy anomalies propagating westward at this latitude, how robust is the bi-decadal timescale of North Atlantic variability? What is the role of salinity for the mean state of the AMOC, its variability and its stability? What is the impact of mesoscale eddies or, in other words, how robust are the mechanisms described from coarse resolution models simulations? How does the AMOC transport heat, how does this impact the SST and the AMV, and finally the atmosphere and the climate? Links to variability in other basins, which I didn't discuss in this report are also important to identify and understand.

This series of questions constitutes the background of my research. Not all of them could be addressed in one life time probably, but I list them here to underline the crucial need for pursuing mechanism studies on these questions. Long control coupled simulations are a useful tool for this, and I will thus pursue my collaboration with the climate model development team at IPSL. At present, the climate modelling group puts lots of efforts in the development of the IPSL-CM6 climate model, and I modestly contribute to the diagnostic and validation of the oceanic state in the subsequent versions. This is a very exciting experience, that force me to re-think about basic questions of the climate system and climate modelling: how do climate interactions, feedbacks and equilibrium set up, how do

climate components influence each other, what are the most sensitive parametrizations, etc. With the aim of entering deeper into the ocean processes and the ocean modelling issues, I have also began to interact more closely with the NEMO R&D group in charge of developing and maintaining the oceanic module NEMO. Beyond the development of the IPSL climate model, I wish to bring my expertise to tackle together fundamental questions on the dynamics of the AMOC (deep convection, mixing) using cheaper forced oceanic configurations and dedicated sensitivity experiments. This work is just emerging. Finally, conceptual approaches, such as the one proposed by Born and Stocker (2014) for the variations of western part of the subpolar gyre as a response to surface buoyancy forcing and deep convection in the Labrador Sea, allow a fundamental understanding of the processes at play. Through a master internship recently supervised at the University of Bern with A. Born, we realised however that this model needs to be improved in order to represent the full (internal + forced) variability. Indeed, in climate models, deep convection in the Labrador Sea can be sensitive to anomalous sea surface salinity, and thus freshwater fluxes, but in the case of external forcing such as volcanic eruptions, which induce a strong and abrupt cooling, this sensitivity can change. Developments are ongoing to improve the modularity of the sensitivity of this conceptual model to components of the buoyancy fluxes, and potential improvements for the representation of the variability of the gyre will have to be performed.

6.2 Reconstruction of the climate variability

Our involvement in the CMIP5 decadal prediction exercise has been very instructive and productive. From a personal point of view, it has pushed me to move more towards the 'real'/observed climate variability. The global warming hiatus discussed above, the North Atlantic anomalous cooling (e.g. Rahmstorf et al., 2015), and the recent cold blob Robson et al. (2015) are fascinating events of climate variability which have been relatively well observed as compared to previous events. They are nevertheless associated with variations of the -poorly observed- oceanic circulation, namely the subpolar gyre and the AMOC. Climate simulations constrained by observations allow a great step forward in addressing these issues, as done for example by Robson et al. (2014); Msadek et al. (2014); Yeager and Danabasoglu (2014).

Several centers (ECMWF, NCEP, JMA...) produce atmospheric (and more recently coupled) reanalysis for the 20th century with sophisticated data assimilation processes. These reanalysis products can be used to constrain the atmospheric model to follow the observed day-to-day variation of the actual weather by nudging (relaxing) the model state variables (winds and optionally temperature and humidity). Atmospheric nudging techniques have been successfully used at IPSL for a long time in global (Coindreau et al., 2007) and regional modelling for the purpose of downscaling (Omrani et al., 2012). They allow to minimise the intrinsic chaotic nature of the atmospheric flow and possible dynamical model biases. Furthermore, atmospheric reconstructions driven only by wind and not by temperature nudging only disrupts the kinetic energy, which is known to be a small part of the energy budget. Such reconstructions could thus be used for attribution purposes: by deactivating components of the forcing in simulations where the natural dynamical variability is constrained, one may expect to better understand the role of each forcing component, as well as internal variability, in shaping the observed variations (e.g. Schaller et al., 2016; Vautard and Yiou, 2009). Such "conditional attribution"

remains a major challenge for the understanding of climate change. Yet, given the central role of the ocean in the global scale variability, a complementary approach is to perform such reconstructions in coupled mode, using the IPSL climate model. Conditional attribution experiments could be compared to atmospheric only simulations, thereby sheding light on fundamental mechanisms yielding low frequency climate variability and sensitivity to external forcing.

In addition, so as to better understand the important processes giving rise to decadal climate variability, more constrains can be added to the climate system and in particular to the ocean. In order not to hamper too much the oceanic dynamical integrity, one could stick to the previous strategy of nudging only the ocean surface, building on the expertise we recently developed in the framework of CMIP5 near-term predictions. SST is an obvious candidate for the nudging. I would first like to build on our recent developments in terms of using a variable restoring coefficient. As seen above, SSS is also crucial to reconstruct the oceanic decadal variability but observations of this variable still suffers great uncertainty at the global scale. Together with colleagues from LOCEAN and EPOC, I wish to pursue some ongoing tests on the use of regional data sets (Reverdin et al. pers. com.) and/or diagnosed statistical relationship between SST and SSS.

Oceanic and coupled reanalysis have been a topic of intense development in the recent years in the international community (e.g. Balmaseda et al., 2007; Wang et al., 2010; Heimbach et al., 2011), but they are still strongly model-dependent and show little agreement (e.g. Munoz et al., 2011; Tett et al., 2014; Karspeck et al., 2015; Born et al., 2015). My aim is not to add one extra reanalysis in this zoology, but rather to contribute to process studies and federate research on the climate variability. The idea is to build on expertise of the "local" climate model dynamics and variability (IPSL-CM6) and examine its sensitivity to external constraints. Furthermore, while it is generally accepted that climate reanalysis depend on the data they have assimilated, knowledge of the underlying climate model is generally overlook. Its biases and strengths, and specificities of its internal variability are nevertheless crucial in order to interpret the associated reanalysis. Therefore, I believe that reconstructing the climate variability with the IPSL climate model may offer interesting opportunities to gain understanding on the past climate variability as well as opportunities for advances on the IPSL climate model development. This idea to is supported by the LABEX L-IPSL. It has also been submitted to one international call.

As illustrated in the previous sections, the historical period of observations is still too short for robust conclusions and assessments of the decadal climate variability. In particular, it is necessary to put the observed 20th century trends, decadal frequency, magnitude of extremes in a longer-term context to evaluate the stationarity of the identified mechanisms. The last 1000 years constitute a good framework for this. Highly-resolved and diverse climate proxies over last 2000 years are becoming available, in close link with the PAGES 2k program (Tierney et al., 2015; McGregor et al., 2015), while state-of-the art climate models can be integrated quasi-routinely over this time period. In the near future, these proxies could be integrated in the IPSL climate model, so as to yield a seamless reconstruction of the ocean circulation and climate variability over a long time period. This idea has been submitted to another international call.

6.3 Past and future variability in the northeastern tropical Atlantic and Sahel region.

Tropical hydroclimate is extremely sensitive to climate change, with severe impacts on natural resources and society (fresh water, rain-agriculture, etc.) in drought and flood prone regions such as the Sahel region. The sahelian monsoon, and its variability in terms of duration, seasonality and intensity is thus a crucial research topic, which has been the focus of an abundant literature. One of the questions arising from decadal prediction systems concerns their capability to provide any useful information for monsoon regions at the decadal time scale (Gaetani and Mohino, 2013).

Besides, by replenishing the nutrients needed for the biochemical activity, the seasonal wind-driven upwelling occurring in boreal winter along the Senegal-Mauritanian coast is another very important element of the local environment. Fisheries produce 70% of the proteins to local population and are of large economic importance for these countries. As opposed to the Canaries permanent upwelling system, the Senegal-Mauritanian upwelling system is seasonal, setting up, as the sahelian monsoon, according to the ITCZ migration. In boreal winter, when the ITCZ is at its southernmost position, strong trade winds over the Mauritania, Senegal and Guinea coast induce the upwelling. In this season, the Sahel is essentially dry. In boreal summer, the ITCZ is at its northernmost position, and the winds along the coast are very weak. Precipitations are on the other hand favoured by convective events under the ITCZ: this is the monsoon season.

Several studies have shown that SST variations control a large part of the variations of the Sahel monsoon (e.g. Folland et al., 1986; Rowell et al., 1995; Ward, 1998; Janicot et al., 2001; Giannini et al., 2003; Hagos and Cook, 2008). At interannual to decadal timescales, the influence of the AMO seems to dominate (Mohino et al., 2011; Rodríguez-Fonseca et al., 2011; Hoerling et al., 2006; Zhang and Delworth, 2006). The AMO is itself partly constrained by the AMOC, as discussed in this report for example. The other oceanic basins, such as the tropical Pacific via ENSO (Joly et al., 2007; Mohino et al., 2011), the indian ocean (Palmer, 1986; Bader and Latif, 2003; Giannini et al., 2003; Lu and Delworth, 2005; Mohino et al., 2011) or the Mediterranean Sea (Rowell, 2003) have also been suggested to play a role. Hastenrath (1990) suggest a role of internal SST variation in this basin, but in fine all the mechanisms of natural variability listed here act on the inter-hemispheric SST gradient of the tropical Atlantic, which is strongly coupled to sahelian precipitations via the ITCZ (Folland et al., 1986; Zeng, 2003). Fewer studies have focused on the variability of the intensity and extent of the eastern tropical Atlantic upwelling. Yet, given their link with the ITCZ migration, past and future variability of the upwelling and monsoon seasons may well be anti-correlated. How does a stronger, longer or later monsoon (and thus cropping) season translate in terms of upwelling (and thus fishing) season? What is the role of the ITCZ anomalous migration in setting a possible link between the two? A related question is the influence of the major modes of climate variability (NAO, ENSO, AMO, Interdecadal Pacific Oscillation...) and the oceanic circulation (AMOC) on the ITCZ migration.

As in other regions, external forcings also act on these systems, and may interplay with the internal variability. Although statistical studies suggest that the drought around the 1980s may have been caused by a simple natural variation (Mohino et al., 2011), Ackerley et al. (2011); Chang et al. (2011) suggest an important influence of the anthropogenic aerosols, via their role on the SST gradient in

the Atlantic. Haarsma (2005); Dong and Sutton (2015) plead instead for a response to the increase of greenhouse gases. The role of the latter recently gained increased interest in the literature, in particular given the demonstrated importance of differential warming between the tropics and the high latitudes (Park et al., 2015). As discussed in section 4.1, large stratospheric tropical volcanic eruptions induce an abrupt cooling in the Tropics, even stronger over land than over the ocean, given the stronger heat capacity of the ocean. Thus, volcanic eruptions may be expected to produce an anomalous air-sea gradient with the opposite sign as compared to global warming, and to decrease the monsoon flux (Iles and Hegerl, 2014; Bourassa et al., 2012). Furthermore, the ocean cooling in response to eruptions is not homogeneous (e.g. Mignot et al., 2011), and it perturbs the temperature gradient in the tropical Atlantic (Evan et al., 2009), and thereby the seasonal to interannual ITCZ variability. At decadal timescales, the AMOC response to tropical volcanic eruptions is still poorly understood, as seen above, although it can largely control the the SST inter-hemispheric gradient at this timescale. The consequences of these phenomena have not been studied in details for the west african monsoon, but the complexity and the heterogeneity of the response has been highlighted for the asiatic monsoon for example (Anchukaitis et al., 2010) and suggested for the south american monsoon (Apaéstegui et al., 2014). Furthermore, several studies have recently suggested an even more important role for the volcanic eruptions on the climate. First, the eruptions that do not reach the stratosphere (thus weaker eruptions) also influence durably the climate, since they are numerous and thus have a non negligible cumulative effect (Santer et al., 2014, 2015). Second, extra-tropical eruptions also seem to have a major impact on the climate, in particular on tropical climate, as they induce a reduction of the west african monsoon (Oman et al., 2006; Haywood et al., 2013). Wegmann et al. (2014) have shown that this reduction weakens the northern branch of the Hadley circulation, thereby altering the atmospheric circulation on the Atlantic-Europe sector and increasing the precipitations over Europe. To conclude, the response of the west african monsoon to external forcing is still poorly understood.

As for the natural variability, much less studies have ben dedicated to the response of the upwelling system to these external forcing. Bakun (1990) suggested in a pioneering work that by intensifying the alongshore wind stress on the ocean surface, increased greenhouse gases concentration in the atmosphere and associated global climate warming may induce an intensification of coastal upwellings. Since then, several papers have investigated this hypothesis using modern data Narayan et al. (2010); Cropper et al. (2014), paleoproxies (McGregor et al., 2007; Barton et al., 2013) and climate models Mote (2002); Wang et al. (2015). However, this mechanism is not robustly confirmed in products based on observations (reanalysis, proxies) (Barton et al., 2013). It is worth noting that all these studies focused on the permanent upwelling system in each oceanic basins, which may have a different sensitivity than the seasonal senegalo-mauritanian upwelling.

This brief review shows that the past and future atmospheric and oceanic natural and forced variability in the eastern tropical Atlantic sector remains under debate. Given the strong societal impact of both the Sahel monsoon and the coastal upwelling, I find important and urgent to address key questions such as (i) what are the key sources of predictability for the vulnerable regions surrounding the tropical Atlantic? (ii) What are the underlying mechanisms? What is the role of the AMOC and the Atlantic decadal variability? What is the impact of volcanic eruptions? (iii) Do identified processes improve predictions skills of the climate impact? These questions are challenging because simulating

the WAM and details of the eastern tropical Atlantic ocean features is still highly uncertain, and long-term observations are still rare. I have recently launched or been associated to various works related to these topics: reconstructions of the west african monsoon variability over the last millennium or snapshots of the last millennium, using proxies and/or a general circulation atmospheric model forced by reconstructions of the sea surface temperature. around the second half of the nineteenth century. Results are not always easy to reconcile with expected variations of the climate of this time period. I have also began to co-supervise a phD student from the University of Dakar on the interannual to decadal variability of the upwelling and its long term changes as represented by climate models and reanalysis. The idea is to diagnose the decadal variability of this feature, its link with the large scale climate variability and external forcing. In parallel, I have been exchanging expertise with a phD student at the university of Bern on the evolution of the Oxygen Minimum zone, located in the vicinity and below the tropical upwelling systems, in a climate simulation of the last millennium. These research directions are for the moment independent and should eventually converge.

Chapter 7

Curriculum Vitae and publication list

Juliette MIGNOT
juliette.mignot@locean-ipsl.upmc.fr

Born December 7th, 1976 (39 yrs old)
French

LOCEAN (UPMC-CNRS-IRD-MNHN)
Tour 45-55 5e étage. Case courier 100
4 place Jussieu 75252 Paris Cedex 05. France
Tel/fax: +33 1 44 27 33 / 71 59

KUP, Univ. Bern
Physics Institute Sidlerstrasse 5
CH-3012 Bern, Switzerland
Tel/fax: +4131 631 4275 / 8742

Researcher at IRD (since 2006) CR1
Physical oceanography / Climatology

Research topics

- Circulation océanique dans l'Atlantique: stabilité, variabilité et prévisibilité, influence des tropiques, rôle de la salinité océanique, rôle des forçages externes,
- modélisation, modèles globaux couplés océan-atmosphère-glace,
- climat de la région Atlantique

Ongoing research projects

- SPECS (Seasonal-to-decadal climate Prediction for the improvement of European Climate Services 2012-2016, EU-FP7, P.I. P. Doblas-Reyes) Principal Investigator for IPSL/LOCEAN.
- PREFACE (Enhancing prediction of tropical Atlantic climate and its impacts, 2013-2016, EU-FP7, PI N. Keenlyside) Co-investigator.
- MORDICUS (Oscillations et rétroactions climatiques aux échelles décennales : mécanismes, sensibilité et incertitudes, ANR, 2013-2018 PI C. Cassou) Co-investigator.
- SALOUM (Variabilité séculaire de la mousson dans l'Ouest du Sahel, 2014-2016, INSU-LEFE-IMAGO, PI M. Carré, ISEM, France) Co-investigator.
- LMI ECLAIRS (Etude du climat en Afrique de l'Ouest, IRD, 2012-2017 PI A. Lazar & A. T. Gaye) Co-responsible for WP 4: plateforme de modélisation et d'observations.
- MISSTERRE (Modélisation intégrée du système Terre, LEFE, 2009-2016 P.I. P. Braconnot & S. Planton) Co-investigator.

Main Affiliation

LOCEAN (UPMC-CNRS-IRD-MNHN)

Research visits and other affiliations

2012-2016	« Physics and Climate Environment » laboratory (KUP), Department of Physics, Bern University, Switzerland (T. Stocker)
2011, 2014, 2015 (2 mois)	Laboratoire de Physique de l'océan et de l'atmophère Siméon Fongang, Université Cheikh Anta Diop de Dakar, Senegal (A. T. Gaye).

Ongoing supervisions

phD students

A.Sylla (2016-, LPAOSF, Sénégal, co-encadrement A. Gaye)

A. Hameau (2016-, Univ. Berne, Suisse, co-encadrement F. Joos)

Past supervisions

Post-doc.

P. Ortega (2013-2015, EU-FP7 SPECS)

P. Ortega, J. Mignot, D.Swingedouw, F. Sévellec, E. Guilyardi (2015) Reconciling two alternative mechanisms behind bi-decadal AMOC variability *Prog. Ocean*. 137(A), pp237-249 doi:10.1016/j.pocean.2015.06.009

A. Germe (2013-2015, EU-FP7 SPECS)

A. Germe, F. Sévellec, J. Mignot, D. Swingedouw, S. Nguyen (2016). On the robustness of near term climate predictability regarding initial state uncertainties *Clim. Dyn., in press*

S. Ray (2012-2013, GICC MEDDEM EPIDOM)

Ray S, Swingedouw D, Mignot J, Guilyardi E, (2015) Effect of surface restoring on subsurface variability in a climate model during 1949-2005 *Clim Dyn*, 44(19) 2333-2349, doi 10.1007/s00382-014-2358-3

J. Servonnat (2011, GICC MEDDEM EPIDOM)

Servonnat J., J. Mignot, E. Guilyardi, D. Swingedouw, R. Séférian, S. Labetoulle, (2015) Reconstructing the subsurface ocean decadal variability using surface nudging in a perfect model framework, *Clim. Dyn*. doi: 10.1007/s00382-014-2184-7

M. Wade (2011-2015, LEFE SALOUM, LPAOSF Dakar Sénégal)

Wade M Mignot J Lazar A Gaye A T (2015) On the spatial coherence of rainfall over the Saloum delta (Senegal) from seasonal to decadal time scales, *Frontiers in Earth science*. 3-00030, doi :10.3389/feart.2015.00030

phD students

I. Camara (2012-2016 LPAOSF, co-encadrement A. Gaye et A. Lazar)

Camara I, Kolodziejczyk N, Mignot J Lazar A and Gaye A.T. (2015) On the seasonal variability of salinity in the tropical Atlantic mixed layer, *J. Geophys. Res.,* 120(6) pp4441-4462, doi : 10.1002/2015JC010865

H. Goelzer (2004-2007, PIK, Potsdam, Allemagne, co-encadrement S. Rahmstorf, A. Levermann)

Goelzer H., Mignot J., Levermann A., Rahmstorf S. Tropical versus high latitude freshwater influence on the Atlantic circulation. Climate Dynamics, 2006, 27 (7-8), p. 715-725

Laboratory engineer

R. Waldman (2011-2012, ecole Ponts Paritech)

M2 Univ. Paris VI

R. Waldman (2011)

R. Escudier (2010)

Escudier R., Mignot J. and Swingedouw D. : A 20-yrs coupled ocean-sea ice-atmosphere variablility mode in the North Atlantic in an AOGCM (2013) Clim. Dyn., 2012, 40, 619-636, DOI: 10.1007/s00382-012-1402-4,

M2 Univ. P. Sabatier, Toulouse

C.Porchier (2016, supervision at the Bern university, Swtzerland, with A. Born)

M2 LPAOSF, Dakar, Senegal

A.Sylla (2015)

O. Diankha (Co-supervision A. Lazar, 2009)

M2 CIPMA, Cotonou, Benin

C.Da-Allada (Co-supervision F. Durand, 2009)

M2 PIK, Potsdam, Gemany

A.Born (Co-supervision S. Rahmstorf, A. Levermann)

Born A., Levermann A., Mignot J.. Sensitivity of the Atlantic Ocean circulation to a hydraulic overflow parameterisation in a coarse resolution model : response of the subpolar gyre. Ocean Modelling, 2009, 27 (3-4), p. 130-142.

M1 Univ. Paris VI

A. Supply (co-supervision M. Khodri 2013)

F. Rouvière (2009)

M. Lacarra (co-supervision A. Lazar 2008)

Mignot, J., A. Lazar and M. Lacarra On the formation of Barrier Layers and associated vertical temperature inversions: a focus on the northwestern tropical Atlantic. 2012, J. Geophy.Res 117, C2, doi:10.1029/2011JC007435

Research engineer

S. Labetoulle (2011-2012, GICC MEDDEM EPIDOM)

S. Nguyen (2013-2016, EU-FP7 SPECS)

phD committes

External committee	A. Révelard (2013-, LOCEAN, C. Frankignoul) T. Bouinot (2009-2013, LSCE, E. Cortijo) Y. Ruprich-Robert (2010-2013, Cerfacs, C. Cassou)
Defense examiner	Y Ruprich-Robert (2014, Université Paul Sabatier), N. Barrier (2013, Université de Bretagne Occidentale) M. Minvielle (2009, Université Paul Sabatier)
Written reviewer	I. Medhaug (2011, University of geophysics, Bergen, Norway), P. Ortega (2011, Universidad de Computense Madrid, Spain), M. MartinDelRey (2015, Universidad de Computense Madrid, Spain)

Teaching activities

Statistics applied to oceanography

2009, 2010, 2012, 2013, 2015, 2016	LPAOSF (UCAD, Dakar, Senegal) 12 h + 8h lab work matlab/octave
2009, 2010, 2012, 2014, 2015, 2016	CIPMA (Cotonou, Bénin). 12 h + 8 lab work matlab
2008	Summer school of statistical modelisation and environment, Dakar, Sénégal 7 h lab work

Others

2000-2003	Tutoring at l'ESPCI « les Etats de la matière » (Prof. P. Papon.) 12h/an.

At-sea experience

Jun-Jul 2007	EGEE5 campaign, on board R/V Antea (Cotonou, Benin – Cotnou, Benin). Bernard Bourles / Fréderic Marin. CTD, ADCP measurements, XBT launching, help to PIRATA moorings maintenance.
Dec. 2001	Opportunity campaign on board M/V Skogafoss (EIMSKIP, Island) Reykjavik-Boston (10 days). Water sampling collection and XBT launching (Dr G. Reverdin).

Other activities for the community

Member of the expert board of Dept Océans at l'IRD (2016-)
Member of executive committee of modeling working group at IPSL (2010-)
Member of users committee at IDRIS (CNRS supercomputing center) (2009-2013)

Reviewer for specialized journals: Journal of Geophysical Research, Journal of Climate, Geophysical Research Letters, Climate Dynamics, J. Oceanography, Ocean science, Climate of the past, Science, Nature Climate Change, La Météorologie.
Reviewer for research projects: NSF, LEFE, NERC

Past research projects:
- Influence des fluctuations de la circulation océanique sur l'atmosphère et le climat (LEFE/IDAHO, 2012-2014 P.I. C. Frankignoul),
- NAIV - North Atlantic Inflow Variability, 2012-2014, INSU-LEFE-IMAGO, PI M.A. Sicre, LSCE, France
- EPIDOM (GICC-MEDDEM, 2011-2013, P.I. C. Cassou) PI pour l'IPSL.
- THOR (EU-FP7 2009-2012 P.I. D. Quadfasel),
- SALOUM (INSU/EC2CO 2011-2012, P.I. M. Carré)
- DYNAMITE (EU-FP6 2005-2008 P.I.H. Drange),
- Variabilité de la circulation thermohaline dans l'Atlantique Nord et changements du climat (LEFE IDAO 2006-2008 P.I. C. Frankignoul),
- MISSTERRE (LEFE EVE 2006-2008 P.I. P. Braconnot & S. Planton),
- Kelvin waves and eddies in the tropical off-equatorial basins : morphology, forcing and interactions (CNES/EUMETSAT/NASA/NOAA 2008-2011 P.I A. Lazar)

Past experience

2005-2006	**Post Doc.** at LOCEAN (France) with C. Frankignoul on contract from european project **DYNAMITE**
2004-2005	**Post Doc.** at Potsdam Institute for Climate Impact Research (PIK, Germany). Dept : Climate System (S. Rahmstorf). **Funding from Comer foundation on abrupt climate changes**
2000-2003	**phD in physical oceanography.** Laboratoire d'Océanographie DYnamique et de Climatologie (LODYC, France). Supervision: Prof. C. Frankignoul. Funding from DGA. *Sur la variabilité climatique de la salinité de surface en Atlantique Nord et son lien avec la circulation océanique dans un modèle couplé* Defended on November 28th 2003, with honours
Apr. –Juin 2000	**Internship at LODYC.** Encadrant: Pr.. C. Frankignoul . On the interannual variability of sea surface salinity in a coupled model
Sept.-Dec. 1998	**Internship at Elf Exploration Production** Analysis of current meters data from a mooring in Block 17 (Angola)

Education

2000-2003	**phD physical oceanography** (LODYC, Paris VI). Prof. C. Frankignoul.
Sept. 2001	Geophysical and Environmental Fluid Dynamics **Summer school**. DAMTP. Cambridge (GB). 15 days
1999-2000	**Master Océanologie, Météorologie et Environnement,** Univ. Paris VI Speciality: atmosphere and ocean dynamics. Honours
1996-2000	Engineer at Ecole Supérieure de Physique et de Chimie Industrielles de la Ville de Paris, France. Spécialisation : Physique.

Publications list

The names of co-authors that were students or post-doc under my supervision at the time of the study are underlined.

Peer-reviewed articles published in international scientific journals

Articles submitted

Khodri, M., Izumo, T., Vialard, J., Cassou, C., Lengaigne, M., **Mignot, J**., Guilyardi, E., Lebas, N., Ruprich-Robert, Y., Robock, A., and McPhaden, M. J. M. 2016. How tropical explosive volcanic eruptions trigger El Niño events. Nature Communications, submitted

Articles published or accepted

53. Agathe Germe, Florian Sévellec, **Juliette Mignot**, Didier Swingedouw and Sebastien Nguyen. On the robustness of near term climate predictability regarding initial state uncertainties *Clim. Dyn.,* in press, 10.1007/s00382-016-3078-7

52. **Mignot J**., Garcia-Serrano J, Swingedouw D, Germe A, Nguyen S, Ortega P, Guilyardi E, Ray S Decadal prediction skill in the ocean with surface nudging in the IPSL-CM5A-LR climate model, *Clim. Dyn*. DOI 10.1007/s00382-015-2898-1

2015

51. Born A. **Mignot J.** Stocker T. Multiple Equilibria as a Possible Mechanism for Decadal Variability in the North Atlantic Ocean *Journal of Climate* **28**, 8907-8922. doi: 10.1175/JCLI-D-14-00813.1

50. Polo I., Lazar A. Rodriguez-Fonseca B. and **Mignot J.** (2015) Growth and decay of the Equatorial-South Atlantic SST mode by means of closed heat budget in a coupled General Circulation Model, *Front. Earth Sci*. 3:37. doi: 10.3389/feart.2015.00037

49. Pablo Ortega, **Juliette Mignot**, Didier Swingedouw, Florian Sévellec, Eric Guilyardi (2015) Reconciling two alternative mechanisms behind bi-decadal AMOC variability *Prog. Ocean*. 137(A), pp237-249 doi:10.1016/j.pocean.2015.06.009

48. Lehner, F., F. Joos, C. C. Raible**, J. Mignot**, A. Born, K. Keller, and T. F. Stocker, 2015: Climate and carbon cycle dynamics in a CESM simulation from 850-2100CE. *Earth System Dynamics.* . 6, 411-434, doi:10.5194/esd-6-411-2015

47. Wade M **Mignot J** Lazar A Gaye A T (2015) On the spatial coherence of rainfall over the Saloum delta (Senegal) from seasonal to decadal time scales, *Frontiers in Earth science*. 3-00030, doi :10.3389/feart.2015.00030

46. Camara I, Kolodziejczyk N, **Mignot J** Lazar A and Gaye A.T. (2015) On the seasonal variability of salinity in the tropical Atlantic mixed layer, *J. Geophys. Res.,* 120(6) pp4441-4462, doi : 10.1002/2015JC010865

45. Ray S, Swingedouw D, **Mignot J**, Guilyardi E, (2015) Effect of surface restoring on subsurface variability in a climate model during 1949-2005 *Clim Dyn*, 44(19) 2333-2349, doi 10.1007/s00382-014-2358-3

44. Servonnat J., **J. Mignot**, E. Guilyardi, D. Swingedouw, R. Séférian, S. Labetoulle, (2015) Reconstructing the subsurface ocean decadal variability using surface nudging in a perfect model framework, *Clim. Dyn*. doi: 10.1007/s00382-014-2184-7

43. Lohmann K., **Mignot J.**, Langehaug R., Jungclaus J. H., Matei D., Ottera O.H. Gao Y., Mjell T.L., Ninnemann U. and Kleiven H.F. (2015) Using simulations of the last millennium to understand variability seen in paleo-observations: Similar variation of Iceland-Scotland overflow strength and Atlantic Multidecadal Oscillation, *Climate of the Past*, doi: 10.5194/cp-11-203-2015

42. Swingedouw D., P. Ortega, **J. Mignot**, E. Guilyardi, V. Masson-Delmotte, P. G. Butler and M. Khodri (2015) Bidecadal North Atlantic ocean circulation variability controlled by timing of volcanic eruptions , Nature Communications, doi : 10.1038/ncoms7545

41. Swingedouw D., Rodehacke C., Olsen S., Menary M., Gao Y., Mikolajewicz U., **Mignot J.** (2015) Impact of Greenland ice sheet melting on the Atlantic overturning: A multi-model assessment *Climate Dynamics*, doi : 10.1007/s00382-014-2270-x

2014

40. Séférian R., Bopp L., Gehlen M., Swingedouw D., **Mignot J.**, Guilyardi E., Servonnat J. (2014) The multi-year prediction of Tropical Pacific Marine Productivity, *PNAS*, 111(32) pp. 11646–11651, doi: 10.1073/pnas.1315855111

39. Lohmann, K. Jungclaus J.H., Matei D., **Mignot J.,** Menary M., Langehaug H. R., Ba J., Gao Y., Otterå O. H., Park W. and Lorenz S. (2014) The role of subpolar deep water formation and Nordic Seas overflows in simulated multidecadal variability of the Atlantic overturning, Ocean Science, 10, 227-241, doi:10.5194/os-10-227-2014

38. Sicre, M.A. ; Weckström K. ; Seidenkrantz M. S. ; Kuijpers A. ; Benetti M.; Massé G. ; Ezat U. ; Schmidt S. ; Bouloubassi I. ; Olsen J. ; Khodri M. ; **Mignot J**. (2014) Labrador Current variability over the last 2000 years EPSL, 400, 26-32, DOI: 10.1016/j.epsl.2014.05.016

37. Ba J., Keenlyside N., Latif M., Park W., Ding H., Lohmann K. **Mignot J.,** Menary M., Otterå O.H., Wouters B., Salas-Mélia D., Oka A., Bellucci A., Volodin E. (2014)A multi-model comparison for Atlantic multidecadal variability, *Clim. Dyn*., DOI :10.1007/s00382-014-2056-1

2013

36. Sicre, M.A., M. Khodri **J. Mignot** J. Eiríksson K.L. Knudsen U. Ezat I. Closset P. Nogues G. Massé Sea-surface temperature and sea-ice variability in the sub-polar North Atlantic from explosive volcanism of the Late 13th century, (2013) Geophys. Res. Let., 40-20, 5526-5530, DOI: 10.1002/2013GL057282, 2013

35. **Mignot J.**, D. Swingedouw, J. Deshayes, O. Marti, C. Talandier, R. Séférian, M. Lengaigne, G. Madec, On the evolution of the oceanic component of the IPSL climate models: from CMIP3 to CMIP5, (2013) Ocean Modelling, 72, 167-184 DOI : 10.1016/j.ocemod.2013.09.001, 2013

34.Swingedouw D., Rodehacke C., Behrens E., Menary M., Olsen S., Gao Y., Mikolajewicz U., **Mignot J.**, Biastoch A. Decadal fingerprints of fresh water discharge around Greenland in a multi-models ensemble. *Climate Dynamics*. Accepted DOI: 10.1007/s00382-012-1479-9

33.Langehaug H. R., P. B. Rhines, T. Eldevik, **J. Mignot** and K. Lohmann Water mass transformation and the North Atlantic Current in three multi-century climate model simulations, JGR, accepted

32. Gerald A. Meehl, Lisa Goddard, Ben Kirtman, Grant Branstator, Gokhan Danabasoglu, Ed Hawkins, Arun Kumar, Tony Rosati, Doug Smith, Rowan Sutton, George Boer, Robert Burgman, Christophe Cassou, Susanna Corti, Alicia Karspeck, Noel Keenlyside, Masahide Kimoto, Daniela Matei, **Juliette Mignot**, Rym Msadek, Antonio Navarra, Holger Pohlmann, Michele Rienecker, Edwin Schneider, Claudia Tebaldi, Haiyan Teng, Geert Jan van Oldenborgh, Gabriel Vecchi, and Steve Yeager Decadal Climate Prediction: An Update from the Trenches, BAMS, accepted.

31.Dufresne J-L · Foujols, M-A · Denvil, S. · Caubel, A. · Marti, O. · Aumont, O · Balkanski, Y · Bekki, S · Bellenger, H · Benshila, R · Bony, S · Bopp, L · Braconnot, P · Brockmann, P · Cadule, P · Cheruy, F · Codron, F · Cozic, A · Cugnet,D · deNoblet,N · Duvel,J-P · Eth´e,C · Fairhead, L · Fichefet, T · Flavoni, S · Friedlingstein, P · Grandpeix, J-Y · Guez, L · Guilyardi, E · Hauglustaine, D · Hourdin, F · Idelkadi, A · Ghattas, J · Joussaume, S · Kageyama, M · Krinner, G · Labetoulle, S · Lahellec, A · Lefebvre, M-P · Lefevre, F · Levy, C · Li, Z. X. · Lloyd, J · Lott, F · Madec, G · Mancip, M · Marchand, M · Masson, S · Meurdesoif, Y · **Mignot, J** · Musat, I · Parouty, S · Polcher, J · Rio, C · Schulz, M · Swingedouw, D · Szopa, S · Talandier, C · Terray, P · Viovy, N Climate change projections using the IPSL-CM5 Earth System Model: from CMIP3 to CMIP5, ClimDyn., 40, 2123-2165, 2013

30. Swingedouw D., **Mignot J.,** Labetoulle S., Guilyardi E., Madec G. : Initialisation and predictability of the AMOC over the last 50 years in a climate model, Clim. Dyn., 40, 2381-2399. DOI: 10.1007/s00382-012-1516-8, 2013

29.Persechino A., **Mignot J.,** Swingedouw D., Labetoulle, S. and Guilyardi E. : Decadal predictability of the Atlantic Meridional Overturning Circulation and Climate in the IPSLCM5A-LR model Clim. Dyn., 40, 2359-2380. DOI: 10.1007/s00382-012-1466-1, 2013.

28.Escudier R., **Mignot J.** and Swingedouw D. : A 20-yrs coupled ocean-sea ice-atmosphere variablility mode in the North Atlantic in an AOGCM Clim. Dyn., 2012, 40, 619-636, DOI: 10.1007/s00382-012-1402-4, 2013

2012

27. Vecchi G. A.,Msadek R., Delworth T.L., Dixon K. W., Guilyardi E., Hawkins E. Karspeck A.R. **Mignot J.** Robson J. Rosati A. Zhang R. Comment on "Multiyear Prediction of Monthly Mean Atlantic Meridional Overturning Circulation at 26.5°N", by D. Matei and co-authors, *Science* (2012) 338 no. 6107 p. 604
DOI: 10.1126/science.1222566

26. **Mignot, J.**, A. Lazar and M. Lacarra On the formation of Barrier Layers and associated vertical temperature inversions: a focus on the northwestern tropical Atlantic. 2012, J. Geophy.Res 117, C2, doi:10.1029/2011JC007435

25. Ortega P., Montoya M., González-Rouco F., **Mignot J.**, and Legutke S. Variability of the Atlantic meridional overturning circulation in the last millennium and two IPCC scenarios, Climate Dynamics, 2012, 38 (9-10), p. 1925-1947, doi: 10.1007/s00382-011-1081-6

24.Born A. and **J. Mignot** Dynamics of decadal variability in the Atlantic subpolar gyre: a stochastically forced oscillator Climate Dynamics 2012, 39 (1), p. 461-474, doi : 10.1007/s00382-011-1180-4

2011

23. **Mignot, J.**, M. Khodri, C. Frankignoul, J. Servonnat Volcanic impact on the Atlantic ocean over the last millennium. 2011. Climate of the Past 2011 7(4). pp1439-1455, doi: 10.5194/cp-7-1439-2011

22.Sicre M.-A., I. Hall, **J. Mignot**, M. Khodri, Ezat, Truong, Eiriksson , Knudsen Sea surface temperature variability in the subpolar Atlantic over the last millennium: a model/data comparison, 2011, Paleoceanography 26, 4, doi:10.1029/2011PA002169

21.Marini C., Frankignoul C., **Mignot J.**. Links between the southern annular mode and the Atlantic meridional overturning circulation in a climate model. Journal of Climate, 2011, 24 (3), p. 624-640, doi: 10.1175/2010JCLI3576.1

2010

20.Marti O., Braconnot P., Dufresne J. L., Bellier J., Benshila R., Bony S., Brockmann P., Cadule P., Caubel A., Codron F., Noblet de N., Denvil S., Fairhead L., Fichefet T., Foujols M. A., Friedlingstein P., Goosse H., Grandpeix J. Y., Guilyardi E., Hourdin F., Idelkadi A., Kageyama M., Krinner G., Levy C., Madec G., **Mignot J.**, Musat I., Swingedouw D.,

Talandier C. Key features of the IPSL ocean atmosphere model and its sensitivity to atmospheric resolution. Climate Dynamics, 2010, 34 (1), p. 1-26.

19.Marzeion B., Levermann A., **Mignot J.**. Sensitivity of North Atlantic subpolar gyre and overturning to stratification-dependent mixing : response to global warming. Climate Dynamics, 2010, 34 (5), p. 661-668.

18.Mignot J., Frankignoul C. Local and remote impacts of a tropical Atlantic salinity anomaly. Climate Dynamics, 2010, 35 (7-8), p. 1133-1147, doi: 10.1007/s00382-009-0621-9

2009

17.Born A., Levermann A., **Mignot J.**. Sensitivity of the Atlantic Ocean circulation to a hydraulic overflow parameterisation in a coarse resolution model : response of the subpolar gyre. Ocean Modelling, 2009, 27 (3-4), p. 130-142.

16.Kageyama M., **Mignot J.**, Swingedouw D., Marzin C., Alkama R., Marti O. Glacial climate sensitivity to different states of the Atlantic Meridional overturning circulation : results from the IPSL model. Climate of the Past, 2009, 5 (3), p. 551-570.

15.Mignot J., Boyer Montégut de C., Tomczak M. On the porosity of barrier layers. Ocean Science, 2009, 5 (3), p. 379-387.

14.Swingedouw D., Mignot J., Braconnot P., Mosquet E., Kageyama M., Alkama R. Impact of freshwater release in the North Atlantic under different climate conditions in an OAGCM. Journal of Climate, 2009, 22 (23), p. 6377-6403.

2008

13.Breugem W.P., Chang P., Jang C.J., **Mignot J.**, Hazeleger W. Barrier layers and tropical Atlantic SST biases in coupled GCMs. Tellus, 2008, 60 (5), p. 885-897.

2007

12.Levermann A., **Mignot J.**, Nawrath S., Rahmstorf S. The role of Northern Sea ice cover for the weakening of the thermohaline circulation under global warming. Journal of Climate, 2007, 20 (16), p. 4160-4170.

11.Marzeion B., Levermann A., **Mignot J**.. The role of stratification-dependent mixing for the stability of the Atlantic overturning in a global climate model. Journal of Physical Oceanography, 2007, 37 (11), p. 2672-2681 + p. 273.

10.Mignot J., Ganopolski A., Levermann A. Atlantic surface temperatures : response to a shutdown of the overturning circulation and consequences for its recovery. Journal of Climate, 2007, 20 (19), p. 4884-4898, doi: 10.1175/JCLI4280.1

9.Mignot J., Boyer Montégut de C. D., Lazar A., Cravatte Sophie. Control of salinity on the mixed layer depth in the world ocean : 2. Tropical areas - art. no. C10010. Journal of Geophysical Research Oceans, 2007, 112 (C10), p. 48-59.

8.Montégut C. D., **Mignot J.** Lazar A., Cravatte Sophie. Control of salinity on the mixed layer depth in the worl. ocean : 1. General description - art. no. C06011. Journal of Geophysical Research Oceans, 2007, 112 (C6), p. 30-41.

2006

7. **Mignot J**., A . Levermann, A. Griesel A Decomposition of the Atlantic Meridional Overturning Circulation into Physical Components Using Its Sensitivity to Vertical Diffusivity 2006, J. Phys. Oceanogr., 36, 636–650. doi: http://dx.doi.org/10.1175/JPO2891.1

6.Goelzer H., **Mignot J.,** Levermann A., Rahmstorf S. Tropical versus high latitude freshwater influence on the Atlantic circulation. Climate Dynamics, 2006, 27 (7-8), p. 715-725.

2005

5. Montoya M., Griesel A., Levermann A., **Mignot J.,** Hofmann M., Ganopolski A., Rahmstorf S. The earth system model of intermediate complexity CLIMBER-3alpha : part 1. Description and performance for present-day conditions. Climate Dynamics, 2005, 25 (2-3), p. 237-263.

4.Mignot J. and Frankignoul C. (2005) On the variability of the Atlantic meridional overturning circulation, the NAO and the ENSO in the Bergen Climate Model. *Journal of Climate* 18(13)2361-2375, doi : 10.1175/JCLI3405.1

2004

3.Mignot J. and Frankignoul C. (2004) Interannual to interdecadal variability of sea surface salinity in the Atlantic and its link to the atmosphere in a coupled model.. *JGR-Oceans*. 9 (C4) C04005 (doi 10.1029/2003JC002005).

2003

2.Mignot J. and Frankignoul C. (2003) On the interannual variability of surface salinity in the Atlantic. *Climate Dynamics*. 20:555-565

2002

1.Frankignoul C., Kestenare E. and **Mignot J.** (2002): The surface heat flux feedback. Part II: direct and indirect estimates in the ECHAM4/OPA8 coupled GCM. *Climate Dynamics*. 19:649-655, doi : 10.1007/s00382-002-0253-9

Non peer-reviewed articles in international scientific journals

1. **Mignot J.** and Bony S. Presentation and analysis of the IPSL and CNRM climate

models used in CMIP5, special issue cover letter, Clim. Dyn., DOI 10.1007/s00382-013-1720-1

2. Tomczak, M., **Mignot, J.** And de Boyer Montégut C., How permeable is the barrier layer ? Bulletin of the Australian Meteorological and oceanographic society, 2008, vol. 21, p 129-132

Non peer-reviewed articles in collective production

1. Sicre, M.A., M. Khodri, J. Mignot, P. Allard, Y. Balkanski, E. Bard, effet des eruptions volcaniques sur le climat,, dans "Le climat à découvert, outils et méthode en recherche climatique», sous la direction de Catherine Jeandel et Rémy Mosseri (édition CNRS, 288 pages)

2. Céron, J.P. M. Déqué et J. Mignot, les previsions climatiques, dans "Le climat à découvert, outils et méthode en recherche climatique», sous la direction de Catherine Jeandel et Rémy Mosseri (édition CNRS, 288 pages)

Peer-reviewed articles in national journals

Cassou C. and **Mignot J.** Enjeux, méthodes et fondamentaux de prévisibilité et prévision décennale, La Météorologie, 2013, n°81, pp23-30.

Khodri M., Swingedouw D., **Mignot J.**, Sicre M.A., Garnier E., Masson-Delmotte V., Ribes A., Terray L. (2015) Le climat du dernier millénaire, *La Météorologie*, 88, 36-47.

Boucher, Olivier; Dufresne, Jean-Louis; Vial, Jessica; Brun, Eric; Cattiaux, Julien; Chauvin, Fabrice; Salas y Mélia, David; Voldoire, Aurore; Bopp, Laurent; Braconnot, Pascale; Ciais, Philippe; Yiou, Pascal; Guilyardi, Eric; **Mignot, Juliette**; Guivarch, Céline (2015) Projection des changements climatiques futurs, *La Météorologie,* 88, DOI : 10.4267/2042/56362

Non peer-reviewed articles in national journals

Mignot J. and Swingedouw D. : A 20-yrs coupled ocean-sea ice-atmosphere variablility mode in the North Atlantic in an AOGCM, LMDZ Info 2012

Invited presentations

International conferences:

Mignot J. *modeling of the Atlantic meridional circulation, shut-down and recovery* 9th International Conference on Paleoceanography, Shanghai, September 3rd-7th 2007.

Mignot J. *The impact of volcanic activity on Atlantic Meridional Overturning Circulation variability* CLIVAR-ICTP International Workshop on Decadal Climate Variability and Predictability: Challenge and Opportunity, ICTP, Trieste, oct 16-20 2015

International workshops

Mignot J.,Swingedouw D., Labetoulle S. Guiyardi E., Persechino A., Servonnat J. *Decadal predictions at IPSL*, Aspen Global Change Institute workshop "Making sense of the multi-model decadal prediction experiments from CMIP5.", June 2011

Chapter 8

Selection of 5 Publications

Mignot J. and Frankignoul C. (2005) On the variability of the Atlantic meridional overturning circulation, the NAO and the ENSO in the Bergen Climate Model. Journal of Climate 18(13)2361-2375, doi: 10.1175/JCLI3405.1

Mignot J., Ganopolski A., Levermann A. Atlantic surface temperatures : response to a shutdown of the overturning circulation and consequences for its recovery. Journal of Climate, 2007, 20 (19), p. 4884-4898, doi: 10.1175/JCLI4280.1

Mignot, J., M. Khodri, C. Frankignoul, J. Servonnat Volcanic impact on the Atlantic ocean over the last millennium. 2011. Climate of the Past 2011 7(4). pp1439-1455, doi: 10.5194/cp-7-1439-2011

Mignot, J., A. Lazar and M. Lacarra On the formation of Barrier Layers and associated vertical temperature inversions: a focus on the northwestern tropical Atlantic. 2012, J. Geophy.Res 117, C2, doi:10.1029/2011JC007435

Mignot J., Garcia-Serrano J, Swingedouw D, Germe A, Nguyen S, Ortega P, Guilyardi E, Ray S Decadal prediction skill in the ocean with surface nudging in the IPSL-CM5A-LR climate model, Clim. Dyn, doi: 10.1007/s00382-015-2898-1

The Variability of the Atlantic Meridional Overturning Circulation, the North Atlantic Oscillation, and the El Niño–Southern Oscillation in the Bergen Climate Model

JULIETTE MIGNOT

Potsdam Institute for Climate Research Impact, Potsdam, Germany, and Laboratoire d'Océanographie Dynamique et de Climatologie, Institut Pierre-Simon Laplace, Université Pierre et Marie Curie, Paris, France

CLAUDE FRANKIGNOUL

Laboratoire d'Océanographie Dynamique et de Climatologie, Institut Pierre-Simon Laplace, Université Pierre et Marie Curie, Paris, France

(Manuscript received 28 May 2004, in final form 29 October 2004)

ABSTRACT

The link between the interannual to interdecadal variability of the Atlantic meridional overturning circulation (AMOC) and the atmospheric forcing is investigated using 200 yr of a control simulation of the Bergen Climate Model, where the mean circulation cell is rather realistic, as is also the location of deep convection in the northern North Atlantic. The AMOC variability has a slightly red frequency spectrum and is primarily forced by the atmosphere. The maximum value of the AMOC is mostly sensitive to the deep convection in the Irminger Sea, which it lags by about 5 yr. The latter is mostly forced by a succession of atmospheric patterns that induce anomalous northerly winds over the area. The impact of the North Atlantic Oscillation on deep convection in the Labrador and Greenland Seas is represented realistically, but its influence on the AMOC is limited to the interannual time scale and is primarily associated with wind forcing. The tropical Pacific shows a strong variability in the model, with too strong an influence on the North Atlantic. However, its influence on the tropical Atlantic is realistic. Based on lagged correlations and the release of fictitious Lagrangian drifters, the tropical Pacific seems to influence the AMOC with a time lag of about 40 yr. The mechanism is as follows: El Niño events induce positive sea surface salinity anomalies in the tropical Atlantic that are advected northward, circulate in the subtropical gyre, and then subduct. In the ocean interior, part of the salinity anomaly is advected along the North Atlantic current, eventually reaching the Irminger and Labrador Seas after about 35 yr where they destabilize the water column and favor deep convection.

1. Introduction

The Atlantic meridional overturning circulation (AMOC), defined here as the integrated meridional transport in the Atlantic as, for example, in Wunsch (2002), plays an essential role in the maintenance of the Northern Hemisphere climate as it transports a substantial amount of warm and saline waters poleward. Ganachaud and Wunsch (2000) estimated the maximum value of the northward heat transport to 1.3 PW around 25°N, associated to a volume of 15 ± 2 Sv (1 Sv $\equiv 10^6$ m^3 s^{-1}) of North Atlantic Deep Water circulating in the Atlantic. Talley et al. (2003) recently estimated this volume to be 18 Sv. Variations of this intensity are likely to significantly alter the climate in the North Atlantic (e.g., Manabe and Stouffer 1999). Direct observations are still lacking (Siedler et al. 2001), but modeling studies suggest that the AMOC substantially varies on the decadal to centennial time scales. The relative importance of atmosphere forcing, air–sea feedback, oceanic feedback, and nonlinearities in generating this variability remains however to be clarified. Decadal to centennial oscillations linked to oceanic processes have been found in oceanic general circulation models (OGCMs) using idealized surface boundary conditions or coupled to a simple energy balance atmospheric model (e.g., Mikolajewicz and Maier-Reimer 1990; Weaver et al. 1991; Chen and Ghil 1996; among many others). A substantial interdecadal vari-

Corresponding author address: Dr. Juliette Mignot, Potsdam Institute for Climate Research Impact, Telegrafenberg A26, 14412 Potsdam, Germany.
E-mail: juliette.mignot@pik-potsdam.de

ability is also found in more realistic climate models. Delworth et al. (1993) suggested that North Atlantic fluctuations with a dominant time scale of approximately 50 yr appeared in the Geophysical Fluid Dynamics Laboratory (GFDL) model because salinity anomalies advected toward the high latitudes were influencing the strength of the meridional overturning circulation. A phase lag between the horizontal and the meridional circulations was responsible for the quasi-oscillatory behavior, but the variability appeared to be primarily forced by the natural variability of the surface heat flux, without significant back action on the atmosphere (Delworth and Greatbatch 2000). On the other hand, Timmermann et al. (1998) proposed a coupled mechanism to explain a 35-yr mode of North Atlantic variability in the ECHAM3–LSG model. When the AMOC was anomalously strong, a warm sea surface temperature (SST) anomaly appeared in the North Atlantic, and its impact on the atmosphere resulted in a strengthened North Atlantic Oscillation (NAO) and hence decreased evaporation and Ekman transport in the Greenland Sea and off Newfoundland. This led to negative sea surface salinity (SSS) anomalies in the oceanic sinking regions, weakening the deep convection and subsequently the AMOC, thus reversing the changes. A different coupled mechanism was suggested by Vellinga et al. (2002) for the Third Hadley Centre Coupled Ocean–Atmosphere General Circulation Model (HadCM3). When the AMOC was anomalously weak, the North Atlantic was anomalously cold and the tropical South Atlantic was anomalously warm, which displaced the intertropical convergence zone southward. There was thus less precipitation north of the equator, which reduced the northward oceanic freshwater transport and led after about six decades to more saline surface conditions in the North Atlantic. This increased the AMOC and reversed the changes. Remote atmospheric forcing may also lead to a substantial AMOC variability, as shown by Latif et al. (2000) and Thorpe et al. (2001) in global warming conditions. In both models, the global warming led to a freshening and warming of the high latitudes, but positive SSS anomalies were created in the tropical Atlantic by enhanced large-scale air–sea interactions with the tropical Pacific. The AMOC was thus stabilized by the compensating advection of high salinity anomalies into the sinking region. In Latif et al. (2000), the interactions between the tropical Atlantic and Pacific were similar to those operating during present-day El Niño–Southern Oscillation (ENSO), but whether ENSO could have a direct impact on the AMOC in present-day conditions has not been established.

In summary, the strength and the nature of the AMOC coupling with the atmosphere remains an open question. In this paper, we focus on the response of the AMOC to the atmospheric forcing in a control run with the Bergen Climate Model (BCM). The simulation is presented in section 2. The AMOC variability is briefly described in section 3, as well as its link with deep convection in the North Atlantic. The influence of the NAO is investigated in section 4. In section 5, we show that ENSO could have a delayed impact on the model AMOC. Conclusions are given in section 6.

2. Data

The BCM is described in Furevik et al. (2003), where specific details on the model and experiment setup can be found, so that only a brief outline is given here. The model couples the Action de Recherche Petite Echelle Grand Echelle/Integrated Forecasting System (ARPEGE/IFS) atmospheric general circulation model (Déqué et al. 1994) in T_L63 resolution (2.8° along the equator) with 31 vertical levels to a global, 24-layer version of the Miami Isopycnic Coordinate Ocean Model (MICOM; Bleck et al. 1992) that incorporates the dynamic and thermodynamic sea ice modules of Drange (1999). The oceanic grid has a 2.4° zonal resolution. The meridional resolution is 2.4° except equatorward of about 10° of latitude, where it gradually increases to 0.8°. The data on isopycnal levels were interpolated on the Levitus z-levels with a simple first-order remapping scheme. After spinup of 20 yr, the BCM was integrated for 300 yr with fixed heat and freshwater flux adjustments that contribute to the realism of the model climate state and reduce the model drift. As described by Furevik et al. (2003), the (seasonally varying) flux adjustment had been estimated in a prior run where SST and SSS were restored to the observed climatology. The time series of the maximum of the Atlantic meridional streamfunction in the North Atlantic between 10° and 70°N, and between 500 and 5000-m depth, hereafter called the Meridional Overturning Index (MOI; see section 3) is shown in Fig. 1. As in Mignot and Frankignoul (2004), we only considered the middle 200 yr of the simulation. The last 50 yr were not considered, as the meridional overturning streamfunction started drifting during the last 10 yr—presumably because of a slight imbalance in the flux adjustments in the northern North Atlantic—nor were the first 50 yr, in order to leave more time for the ocean to reach an approximate steady state (a very conservative choice).

The main characteristics of the AMOC have been discussed by Bentsen et al. (2004). Here, we focus on

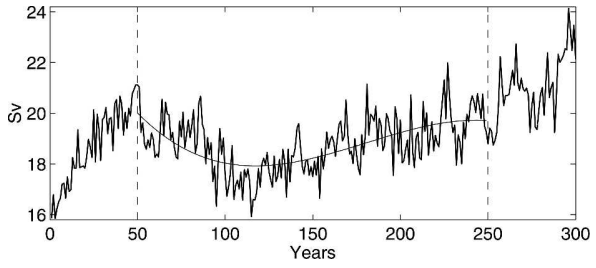

FIG. 1. Raw MOI time series over the 300 yr of the model run. The vertical dashed lines show the limits of the 200 yr that are considered in the present study. The smooth curve indicates the third-order polynomial fit of the time series.

the AMOC variability on annual to multidecadal time scales in the 200 yr of data. As a drift may influence the lowest frequencies, a third-order polynomial was first removed by least squares fit from each variable at each grid point. This is illustrated for the MOI in Fig. 1, which shows that only centennial and longer time scales are affected by the detrending. The shorter (interannual) time scales are investigated below using the detrended annual means, and the longer (decadal) ones by further filtering periods smaller than 10 yr with the continuous wavelet transform technique (e.g., Daubechies 1992) from the detrended annual means. Monthly anomalies were also considered by subtracting the mean seasonal cycle from the detrended monthly averages. Significance of correlations between annual (decadal) time series are calculated using the Student's *t* test assuming independent samples at a 1-yr (5-yr) interval.

3. The natural variability of the Atlantic meridional overturning circulation

The 200-yr mean Atlantic meridional streamfunction is shown in Fig. 2. It has features similar to the mean AMOC inferred from observational estimates (Ganachaud and Wunsch 2000; Talley et al. 2003): about 18 Sv of warm water flows northward in the upper ocean, mainly in the Gulf Stream and North Atlantic Current, sinks at high latitudes, and returns southward at depth as North Atlantic Deep Water (NADW). The simulated poleward transport of Atlantic Water across the Greenland–Scotland ridge (8.2 Sv) is very close to observation-based estimates, as discussed by Otterå et al. (2003). Note that the overflow of very deep waters over the ridges between Greenland and Scotland and the associated changes of water mass properties occurring northward appear more clearly when the streamfunction is represented as a function of density rather than depth (Gao et al. 2003). The deep circulation cell of

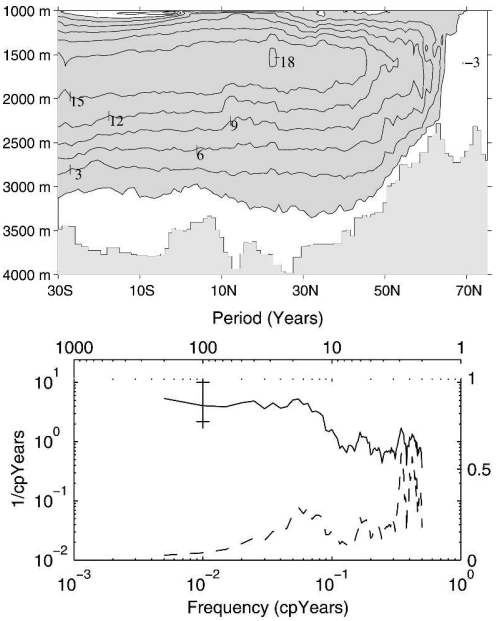

FIG. 2. (top) Mean AMOC in the BCM. (bottom) Spectrum of the (detrended) MOI, in log–log units (solid line) and in log–linear units (variance preserving spectrum: dashed line). The spectrum was calculated by the multi-taper method using four tapers. The vertical line indicates the 90% confidence interval.

Antarctic Bottom Water (AABW) that should lie beneath the NADW is not simulated. This is a common default of isopycnic models that use a reference pressure at the surface when computing potential density, which results in an incorrect representation of the cold deep waters from the Antarctic (DYNAMO Group 1997). Although interactions between NADW and AABW are still poorly known, we focus on the NADW cell variability and its link with the atmospheric forcing, and this deficiency should have limited influence.

In their analysis, Bentsen et al. (2004) characterized the natural variability of the AMOC using the time series [principal component (PC)] of its leading empirical orthogonal function (hereafter PC1). However, the latter may be too constraining to fully represent the AMOC variability as it refers to a fixed spatial pattern. Thus, we use instead the (detrended) time series of the maximum value reached by the AMOC between 10° and 70°N, and 500- and 5000-m depth, which can be seen in Fig. 1. In the BCM simulation, the latitude of the maximum is almost constant in time, around 23°N, and its value is strongly correlated (0.8) to PC1. The results below are thus very similar to both time series. Following Delworth et al. (1993), we refer to our index as the Meridional Overturning Index. Most of its variance is found at decadal time scales, but its frequency spectrum has no significant peak on time scales shorter

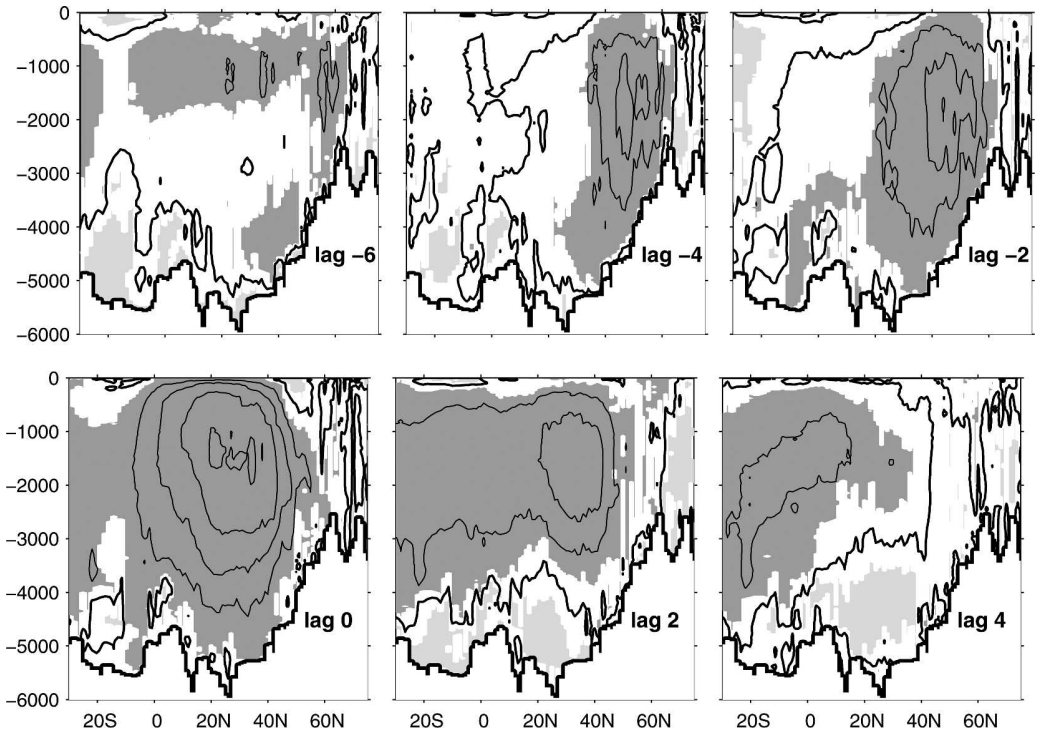

FIG. 3. Regression of the AMOC on the MOI. AMOC leads at negative lags (in years). The contour interval is 0.2 Sv, continuous for positive and dashed for negative values. The thick contour denotes zero. Light (dark) shaded areas are negative (positive) and significant at the 10% level.

than 50 yr (not shown). Note that the time series is too short to see oscillations on longer time scales.

To investigate the variability of the AMOC, we regressed it on the MOI as a function of time lag (Fig. 3). A significant anomalous positive overturning cell appears at high latitudes about 5 yr prior to the AMOC maximum and progressively expands to the south, occupying the whole North Atlantic basin by lag −1 (cf. lags −2 and 0 in the figure). The maximum anomaly keeps progressing southward and loses significance at high and midlatitudes after a lag of 4 yr. As the AMOC variability seems to originate from the high latitudes, it is likely to be linked to deep convection in the North Atlantic. To account for the intermittent character of the deep convection phenomenon, the deep convection sites were defined by a criterion on mixed layer depth variability, namely where the standard deviation of the mixed layer depth in March exceeds 320 m. Results are identical when using as a criterion that the maximal depth reached over the average annual cycle exceeds 1000 m (Fig. 4). Note that we use the mixed-layer depth directly coming from the isopycnal integration, as detailed in Furevik et al. (2003). As in Bentsen et al. (2004), three deep-water formation sites are identified: the Labrador Sea; the Greenland, Iceland, and Norwegian (GIN) Seas; and the Irminger Sea. Maximum mixed layer depths in the model are reached in the Irminger Sea. Observational evidence for deep convection in this area is recent (Bacon et al. 2003; Pickart et al. 2003b), and it seems to only reach depths of about 1000 m, versus 2000 m in the model. In the Labrador and GIN Seas, deep convection has often been ob-

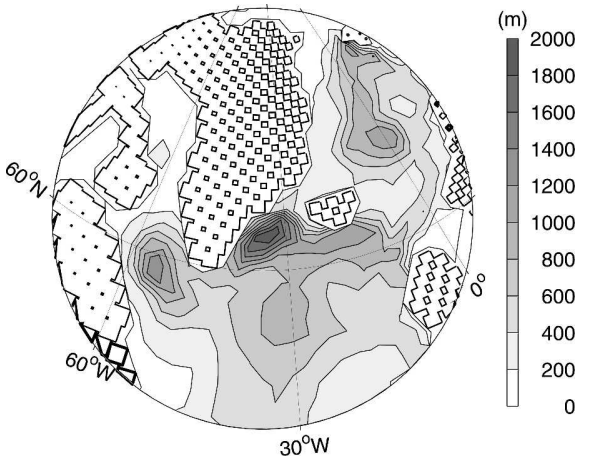

FIG. 4. Maximal depth of the mixed layer over the annual cycle.

served (e.g., Clarke and Gascard 1983; Schott et al. 1993), reaching about a 2000- and 1500-m depth, respectively (Marshall and Schott 1999). In the model, deep convection is also found at these locations, but it is too shallow by about 400 m.

Dickson et al. (1996) showed in the observations that a positive phase of the NAO enhances deep convection in the Labrador Sea but reduces it in the GIN Seas, and vice versa. In the BCM simulation, the atmospheric patterns associated with deep convection in the two areas are indeed very similar to the NAO (see Bentsen et al. 2004, their Fig. 9), and the winter mixed layer depth is well correlated with the NAO time series (Fig. 5). The NAO index is defined here as the time series of the leading empirical function of the sea level pressure (SLP) over the North Atlantic sector, which compares well with the observations (Furevik et al. 2003). It typically varies on time scales of a few weeks, as in the observations (Feldstein 2000), and has only a little month-to-month persistence and none from one year to the next in the model. Monthly anomalies indicate that the NAO leads enhanced (weakened) deep convection in the Labrador (GIN) Sea by 1 month (not shown).

Deep convection in the Irminger Sea might also occur during positive NAO phases in the observations (Pickart et al. 2003a). In the model, however, it is only weakly related to the NAO (Fig. 5), presumably because of the limited spatial resolution. Instead it seems to respond to a complex series of atmospheric conditions in the North Atlantic, starting on the average 3 yr prior to a deep convection maximum (Fig. 6). The anomalous SLP pattern first resembles a negative NAO phase (lag −3), but it then mostly reduces to a low pressure monopole centered west (lag −2) and then east (lag −1) of Iceland. As shown by the arrows in Fig. 6, the cyclonic circulation induces significant anomalous cold northerly winds and evaporation over the Irminger Sea (see also Bentsen et al. 2004). The surface waters become colder and saltier, and they sink when dense enough. As opposed to the Labrador and GIN Seas where deep convection is forced by short-term changes in a standing atmospheric pattern (the NAO), the Irminger Sea deep convection is thus forced by a long-term succession of atmospheric patterns. It is interesting to note that in the GFDL coupled model, anomalously cold SSTs in the Irminger Sea are also associated with surface pressure and northerly wind anomalies that have their largest amplitude approximately 2 yr before (Delworth et al. 1997). In both models, the northerly winds increase the East Greenland current by lag −1, but SSS anomalies are advected from the Arctic in the GFDL model while no evidence of an advective mechanism is found in the BCM, where density anomalies are mostly created by the local atmospheric fluxes, as described above.

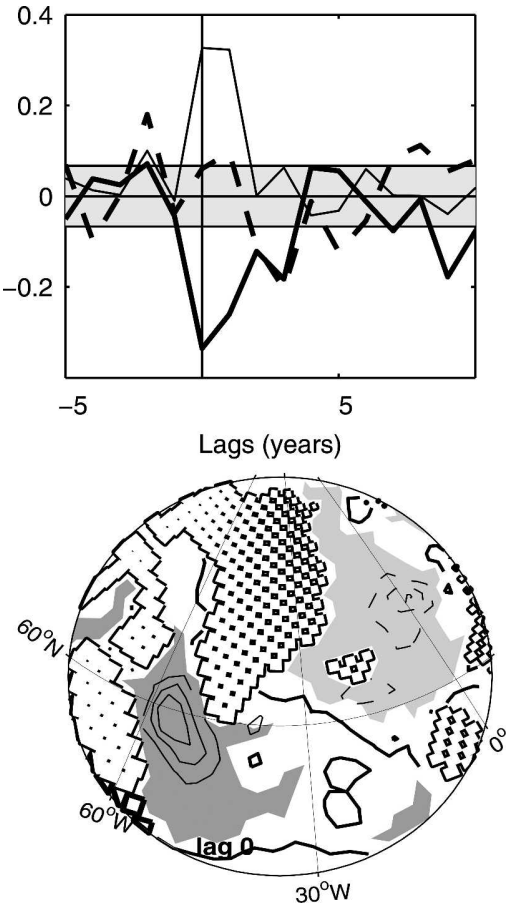

FIG. 5. (top) Cross correlation between the annual NAO time series and the mixed layer depth averaged over the areas of deep convection during the winter season (Jan–Apr). The NAO leads at positive lags. The thin line refers to the Labrador Sea, the dashed line to the Irminger Sea, and the thick line to the GIN Seas. The gray area limits the 10% significant domain. (bottom) Regression of the annual mixed layer depth on the normalized annual NAO time series. The contour interval is 10 m. The contours and shadings are as in Fig. 3.

The strength of the cross correlations between the oceanic surface characteristics in the deep convection areas and the MOI shown in Fig. 7 indicates that in the BCM simulation, the AMOC is most sensitive to deep convection in the Irminger Sea, where an anomalously deep, dense, salty, and cold mixed layer leads the MOI by about 5 yr. The correlations between the MOI and the deep convection parameters in the Labrador and GIN Seas are much weaker, suggesting that they play a lesser role. Bentsen et al. (2004) have shown that the high-latitude AMOC anomalies propagate southward in the Atlantic basin as a coastally trapped wave, as in

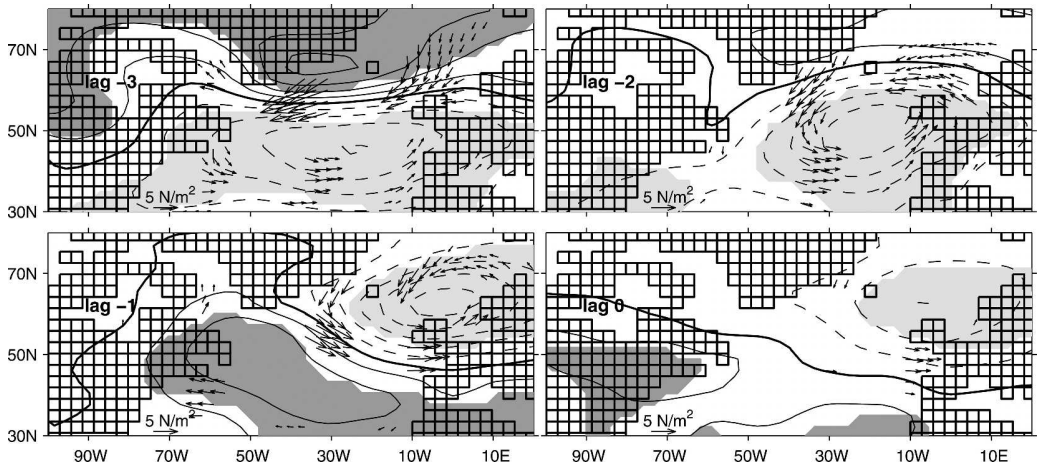

FIG. 6. Lagged regression of SLP (contours) and wind stress (arrows) anomalies onto the anomalous deep convection in the Irminger Sea. The atmosphere leads at negative lags (in years). Only the vectors with at least one significant component at the 10% level are shown. The contour interval is 0.1 hPa. The contours and shadings are as in Fig. 3.

Kawase (1987) and Yang (1999). The time scale is however longer since Kelvin baroclinic waves are not present in coarse resolution models where the Rossby radius is not resolved but replaced by viscous boundary waves (e.g., Hsieh et al. 1983; Killworth 1985), which have a much slower propagation speed. This may explain why the perturbation takes about 6 yr to reach the equator. The exact time scale also probably depends on the resolution and the type of grid. Note that it is of the same order of magnitude as that found by Eden and Willebrand (2001) in a low-resolution OGCM.

4. The Atlantic meridional overturning circulation and the NAO

Previous modeling studies have suggested that the NAO has a strong impact on the thermohaline circulation (THC) through mechanical wind or buoyancy forcing (Timmermann et al. 1998; Delworth and Greatbatch 2000; Eden and Willebrand 2001). Since in the BCM simulation the NAO triggers deep convection in the Labrador and GIN Seas (Fig. 5), it is of interest to investigate its influence on the AMOC. Regressing the AMOC on the monthly NAO time series only shows significant correlation when the AMOC is in phase with the NAO or follows by a few months. The monthly AMOC anomaly that covaries with the NAO is very significant (Fig. 8) and is essentially due to Ekman pumping. During a positive NAO phase, the Ekman pumping is anomalously negative between 32° and 55°N as a consequence of the convergence of the Ekman currents due to the intensification of the westerlies and the trade winds, and anomalously positive elsewhere. The horizontal circulation is maximum at the surface and almost constant beneath the mixed layer, suggesting a barotropic response to the wind forcing, as in Eden and Willebrand (2001) and Hakkinen (1999). The barotropic response persists little, about 1 month at extratropical latitudes and up to 4 months in the subtropics, with a weak southward propagation.

To search for the baroclinic AMOC response that should appear at longer time lags, the same analysis is repeated with annual means (Fig. 9). At lag 0, we primarily detect the rapid wind-induced barotropic response (left). When the AMOC follows the NAO by 1 yr (middle), the AMOC response is composed of two cells that are almost opposite to the ones in phase. A large positive cell that is weak at the surface and maximum between 1000 and 2000 m is centered at 50°N and persists up to lag 3. A weak negative cell is located farther south around 20°N, with a maximum near 500 m, but significance is lost by lag 2. This pattern resembles the baroclinic response to the NAO winds found by Eden and Willebrand (2001), except that it only appears after 3 yr in their model. Note that the associated horizontal currents (not shown) resemble the gyre variability discussed by Curry and McCartney (2001) and Marshall et al. (2001). No significant signal is found when the AMOC leads.

In spite of their different structure, the NAO-induced AMOC patterns are not independent from that associated with the MOI, as defined by lag 0 in Fig. 3: the spatial correlation is 0.64 for the in-phase barotropic structure of Fig. 9 (left) and −0.56 for the baroclinic

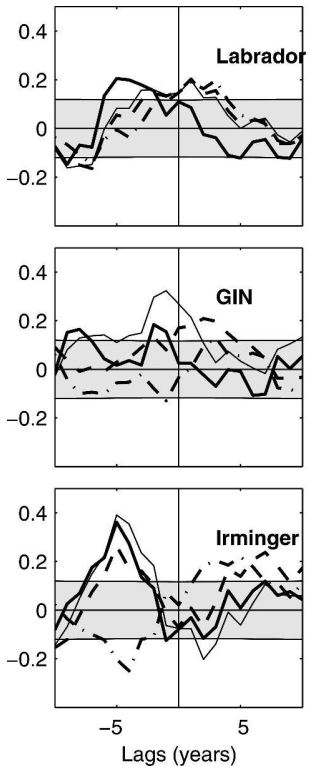

FIG. 7. Cross correlation between the annual MOI and the winter (Jan–Apr) mixed layer depth (thick line), sea surface density (thin line), SSS (dashed line), and SST (mixed line). The gray area delimits the 10% significant domain. The MOC leads at positive lags.

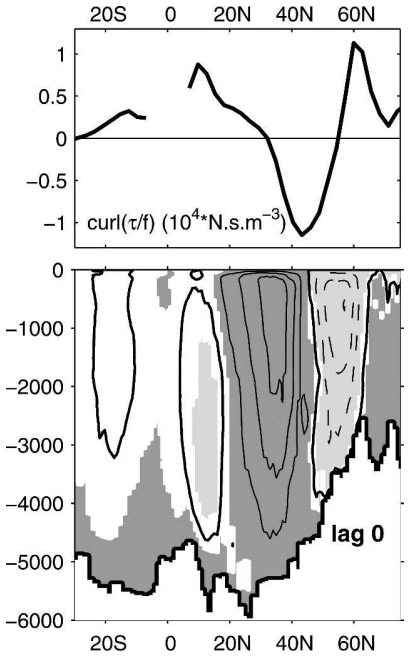

FIG. 8. (top) In-phase regression of the zonal mean Ekman pumping anomalies on the normalized time series of monthly NAO anomalies. Note that the Ekman pumping is not defined near the equator. (bottom) Same for the AMOC monthly anomalies. The contour interval is 0.4 Sv. The contours and shadings are as in Fig. 3, with the continuous line for positive and the dashed line for negative values.

structure at lag 1 (Fig. 9, right). Consistently, the NAO index and the MOI are significantly correlated in phase and weakly anticorrelated at lag 1 (Fig. 10). When the data are low-pass filtered (section 2) to focus on the decadal time scales, the correlation between NAO and MOI is small (Fig. 10, dashed line), and correspondingly, the regression of the AMOC on the NAO time series shows no significant signal. We speculate that it is primarily due to a near compensation at low frequency between the barotropic and the baroclinic responses seen in Fig. 9. This differs from Timmermann et al. (1998) and Delworth and Greatbatch (2000), who suggested that low-frequency changes in the NAO force a basin-scale acceleration of the THC via persistent buoyancy fluxes at high latitudes that enhance deep convection. However, the deep convection in these models was occurring south of Greenland, where the buoyancy forcing of the NAO was strong, while in the BCM the main convection site is in the Irminger Sea and is not directly forced by the NAO. Note that we do not exclude that the baroclinic response in Fig. 9 may be driven in part by buoyancy forcing as well, but our two-cell response widely differs from the buoyancy forced basin-scale cell seen in the other models.

5. The Atlantic meridional overturning circulation and ENSO

a. ENSO in the BCM

In the BCM simulation, the ENSO phenomenon is strong and rather realistic. It is well described by the first mode of SST variability in the tropical Pacific (not shown) that explains 55% of the monthly SST anomaly variance between 12°N and 12°S, versus 64% in the National Centers for Environmental Prediction–National Center for Atmospheric Research (NCEP–NCAR) reanalysis. The mode time series, or ENSO index (positive for a warm El Niño phase) is anticorrelated at a 17-month lag, versus 20 in the NCEP–NCAR reanalysis, and is more strongly autocorrelated at a 3–4-yr lag. Its spectrum (Fig. 11, top) thus shows significantly enhanced variance around 35 months. In the Indo-Pacific, the associated SLP structure compares rather well with the observed Southern Oscillation even though the eastern Pacific lobe extends farther west-

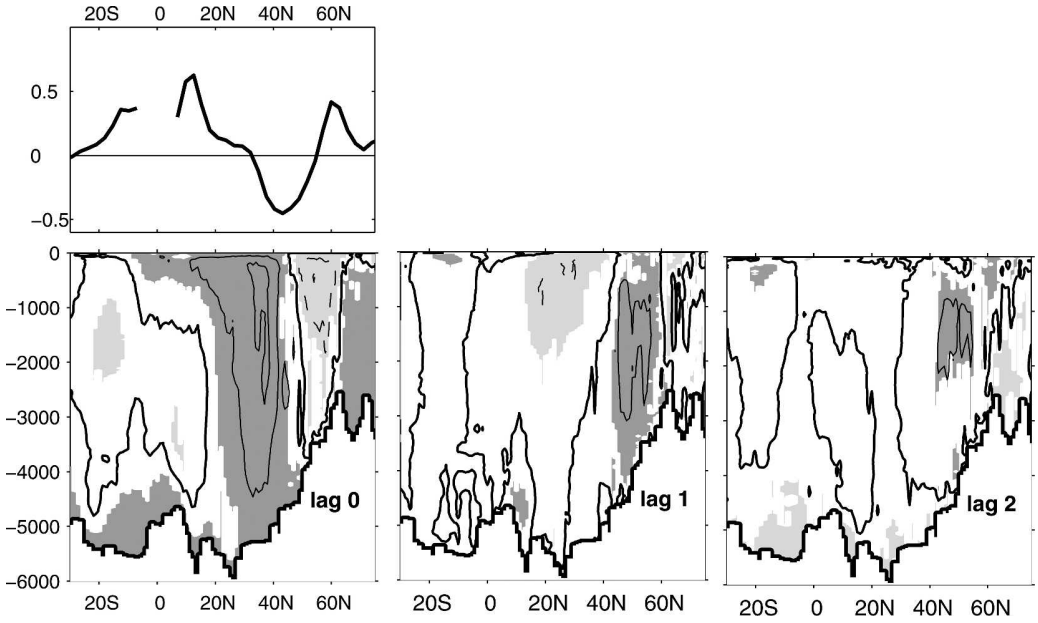

FIG. 9. Same as Fig. 8, but for annual means and various lags (in years). NAO leads at positive lags. The contour interval is 0.2 Sv.

ward along the equator (Fig. 12). In the North Atlantic, however, the SLP signal is 2.5 times too strong in the BCM, and the observed southwest–northeast pattern is replaced by a dipole that has some similarity with a negative phase of the NAO, except that it is shifted northward and strongly dominated by the southern pole. The too-strong impact of ENSO on the North Atlantic is a known deficiency of the ARPEGE atmospheric model (Cassou and Terray 2001). It results in an unrealistic in-phase anticorrelation ($r = -0.35$) between the NAO and ENSO indices that makes it harder to distinguish between NAO and ENSO influences on the northern North Atlantic, as discussed below. On the other hand, the ENSO signal is fairly well reproduced in the tropical and subtropical Atlantic, and the ENSO-induced anomalous precipitation pattern is significant and realistic, as shown in Fig. 13 by a comparison with the NCEP–NCAR reanalysis (for clarity, we did not indicate statistical significance). During the late rainy season in the Caribbean Sea (August–November; Fig.

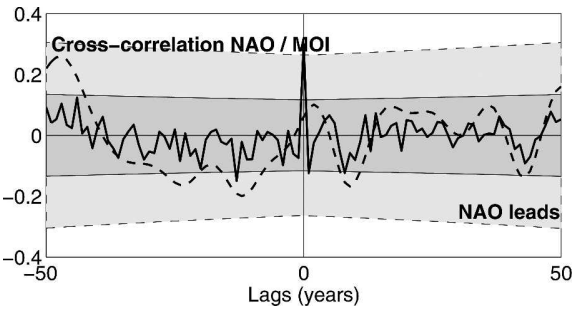

FIG. 10. Cross correlation between the NAO time series and the MOI, in annual means (solid line) and after low-pass filtering (dashed line). The dark (light) area delimits the 10% significant domain for the annual (decadal) data.

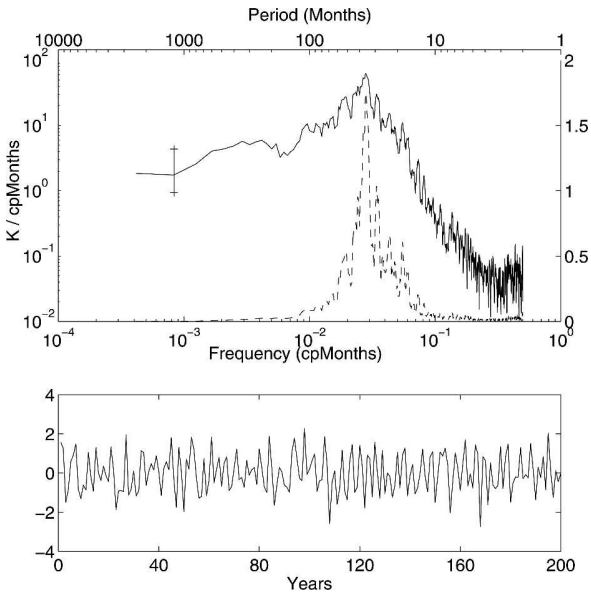

FIG. 11. (top) Same as in bottom of Fig. 2, but for the ENSO time series. (bottom) Normalized ENSO time series of annual mean.

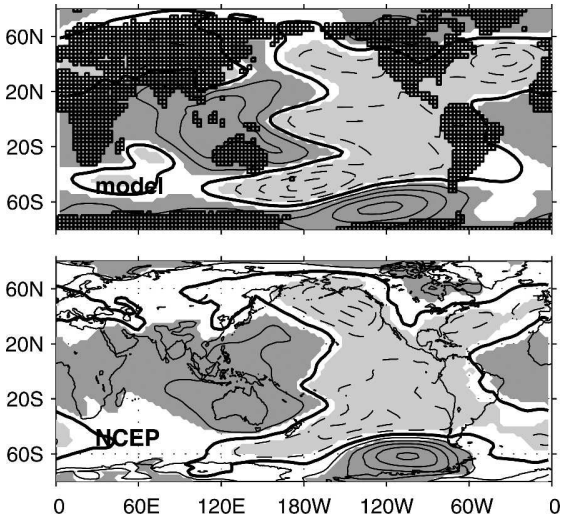

FIG. 12. Southern Oscillation associated with a positive phase of the leading tropical Pacific "El Niño" SST mode in (top) BCM and (bottom) NCEP–NCAR. The contour interval is 0.4 hPa. The contour and shadings are as in Fig. 3.

13, left) preceding a mature ENSO phase (December–January–February), a divergent surface flow dominates the eastern tropical Atlantic, contributing to anomalously weak precipitation over the Caribbean, as in the "dry Caribbean–ENSO relationship" of Hastenrath (1976). During the following months (middle), high pressure over the equatorial Atlantic reduces the meridional SLP gradient, yielding weaker trade winds and a gradual warming of the sea surface, consistent with Enfield and Mayer (1997). The warm SST anomaly reaches its maximum 4–6 months after the mature ENSO phase (i.e., in boreal spring of the ensuing year; right) and is associated with a wetter Caribbean at the start of the new rainy season, as discussed in Giannini et al. (2000). This realistic behavior of ENSO in the tropical Atlantic is of particular interest in view of the previous studies that have linked ENSO to the AMOC (e.g., Latif 2001).

b. Interannual time scales

Lagged regression based on annual means shows no significant link when the AMOC leads ENSO. In phase with ENSO events (Fig. 14, left), the AMOC is weaker at midlatitudes (typically by 0.3 Sv), as during a negative NAO phase but with less intensity (Fig. 9, left), consistent with the anticorrelation between the two atmospheric indices, and mechanical forcing by anomalous Ekman pumping (Fig. 14, top). The difference with the NAO case is that the AMOC southern cell extends less toward the Tropics, and there is an opposite cell at 15°S. The correlation loses significance 1 yr after ENSO, but 2 yr after (lag 2), a significant response of the opposite sign and slightly shifted southward appears with a similar intensity (Fig. 14, middle). There is some similarity with the baroclinic response to the NAO, but the pattern persists much longer and slowly propagates southward, so that 6 yr after ENSO (right), the weakening of the meridional circulation is centered at 35°N, resembling to some extent the lag-0 barotropic response, but without significant positive cells. Significance is lost by lag 7. Consistent with this picture, the MOI and ENSO index are significantly correlated in phase and also when the MOI lags by 6 yr (Fig. 15). The AMOC weakening following a positive ENSO event persists longer than that following a negative NAO phase because the ENSO forcing is more persistent and affects the deep convection sites differently. As shown in Fig. 16, the ENSO teleconnections simultaneously reduce the deep convection in the Labrador and Irminger Seas without significantly affecting the GIN Seas, while a negative NAO phase reduces the deep convection in the Labrador Sea and enhances it in the

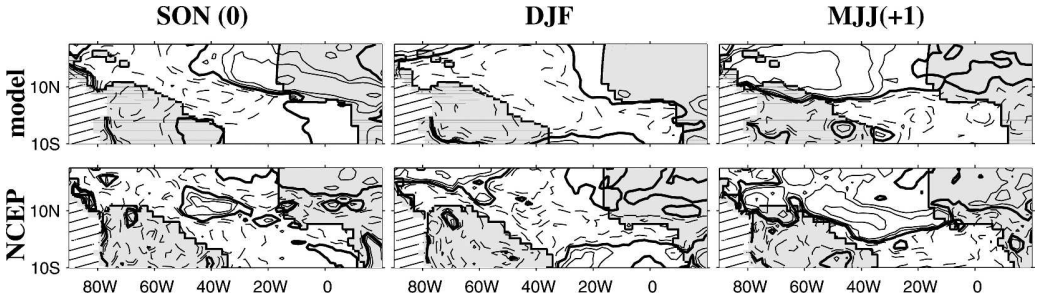

FIG. 13. Lagged regression of precipitation on ENSO in Dec–Jan–Feb in (top) BCM and in (bottom) NCEP–NCAR. SON (0) indicates that precipitation is considered from Sep to Nov prior to the mature phase of ENSO and MJJ(+1) indicates that precipitation is considered from May to Jul after the mature phase. The contours correspond to 0, 2.5, 5, 12.5, 22.5, and 50 mm month^{-1}, with continuous (dashed) line for positive (negative) values. The thick contour denotes zero.

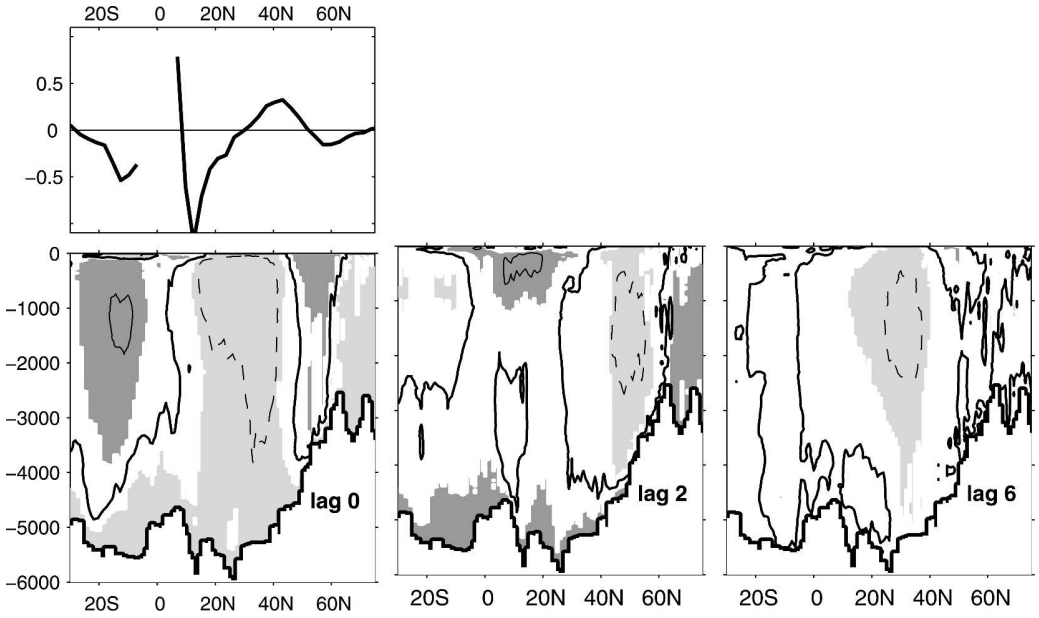

FIG. 14. Same as Fig. 9, but for the normalized annual ENSO time series when the latter is (left) in phase and leads by (middle) 2 and (right) 6 yr. The contours and shadings are as in Fig. 3.

GIN Seas, without much effect in the Irminger Sea (see Fig. 5, right). The effect of ENSO might in addition be further prolonged by the advection of a negative salinity anomaly created in phase off Newfoundland and that propagates toward the Irminger Sea in 3–4 yr, as described in Mignot and Frankignoul (2004). In conclusion, ENSO forcing explains why Bentsen et al. (2004) found that regimes can exist in the BCM simulation where deep convection in the Irminger and Labrador Seas act together.

c. Decadal time scales

To filter out the fast response to the wind forcing that may obscure slower changes, we now consider the data filtered at decadal time scales. We thus now consider the response to decade-long ENSO fluctuations or to successions of shorter events of the same signs, both referred to as decadal changes of ENSO. Contrary to the NAO case where statistical significance was lost, low-pass filtering strongly enhances the AMOC weakening that follows ENSO events, and it makes its slow southward propagation more visible (not shown). The AMOC weakening is initiated at high latitudes, reaches its maximum (0.5 Sv) about 4 yr after decade-long warm ENSO events or decadal succession of short

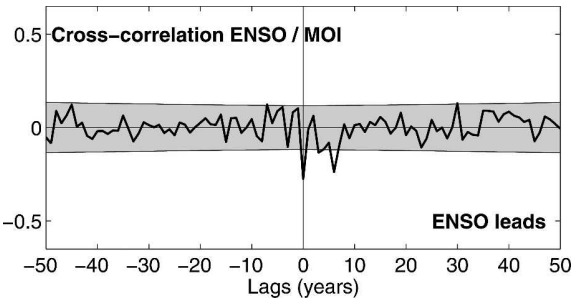

FIG. 15. Cross correlation between the annual MOI and ENSO index. The shaded area indicates the 10% two-sided significant level.

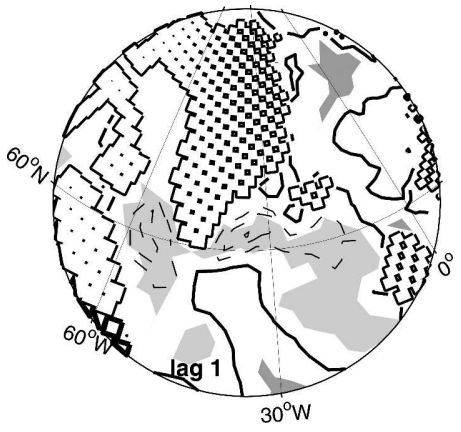

FIG. 16. Regression of the annual mixed layer depth to the normalized annual ENSO time series. The mixed layer depth follows the ENSO time series by 1 yr. The contour interval is 10 m (contours and shadings are as in Fig. 3).

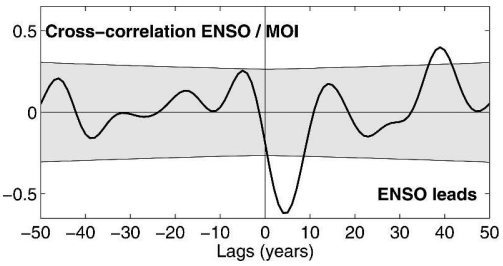

FIG. 17. Lagged correlation between the low-passed ENSO and MOI time series. The shaded area indicates the 10% significant level.

warm ENSO events, and expands to the Southern Hemisphere after about 8 yr, consistent with the AMOC propagation in Fig. 3.

The cross correlation between the low-pass-filtered ENSO and MOI time series confirms the strong anticorrelation when ENSO leads by about 4 yr (Fig. 17) but, in addition, shows a significant positive correlation when ENSO leads by about 39 yr. Note that this peak is significant (at the estimated 10% level) independently of the trend removal, although artificially large correlations are found at positive lags when no trend is removed. It is also significant when periods lower than 5 yr only are filtered out. To document the associated patterns, the global SST field was regressed on the MOI with the same time lag (Fig. 18, left), showing indeed a significant positive SST monopole in the tropical Pacific that resembles the model El Niño.

To confirm the relationship between tropical Pacific SST and the AMOC, we used a lagged maximum covariance analysis (MCA) based on a singular value decomposition. As in Frankignoul et al. (2001), statistical significance was estimated using a moving block bootstrap approach. The first covariance mode between the low-pass-filtered global SST and low-pass-filtered AMOC is highly significant when AMOC follows SST by a few years, confirming that a positive ENSO phase is followed by a basin-scale weakening of the AMOC (Fig. 19). No other significant first mode was found, but the second mode of covariability is significant when SST leads the AMOC by 36 yr. The associated patterns (Fig. 20) show that a positive ENSO phase is followed by a dipole-like AMOC fluctuation with anomalously strong meridional circulation at high latitudes and an anomalously weak one in the Tropics. This structure is very close to the second EOF of the AMOC (not shown), and it has some similarity with the lag −4 pattern in Fig. 3. Based on the latter, we can thus expect a basin-scale acceleration of the AMOC about 36 + 4 = 40 yr after a decade with warm ENSO events, as seen in Fig. 17. However, no significant covariance could be found near this lag, possibly because the simulation is too short for the signal to be robust when only using SST data.

We saw that warm ENSO events lead to a salinification of the western tropical Atlantic via anomalous freshwater fluxes (section 5a), and the surface waters are indeed anomalously salty 39 yr prior to the AMOC maximum (Fig. 18, right). The delayed ENSO influence could thus occur via salinity advection, as suggested in the observations by Latif (2001). To investigate this mechanism in the BCM, we released fictitious Lagrangian drifters in the surface mixed layer at the center of the positive haline anomaly in the tropical North Atlantic and followed their advection by the model climatological monthly currents, as in Mignot and Frankignoul [2004; see Blanke and Raynaud (1997) for a description of the Lagrangian advective tool]. The trajectories of the floats calculated over 40 yr are shown in Fig. 21 as a function of depth. The releases were distributed throughout the year, but, for clarity, we only show the trajectories of particles released in January and July. The time step used for the calculation is 10 days. Most drifters propagate twice around the

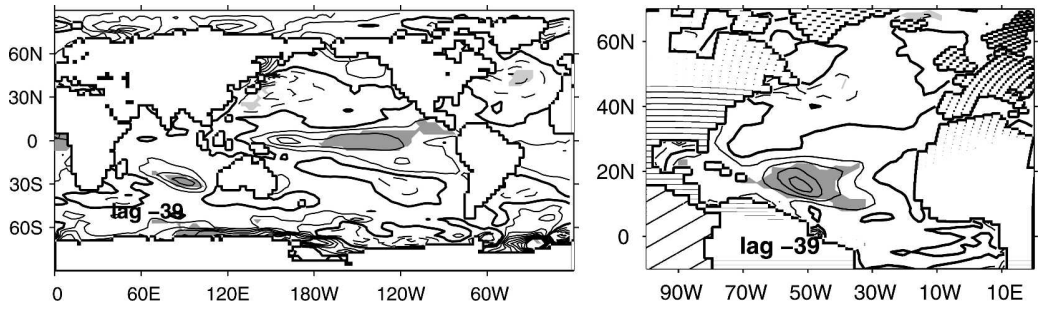

FIG. 18. Lagged regression of (left) the global decadal SST (contour interval: 0.4 K) and (right) the North Atlantic SSS (contour interval: 0.15 psu) on the normalized low-pass-filtered MOI. The MOI lags by 39 yr in both cases. The contours and shadings are as in Fig. 3.

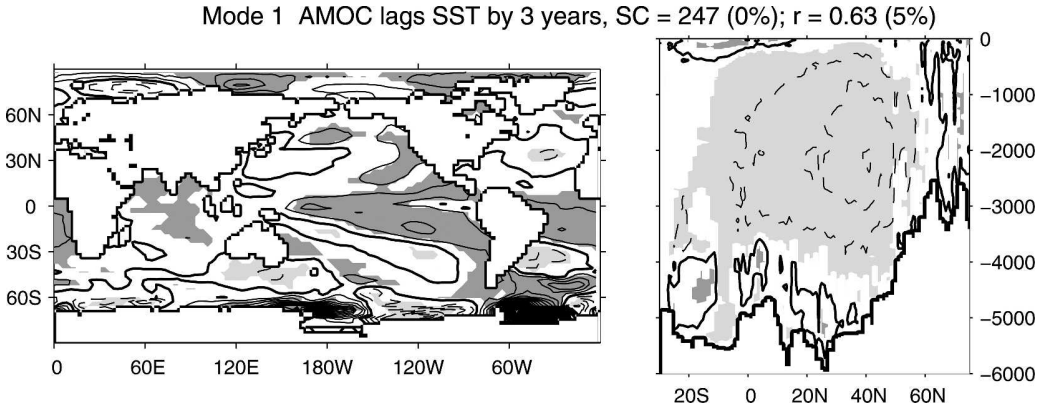

FIG. 19. Leading mode of the MCA between low-pass-filtered SST and AMOC when the former leads the latter by 3 yr. (left) SST homogeneous field (projection of the SST on the MCA time series associated to the SST). The contour interval is 0.08 K. (right) AMOC heterogenous field (projection of the AMOC on the same time series). The contour interval is 0.2 Sv. The contours and shadings are as in Fig. 3. SC is the square covariance and *r* is the correlation of the two MCA time series. The value in parentheses indicates the estimated significance level.

subtropical gyre, first remaining in the mixed layer, then subducting in the center of the gyre and recirculating at greater depth in the Caribbean Sea and along the coast of the United States. Some drifters then escape the subtropical gyre along the North Atlantic Current and are seen to finally reach the high latitudes, essentially the Irminger and Labrador Seas, between 500- and 1500-m depth. We emphasize that these trajectories were calculated using the monthly climatological currents of the model and are thus independent of the filtering applied to the data. They show that a 40-yr delay between decade-long warm ENSO events or a decadal succession of short warm ENSO events and a weakening of the AMOC is consistent with the northward advection of salinity anomalies created by ENSO in the tropical Atlantic. The good correspondence between the time scales found in the two independent analyses gives credit to the proposed long-term link. The propagation of salinity anomalies was difficult to follow. However, the lagged regression of the anomalous potential density at 600 m on the ENSO time series indeed shows that the water becomes anomalously dense in the North Atlantic about 35 yr after the warm ENSO events (Fig. 22). This could destabilize the water column and, presumably, favor deep convection.

6. Conclusions

In the BCM, the natural variability of the AMOC is dominated by a basin-scale adjustment to changes in the deep convection in the Irminger Sea. Although the relevance of deep convection in the Irminger Sea has been confirmed by recent observations (Pickart et al. 2003b; Bacon et al. 2003), its relative importance seems overestimated, as the Labrador and GIN Seas are generally considered as the main areas of deep-water for-

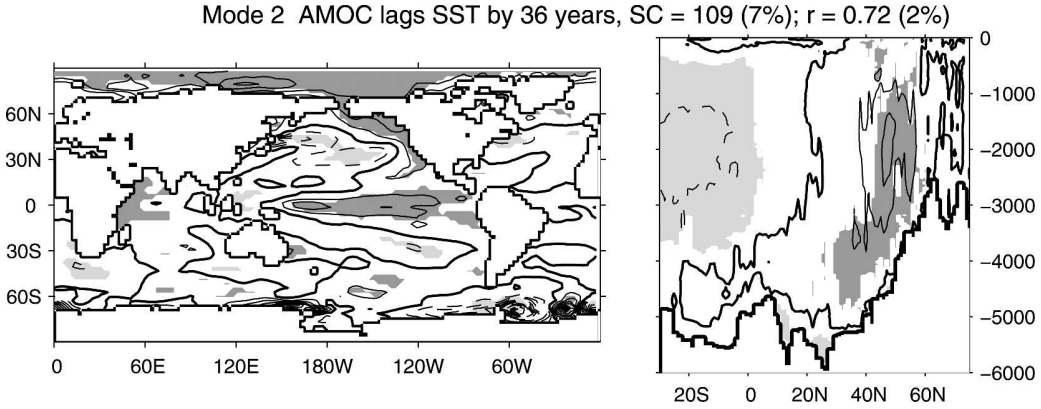

FIG. 20. Same as Fig. 19, but for the second mode of covariability. The SST leads the AMOC by 36 yr.

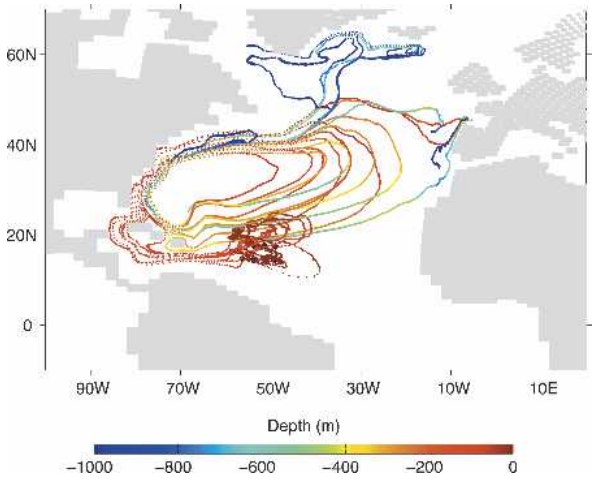

FIG. 21. Lagrangian trajectories of the fictitious drifters launched in the Tropics (black diamonds) and advected by the model mean currents for 39 yr. The colors indicate the depth of the drifters.

mation in the northern North Atlantic (e.g., Lazier et al. 2001). In the model, enhanced deep convection in the Irminger Sea is due to a succession of atmospheric patterns that bring anomalous northerly winds over the area, evaporation, and cooling. Unlike in the observations (Pickart et al. 2003a), the atmospheric forcing is not linked to the NAO. Note however that observations are partly influenced by noise and perhaps also by changes in radiative forcing, composition of the atmosphere, etc.

The influence of the NAO on the AMOC was explored. Although a positive NAO phase enhances deep convection in the Labrador Sea and inhibits it in the GIN Seas (and conversely), as in the observations, it primarily influences the AMOC through the mechanical action of the wind. The AMOC is indeed rapidly intensified south of 40°N and weakened to the north, consistent with a barotropic response to NAO winds. The baroclinic response appears 1 yr later and almost has the opposite polarity. At longer time scales, the barotropic and baroclinic responses thus largely compensate, and the AMOC response to the NAO is weak. We found no evidence of a significant low-frequency impact of the NAO through buoyancy forcing. This differs from previous studies of Timmermann et al. (1998) and Delworth and Greatbatch (2000), where the buoyancy forcing associated to the NAO caused a basin-scale change of the AMOC. The weaker NAO influence in the BCM is presumably due to the strength of the deep convection in the Irminger Sea, which is not directly affected by the NAO in the model. Although of questionable realism, this result emphasizes that the location of deep convection and the high-latitude atmospheric forcing must both be well represented in coupled models in order to correctly simulate the AMOC variability.

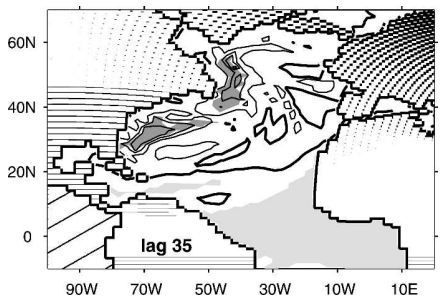

FIG. 22. Regression at lag 35 of the potential density at 600 m on the ENSO time series (ENSO leads); all data are low-pass filtered.

Finally, we investigated the link between ENSO and the AMOC. In the BCM, the ENSO phenomenon is fairly realistic, but its influence on the atmospheric circulation in the North Atlantic sector is too strong, and ENSO and NAO are significantly anticorrelated, unlike in the observations. As a result, the ENSO teleconnections affect the AMOC through both wind forcing and a direct impact on deep convection in the Labrador and Irminger Seas, resulting in a more persistent influence—a slower overturning following a positive ENSO phase by about 6 yr. However, as these impacts are directly linked to the artificial ENSO influence on the northern North Atlantic, they are unlikely to be realistic.

Some evidence of more realistic influence of ENSO on the AMOC was found at low frequency with a time lag of about 40 yr. The mechanism is based on the advection of salinity anomalies that appear in the tropical Atlantic during El Niño events, consistent with the observed ENSO impact that was suggested by Latif (2001). Their northward propagation is primarily due to the mean oceanic circulation and takes approximately 35 yr. The salinity anomalies would first circulate in the subtropical gyre, then subduct, and recirculate at depths along the coast of northern America. They would then be in part advected along the North Atlantic current, eventually reaching the Irminger and Labrador Seas, where they tend to destabilize the water column and thus presumably enhance deep convection, hence the AMOC. However, this delayed ENSO impact was difficult to detect in only 200 yr of model data, and it should be investigated further in longer simulations or through specific experiments in forced conditions. It is interesting to note that several sensitivity experiments with coupled models highlight a similar mechanism. Latif et al. (2000) described a scenario

simulation where the AMOC is stabilized in global warming conditions by the advection of salinity anomalies from the tropical Atlantic that were created by strong ENSO events. A similar mechanism is suggested by Thorpe et al. (2001), except that it does not involve ENSO. In a BCM simulation perturbed by an artificial freshening in the high latitudes, Otterå et al. (2003) observed a stabilization of the AMOC because salinity anomalies that were created by the weakening of the Guyana Current in the tropical Atlantic were advected northward, countering after about 50 yr the imposed freshening. Subtropical salinity anomalies due to a shift of the ITCZ position acted similarly in two simulations with the HadCM3 model, one in control conditions (Vellinga and Wu 2004) and one perturbed by an anomalous freshwater anomaly in the high latitudes (Vellinga et al. 2002). Our study does not tell whether salinity advection from the tropical Atlantic would be sufficient to stabilize the AMOC in a global warming scenario with the BCM, but it emphasizes its possible role in the long-term variability of the thermohaline circulation.

Acknowledgments. We thank Helge Drange, Mats Bentsen, and Ina Karin Kindem for providing the BCM run, and Bruno Blanke and Daniele Iudicone for making available the Lagrangian tool. Thanks are also due to the reviewers, whose comments led to an improved presentation of the work. Useful discussions with Gilles Reverdin and Jean-Luc Mélice are acknowledged. The NCEP–NCAR reanalysis data were provided through the NOAA Climate Diagnostics Center (http://www.cdc.noaa.gov/). This research was supported in part by the PREDICATE project of the European Community, the PNEDC, and the Institut Universitaire de France. J. M. was supported during her doctoral thesis by a scholarship from the DGA–CNRS.

REFERENCES

Bacon, S., W. J. Gould, and Y. Jia, 2003: Open-ocean convection in the Irminger Sea. *Geophys. Res. Lett.,* **30,** 1246, doi:10.1029/2002GL016271.

Bentsen, M., H. Drange, T. Furevik, and T. Zhou, 2004: Simulated variability of the Atlantic meridional overturning circulation. *Climate Dyn.,* **22,** 701–720.

Blanke, B., and S. Raynaud, 1997: Kinematics of the Pacific Equatorial Undercurrent: An Eulerian and Lagrangian approach from GCM results. *J. Phys. Oceanogr.,* **27,** 1038–1053.

Bleck, R., C. Rooth, D. Hu, and L. T. Smith, 1992: Salinity-driven thermohaline transients in a wind- and thermohaline-forced isopycnic coordinate model of the North Atlantic. *J. Phys. Oceanogr.,* **22,** 1486–1505.

Cassou, C., and L. Terray, 2001: Oceanic forcing of the wintertime low-frequency atmospheric variability in the North Atlantic European sector: A study with the ARPEGE model. *J. Climate,* **14,** 4266–4291.

Chen, F., and M. Ghil, 1996: Interdecadal variability in a hybrid coupled ocean–atmosphere model. *J. Phys. Oceanogr.,* **26,** 1561–1578.

Clarke, R. A., and J.-C. Gascard, 1983: The formation of Labrador Sea Water. Part I: Large-scale processes. *J. Phys. Oceanogr.,* **13,** 1764–1778.

Curry, R. G., and M. S. McCartney, 2001: Ocean gyre circulation changes associated with the North Atlantic Oscillation. *J. Phys. Oceanogr.,* **31,** 3374–3400.

Daubechies, I., 1992: Ten lectures on wavelets. Society for Industrial and Applied Mathematics CBMS-NSF Lecture Notes 61, 357 pp.

Delworth, T. L., and R. J. Greatbatch, 2000: Multidecadal thermohaline circulation variability driven by atmospheric surface flux forcing. *J. Climate,* **13,** 1481–1495.

——, S. Manabe, and R. J. Stouffer, 1993: Interdecadal variations of the thermohaline circulation in a coupled ocean–atmosphere model. *J. Climate,* **6,** 1993–2011.

——, ——, and ——, 1997: Multidecadal climate variability in the Greenland Sea and surrounding regions: A coupled model simulation. *Geophys. Res. Lett.,* **24,** 257–260.

Déqué, M., C. Dreveton, A. Braun, and D. Cariolle, 1994: The ARPEGE/IFS atmosphere model: A contribution to the French community climate modelling. *Climate Dyn.,* **10,** 249–266.

Dickson, R., J. Lazier, J. Meincke, P. Rhines, and J. Swift, 1996: Long term coordinated changes in the convective activity of the North Atlantic. *Progress in Oceanography,* Vol. 38, Pergamon, 241–295.

Drange, H., 1999: RegClim ocean modelling at NERSC. Regclim: Regional Climate Development under Global Warming, General Tech. Rep. 2, Norwegian Institute for Air–Sea Research, 93–102.

DYNAMO Group, 1997: DYNAMO—Dynamics of the North Atlantic Models: Simulation and assimilation with high resolution models. Tech. Rep. 294, Institüt für Meereskunde, Christian Albrechts Universität, Kiel, Germany, 334 pp.

Eden, C., and J. Willebrand, 2001: Mechanisms of interannual to decadal variability of the North Atlantic circulation. *J. Climate,* **14,** 2266–2280.

Enfield, D. B., and D. A. Mayer, 1997: Tropical Atlantic sea surface temperature variability and its relation to El Niño–Southern Oscillation. *J. Geophys. Res.,* **102** (C1), 929–945.

Feldstein, S. B., 2000: Teleconnections and ENSO: The timescale, power spectra, and climate noise properties. *J. Climate,* **13,** 4430–4440.

Frankignoul, C., G. De Coëtlogon, T. M. Joyce, and S. Dong, 2001: Gulf Stream variability and ocean–atmosphere interactions. *J. Phys. Oceanogr.,* **31,** 3516–3529.

Furevik, T., M. Bentsen, H. Drange, I. K. T. Kindem, N. G. Kvamstø, and A. Sorteberg, 2003: Description and evaluation of the Bergen Climate Model: ARPEGE coupled with MICOM. *Climate Dyn.,* **21,** 27–51.

Ganachaud, A., and C. Wunsch, 2000: Improved estimates of global ocean circulation, heat transport and mixing from hydrographic data. *Nature,* **408,** 453–456.

Gao, Y., H. Drange, and M. Bentsen, 2003: Effects of diapycnal and isopycnal mixing on the ventilation of CFCs in the North Atlantic in an isopycnic coordinate OGCM. *Tellus,* **55B,** 837–854.

Giannini, A., Y. Kushnir, and M. C. Cane, 2000: Interannual vari-

ability of Caribbean rainfall, ENSO, and the Atlantic Ocean. *J. Climate,* **13,** 297–310.

Hakkinen, S., 1999: Variability of the simulated meridional heat transport in the North Atlantic for the period 1951–1993. *J. Geophys. Res.,* **104** (C5), 10 991–11 007.

Hastenrath, S., 1976: Variations in the low-latitude circulation and extreme climatic events in the tropical Americas. *J. Atmos. Sci.,* **33,** 202–215.

Hsieh, W. W., M. K. Daney, and R. C. Wajsowicz, 1983: The free Kelvin wave in finite-difference numerical models. *J. Phys. Oceanogr.,* **13,** 1383–1397.

Kawase, M., 1987: Establishment of deep ocean circulation driven by deep-water production. *J. Phys. Oceanogr.,* **17,** 2294–2317.

Killworth, P. D., 1985: A two-level wind and buoyancy driven thermocline model. *J. Phys. Oceanogr.,* **15,** 1414–1432.

Latif, M., 2001: Tropical Pacific/Atlantic ocean interactions at multi-decadal time scales. *Geophys. Res. Lett.,* **28,** 539–542.

——, E. Roeckner, U. Mikolajewicz, and R. Voss, 2000: Tropical stabilization of the thermohaline circulation in a greenhouse warming simulation. *J. Climate,* **13,** 1809–1813.

Lazier, J. R. N., R. Pickart, and P. Rhines, 2001: Deep convection. *Ocean Circulation and Climate: Observing and Modelling the Global Ocean,* G. Siedler, J. Church, and J. Gould, Eds., International Geophysics Series, Vol. 77, Academic Press, 387–400.

Manabe, S., and R. J. Stouffer, 1999: The role of thermohaline circulation in climate. *Tellus,* **51A–B,** 91–109.

Marshall, J. C., and F. Schott, 1999: Open-ocean convection: Observations, theory and models. *Rev. Geophys.,* **37,** 1–64.

——, H. Johnson, and J. Goodman, 2001: A study of the interaction of the North Atlantic Oscillation with the ocean circulation. *J. Climate,* **14,** 1399–1421.

Mignot, J., and C. Frankignoul, 2004: Interannual to interdecadal variability of sea surface salinity in the Atlantic and its link to the atmosphere in a coupled model. *J. Geophys. Res.,* **109,** C04005, doi:10.1029/2003JC002005.

Mikolajewicz, U., and E. Maier-Reimer, 1990: Internal secular variability in an ocean general circulation model. *Climate Dyn.,* **4,** 145–156.

Otterå, O. H., H. Drange, M. Bentsen, N. G. Kvamstø, and D. Jiang, 2003: The sensitivity of the present-day Atlantic meridional overturning circulation to freshwater forcing. *Geophys. Res. Lett.,* **30,** 1898, doi:10.1029/2003GL017578.

Pickart, R. S., M. A. Spall, M. H. Ribergaard, G. W. K. Moore, and R. F. Milliff, 2003a: Deep convection in the Irminger Sea forced by the Greenland tip jet. *Nature,* **424,** 152–156.

——, F. Straneo, and G. W. K. Moore, 2003b: Is the Labrador Sea Water formed in the Irminger basin? *Deep-Sea Res.,* **50A,** 23–52.

Schott, F., M. Visbeck, and J. Fischer, 1993: Observations of vertical currents and convection in the central Greenland Sea during the winter of 1988/1989. *J. Geophys. Res.,* **98,** 14 401–14 421.

Siedler, G., J. Church, and J. Gould, Eds., 2001: *Ocean Circulation and Climate: Observing and Modelling the Global Ocean.* International Geophysics Series, Vol. 77, Academic Press, 715 pp.

Talley, L. D., J. L. Reid, and P. E. Robbins, 2003: Data-based meridional overturning streamfunctions for the global oceans. *J. Climate,* **16,** 3213–3226.

Thorpe, R. B., J. M. Gregory, T. C. Johns, R. A. Wood, and J. F. B. Mitchell, 2001: Mechanisms determining the Atlantic thermohaline circulation response to greenhouse gas forcing in a non-adjusted coupled climate model. *J. Climate,* **14,** 3102–3116.

Timmermann, A., M. Latif, R. Voss, and A. Grötzner, 1998: Northern Hemispheric interdecadal variability: A coupled air–sea mode. *J. Climate,* **11,** 1906–1931.

Vellinga, M., and P. Wu, 2004: Low-latitude freshwater influence on centennial variability of the Atlantic thermohaline circulation. *J. Climate,* **17,** 4498–4511.

——, R. Wood, and J. Gregory, 2002: Processes governing the recovery of a perturbed thermohaline circulation in HadCM3. *J. Climate,* **15,** 764–780.

Weaver, A. J., E. S. Sarachik, and J. Marotzke, 1991: Freshwater flux forcing of decadal and interdecadal oceanic variability. *Nature,* **353,** 836–838.

Wunsch, C., 2002: What is the thermohaline circulation? *Science,* **298,** 1179–1181.

Yang, J., 1999: A linkage between decadal climate variations in the Labrador Sea and the tropical Atlantic Ocean. *Geophys. Res. Lett.,* **26,** 1023–1026.

Atlantic Subsurface Temperatures: Response to a Shutdown of the Overturning Circulation and Consequences for Its Recovery

J. MIGNOT,* A. GANOPOLSKI, AND A. LEVERMANN+

Potsdam Institute for Climate Impact Research, Potsdam, Germany

(Manuscript received 28 September 2006, in final form 13 February 2007)

ABSTRACT

Using the coupled climate model of intermediate complexity, CLIMBER-3α, changes in the vertical thermal structure associated with a shutdown of the Atlantic meridional overturning circulation (AMOC) are investigated. When North Atlantic Deep Water formation is inhibited by anomalous freshwater forcing, intermediate depth ventilation can remain active and cool the subsurface water masses (i.e., the "cold case"). However, if intermediate ventilation is completely suppressed, relatively warm water coming from the south penetrates to a high northern latitude beneath the halocline and induces a strong vertical temperature inversion between the surface and intermediate depth (i.e., the "warm case"). Both types of temperature anomalies emerge within the first decade after the beginning of the freshwater perturbation. The sign of subsurface temperature anomaly has a strong implication for the recovery of the AMOC once the anomalous freshwater forcing is removed. While the AMOC recovers from the cold case on centennial time scales, the recovery is much more rapid (decadal time scales) when ventilation is completely suppressed and intermediate depths are anomalously warm. This is explained by a more rapid destabilization of the water column after cessation of the anomalous flux due to a strong vertical temperature inversion. A suite of sensitivity experiments with varying strength and duration of the freshwater perturbation and a larger value of background vertical diffusivity demonstrate robustness of the phenomenon. Implications of the simulated subsurface temperature response to the shutdown of the AMOC for future climate and abrupt climate changes of the past are discussed.

1. Introduction

Because of its importance for the climate system, the Atlantic meridional overturning circulation (AMOC) has received considerable attention in recent years (e.g., Vellinga and Wood 2002; Winton 2003; Herweijer et al. 2005). The AMOC is responsible for a large part of meridional heat transport in the Atlantic Ocean (e.g., Ganachaud and Wunsch 2000; Trenberth and Caron 2001) and numerous modeling experiments have shown that changes in its strength and spatial structure can considerably affect regional and global climate (Crowley 1992; Stocker 1998; Vellinga and Wood 2002; Timmermann et al. 2005; Levermann et al. 2005). Rapid reorganizations of the AMOC are considered as the prime candidates for explaining abrupt climate changes recorded during glacial times (Clarke et al. 2002; Rahmstorf 2002). The possibility of an AMOC shutdown in the future in response to global warming has been demonstrated with a number of climate models (Manabe and Stouffer 1993; Rahmstorf and Ganopolski 1999; Houghton et al. 2001).

So-called water hosing experiments, where anomalous freshwater flux (or equivalent negative salinity flux) is applied to some regions of the ocean are widely used to study the stability of the AMOC and its impact on climate (e.g., Stocker and Wright 1991; Manabe and Stouffer 1995; Rahmstorf 1996; Fanning and Weaver 1997; Schiller et al. 1997; Rind et al. 2001; Rahmstorf et al. 2005; Stouffer et al. 2006). These idealized experiments are motivated by the necessity to understand past abrupt changes of the ocean circulation, as well as its response to future climate change. A large discharge of freshwater into the North Atlantic during glacial

* Current affiliation: LOCEAN, Unité Mixte de Recherché, CNRS-IRD-UPMC-MNHN, Université Pierre et Marie Curie, Paris, France.

+ Additional affiliation: Institute of Physics, Potsdam University, Potsdam, Germany.

Corresponding author address: J. Mignot, LOCEAN, Université Pierre et Marie Curie, Case courrier 100, 4 place Jussieu, 75252 Paris CEDEX 05, France.
E-mail: juliette.mignot@locean-ipsl.upmc.fr

DOI: 10.1175/JCLI4280.1

time and deglaciation is believed to be responsible for major shifts in the ocean circulation recorded by various paleoclimate proxies (e.g., Bond et al. 1992; McManus et al. 2004). Concerning future climate change, model simulations suggest that global warming would intensify the freshwater input into the North Atlantic, as a consequence of an intensification of northward atmospheric moisture transport, increase of river discharge into the Arctic Ocean, and melting of the Greenland ice sheet (Church et al. 2001). Recent observations give consistent indications (Peterson et al. 2002; Dickson et al. 2002).

In most hosing experiments, anomalous freshwater flux has been applied to the North Atlantic and, in spite of differences in models, areas and magnitudes of the applied freshwater flux, a number of robust features of the models' response emerged. In particular, it has been shown that a sufficiently large anomalous freshwater flux [typically 0.1–1 Sv (1 Sv = 10^6 m^3 s^{-1}), this value being strongly model dependent] can shut down the AMOC completely on decadal to centennial time scales (e.g., Rahmstorf et al. 2005; Stouffer et al. 2006). This leads to a strong surface oceanic and atmospheric cooling in the North Atlantic realm (order of 10 K) and a pronounced cooling over most of the Northern Hemisphere. At the same time, in the southern Atlantic, surface and subsurface warming occurs on decadal time scales (i.e., the Atlantic seesaw; Crowley 1992) after the shutdown of the AMOC. These warm anomalies gradually propagate into high latitudes of the Southern Hemisphere. This process occurs on multicentennial time scales and is thus not clearly seen in short-term water hosing experiments (e.g., Rind et al. 2001). Apart from a direct atmospheric temperature response, the shutdown of AMOC leads to a pronounced reorganization of atmospheric circulation, in particular to a southward shift of the intertropical convergence zone, which results in large changes in precipitation in the Tropics [e.g., Manabe and Stouffer (1988); Vellinga and Wood (2002); Broccoli et al. (2006) in models; Peterson et al. (2000) using paleo-observations].

At the same time, experiments with different climate models reveal important discrepancies that have not received much attention and remain unexplained. It has been shown that the magnitude and time scale of the AMOC weakening in response to a fixed amount of anomalous freshwater depends, among other factors, on the location of the anomaly, with a stronger and more rapid response if the latter is applied directly in the area of deep-water formation as compared to a more southern perturbation (Rahmstorf 1996; Manabe and Stouffer 1997; Gregory et al. 2003; Goelzer et al. 2006). Furthermore, while the models agree on the surface cooling in the North Atlantic and the surface and subsurface warming in the southern and tropical Atlantic, different authors report subsurface temperature changes in the mid- and high latitudes of the North Atlantic of the opposite sign: Manabe and Stouffer (1988, 1997) and Rind et al. (2001) show strong negative temperature anomalies developing in mid- and high latitudes of the North Atlantic from the surface to the bottom, while Knutti et al. (2004) and Rühlemann et al. (2004) report on strong subsurface warming (with a magnitude of several degrees) within the upper 1000 m in the Atlantic northern high latitudes. Together with the surface cooling, this can induce significant reversed vertical temperature gradients. Apart from that, the rate of recovery differs strongly between model experiments (e.g., Stouffer et al. 2006).

It is natural that surface changes associated with a weakening or a complete shutdown of the AMOC attracted the primary attention, because they can directly affect the regional and global climate. However, as we will show below, subsurface temperature and salinity changes are important because they determine the mechanism and rate of the AMOC recovery after cessation of the anomalous freshwater flux. This plays a role in the interpretation of paleoclimate data and the understanding of mechanisms of past abrupt climate changes. For example, the strong vertical temperature inversion in high latitudes of the North Atlantic during stadial (cold) Atlantic events is crucial for the rapid onset of Dansgaard–Oeschger warm events simulated by Ganopolski and Rahmstorf (2001). They are also an essential element of the mechanism of self-sustained deep-decoupling oscillations found in some models. These have been proposed to explain millennium-scale climate variability during glacial times (Winton 1997; Shaffer et al. 2004).

Here, we show that opposite subsurface temperature patterns in the northern North Atlantic are obtained in experiments with different locations of freshwater perturbations. First, this result is interesting in the framework of model intercomparison. In all the experiments cited above, hosing is alternatively applied in the high northern latitudes (e.g., Stouffer et al. 2006), farther south in the subtropics (e.g., Rahmstorf et al. 2005) or in an intermediate region around 50°N (e.g., Knutti et al. 2004; Rühlemann et al. 2004), and results are usually compared without special care. We will show that different experimental setups can induce very different oceanic subsurface anomalies and AMOC recovery mechanisms. Second, we will discuss some paleoclimatic implications of subsurface response to changes in the AMOC. These changes might be relevant for the

assessment of environmental impacts of a possible future AMOC reduction in response to global warming.

The model and experiments are described in section 2. Subsurface temperature anomalies are discussed in section 3 and implications for the AMOC recovery are discussed in section 4. Robustness of the results to details of the perturbation and to oceanic mixing parameterization is tested in section 5. Results are discussed in section 6.

2. Model and experimental setup

The model used in this study is the CLIMBER-3α coupled climate model of intermediate complexity (Montoya et al. 2005). It consists of the Potsdam statistical–dynamical atmospheric model version 2 (POTSDAM-2; Petoukhov et al. 2000) coupled to a global, 24-layer ocean general circulation model based on the Geophysical Fluid Dynamics Laboratory (GFDL) Modular Ocean Model version 3 (MOM-3) code and to the dynamic and thermodynamic sea ice module of Fichefet and Maqueda (1997). The oceanic model has a horizontal resolution of 3.75° × 3.75°. It uses a weak background vertical diffusivity ($\kappa = 0.1 \times 10^{-4}$ m^2 s^{-1}) and a second-order-moment advection scheme for tracers (Prather 1986) that strongly reduces numerical diffusivity (Hofmann and Maqueda 2006). A parameterization of boundary enhanced mixing depending both on near-bottom stratification and roughness of topography (Ledwell et al. 2000) is implemented, following Hasumi and Suginohara (1999). This leads locally to vertical diffusion coefficients of up to 10^{-4} m^2 s^{-1} for example over rough topography. Instead of a grid-based horizontal diffusivity, an isopycnal diffusion coefficient of $\kappa_{iso} = 1000$ m^2 s^{-1}is applied. In the upper layer, the K-profile parameterization (Large et al. 1994) is used in order to better represent the mixed layer. The atmospheric POTSDAM-2 model has a coarse horizontal resolution (7.5° latitude and 22.5° longitude) and is based on the assumption of a universal vertical structure of temperature and humidity, which allows reducing the three-dimensional description to a set of two-dimensional prognostic equations for temperature and humidity. Description of atmospheric dynamics is based on a quasigeostrophic approach and a parameterization of the zonally averaged meridional atmospheric circulation. The synoptic processes are parameterized as diffusion terms with a turbulent diffusivity computed from the atmospheric stability and horizontal temperature gradients. Heat and freshwater fluxes between the ocean and the atmosphere are computed on the oceanic grid and applied without any flux adjustments. The wind stress is computed as the sum of the National Centers for Environmental Prediction–National Center for Atmospheric Research (NCEP–NCAR) reanalysis wind stress climatology (Kalnay et al. 1996) and the wind stress anomaly calculated by the atmospheric model relative to the control run. The reader is referred to Montoya et al. (2005) for a description of the coupling and more details on the oceanic mixing parameterization, and to Mignot et al. (2006) for a discussion on the model's sensitivity to oceanic vertical diffusivity.

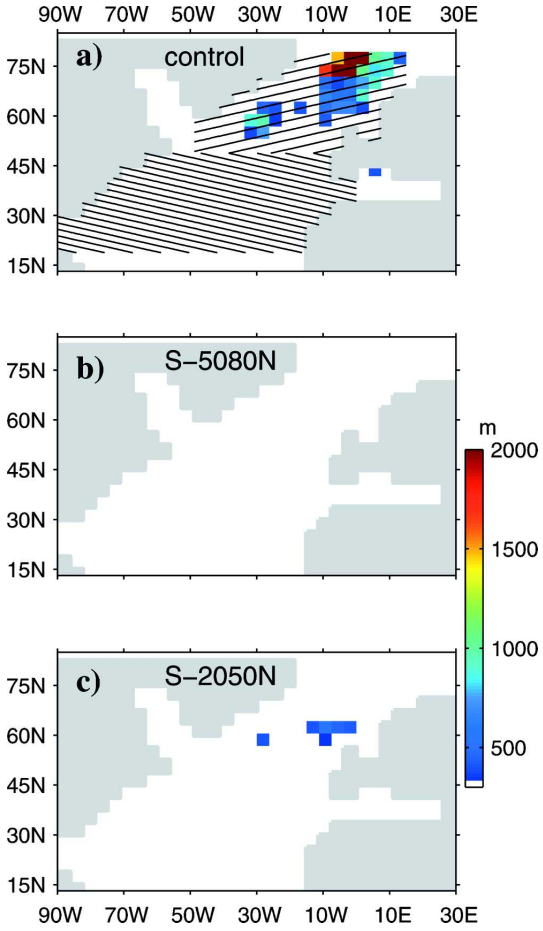

FIG. 1. Maximal depth of the turbulent mixed layer given by the model over the annual cycle in (a) the control run and in experiments (b) S-5080N and (c) S-2050N after 100 yr of anomalous forcing. In (a), the hatched areas represent the two forcing areas used in the study (see text).

The control model run has been integrated under present-day boundary conditions for more than 5000 yr. It yields an overturning circulation in the Atlantic of about 12 Sv, with deep-water formation occurring both in the Nordic Seas and in the Irminger Sea south of the Greenland–Scotland ridge (Fig. 1a). Note that it reaches much shallower depths in this latter area. Two specific experiments that differ in the location where the forcing is applied constitute the core of the study

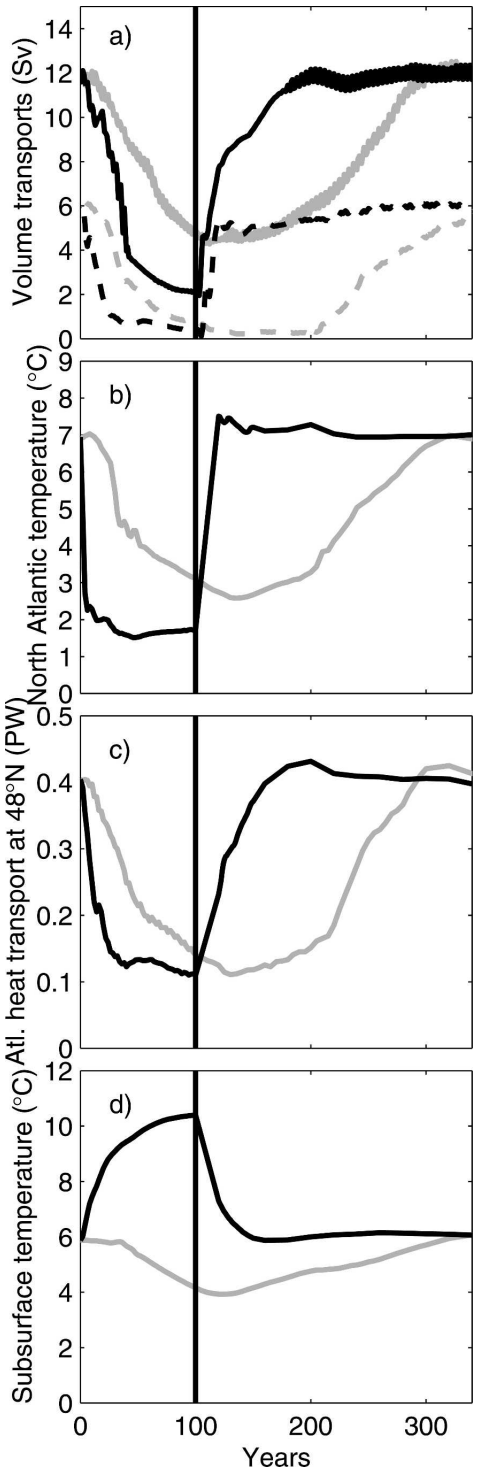

FIG. 2. (a) Time series of the maximum overturning circulation (solid) and overflow over the Greenland–Scotland ridge (dashed) annual averages in experiments S-2050N (cold case, gray) and S-5080N (warm case, black), respectively. The perturbation (equivalent to a freshwater flux of 0.35 Sv) was applied during 100 yr (black vertical line) before being removed. (b)–(d) The corresponding time series for the surface air temperature in the North Atlantic region (60°–90°N), the Atlantic ocean heat transport at 48°N, and the Atlantic subsurface temperature averaged between 40° and 80°N and between 100 and 700 m for the two experiments, respectively.

(Fig. 1a). Note that in all experiments, in spite of the fact that the model uses an explicit free surface, the perturbation consists in an extraction of salt, so that the volume of the ocean is unperturbed. In the first experiment (S-5080N), a negative anomalous salt flux corresponding to 0.35 Sv of freshwater flux was uniformly added in the high latitudes of the North Atlantic, between 50° and 80°N. This region covers the sites of deep-water formation in the model. This setup is similar to the one of the Coupled Model Intercomparison Project (CMIP; Stouffer et al. 2006). In the second experiment (S-2050N), an anomalous salt flux of identical amplitude (0.35 Sv) was added to the North Atlantic between 20° and 50°N. This region is located south of the deep-water formation sites and was used by several authors to investigate the possible bistability of the meridional overturning circulation (e.g., Wang 2005; Rahmstorf et al. 2005). Note that since the forcing areas differ in both experiments, the anomalous flux imposed at each grid cell (expressed in $m\,s^{-1}$) differs. Both experiments were integrated for 100 yr with anomalous forcing and an additional 300 yr without the forcing. Additional experiments were performed in order to investigate the sensitivity of the results to the strength and duration of the freshwater perturbation and to the oceanic vertical diffusivity. Details will be given below.

3. Subsurface temperature anomalies

After 100 yr of integration with 0.35-Sv anomalous equivalent freshwater flux, the AMOC is strongly reduced in both experiments. Deep-water formation in the Nordic Seas and south of the Greenland–Scotland ridge has ceased, as can be inferred from the very shallow mixed layer depth in Figs. 1b,c compared to the control run (Fig. 1a). In the case of the southern forcing region (S-2050N), ventilation down to about 600-m depth is still enabled around 60°N (Fig. 1c). This is much shallower than the maximum depths reached in the control simulation (more than 2000 m, Fig. 1a) and does not result in deep-water formation. The time scale for the AMOC shutdown also differs in the two experiments, as seen in Fig. 2a: it is much more abrupt in experiment S-5080N where deep-water formation sites are directly capped by the surface freshwater anomaly.

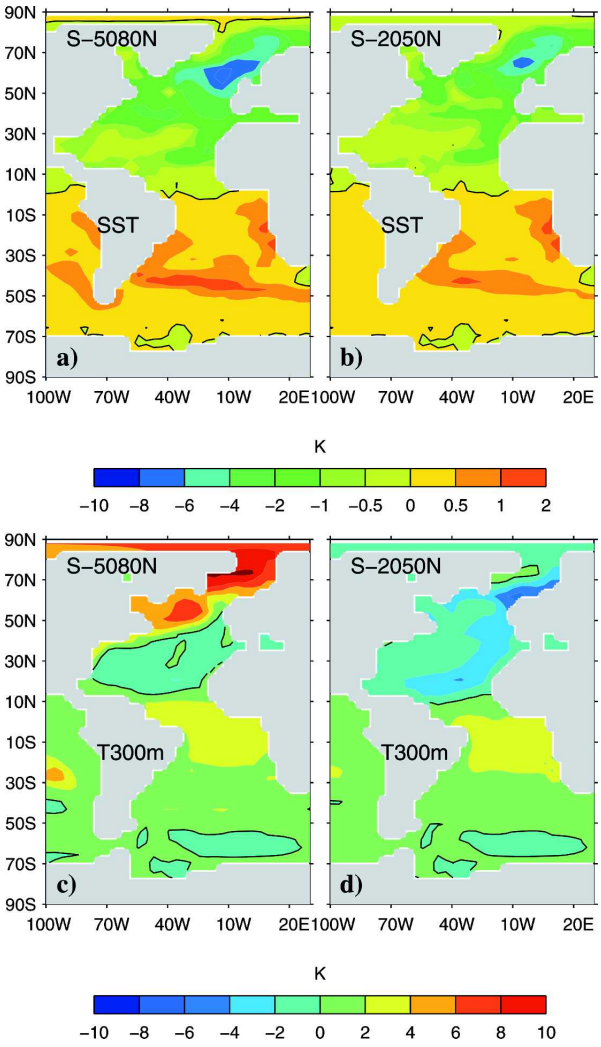

FIG. 3. Sea surface temperature anomaly in the Atlantic after 100 yr of anomalous forcing as compared to the control run in experiments (a) S-5080N (warm case) and (b) S-2050N (cold case), respectively. The black contour lines represent 0 K. (c), (d) Same as (a), (b), but for the temperature at 300-m depth.

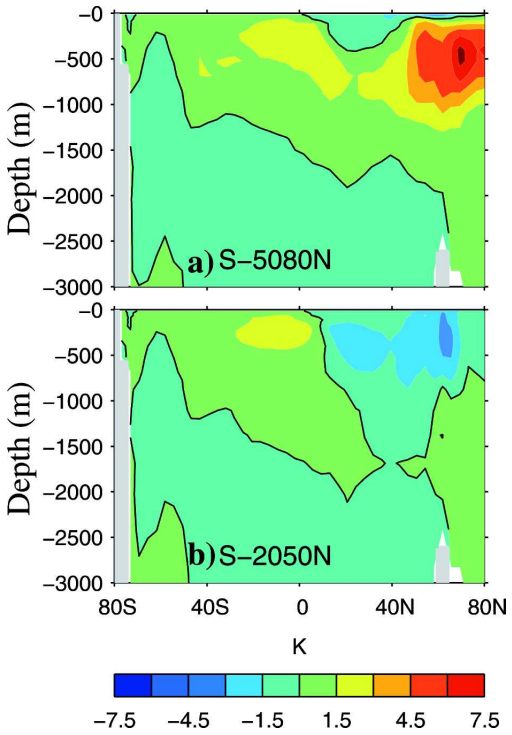

FIG. 4. Zonally averaged temperature anomaly in the Atlantic after 100 yr of anomalous forcing in experiments (a) S-5080N (warm case) and (b) S-2050N (cold case), respectively, as compared to the control run. The black contour line represents 0 K.

In S-2050N, the freshwater-induced salinity anomalies are carried to the north by the oceanic circulation itself (e.g., Goelzer et al. 2006). This is why time scales are longer while the amplitude of the reduction is smaller (see also Rahmstorf 1996; Manabe and Stouffer 1997).

The pattern of sea surface temperature difference to the control run is qualitatively the same for both experiments (Figs. 3a,b), and corresponds to the classic picture associated with a reduction of the northward oceanic heat transport [e.g., Manabe and Stouffer (1988) in equilibrium experiments; Vellinga and Wood (2002) in transient experiments]: the South Atlantic is warmer than the control run by 0.5–2 K while a cooling of up to 8 K occurs in the North Atlantic. In the latter basin, cooling is maximal (12 K in S-5080N and 10 K in S-2050N) in the deep-water formation regions as a result of the shutdown of deep convection. The anomalous surface air temperature show the same qualitative north–south dipole, with maximum amplitude over the Nordic Seas being higher in S-5080N, as shown in Fig. 2b.

On the other hand, strong differences between the two experiments arise at an intermediate depth in the northern North Atlantic (Figs. 3c,d). In the S-2050N experiment, temperature anomalies at 300 m are of the same sign as surface anomalies. In S-5080N, a strong warm anomaly is found north of 50°N. In the North Atlantic Tropics and subtropics, the waters at 300 m are colder than in the control run, but the anomaly is much reduced as compared to S-2050N at corresponding latitudes. Southern Atlantic subsurface is anomalously warm in both experiments.

The zonally averaged fields further document these Atlantic subsurface temperature anomalies (Fig. 4). The warming of the northern North Atlantic in S-5080N is maximal between 300 and 700 m, and reaches more than 8 K locally. We will refer to this

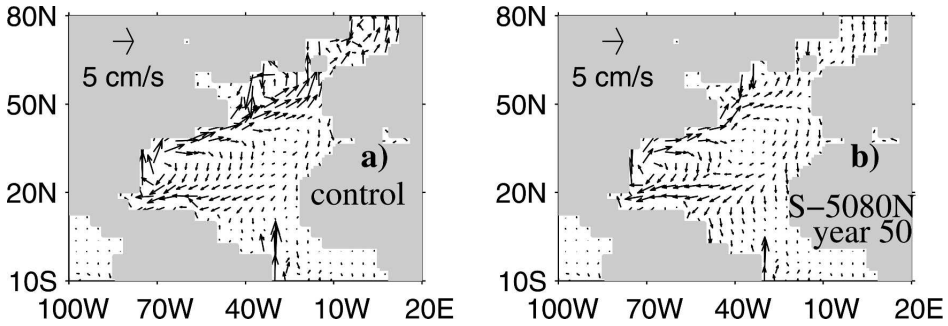

FIG. 5. Horizontal oceanic currents at 300-m depth in (a) the control run and (b) 50 yr after the beginning of the perturbation in experiment S-5080N.

situation as the "warm case." Together with a strong surface cooling, this implies vertical temperature inversions of more than 10 K within the upper 300 m. When the forcing is applied between 20° and 50°N, the cold surface anomalies reach down to about 1000-m depth ("cold case"). They are maximal above 600-m depth, which is approximately the pycnocline depth in the control run (Mignot et al. 2006).

The fundamental difference between the two experiments arises from different ventilation patterns and emerges already during the first years after the beginning of the perturbation (Fig. 2d). In the high-latitude forcing case (S-5080N, warm case), ventilation is rapidly and completely suppressed in the northern North Atlantic (Fig. 1b). Without any contact to the surface, the intermediate waters of the northern North Atlantic are protected from intense atmospheric cooling. On the other hand, the wind-induced circulation still enables ventilation in the tropical and subtropical Atlantic (e.g., Luyten et al. 1983) and northward transport of warm waters. This pathway is illustrated in Fig. 5b showing the horizontal circulation in the North Atlantic at 300-m depth 50 yr after the beginning the perturbation. It can be shown that this circulation pattern is established within the first decades after the beginning of the perturbation and then remains stable as long as the freshwater is applied. Obviously, the intergyre connection is strongly reduced as compared to the initial state with an active AMOC (Fig. 5a), but it still exists. However, in the absence of convection, surface heat loss is drastically reduced and this small transport of warm waters from the south is sufficient to distort the vertical isotherms resulting from deep-water formation in the control run. This explains the warm subsurface anomaly seen in Figs. 3c and Fig. 4a. In the cold case (S-2050N), on the other hand, ventilation of intermediate layers around 60°N (Fig. 1c) is sufficient for the surface cooling to reach intermediate depths (Fig. 4b). The reduction of the cross-equatorial heat transport explains surface and subsurface warming in the South Atlantic in both experiments.

The intermediate depth ventilation around 60°N also impacts the anomalous salinity structure of the Atlantic (Fig. 6a): in the warm case, the negative salinity anomaly imposed at the surface rather remains strictly confined to the upper 200 m. Below this upper layer, water masses are anomalously salty as compared to the control run. This results from northward advection of tropical waters, the same mechanism that induces the warm subsurface anomalies (e.g., Fig. 6b). In the cold case, the negative salinity anomaly penetrates down through ventilation to about 1000-m depth (Fig. 6a), as does the negative temperature anomaly (Fig. 6b). The fact that the subtropical anomaly reaches the high latitudes after subduction also contributes to the subsurface fresh anomaly in Fig. 6a. However, this does not explain the cold temperature anomaly in Fig. 6b. Finally, the vertical density structure from the two experiments is rather similar below the surface layer (Fig. 6c): the deep and intermediate water masses in the North Atlantic are slightly lighter than in the control run, because of the warm anomaly in the warm case (S-5080N) and of the fresh anomaly in the cold case (S-2050N). Note that Levermann and Griesel (2004) showed that the pycnocline depth is stable under hosing perturbations in the model.

4. Consequences for the recovery of the AMOC

The preindustrial climate as simulated by the control run of CLIMBER-3α is monostable in response to the water flux anomalies imposed here: the AMOC recovers as soon as the anomalous salt forcing is removed. Time series of this recovery are yet very different in the two experiments (Fig. 2a). The resumption from the warm case is abrupt and very fast (decadal time scales), while it is much more gradual (centennial time scales) for the cold case. As seen from Fig. 2, the average

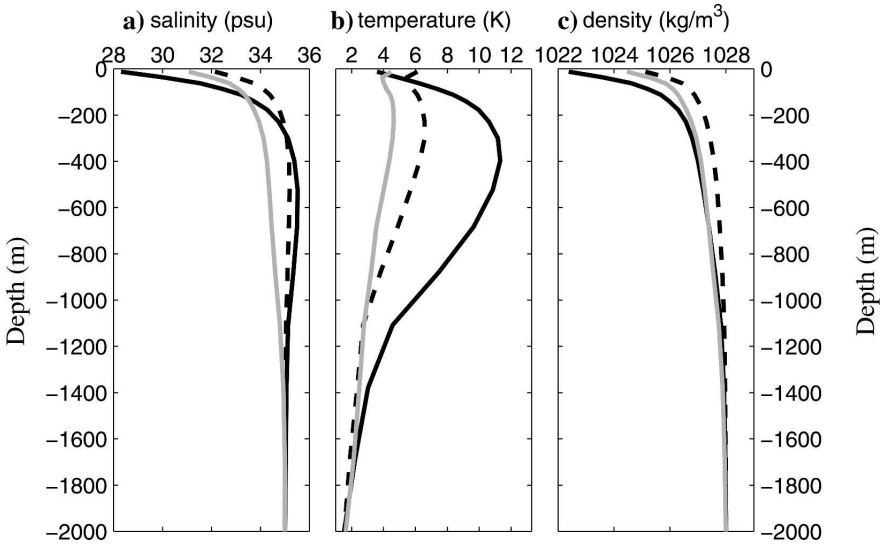

FIG. 6. (a) Salinity, (b) temperature, and (c) density profiles averaged in the Atlantic between 40° and 80°N after 100 yr of anomalous forcing in the Atlantic northern high latitudes (warm case, black lines) and in the Atlantic midlatitudes (cold case, gray lines). The dashed black line shows the same profiles in the control run.

surface air temperature in the North Atlantic (Fig. 2b) and the oceanic heat transport in the Atlantic at 48°N (Fig. 2c) closely follow the recovery of the AMOC (Fig. 2a). Salinity stratification is in fact much less favorable for the recovery in the warm case because of a much more pronounced halocline (Fig. 6a). In the absence of meridional heat transport, this difference in recovery time scales must thus result from the difference in temperature stratification.

In the warm case, sea surface salinity (SSS) in the hosing area starts to increase rapidly after the cessation of the anomalous freshwater flux, while SST changes little (Fig. 7c). This leads to an increase of mixed layer density that eventually exceeds that of the underlying layer. Convection starts first in the area where the SSS anomalies are smallest (compared to surrounding area) and the temperature inversion is strongest. These conditions are met in the area of strong wind-driven upwelling southeast of Greenland (Fig. 7a). Here, the mixed layer depth reaches several hundred meters already a few months after the cessation of anomalous freshwater flux (Fig. 8a, years 102–105). Consequently, the subsurface layer cools rapidly through air–sea interactions. Convection thus gradually weakens as the subsurface reservoir is damped, while it starts again in a more northward location (Fig. 8a, years 105–107). This is still not sufficient to switch deep convection on permanently (Fig. 8a, years 108–110), but it has enabled an increase of the density of intermediate water masses in the northern North Atlantic by cooling the relatively salty water mass (Fig. 9). This increases the meridional density gradient and drives the AMOC recovery. A weak circulation and shallow ventilation (Fig. 8a, around year 110) then brings salty water to high latitudes. As the fresh anomaly has at least partly been evacuated by the early convective spikes, it only takes about a decade for full deep convection to recover in the Nordic Seas. Note that the recovery of Atlantic overflow in S-5080N experiment starts simultaneously with the increase of the AMOC and reaches its full strength already during the first decade after the end of the hosing experiment.

The situation is very different in the experiment S-2050N where ventilation operates only south of the sill for 200 yr after the end of hosing. It is only then that the convection resumes north of the sill and that the overflow starts to recover (Fig. 8b). In this experiment, the persisting intermediate depth ventilation around 60°N is enough to progressively evacuate the fresh surface anomaly, reestablish the northward density gradient, and allow the circulation to slowly intensify (Fig. 2a). This is a relatively slow process because unlike temperature, salinity is a conservative tracer that can only be evacuated by ocean circulation. Advection of salt from the Tropics by the resuming overturning circulation itself further contributes to this gradual recovery (e.g., Stommel 1961). However, since the freshwater perturbation was applied in the subtropics, at least part of it subducted in the center of the subtropical gyre. Therefore, the subtropical waters advected by the

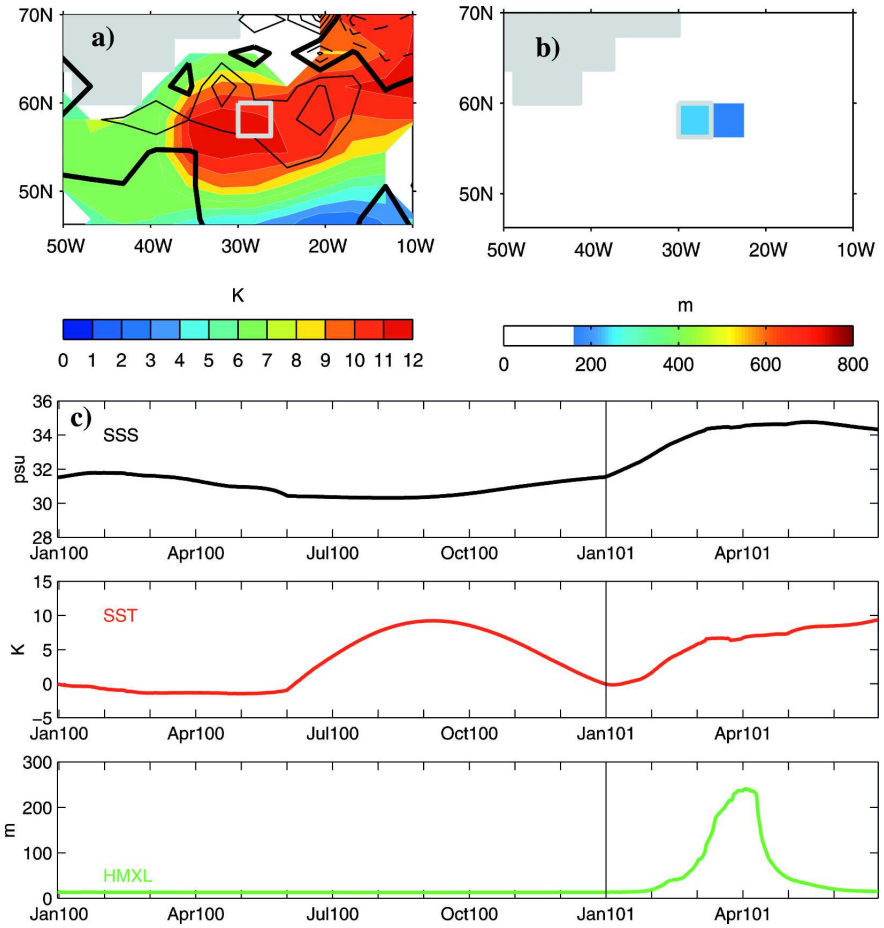

FIG. 7. Resumption mechanism in S-5080N. (a) (colors) Difference between SST and temperature at 300 m at year 100, i.e., at the end of the perturbation; a positive difference corresponds to subsurface temperatures warmer than SST. (contours) Curl of the wind stress in winter (January–March) of the first year after the end of the perturbation; continuous (dashed) contours are for positive (negative) values and are every 1×10^{-8} dyn cm^{-3} with the zero line in bold. Positive wind stress curl corresponds to upward Ekman velocity (upwelling). (b) Maximum oceanic mixed layer depth during the first winter of year 101, i.e., the year following the end of the perturbation. (c) Sea surface salinity, sea surface temperature, and turbulent mixed layer depth evolution at grid box marked in gray in (a), (b). The end of the perturbation is marked with the vertical black line at Jan101.

resuming circulation itself are not as salty as in the warm case. This further delays the recovery. The mixed layer gradually deepens during this slow process. More than 200 yr after the cessation of the perturbation, mixed layer depths exceed 1200 m both in the Irminger and Nordic Seas. It further deepens in the Nordic Seas during the following 100 yr.

The gradual recovery of the AMOC from the cold case thus occurs through the progressive deepening of initially shallow ventilation in high latitudes and evacuation of the freshwater locally while the intensifying circulation further evacuates the freshwater that was added in the subtropics and progressively brings relatively salty tropical waters to the north. Note that the cyclonic wind forcing and the associated Ekman upwelling operates essentially equally in both experiments. However, in the cold case, it is not sufficient to induce an abrupt recovery because stability of the water column is strongly maintained by the subsurface cold anomalies. In the warm case, it is combined with the strong vertical temperature inversion that facilitates destabilization of the water column. Note also that in the warm case, convection starts as soon as a few months after the end of the perturbation. This initial fast response is inconsistent with a purely advective mechanism. It is rather due to an initial destabilization of the

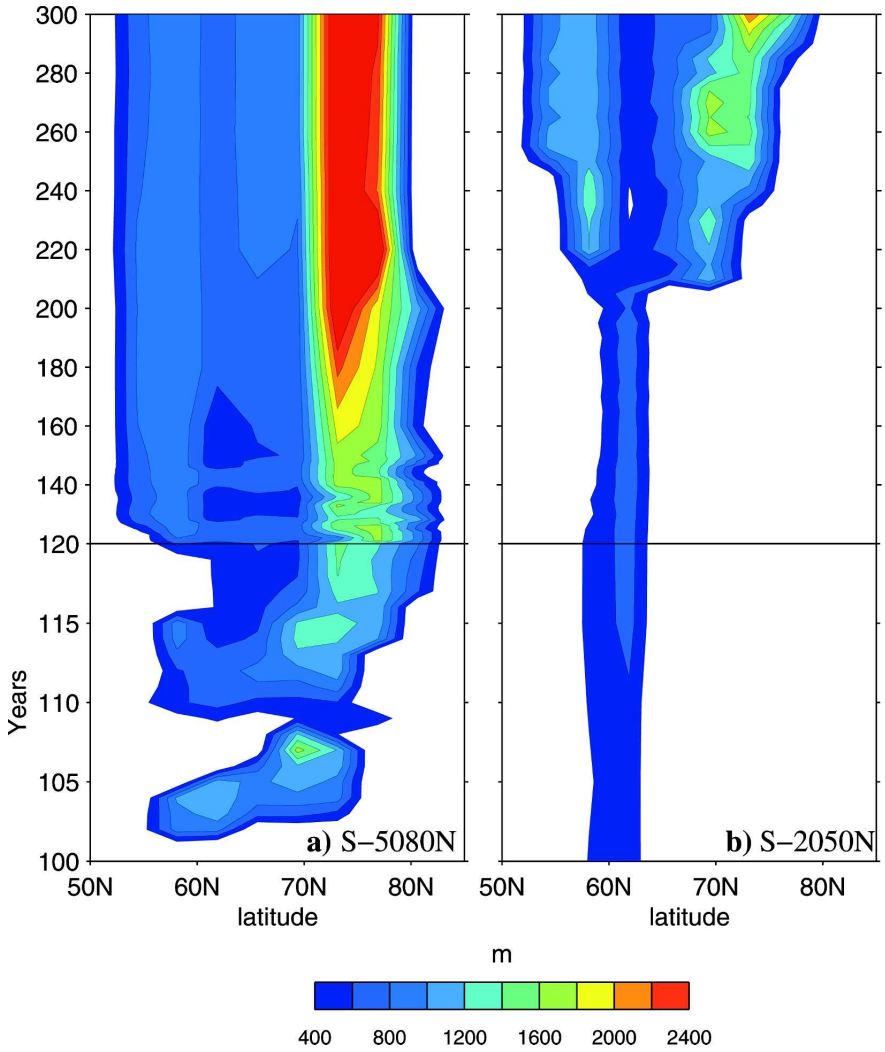

FIG. 8. Latitude–time evolution of maximum mixed layer depth in the northern North Atlantic for experiment (a) S-5080N (warm case) and (b) S-2050N (cold case). Note the change of time scale at year 120. In (a), contours are interpolated from yearly data until year 150 and from data sampled every 20 yr from year 160 on. In (b), snapshot results recorded every 5 yr are used.

water column as explained above. Only then does the salt advection mechanism come into play. The latter is more efficient in the warm case since saltier subtropical waters were less affected by the freshwater perturbation.

The dynamics of the AMOC recovery is thus very different in both experiments, yielding time scales of the order of decades in the warm case and centuries in the cold case. In the next section, we analyze the robustness of these findings to details of the experimental setup, namely, the magnitude and duration of the perturbation, its time evolution, and the oceanic vertical diffusivity.

5. Sensitivity analysis

Let us first investigate the sensitivity of the results to the magnitude of anomalous freshwater flux imposed on the North Atlantic. Experiments similar to the ones described above were performed with an anomalous salt flux equivalent to 0.1, 0.2, and 0.5 Sv of freshwater, respectively. The same types of anomalies develop in all cases, irrespective of the forcing magnitude (Fig. 10a). The magnitude of the anomaly increases with the strength of the perturbation. This increase is rather linear in the cold case while it saturates for strong perturbations in the warm case. The warm anomaly is the

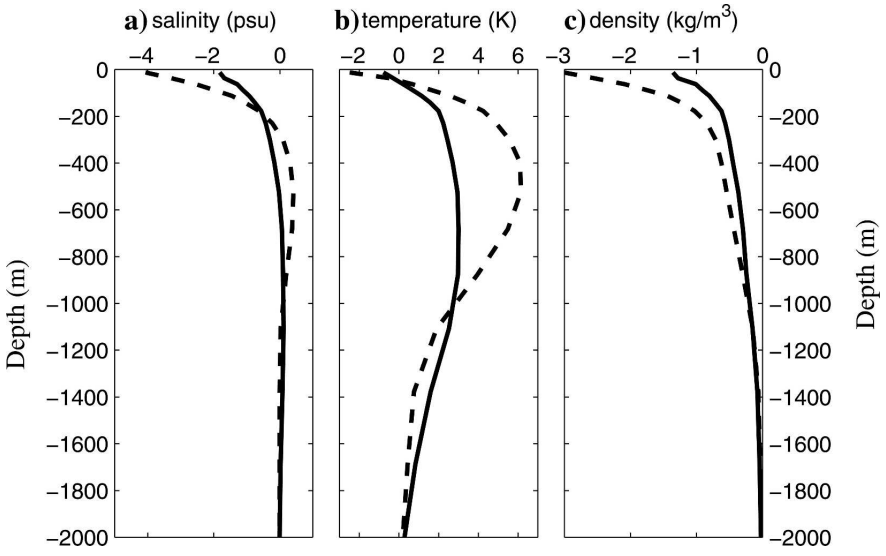

FIG. 9. Anomalous (a) salinity, (b) temperature, and (c) density profiles in the warm case. The profiles are Atlantic averages between 55° and 80°N and computed as the difference to the control run. The dashed line shows the anomalous profile after 100 yr of anomalous forcing and the continuous line is at year 110, i.e., 10 yr after the end of the perturbation.

result of a balance between horizontal circulation and diffusion. The saturation can be understood through the maximum distortion of isotherms that can be induced by this balance. The AMOC recovery time is always longer in the corresponding cold case (Fig. 10b). In the warm case, it is of the order of a few decades for all the perturbation magnitudes that we tested. In the cold case, it increases approximately linearly with the magnitude of the perturbation and is of the order of one to two centuries.

An additional pair of experiments was performed to investigate the sensitivity of the results to the perturbation duration. Figure 11 shows the response of AMOC and overflow to 0.35 Sv of anomalous freshwater imposed over 1000 yr. This experiment is admittedly rather extreme but it shows that qualitative differences between the cold (gray) and warm (black) cases are the same as for shorter perturbations (cf. Fig. 2). Subsurface temperature anomalies are slightly stronger in case of a longer forcing (Fig. 10a, open circles), because the equilibrium is not reached in the shorter experiments (100 yr). This supports the fact that the sign of subsurface temperature changes is not a transient effect and does not depend on the duration of the water hosing. It is an important point in order to compare the results to previous work. More discussion is given in section 6. In the cold case, time needed for the AMOC to recover 80% of its initial value is slightly longer than in the 100-yr perturbation experiment (Fig. 10b, open circles). In the warm case, it is even shorter and the AMOC overshoots before eventually stabilizing.

The steplike forcing scenarios applied above are extremely simplified, and probably not realistic to represent, for example, the massive discharges of icebergs that are believed to have taken place in the past (e.g., Heinrich 1988). A freshwater input increasing and decreasing more progressively with time (e.g., linearly) is less straightforward in terms of interpretation but probably more realistic. Several experiments were carried out with such forcing scenarios, and Fig. 12 shows that the results presented above are robust: in the warm case, both the shutdown and the recovery of the AMOC are much more abrupt than in the cold one. Note that the recovery begins before the perturbation ceases completely. It only requires that the imposed freshwater anomaly is weaker than a threshold value that can be counteracted by the ventilation and the circulation itself in the cold case and the temperature-induced destabilization of the water column associated to wind-driven upwelling in the warm case, as explained in section 4.

Finally, robustness of the results to the oceanic vertical diffusivity κ was tested. No qualitative differences in the results were found when the standard background value $\kappa = 0.1 \times 10^{-4}$ m^2 s^{-1} was increased to $\kappa = 0.3 \times 10^{-4}$ m^2 s^{-1} (Fig. 10, triangles). Maximum subsurface temperature anomalies are of the same order of magnitude. Recovery time scales are also well

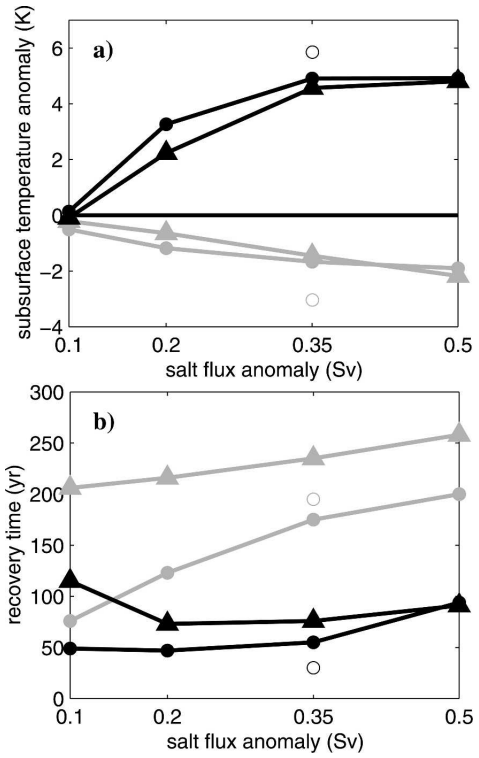

FIG. 10. (filled circles) (a) Subsurface temperature anomaly averaged in the North Atlantic between 40° and 80°N and between 300- and 700-m depth and (b) time (years) needed for the AMOC to reach 80% of its initial value after cessation of anomalous freshwater flux in experiments S-2050N (cold case, gray) and S-5080N (warm case, black), respectively, with different magnitudes of the freshwater anomaly. For each experiment, the anomaly has been applied for 100 yr. (open circles) Same but for the experiments where the 0.35Sv of equivalent freshwater anomaly are applied during 1000 yr. (triangles) Same as filled circles, but with an increased oceanic vertical diffusivity ($\kappa = 0.3 \times 10^{-4}$ m^2 s^{-1}).

separated for both experiments. It is larger by up to 50 yr in S-5080N and by 75 yr in S-2050N for $\kappa = 0.3 \times 10^{-4}$ m^2 s^{-1} as compared to $\kappa = 0.1 \times 10^{-4}$ m^2 s^{-1}.

These findings give us confidence in the robustness of the results. A discussion of the applicability of our results to other models and to the findings of previous studies is given in section 6.

6. Conclusions and discussion

We used the coupled climate model CLIMBER-3α to investigate the vertical thermal structure in the Atlantic following a cessation of deep-water formation. For this, we analyzed several experiments where a surface freshwater perturbation was applied either in the high latitudes of the North Atlantic (over the deep convection sites) or in the Atlantic midlatitudes. We found that although both experiments lead to a rapid shutdown of deep-water formation and the AMOC and to a surface cooling in the North Atlantic, they induce radically different subsurface temperature anomalies, depending on the possibility for intermediate depth ventilation to take place or not. When the latter is suppressed, the subsurface waters in the North Atlantic are completely isolated from the cold atmosphere in the northern North Atlantic and only the subtropical ventilation is active. Propagation of warm water masses at the intermediate depth into the northern North Atlantic leads to robust warm subsurface anomalies and the development of a strong vertical temperature inversion in the Nordic Seas (warm case). In the case of active intermediate depth ventilation, subsurface waters are cooled by contact with the atmosphere (cold case).

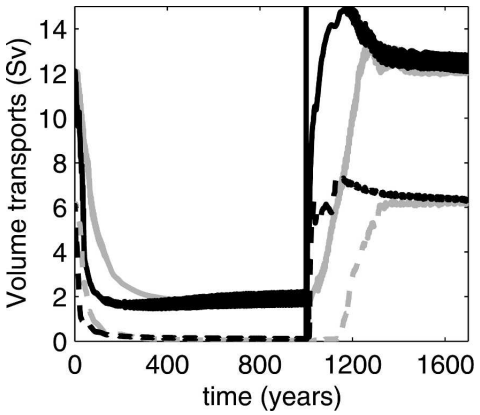

FIG. 11. As in Fig. 2a, but when the anomalous forcing is applied for 1000 yr.

These two cases have been observed in previous studies: Manabe and Stouffer (1997) and Rind et al. (2001) reported a subsurface cooling in response to the

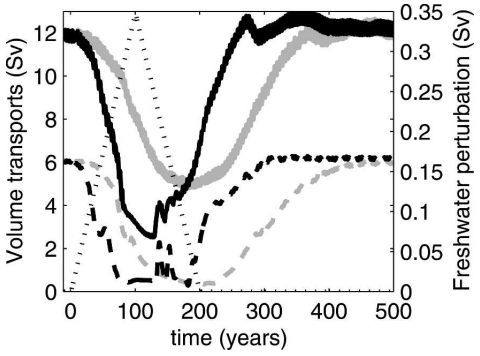

FIG. 12. As in Fig. 2a, but for the forcing scenario represented with the dotted black line (right scale).

shutdown of the AMOC while Rühlemann et al. (2004) and Knutti et al. (2004) observed a warming. Our study sheds light on understanding these differences: the sign of the anomaly depends on whether intermediate ventilation continues or is shut down completely under freshwater perturbation and the magnitude and region of water hosing required to completely shut down intermediate water formation is model dependent. This might explain the apparent difference of our results with those from Manabe and Stouffer (1997). In their experiments where freshwater hosing is applied between 50° and 70°N, a strong subsurface cooling developed, while in similar experiment S-5080N, we found a subsurface warming. A possible explanation for this difference is that intermediate convection was still active in their experiment, which should thus rather be compared to our S-2050N experiment, where we also find subsurface cooling. The CMIP intercomparison involves both models of intermediate complexity and fully coupled general circulation models (Stouffer et al. 2006). Subsurface anomalies induced in response to the application of 0.1 Sv of anomalous freshwater over the deep-water formation region are very weak because the freshwater perturbation is not sufficient to significantly alter the overturning. However, warm anomalies are a general feature of the subsurface temperature structure in response to the application of 1 Sv of anomalous freshwater over the deep convection sites of the models, that is, when deep convection is off in all models (J. Yin 2005, personal communication). Using a climate model of intermediate complexity with glacial boundary conditions, Flueckiger et al. (2006) find a strong subsurface cooling for a freshwater perturbation of 0.2 Sv (as compared to an on-state with the same freshwater flux), and a subsurface warming for a large freshwater flux (0.4 Sv). This differs from our results, where the sign of the subsurface anomaly does not depend on the strength of freshwater forcing. It is unclear whether this is due to differences between the models or if it is related to the different climate states.

We showed that the subsurface temperature structure has crucial implications for the recovery of the AMOC once the freshwater perturbation is removed. When a warm reservoir has developed in subsurface, the recovery occurs on decadal time scales. Indeed, SSS rises rapidly and, with the help of wind-driven upwelling, the water column can be easily destabilized. This gives rise to intense flushes of deep-water formation that evacuate the warm subsurface anomaly very quickly through air–sea interactions and erode the surface fresh anomaly. These initial flushes allow a rapid increase of the subsurface northward density gradient. A sustainable AMOC and permanent deep-water formation in the North Atlantic thus occur within another decade. In experiments where the AMOC was perturbed in midlatitudes, and where subsurface cold anomalies were maintained by intermediate depth ventilation, the AMOC recovery is much more gradual (typically over a century). It is the weak and shallow residual circulation associated with this ventilation that progressively evacuates the freshwater and brings at the same time relatively salty tropical waters to the north.

These results where shown to be robust to various details of the experimental setup, such as the duration, magnitude, and time evolution of the freshwater perturbation, and the oceanic vertical mixing. They are consistent with Stouffer and Manabe (2003) who underlined the influence of temperature distribution in subsurface and deeper layers of the Atlantic Ocean on the final state of the AMOC. Furthermore, we believe that they can help understanding and interpreting the diversity of the models' responses to hosing experiments and in particular the AMOC recovery (Stouffer et al. 2006). We emphasize that the relatively "slow" recovery observed in S-2050N is in fact typical for most water hosing experiments. It is associated with a positive advection–salinity feedback as already discussed by Rahmstorf (1996) or Goelzer et al. (2006). The real novelty here is the relatively fast (decadal time scales) recovery detected in S-5080N. The mechanism is initiated by an abrupt startup of convection in the high latitudes, which leads to fast initial recovery of the AMOC. Only after that does the salinity advection feedback come into play. Thus, the decadal recovery time scale in S-5080N is explained as the time scale of baroclinic adjustment to imposed density changes. In S-2050N, a complete recovery of the AMOC can only happen after a complete overturning of Atlantic water masses, that is, indeed on a centennial time scale.

The experiments were carried out with a climate model of intermediate complexity, and we cannot rule out that atmospheric variability (missing in CLIMBER-3α) might be important for the subsurface temperature anomalies. However, a strong subsurface warming was also reported by Knutti et al. (2004) who used the ECBILT-CLIO model, which has a rather realistic extratropical variability. Moreover, the results of the 1-Sv hosing show a subsurface warming in all the coupled GCMs of the CMIP experiment (J. Yin 2005, personal communication). Finally, SST anomalies are very similar in both runs (Figs. 3a,b), so that we do not expect strong differences in the atmospheric response of the two experiments. Therefore, we do not believe that our results are just an artifact due to missing atmospheric

variability. On the other hand, missing atmospheric feedback could possibly be important for the fast recovery mechanism. In particular, Schiller et al. (1997) find an important feedback of SST anomalies on the atmospheric cyclonic circulation over the Norwegian Sea. In their model, this feedback stabilizes deep-water formation in the North Atlantic. More generally, differences in the mean climate state might also be important for the impact of anomalous freshwater input, both in terms of subsurface temperature response and in terms of MOC recovery.

Beyond these modeling results, our findings have a series of more general implications. In particular, large subsurface temperature anomalies associated with a possible future reduction of the AMOC can have significant geochemical impacts (e.g., for the stability of the ocean clathrates reservoir). In the present climate, the latter are present at a depth of several hundred meters and below and several studies have shown that a warming of several degrees would strongly affect their stability. (e.g., Archer and Buffett 2005; Schicks et al. 2006). Furthermore, although our results were obtained in idealized water hosing experiments performed for modern climate conditions, they may also have important implications for understanding mechanisms of abrupt climate changes during the last glacial cycle. Our results demonstrate that if convection and ventilation are completely suppressed in the high latitudes of the North Atlantic by enhanced freshwater flux, the recovery of the AMOC after cessation of anomalous freshwater flux occurs abruptly and air temperature rises within several decades by about 6 K on average over the northern North Atlantic. When the perturbation is applied for a sufficiently long period, AMOC, overflow, and air temperature even overshoot their equilibrium values. This resembles the dynamics of the Dansgaard–Oeschger warm events recorded during the last glacial cycle in Greenland and other locations, and corroborates the results of simulations of Dansgaard–Oeschger events obtained with two-dimensional ocean models (Winton 1997; Ganopolski and Rahmstorf 2001). Interestingly enough, a pronounced warming of the subsurface water masses during cold (stadial) conditions in the Nordic Seas was reported by Rasmussen and Thomsen (2004), though the interpretation of benthic isotopes remains ambiguous. Additional simulations, especially using glacial climate conditions, would be needed to corroborate applicability of our results to the mechanism of Dansgaard–Oeschger events. In particular, some of the Dansgaard–Oeschger events last 3000 yr or more and show a decreasing trend over the whole interstadial. An overshooting phenomenon will probably not last for such a long time period. This implies that other factors are important in setting the shape of the events.

Another interesting implication of our results is related to the timing of the massive iceberg discharges into the North Atlantic. Recently, Moros et al. (2002) proposed that increased iceberg discharge during cold stadial events may have resulted from the destabilization of marine ice shelves by a strong subsurface melting caused, in turn, by enhanced oceanic heat transport. Alternatively, our results suggest that a considerable subsurface warming might be caused by a complete cessation of intermediate ventilation during periods of decreased northward heat transport and the maximum cooling in the Northern Hemisphere. This idea was first introduced by Shaffer et al. (2004), even though subsurface warming in this simplified model as well as in Winton's (1997) deep-coupling–decoupling oscillations reach much deeper down (about 3000 m) than in the experiments shown here. The link between subsurface warming and cessation of intermediate ventilation is further supported by recent findings of Flueckiger et al. (2006). In particular, this mechanism sheds some light on the long-standing problem—why ice-rafted events (including Heinrich events) always occurred during cold (stadial) conditions in the North Atlantic. Here again, glacial simulations are required for a more definitive conclusion. One possible scenario is that the initial suppression of deep-water formation and establishing of a strong halocline in the glacial Nordic Seas are caused by melting or small-scale instability of surrounding ice sheets and ice caps. As soon as the ventilation is ceased completely, a subsurface warming starts to develop and via intense bottom melting of marine ice shelves provokes a large-scale instability of the Laurentide ice sheets. This might explain an apparent synchrony of ice-rafted events observed in different locations during the glacial age. The basal melting of ice shelves, whose depth ranges from a few hundred of meters to more than 1 km for the modern climate (Antarctica), is indeed very sensitive to the water temperature and increases by 10 m yr^{-1} for each 1 K of water temperature rise (e.g., Rignot and Jacobs 2002). Thereby if the subsurface temperature rose during glacial stadials by 0–5 K, it could lead to a complete melting of ice shelf in a matter of decades. While the mechanism of teleconnection between different ice sheets is promising, one has to admit that the degree of coupling between grounded ice and ice shelves remains a controversial issue.

Acknowledgments. JM and AL were funded by the Gary Comer foundation. The authors would also like to

thank S. Rahmstorf for useful comments and J. Yin for providing additional results of the CMIP.

REFERENCES

Archer, D., and B. Buffett, 2005: Time-dependent response of the global ocean clathrate reservoir to climatic and anthropogenic forcing. *Geochem. Geophys. Geosyst.,* **6,** Q03002, doi:10.1029/2004GC000854.

Bond, G., and Coauthors, 1992: Evidence for massive discharge of icebergs into the North Atlantic Ocean during the last glacial. *Nature,* **360,** 245–249.

Broccoli, A. J., K. A. Dahl, and R. J. Stouffer, 2006: Response of the ITCZ to Northern Hemisphere cooling. *Geophys. Res. Lett.,* **33,** L01702, doi:10.1029/2005GL024546.

Church, J. A., J. M. Gregory, P. Huybrechts, M. Kuhn, K. Lambeck, M. T. Nhuan, D. Qin, and P. L. Woodworth, 2001: Change in sea level. *Climate Change 2001: The Scientific Basis,* J. T. Houghton et al., Eds., Cambridge University Press, 640–693.

Clarke, P. U., N. G. Pisias, T. F. Stocker, and A. J. Weaver, 2002: The role of the thermohaline circulation in abrupt climate change. *Nature,* **415,** 863–869.

Crowley, T. J., 1992: North Atlantic deep water cools the southern hemisphere. *Paleoceanography,* **7,** 489–497.

Dickson, B., I. Yashayaev, J. Meincke, B. Turrell, S. Dye, and J. Holfort, 2002: Rapid freshening of the deep North Atlantic Ocean over the past four decades. *Nature,* **416,** 832–837.

Fanning, A. F., and A. J. Weaver, 1997: Temporal-geographical meltwater influences on the North Atlantic Conveyor: Implications for the Younger Dryas. *Paleoceanography,* **12,** 307–320.

Fichefet, T., and M. A. M. Maqueda, 1997: Sensitivity of a global sea ice model to the treatment of ice thermodynamics and dynamics. *J. Geophys. Res.,* **102,** 12 609–12 646.

Flueckiger, J., R. Knutti, and J. W. C. White, 2006: Oceanic processes as potential trigger and amplifying mechanisms for Heinrich Events. *Paleoceanography,* **21,** PA2014, doi:10.1029/2005PA001204.

Ganachaud, A., and C. Wunsch, 2000: Improved estimates of global ocean circulation, heat transport and mixing from hydrographic data. *Nature,* **408,** 453–456.

Ganopolski, A., and S. Rahmstorf, 2001: Rapid changes of glacial climate simulated in a coupled climate model. *Nature,* **409,** 153–158.

Goelzer, H., J. Mignot, A. Levermann, and S. Rahmstorf, 2006: Tropical versus high latitude freshwater influence on the thermohaline circulation. *Climate Dyn.,* **27,** 715–725.

Gregory, J. M., O. A. Saenko, and A. J. Weaver, 2003: The role of the Atlantic freshwater balance in the hysteresis of the meridional overturning circulation. *Climate Dyn.,* **21,** 707–717.

Hasumi, H., and N. Suginohara, 1999: Effects of locally enhanced vertical diffusivity over rough bathymetry on the world ocean circulation. *J. Geophys. Res.,* **104,** 23 364–23 374.

Heinrich, H., 1988: Origin and consequences of cyclic ice rafting in the northeastern Atlantic Ocean during the past 130,000 years. *Quat. Res.,* **29,** 142–152.

Herweijer, C., R. Seager, M. Winton, and A. Clement, 2005: Why ocean heat transport warms the global mean climate. *Tellus,* **57A,** 662–675.

Hofmann, M., and M. A. M. Maqueda, 2006: Performance of a second-order moments advection scheme in an Ocean General Circulation Model. *J. Geophys. Res.,* **111,** C05006, doi:10.1029/2005JC003279.

Houghton, J. T., Y. Ding, D. J. Griggs, M. Noguer, P. J. van der Linden, X. Dai, K. Maskell, and C. A. Johnson, Eds., 2001: *Climate Change 2001: The Scientific Basis*. Cambridge University Press, 881 pp.

Kalnay, E., and Coauthors, 1996: The NCEP/NCAR 40-Year Reanalysis Project. *Bull. Amer. Meteor. Soc.,* **77,** 437–471.

Knutti, R., J. Flueckiger, T. F. Stocker, and A. Timmernmann, 2004: Strong hemispheric coupling of glacial climate through freshwater discharge and ocean circulation. *Nature,* **430,** 851–856.

Large, W. G., J. C. McWilliams, and J. C. Doney, 1994: Oceanic vertical mixing: A review and a model with a nonlocal boundary layer parameterization. *Rev. Geophys.,* **32,** 363–403.

Ledwell, J. R., E. T. Montgomery, K. L. Polzin, L. C. St. Laurent, R. W. Schmitt, and J. M. Toole, 2000: Evidence for enhanced mixing over rough topography in the abyssal ocean. *Nature,* **403,** 179–182.

Levermann, A., and A. Griesel, 2004: Solution of a model for the oceanic pycnocline depth: Scaling of overturning strength and meridional pressure difference. *Geophys. Res. Lett.,* **31,** L17302, doi:10.1029/2004GL020678.

——, ——, M. Hofmann, M. Montoya, and S. Rahmstorf, 2005: Dynamic sea level changes following changes in the thermohaline circulation. *Climate Dyn.,* **24,** 347–354.

Luyten, J. R., J. Pedlosky, and H. Stommel, 1983: The ventilated thermocline. *J. Phys. Oceanogr.,* **13,** 292–309.

Manabe, S., and R. J. Stouffer, 1988: Two stable equilibria of a coupled ocean–atmosphere model. *J. Climate,* **1,** 841–866.

——, and ——, 1993: Century-scale effects of increased atmospheric CO_2 on the ocean-atmosphere system. *Nature,* **364,** 215–218.

——, and ——, 1995: Simulation of abrupt climate change induced by freshwater input to the North Atlantic Ocean. *Nature,* **378,** 165–167.

——, and ——, 1997: Coupled ocean-atmosphere model response to freshwater input: Comparison to Younger Dryas event. *Paleoceanography,* **12,** 321–336.

McManus, J. F., R. Francois, J.-M. Gherardi, L. D. Keigwin, and S. Brown-Leger, 2004: Collapse and rapid resumption of Atlantic meridional circulation linked to deglacial climate changes. *Nature,* **428,** 834–837.

Mignot, J., A. Levermann, and A. Griesel, 2006: A decomposition of the Atlantic meridional overturning circulation into physical components using its sensitivity to vertical diffusivity. *J. Phys. Oceanogr.,* **36,** 636–650.

Montoya, M., A. Griesel, A. Levermann, J. Mignot, M. Hofmann, A. Ganopolski, and S. Rahmstorf, 2005: The Earth system model of intermediate complexity CLIMBER-3α. Part I: Description and performance for present day conditions. *Climate Dyn.,* **25** (2–3), 237–263.

Moros, M., A. Kuijpers, I. Snowball, S. Lassen, D. Bäckström, F. Gingele, and J. McManus, 2002: Were glacial iceberg surges in the North Atlantic triggered by climatic warming? *Mar. Geol.,* **192,** 393–417.

Peterson, B. J., R. M. Holmes, J. W. McClelland, C. J. Vörösmarty, R. B. Lammers, A. I. Shiklomanov, I. A. Shiklomanov, and S. Rahmstorf, 2002: Increasing river discharge to the Arctic Ocean. *Science,* **298** (5601), 2171–2173.

Peterson, L. C., G. H. Haig, K. A. Hughen, and U. Röhl, 2000: Rapid changes in the hydrologic cycle of the tropical Atlantic during the last glacial. *Science,* **290,** 1947–1951.

Petoukhov, V., A. Ganopolski, V. Brovkin, M. Claussen, A. Eliseev, C. Kubatzki, and S. Rahmstorf, 2000: CLIMBER 2: A climate system model of intermediate complexity. Part I: Model description and performance for present climate. *Climate Dyn.,* **16,** 1–17.

Prather, M. J., 1986: Numerical advection by conservation of second-order moments. *J. Geophys. Res.,* **91,** 6671–6681.

Rahmstorf, S., 1996: On the freshwater forcing and transport of the Atlantic thermohaline circulation. *Climate Dyn.,* **12,** 799–811.

——, 2002: Ocean circulation and climate during the past 120, 000 years. *Nature,* **419,** 207–214.

——, and A. Ganopolski, 1999: Long-term global warming scenarios computed with an efficient coupled climate model. *Climatic Change,* **43,** 353–367.

——, and Coauthors, 2005: Thermohaline circulation hysteresis: A model intercomparison. *Geophys. Res. Lett.,* **32,** L23605, doi:10.1029/2005GL023655.

Rasmussen, T. L., and E. Thomsen, 2004: The role of the North Atlantic Drift in the millennial timescale glacial climate fluctuations. *Palaeogeogr. Palaeoclimatol. Palaeoecol.,* **210,** 101–116.

Rignot, E., and S. S. Jacobs, 2002: Rapid bottom melting widespread near Antarctic ice sheet grounding lines. *Science,* **296,** 2020–2023.

Rind, D., G. Russell, G. Schmidt, S. Sheth, D. Collins, P. deMenocal, and J. Teller, 2001: Effects of glacial meltwater in the GISS coupled atmosphere-ocean model 2. A bipolar seesaw in Atlantic Deep Water production. *J. Geophys. Res.,* **106,** 27 355–27 365.

Rühlemann, C., S. Mulitza, G. Lohmann, A. Paul, M. Prange, and G. Wefer, 2004: Intermediate depth warming in the tropical Atlantic related to weakened thermohaline circulation: Combining paleoclimate data and modelling results for the last deglaciation. *Paleoceanography,* **19,** PA1025, doi:10.1029/2003PA000948.

Schicks, J. M., R. Naumann, J. Erzinger, K. C. Hester, C. A. Koh, and E. D. Sloan Jr., 2006: Phase transitions in mixed gas hydrates: Experimental observations versus calculated data. *J. Phys. Chem. B,* **110,** 11 468–11 474.

Schiller, A., U. Mikolajewicz, and R. Voss, 1997: The stability of the North Atlantic thermohaline circulation in a coupled ocean-atmosphere general circulation model. *Climate Dyn.,* **13,** 325–347.

Shaffer, G., S. Malskaer Olsen, and C. J. Bjerrum, 2004: Ocean subsurface warming as a mechanism for coupling Dansgaard-Oeschger climate cycles and ice-rafting events. *Geophys. Res. Lett.,* **31,** L24202, doi:10.1029/2004GL020968.

Stocker, T. F., 1998: The seesaw effect. *Science,* **282,** 61–62.

——, and D. G. Wright, 1991: Rapid transitions of the ocean's deep circulation induced by changes in surface water fluxes. *Nature,* **351,** 729–732.

Stommel, H. M., 1961: Thermohaline convection with two stable regimes of flow. *Tellus,* **13,** 224–230.

Stouffer, R. J., and S. Manabe, 2003: Equilibrium response of thermohaline circulation to large changes in atmospheric CO_2 concentration. *Climate Dyn.,* **20,** 759–773.

——, and Coauthors, 2006: Investigating the causes of the response of the thermohaline circulation to past and future climate changes. *J. Climate,* **19,** 1365–1387.

Timmermann, A., S.-I. An, U. Krebs, and H. Goosse, 2005: ENSO suppression due to weakening of the North Atlantic thermohaline circulation. *J. Climate,* **18,** 3122–3139.

Trenberth, K. E., and J. M. Caron, 2001: Estimates of meridional atmosphere and ocean heat transports. *J. Climate,* **14,** 3433–3443.

Vellinga, M., and R. Wood, 2002: Global climatic impacts of a collapse of the Atlantic thermohaline circulation. *Climatic Change,* **54,** 251–267.

Wang, Z., 2005: Two climatic states and feedbacks on thermohaline circulation in an Earth system model of intermediate complexity. *Climate Dyn.,* **25,** 299–314.

Winton, M., 1997: The effect of cold climate upon North Atlantic Deep Water formation in a simple ocean-atmosphere model. *J. Climate,* **10,** 37–51.

——, 2003: On the climatic impact of ocean circulation. *J. Climate,* **16,** 2875–2889.

Clim. Past, 7, 1439–1455, 2011
www.clim-past.net/7/1439/2011/
doi:10.5194/cp-7-1439-2011

Climate of the Past

Volcanic impact on the Atlantic Ocean over the last millennium

J. Mignot[1], **M. Khodri**[1], **C. Frankignoul**[1], **and J. Servonnat**[2]

[1]LOCEAN-IPSL UMR 7159 CNRS-IRD MNHN-UPMC, Case 100, Université Pierre et Marie Curie, 4 place Jussieu, 75252 Paris Cedex 05, France
[2]LSCE-IPSL UMR 8212, CEA-Orme des Merisiers, 91191 Gif-sur-Yvette Cedex, France

Received: 19 July 2011 – Published in Clim. Past Discuss.: 2 August 2011
Revised: 4 November 2011 – Accepted: 22 November 2011 – Published: 21 December 2011

Abstract. The oceanic response to volcanic eruptions over the last 1000 years is investigated with a focus on the North Atlantic Ocean, using a fully coupled AOGCM forced by a realistic time series of volcanic eruptions, total solar irradiance (TSI) and atmospheric greenhouse gases concentration. The model simulates little response to TSI variations but a strong and long-lasting thermal and dynamical oceanic adjustment to volcanic forcing, which is shown to be a function of the time period of the volcanic eruptions. The thermal response consists of a fast tropical cooling due to the radiative forcing by the volcanic eruptions, followed by a penetration of this cooling in the subtropical ocean interior one to five years after the eruption, and propagation of the anomalies toward the high latitudes. The oceanic circulation first adjusts rapidly to low latitude anomalous wind stress induced by the strong cooling. The Atlantic Meridional Overturning Circulation (AMOC) shows a significant intensification 5 to 10 years after the eruptions of the period post-1400 A.D., in response to anomalous atmospheric momentum forcing, and a slight weakening in the following decade. In response to the stronger eruptions occurring between 1100 and 1300, the AMOC shows no intensification and a stronger reduction after 10 years. This study thus stresses the diversity of AMOC response to volcanic eruptions in climate models and discusses possible explanations.

1 Introduction

Understanding the climate fluctuations at decadal timescales and the climate response to external forcing is of prime importance to anticipate and understand future climate changes. The last millennium constitutes an interesting framework for investigating natural and forced variations, as climate reconstructions are reaching a relatively high temporal resolution (Jones et al. 2001, Mann et al. 2009), and show substantial decadal to multidecadal fluctuations (e.g. Gray et al. 2004). However, reliable oceanic reconstructions are still very rare (Sicre et al. 2008, Masse et al. 2008, Richter et al. 2009), mainly because of the difficulty to obtain undisturbed high sedimentation rate and well-dated marine sediments. Meanwhile, computer resources are increasing so that climate integrations using state-of-the-art coupled ocean-atmospheric general circulation models (OAGCM) are becoming routinely available over this period, allowing investigations of the mechanisms of low frequency climate variability.

Several observational studies have shown that the ocean, and in particular the North Atlantic, plays a large role in decadal climate variability (e.g. Knight et al., 2005 Sutton and Hodson 2003, 2005). The relative importance of the various external forcings, however, remains debated. In model studies, this is partly due to their different representation and partly to divergent model responses. The researchers van der Schrier et al. (2002) and Hofer et al. (2010) suggested that external forcings, primarily variations of the total solar irradiance (TSI), act as modulators of the natural climate variability. Goosse and Renssen (2006) reported a decrease of the large scale Atlantic Meridional Overturning Circulation (AMOC) for increasing TSI, similar to the response to an increased atmospheric CO2 concentration. In Zorita et al. (2004), on the contrary, the TSI does not have a significant impact on the AMOC.

Volcanic eruptions constitute another important external forcing over the last millennium. Their climatic impact has been largely investigated in terms of atmospheric thermal and dynamical anomalies in relation with the North Atlantic Oscillation, the El Nino-Southern Oscillation or the monsoons systems (e.g. Oman 2006, Shindell et al. 2004, Stenchikov et al. 2006, Trenberth and Dai 2007). Probably because of the lack of reliable reconstructions, fewer studies have

Correspondence to: J. Mignot
(juliette.mignot@locean-ipsl.upmc.fr)

Published by Copernicus Publications on behalf of the European Geosciences Union.

focused on their effect on the oceans. Church et al. (2005) and Gleckler et al. (2006) suggested that oceanic anomalies following a volcanic eruption could last more than a decade. Applying sensitivity response studies to relatively recent eruptions (the Pinatubo in 1991 and the Tambora in 1815), Stenchikov et al. (2009) showed that, while radiative forcing produced by these explosive events lasted for about 3 years, the volcanically induced tropospheric temperature anomalies remained significant for seven years, the sea ice responded on decadal time scales, and the deep ocean temperature, sea level, salinity and the AMOC were perturbed for several decades to a century. In particular, the AMOC strengthened by roughly 10 %, but the amplitude to the response scaled less than linearly with the strength of the eruption. In response to a super-eruption with 100 time the Pinatubo amount of sulphuric acid released in the stratosphere, Jones et al. (2005) found that the AMOC doubled in intensity after nine years. Ottera et al. (2010), Ortega et al. (2011) and Zanchettin et al. (2011) all found an intensification of the AMOC in long simulations forced by both reconstructions of volcanic eruptions and variations in TSI. This response was associated to a persistent positive phase of the North Atlantic Oscillation (NAO) in Ottera et al. (2010). In both Ortega et al. (2011) and Zanchettin et al. (2011) (2011), the AMOC intensification is induced by enhanced convection in the Nordic Seas rather than in the Labrador Sea as in Ottera et al. (2010).

Several studies have also begun to point out the specificity of the thirteenth century in terms of intense volcanic activity and the possibility for a cumulative impact on the ocean (e.g. Zhong et al. 2010). The second half of the thirteen century is indeed the most perturbed half century of the past 1500 years (Jansen et al. 2007). In two out of four simulations, Zhong et al. (2010) found a centennial-scale climate change following the succession of decadally paced eruptions following the 1257–1258 mega-eruption. They highlighted a coupled ice-ocean interaction between the subpolar North Atlantic, a reduced extension of the AMOC into the northern North Atlantic, and the Arctic Ocean, which maintained significantly expanded sea ice and reduced surface air temperatures for at least 100 years. However, the feedback mechanism depended on other factors since it was only activated in half of the simulations. In this context, it is important to highlight that while both Stenchikov et al. (2009) and Ottera et al. (2010) found a significant intensification of the AMOC following volcanic eruptions, the first study was based on sensitivity experiments following single eruptions of different intensities and the other based on composite analysis over the last 600 years of the millennium, thereby excluding the particular succession of events of the thirteenth century.

Here, we explore the interannual to decadal oceanic response to volcanic activity in a coupled OAGCM forced by a full set of reconstructed external forcings over the last millennium. Sicre et al. (2011) have shown that the simulated sea surface temperature (SST) in the northern North Atlantic compares well with a recent high resolution SST reconstruction off Iceland. We propose to describe more thoroughly the oceanic response to the major volcanic eruptions of the last millennium and investigate the mechanisms for the oceanic circulation adjustment. The model configuration and the forcings are presented in Sect. 2. The oceanic response to solar and volcanic forcing are compared in Sect. 3 and the temperature response to volcanic eruptions is discussed in Sect. 4. In Sect. 5, we investigate the response of the Atlantic circulation to isolated volcanic eruptions (occurring after year 1400) and in Sect. 6, we highlight the differences with the twelfth and thirteenth century. Conclusions are given in Sect. 7.

2 Model and experiment

2.1 The coupled model

We use the IPSLCM4 v2 climate model developed at the Institut Pierre-Simon Laplace (Marti et al. 2010). This model couples the LMDz4 atmosphere GCM (Hourdin et al. 2006) and the ORCHIDEE 1.9.1 module for continental surfaces (Krinner et al., 2005) to the OPA8.2 ocean model (Madec et al. 1998) and the LIM2 sea-ice model (Fichefet and Maqueda 1997), using the OASIS coupler (Valcke et al. 2000). The resolution in the atmosphere is 3.75° in longitude, 2.5° in latitude, and 19 vertical levels. The ocean and sea-ice are implemented on the ORCA2 grid (averaged horizontal resolution $2 \times 2°$, refined to 0.5° around the equator, 31 vertical levels). In all simulations, the vegetation was set to a modern climatology from Myneni et al. (1997). After a 310 year spin up with preindustrial greenhouse gases (GHG) concentrations and tropospheric aerosols, two simulations were run. The first one is a 1000-year control simulation with the same preindustrial conditions as the spin up, also used in Servonnat et al. (2010). The main characteristics of the AMOC in the model and its sensitivity to freshwater have been discussed by Swingedouw et al. (2007). They showed that an excess of freshwater flux over the Labrador Sea was responsible for the lack of deep convection in this region and the relatively weak AMOC (11 Sv) in the model. Deep convection in the northern North Atlantic only takes place in the Nordic Seas and south of Iceland (Marti et al. 2010). The natural variability of the AMOC, its link to deep convection and its impact on the atmosphere have been studied by Msadek and Frankignoul (2009). They showed that the multidecadal fluctuations of the AMOC are mostly driven by the deep convection in the subpolar gyre with a time lag of 6 to 7 years. Convection in the subpolar gyre is itself primarily influenced by anomalous salinity advection caused by the variability of the East Atlantic Pattern (EAP), second dominant mode of atmospheric variability in the North Atlantic region. The lack of Labrador Sea convection in the model probably

explains the dominance of the EAP (as opposed to the North Atlantic Oscillation) in forcing multidecadal variations of the AMOC. The second simulation (LM2SV) was forced with a reconstruction of TSI, GHGs concentrations, changes in orbital parameters, and radiative effect of volcanic eruptions over the last millennium, from 850 to 2000 A.D. The choice and implementation of the forcings are discussed below. To reduce the influence of the model drift, a quadratic trend was removed from each variable and grid point.

As our main focus is on the oceanic response to volcanic eruptions at interannual to decadal timescales, all data are considered in annual mean, or seasonal mean for such variables as sea ice cover and mixed layer depth.

2.2 External forcing over the last millennium

A number of different reconstructions for TSI variations have been produced (e.g. Jansen et al. 2007), mostly differing in the estimated reduction of total irradiance during the 17th century Maunder Minimum, which ranges from 0.08 % to 0.65 % (1.1 to 8.9 Wm^{-2}) of the contemporary value. Ammann et al. (2007) found that a TSI decrease of about 0.25 % during the Maunder Minimum produces a realistic amplitude of the Northern Hemisphere temperature change in climate models. However, recent progress in solar physics (Foukal et al. 2004, Solanki and Krivova 2006, Gray et al. 2010) imply that the TSI variations between the Maunder Minimum and present day value are about 0.1 %. On the other hand, even more recently, Shapiro et al. (2011) found indications of very large variations of the solar forcing during the Holocene. Nevertheless, as the weak scaling is recommended for the third phase of the paleoclimate modeling inter-comparison project (PMIP III, Schmidt et al. 2011), we use the TSI reconstruction by Vieira and Solanki (2010) and Krivova et al., (personal communication, 2009), which follows it. The corresponding variations of the raw shortwave input at the top of the atmosphere is shown in Fig. (2) (top panel).

Large volcanic eruptions inject sulfur gases into the stratosphere, which convert to sulfate aerosols with a residence time of about a year. The aerosol cloud has several effects on radiative processes, most notably by backscattering part of the incoming solar radiation, which induces a net cooling at the Earth's surface (e.g. Robock 2000). Thus, until recent years, most modelling groups (e.g. Jansen et al. 2007) have represented the volcanic forcing by altering the solar constant. Although such a coarse approach leads to hemispheric averages that compared reasonably well to a "blend" of proxy and/or instrumental reconstructions (e.g. Goosse et al. 2005, Stendel et al. 2006), it does not properly represent regional and seasonal variations. It is indeed known that the climatic impact of volcanic eruptions highly depends on the season, and that latitudinal dependence of the cooling in the troposphere (warming in stratosphere) evolves for at least 2 to 3 years after the eruption. Furthermore, the volcanic aerosols serve as surfaces for heterogeneous chemical

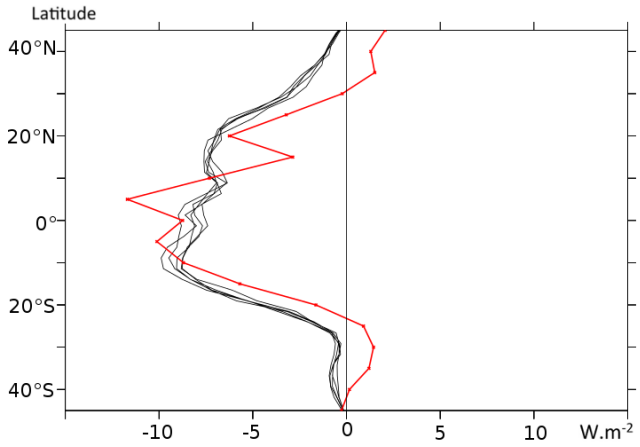

Fig. 1. Comparison of August 1991 absorbed shortwave radiative fluxes (SW, in W m^{-2}) at the top of the atmosphere (TOA) anomalies from Earth Radiation Budget Satellite (ERBS) observations (red) and 5 members simulation ensemble with the IPSLCM4v2 model (black). The simulated anomalies are computed as the differences between the Mt Pinatubo simulations and the control run. ERBS TOA SW radiative fluxes anomalies are expressed relatively to a 1985 to 1989 base climatology.

reactions that destroy stratospheric ozone, which controls solar energy absorption in the stratosphere. Its variations thus alter both the vertical temperature gradient between the troposphere and the stratosphere and the latitudinal temperature gradient in the stratosphere. We implemented in the IPSL model a new radiative module that mimics the direct radiative effect of sulphate aerosols. The input time series is based on the monthly mean optical thickness latitudinal reconstruction by Ammann et al. (2003) and Gao et al. (2008) from A.D. 850 to present. Vertically, the atmosphere in our model is divided into 19 hybrid sigma pressure levels with 4 layers above the tropopause. Due to the rather coarse vertical resolution, the optical properties of stratospheric sulfate aerosols in the visible band are evenly spread over the first two layers of the stratosphere. The optical properties were computed assuming a fixed sulfate aerosol droplet size distribution with a standard deviation of 1.8 μm and an effective radius of 0.5 μm corresponding to the average size of the Mt Pinatubo aerosols. As in Gao et al. (2008), all volcanic aerosols originate in the tropical band between 20° S and 20° N, where they last for few months, then spread poleward before decaying 3 years after the eruption started. As a validation, Fig. (1) shows the responses of reflected solar flux at the top of the atmosphere in August 1991, displayed as zonal averages between 40° S and 40° N in order to be comparable to Earth Radiation Budget Satellite (Minnis et al., 1993) in a series of sensitivity experiments. The model displays an overall agreement with the observations: shortwave anomalies associated with the volcanic eruption reaching 10 $W m^{-2}$ between 10° S and 10° N in both model and observations.

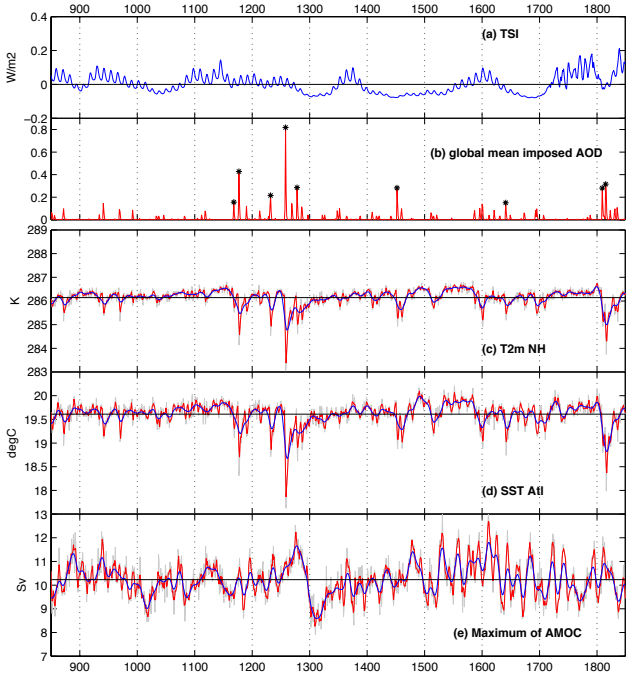

Fig. 2. Time series from 850 to 1850 of **(a)** Anomalous short wave input at the top of the atmosphere, taken as an estimation of variations of the TSI, **(b)** Imposed optical depth of volcanic aerosols. **(c)** Northern Hemisphere air temperature at 2 m **(d)** SST averaged between 30°S and 70°N in the Atlantic **(e)**. Maximum of the meridional overturning circulation between 10°N and 60°N and below 500 m depth in the Atlantic. For **c, d,** and **e**, raw annual mean data are shown in grey and low pass filtered data using a running mean of 3 years in red. Low pass filtered data using a spline function with a cutoff at 20 years are shown in blue.

Figure (2) (second panel) illustrates the time series of implemented stratospheric volcanic aerosols optical depth. Note that a change in the global mean optical depth of 0.1 corresponds to a global anomalous radiative forcing of roughly $-3\,W\,m^{-2}$. However, as discussed in Timmreck et al. (2009), the volcanic module tends to overestimate the radiative effect of the mega eruptions because of the use, for paleo-eruptions, of aerosol effective radius and optical depth derived from observations over the instrumental period, specifically for the Mount Pinatubo (1991) and El Chichón (1982) volcanic eruptions.

The greenhouse gas concentrations are those inferred from ice cores and direct measurements as reported in Servonnat et al. (2010). This simulation does not include the forcing by anthropic aerosols, so that global warming detected over the last decades of the simulation is overestimated (not shown). Hence, this study focuses on the natural external forcings and the period of investigation is limited to years 850 to 1849 A.D.

3 Temperature response to solar and volcanic forcings

Figure (2) also shows the air temperature at 2 m averaged over the Northern Hemisphere (third panel) and he SST averaged over the Atlantic Ocean (fourth panel). These time series highlight the fact that centennial variability is relatively weak in this simulation, and that some centennial features such as temperature shifts between the medieval climate anomaly (MCA) and the Little Ice Age (LIA) are not simulated in the model, unlike several reconstructions. Whether this is due to a model deficiency or the weak TSI variations is difficult to assess. We admit nevertheless that under TSI reconstructions with larger variations (Crowley 2000), the same model led to much larger SST low frequency variations, in relative agreement with paleoreconstructions, except for the onset of the MCA (Servonnat et al. 2010). The most striking signal in these time series are in fact important variations following volcanic eruptions, in particular an abrupt cooling of up to 3 °C in the atmosphere and 1 °C in the ocean. Such signature has also recently been found in temperature reconstructions in the subpolar North Atlantic (Sicre et al., 2011). On the other hand, variations of the solar insolation do not seem to have a strong imprint. The lagged correlation r of the anomalous TSI time series with the averaged surface air temperature in the Northern Hemisphere and with the Atlantic SST have a broad but weak maximum when the TSI leads by 4 years, reaching $r = 0.12$ and 0.13, respectively (significant at the 5 % level) (Fig. 3). The corresponding correlation with the volcanic forcing is much larger, peaking when temperature lags by one year, with $r = -0.63$ and $r = -0.52$, respectively. For both air and sea temperature, the correlation with the volcanic signal remains significant for more than 15 years. Note that the significant correlation at lag -1 in Fig. (3) is due to the use of annual averages, as eruptions might in fact have started during the calendar year preceding the maximum of emission. The stronger influence of volcanic forcing is probably due to our use of a TSI reconstruction with weak variations and to an overestimation of the volcanic radiative effect (Sect. 2.2). In this sense, this simulation could be considered as a sensitivity study to volcanic eruptions over the last millennium.

The frequency dependence of the solar correlation is illustrated by the cross-wavelet coherence spectra in Fig. (4). The wavelet analysis was made with the Morlet wavelet, and the transform performed in Fourier space, using zero padding to reduce wraparound effects (Torrence and Compo 1998). The parameters were chosen to give a total of 57 periods ranging from 0.5 to 256 years, and the square coherency were calculated using smoothing in the time and space domain (Grinsted et al. 2004), with the 5 % significance level determined from a Monte-Carlo simulation of 1000 sets of surrogate time series. The two temperature time series show episodic coherency with the solar forcing at 11 year period (Fig. (4), top panels), in particular around 1200 and 1600. Meehl et al. (2008, 2009) indeed showed that a peak in

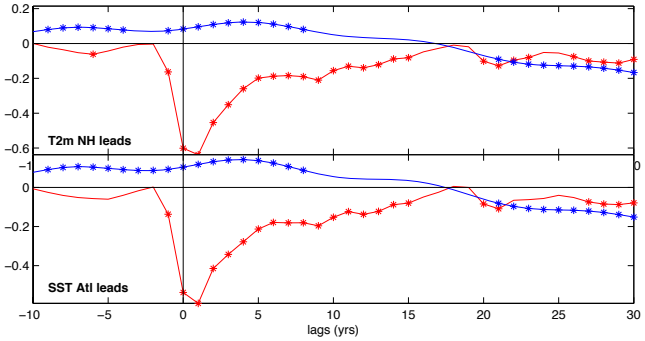

Fig. 3. Cross correlation between the temperature time series in Fig. 2 and the time series of the solar forcing (blue) and the volcanic forcing (red) from 850 to 1850 A.D. Lags with a star are significant at the 5 % level, tested against a bootstrap procedure with 500 permutation of the forcing time series using blocks of 3 years.

the solar activity induces surface cooling in the tropical Pacific. Kuroda et al. (2008) showed that over the historical period, years of anomalously high solar irradiance were associated with a large warming of the lower stratosphere through radiative heating. Such a temperature anomaly in the stratosphere creates anomalous temperature of opposite sign at lower heights. However, these processes require a much higher resolution in the stratosphere to be properly represented. In fact, episodic coherency between SST and TSI variations at 11 years timescale is also seen in the control simulation, suggesting that the significativity test is too liberal. Signal in Fig. (4) is thus most probably internal to the data sets and does not indicate physical response of the ocean to the 11-year cycle. Furthermore, the 11-year cycle Fig. (2) (top) is primarily an extrapolation back in time of the 11-cycle observed in sunspots after year 1600. It is thus largely artificial. The temperature time series also show strong coherency with the TSI variations at multidecadal timescale from 1700, associated to the TSI increase, and at centennial time scales over the whole simulation (Fig. 4, second and third panels).

It is somewhat more difficult to distinguish the response of the Atlantic meridional overturning circulation (AMOC) from its natural variability. As shown in Fig. (2) (bottom panels), the AMOC intensifies during the second half of the thirteenth century, when volcanic activity was intense, peaks around year 1280 and then rapidly decreases, reaching a minimum around year 1320, about 60 years after the major eruption of 1260. There is a hint of a weak response to the eruptive events in the early 1800s. As shown in Fig. (4) (bottom), there is a hint of a weak coherence between the time series of AMOC maximum with the TSI variations at 11-year periods, but this is so sparse that such interpretation is debatable. There is a more significant coherence at about 100-year period, with TSI leading by 15 years (not shown). Correlations with the volcanic forcing are barely significant.

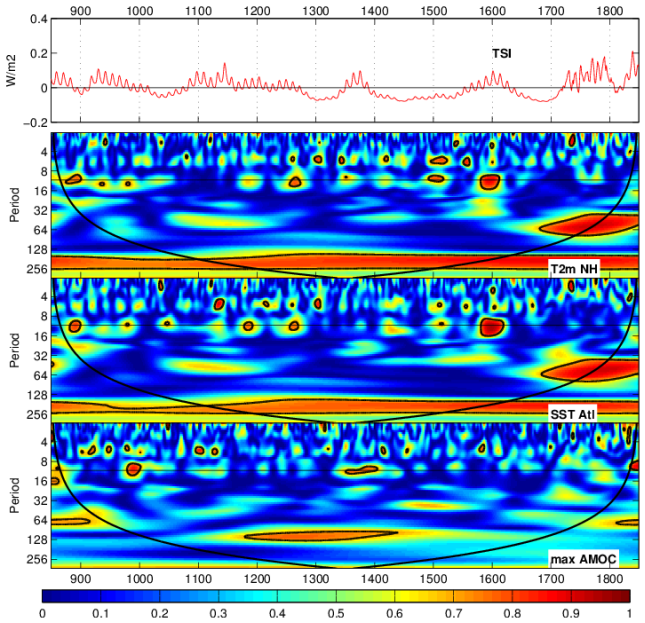

Fig. 4. Time series of the solar forcing (top) and cross-wavelet coherence spectrum of the temperature time series in Fig. 2 (bottom three panels). The thick contours enclose regions of greater than 95 % confidence and the thin lines indicate the limit of the cone of influence. The horizontal line indicates the 11 year period.

As will be shown below, this does not imply that there is no AMOC response to natural forcings, in particular volcanic eruptions. Time series of AMOC maximum represents one mode of AMOC variability, namely a basin scale acceleration, as discussed for example in Msadek and Frankignoul (2009). More local AMOC adjustments require more specific analysis. In the following, we concentrate on the response to volcanic forcing, which has a much stronger impact on the atmospheric and the oceanic temperature than the solar forcing in the model.

4 Anomalous temperature patterns in response to volcanic eruptions

To describe the oceanic response to a volcanic eruption, we construct a composite evolution based on the oceanic anomalies that follow the major eruptions. For each selected eruption, anomalies are computed as the difference between the time evolution of the field after the eruption and a reference defined as the average of the field during the two years preceding the eruption. A longer reference period would have the advantage to filter out inter annual climatic variability, but on the other hand, it would make the composites more sensitive to lower frequency variability. The choice of a shorter reference period was motivated by the focus of this study on the response of Atlantic Ocean circulation which is dominated by relatively long timescale variability. Note,

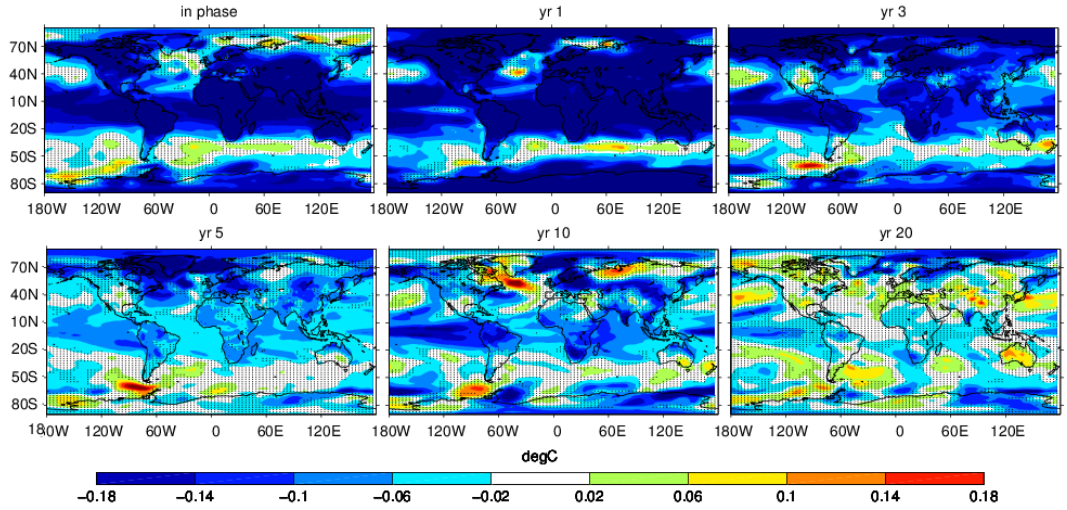

Fig. 5. Composites of annual mean anomalous surface temperature for different time lags (in years) with respect to the volcanic eruptions corresponding to optical depths higher than 0.15. Surface temperature corresponds to SST over the ocean and air temperature otherwise. Dotted areas are not significant at the 5 % level

.

however, that major results are unchanged for a reference period lasting up to five years prior to the eruption. Composites are then defined as the average of these anomalies scaled by the inverse of the magnitude of each eruption, so that possible non linear effects linked to the eruption magnitude are minimized. Note however that our conclusions are unchanged without this normalization. In order to maximize the signal to noise ratio, we focused on relatively large eruptions, and thus selected eruptions corresponding to an increase of stratospheric aerosol optical depth (AOD) by more than 0.15 (eruptions marked with a star in Fig. 2), which is equivalent to a global radiative forcing of at least $-2.8\,W\,m^{-2}$. This corresponds to the 9 strongest eruptions between A.D. 850 and 1849. As seen in Fig. (2) and discussed in Sect. 2.2, several of the selected events follow each other by less than 10 years (1169–1178, 1810–1816). To minimize the interference between successive events, eruptions which precede another one by less than the considered time lag in the composite were omitted. As a consequence, the number of events in the composites may decrease with lag. The resulting composites are rescaled by 0.15 so that the amplitude of the results that are displayed are for an eruption with a stratospheric global mean optical depth equal to 0.15. Significativity is tested with a block bootstrap procedure with 500 permutations of the volcanic time series in blocks of 3 years (the maximum residence time of stratospheric aerosols). Composites are recomputed using each of these, resulting forcing time series in order so as to define the noise level.

Figure (5) shows composites of anomalous global annual mean surface temperature up to 20 years after a volcanic eruption of AOD of 0.15. The first panel (year 0) shows that the maximum cooling occurs in the tropics and on the lands during the year of the eruption. There is also a meridional dipole in the Southern Atlantic and the Indian oceans, which can be shown to be due to a shift of the westerlies, persisting for a year. In winter only, the anomalous winter warming over Eurasia consistent with the observations (e.g. Robock and Mao 1992) is significant at the 10 % level (not shown) and closely related to tropospheric and stratospheric circulation changes. As the lag increases, the tropical oceanic signal extends in latitude, reflecting the spreading of the atmospheric cooling (e.g. Robock 2000), while progressively decaying in the tropics. In the subpolar North Atlantic, the cooling peaks at year 3 and decays thereafter. Note the relatively rapid decay of the cooling in the eastern equatorial Pacific at year 1, also present at year 2 (not shown) which could be due to an El Nino-like response. One to two years after the eruption, there is an anomalous warming in the North Atlantic midlatitudes, the origin of which is discussed below. An anomalous warming near the Drake Passage becomes significant at year 3 and reaches its maximum at year 5. Ten years after the eruption, the whole tropical band is still significantly anomalously cold, as well as some land areas such as in Eurasia. In the North Atlantic, the most striking feature is an anomalous warming in the Labrador Sea, which decays thereafter.

Figure (6) shows similar composites for the zonally averaged global oceanic temperature response as a function of depth up to 20 years after a volcanic eruption. Consistent with Fig. (5), a temperature decrease of up to 0.25 K appears

in the upper tropical ocean during the eruption year, together with a warming below 100 m depth in the deep tropics. The latter results from a thickening of the tropical thermocline and a decrease of equatorial ventilation following a weakening of the trade winds, as discussed below. The surface cooling already reaches 60° N, but its poleward extension is stronger one year after the eruption, consistent with Fig. (5). By year 1, the signal has penetrated in the ocean interior around 30° N and 30° S, where oceanic ventilation mostly takes place. In the subtropics, the downwelling is shifted slightly poleward of the climatological ventilation region, indicated by the mean isotherms in Fig. (6) (white contours). As in Laurian et al. (2009), the shift can be explained by the poleward displacement of the surface isopycnals resulting from the surface cooling. Deep penetration down to 900 m of the cooling is also seen around 60° N at year 1, reflecting enhanced deep convection. Deep convection also mixes the cooling signal down in the Southern Ocean, reaching its largest depth 2 to 3 years after the eruption (not shown). In the following years, the tropical surface cooling decays, while persisting at depth and deepening further (Fig. (6), year 5). As the surface cooling reaches greater depths, the subsurface warming deepens and shifts poleward.

After 10 years, the cooling signal has reached more than 500 m at 40° latitude north and south, which is roughly the maximum depth of the subtropical cells, and 700 m in the Southern Ocean. In the North Atlantic, on the other hand, a warm subsurface anomaly has appeared, reflecting a decrease of deep convection as will be discussed below. At this stage, the response is thus asymmetric in the high latitudes as also found by Stenchikov et al. (2009). Twenty years after an eruption, cooling is still significant in the tropics and at high latitudes, where it reaches 700 to 900 m, while the northern subtropics have warmed, reflecting the dynamical adjustment of the gyres discussed below.

In the following, we focus on the response of the Atlantic Ocean, as a case study and in order to investigate the behavior of the AMOC. From Fig. (2), it seems clear that the behavior of the AMOC after the severe and decadally paced eruptions of the twelfth and thirteenth century is peculiar. Figure (7) illustrates the different response of the ocean to the selected eruptions occurring after 1400, from the ones occurring between 1100 and 1300. In hihgresponse to volcanic eruptions occurring after 1400 (bottom panels), the initial (in phase) cooling is more clearly limited to the tropics and subtropics, while the mid and high latitudes are characterized by an anomalous warming, due to anomalous turbulent heat fluxes as discussed below. The anomalous cooling rapidly reaches the higher latitudes (yr 1 to 4), except for a small patch of anomalous warming at 45° N which reflects a northward shift of the North Atlantic Current. After about a decade, the anomalous cooling has disappeared or lost significance in the Atlantic basin, while a strong and persistent warming has appeared in the subpolar gyre, with maximum amplitude south of Greenland, and extends in the eastern subtropics in a coma shape which resembles the path of the subtropical gyre. This horseshoe-like structure thus is strongly similar to the signature of an AMOC acceleration in the coupled model (e.g. Msadek and Frankignoul 2009).

Table 1. Month of maximum global mean AOD for the selected eruptions. The input time series is based on the monthly mean optical thickness latitudinal reconstruction by Ammann et al. (2003) and Gao et al. (2008).

Period 1100–1300		Period 1400–1850	
eruption year	month of maximum AOD	eruption year	month of maximum AOD
1168	February	1452	May
1177	February	1641	May
1231	November	1809	May
1258	April	1815	September
1278	May to October		

On the other hand, the anomalous cooling occurring in phase with the intense and decadally paced eruptions between 1100 and 1400 is significant not only in the tropics, but also at subpolar latitudes, in particular in the Irminger Sea and the Nordic Seas, where deep convection in the model takes place. There is also a weak, marginally significant, warming at midlatitude, again probably reflecting a shift in the North Atlantic current, but it is short lived and the entire basin becomes anomalously cold in the years following the eruption. At decadal timescales, the anomalous subpolar warming seen after 1400 can be recognized but it is much weaker and not significant at the 5 % level. The fact that the response differs already in phase with the eruption suggests an immediate difference and tends to eliminate the cumulative effect of the decadally-paced eruptions of the twelfth and thirteenth century, as opposed to more isolated eruptions occurring after year 1400. A larger signal to noise ratio in response to stronger eruptions might be an alternative explanation, as discussed e.g. in Shindell et al. (2003) and Schneider et al. (2009). However, the anomalous atmospheric response shown in Fig. (7) (top) is unchanged if the mega eruption of 1258–1259 is omitted for the computation of the composite (not shown). Table 1 suggests rather that the eruptions of the middle age period tend to peak during the cold season, while the ones that occurred during the rest of the last millennium mostly peak during the warm season. Nevertheless, given the relatively strong uncertainty in this seasonality in the reconstruction (Gao et al. 2008), this is quite hypothetical. Investigating the effect of this seasonality requires specific sensitivity experiments and is beyond the point of this study. Finally, Fig. (2) (bottom) suggests that the AMOC variability has a different character pre and post 1300, with more high-frequency variability in the later period, especially after 1500. Whether this could explain some part of the difference will be discussed in the conclusion. Note however that

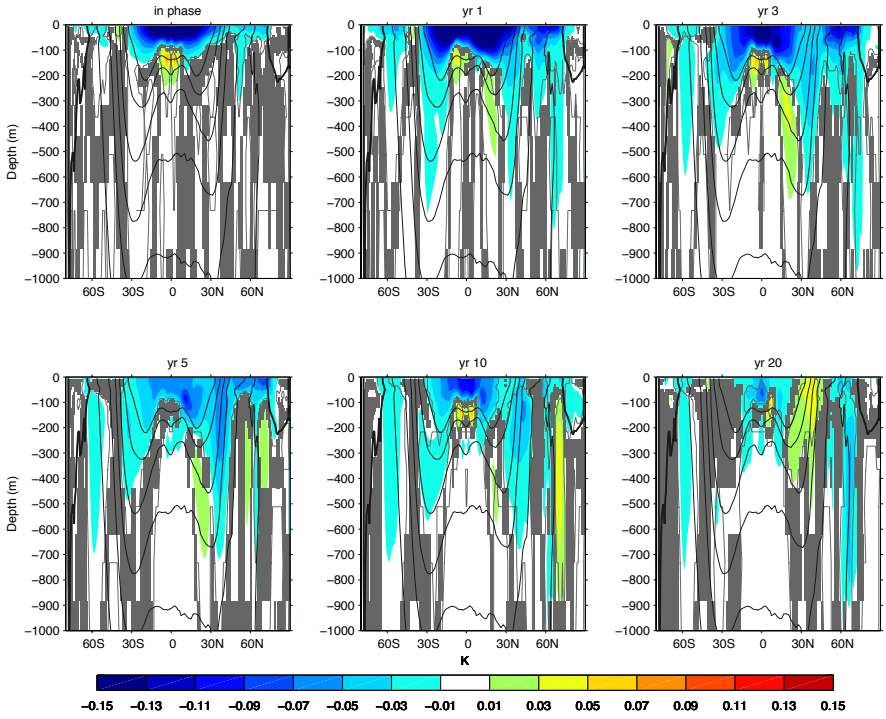

Fig. 6. Composites of anomalous zonally averaged oceanic temperature response at different time lags (in years). Shaded areas are not significant at the 20 % level. Grey contours indicate anomalies significant at the 5 % level. Dark contours show the zonal mean global temperature (contour interval is 3 °C).

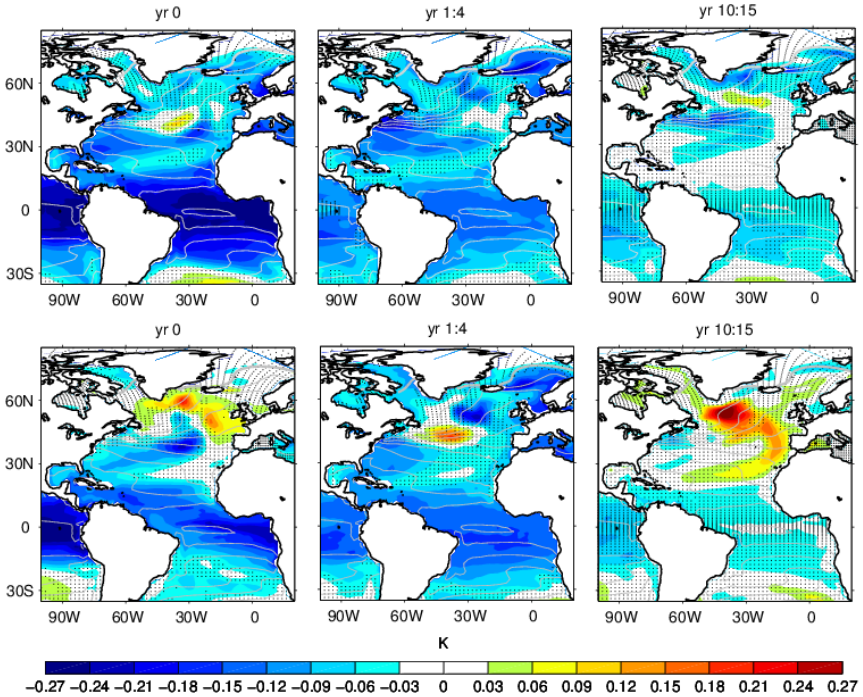

Fig. 7. Composites of anomalous sea surface temperature following volcanic eruptions in different periods. Top: between 1100 A.D. and 1300 A.D., bottom: after 1400 A.D. Dotted areas are not significant at the 5 % level. Grey contours show the annual mean SST. Contour interval is 3 K, the thick line is for the zero contour.

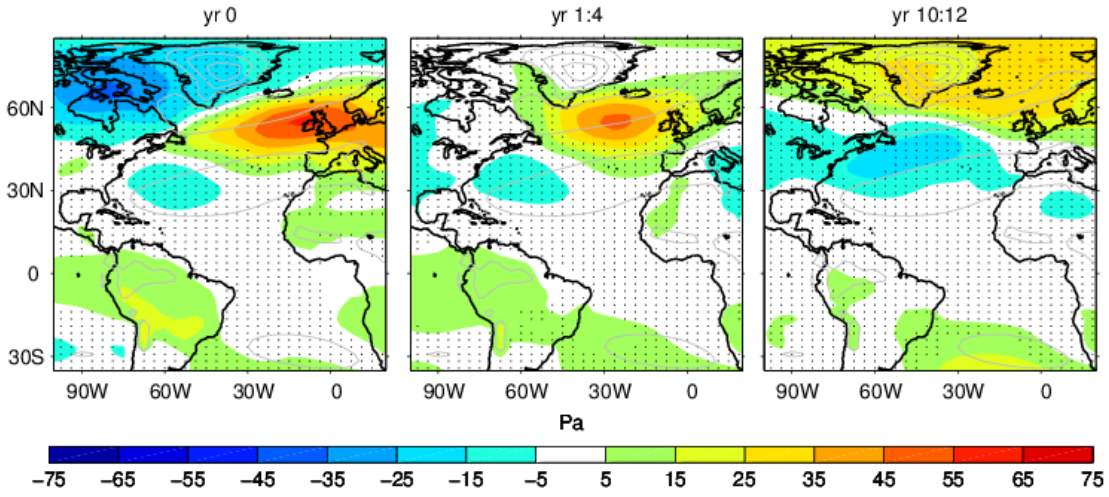

Fig. 8. Composites of annual mean anomalous sea level pressure in phase with the volcanic eruption (left) and following the volcanic eruption (other panels) for the period after 1400 A.D. Grey contours show the SLP annual mean in the model (contour interval is 10^2Pa)

.

Zanchettin et al. (2011) also noted modulation of volcanic-forced perturbations by the background climate. In the following, we will first investigate the response to eruptions occurring after 1400.

5 Interannual to decadal response of the Atlantic Ocean to eruptions post 1400 A.D.

In response to the rapid surface cooling, there is a strong anomalous low over the Canadian Archipelago and an anomalous high over the northeastern Atlantic. In addition, the sea level pressure (SLP) becomes anomalously high over South America and most of Africa, where the cooling is strongest, and an anomalous low in the western subtropics (Fig. 8). Consequently, the Northern Hemisphere trades and westerlies are reduced during the year of the eruption, and shifted southward. Over the tropical lands, the SLP signal weakens at year 1, but it remains significant for almost 2 decades over the Amazonian Basin. At mid to high latitudes, the anomalous low quickly disappears but the anomalous anticyclone shifts slightly westward and persists until year 4, resembling a negative phase of the East Atlantic Pattern (EAP). Later, the signal loses significance (not shown), until year 10, where a response resembling a negative phase of the NAO is detected.

At year 0, the wind changes induce a negative wind stress curl anomaly across the basin between 50 and 60° N and a positive one north and south of it (Fig. 9, left). The depth-integrated oceanic circulation, as described by the barotropic streamfunction, adjusts rapidly to the wind stress curl. At year 0, it is anomalously negative in much of the subtropical Atlantic, reflecting a weakening of the subtropical gyres

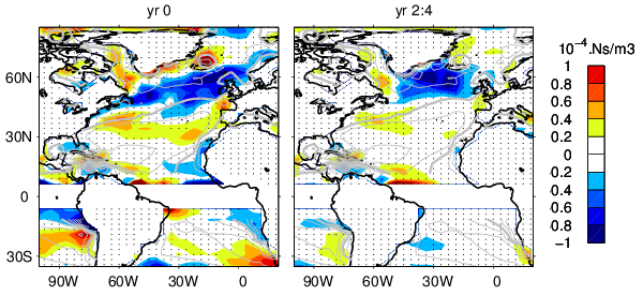

Fig. 9. Composites of anomalous wind stress curl, shown over oceans only, in phase with the volcanic eruption (left) and following the volcanic eruption by two to four years (right) for the period after 1400 A.D. Grey contours show the annual mean values (contour interval is $10^-4 N s\,m^{-3}$), the thick grey line shows the zero contour.

(Fig. 10, left). A weak positive anomaly is also significant in the subpolar region, where the wind stress curl is negative. At following lags, the negative wind stress curl anomaly persists at subpolar latitudes and shifts to the southern Irminger Sea, consistent with the SLP response (Fig. 9, right). Two to four years after the eruption, both gyres of the North Atlantic are thus clearly reduced. At longer lags, the response decays in the subtropics while the subpolar gyre stays anomalously weak for more than a decade after the eruption (Fig. 10, middle). Note also the persistent signal in the Labrador Sea where the cyclonic circulation is reinforced.

The atmospheric response to the eruption also induces vertical circulation in the ocean, resulting from the anomalous Ekman suction at 30° N/S and pumping around 50° N. This appears clearly at year 0 on the meridional streamfunction

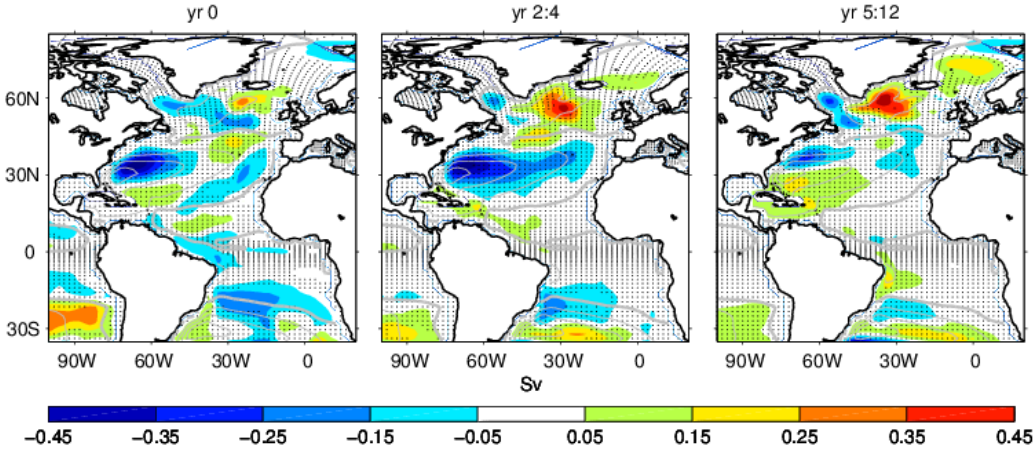

Fig. 10. Composites of anomalous Atlantic barotropic streamfunction in phase with the volcanic eruption (left) and following the volcanic eruption (other panels) for the period after 1400 A.D. Positive (negative) values correspond to an anticyclonic (cyclonic) circulation. Grey lines show the annual mean stream function in the model, with a contour interval of 10 Sv

.

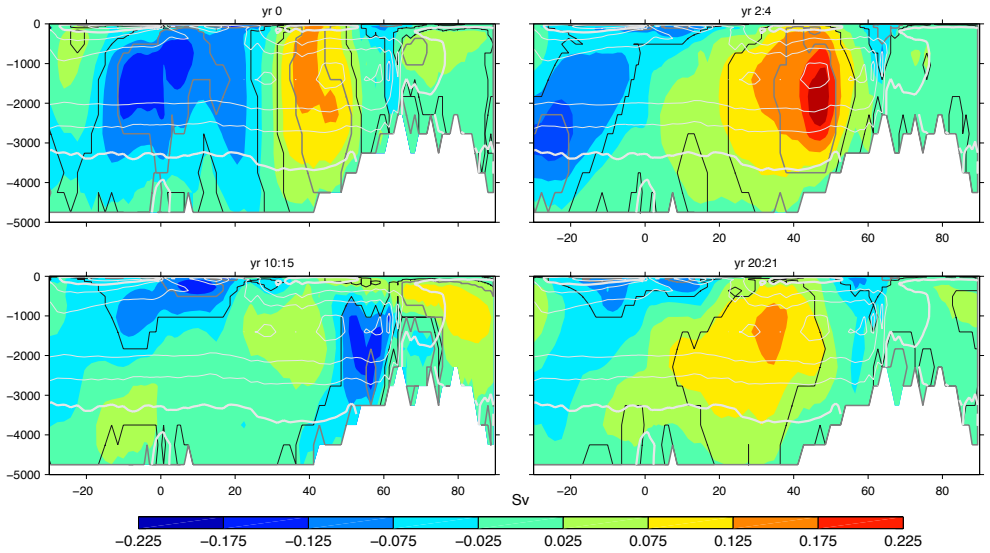

Fig. 11. Composites of anomalous Atlantic meridional streamfunction in phase with the volcanic eruption (left) and following the volcanic eruption (other panels) for the period after 1400 A.D. Positive (negative) values correspond to a clockwise (counter-clockwise) circulation. Black and day grey contours mark significant areas at the 95 % and 80 % level, respectively, according to the Monte Carlo permutation test. Light grey contours show the annual mean Atlantic meridional circulation in the control simulation (contour interval is 3 Sv, thick contour corresponding to the zero contour.)

composite (Fig. 11, left). The signal is equivalent barotropic, with an upwelling around 30° N and a downwelling at 50° N and around the equator. During the following years, the strong negative wind stress curl in the subpolar North Atlantic maintains a positive meridional cell between 20 and 50° N, which can be viewed as an intensification of the AMOC in the North Atlantic, consistent with previous studies (e.g. Stenchikov et al. 2009, Ottera et al. 2010, Ortega et al., 2011). Note that this positive anomaly is probably also favored by the intensified deep convection that occurs during the year of the eruption (Fig. 12, top), and is associated with strong surface cooling. An intensification of deep convection typically leads by several years an acceleration of the AMOC in the North Atlantic Basin (e.g. Mignot and Frankignoul 2005). However, it is short-lived here, loosing significance by year 1, so that the AMOC intensification does not persist more than a few years (Fig. 11, bottom left). On the other hand, there is a weak reduction of the AMOC north

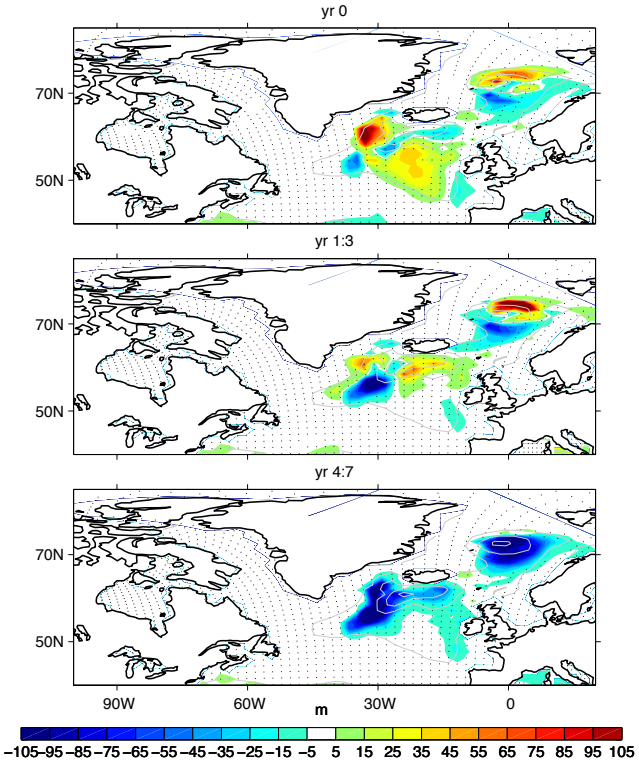

Fig. 12. composites of anomalous March mixed layer depth during the year of the eruption (left), averaged over the following 3 years (middle), and averaged 4 to 7 years later (right) for the period after 1400 A.D. Grey lines show the annual mean mixed layer depth field in the model, with a contour interval of 500 m

.

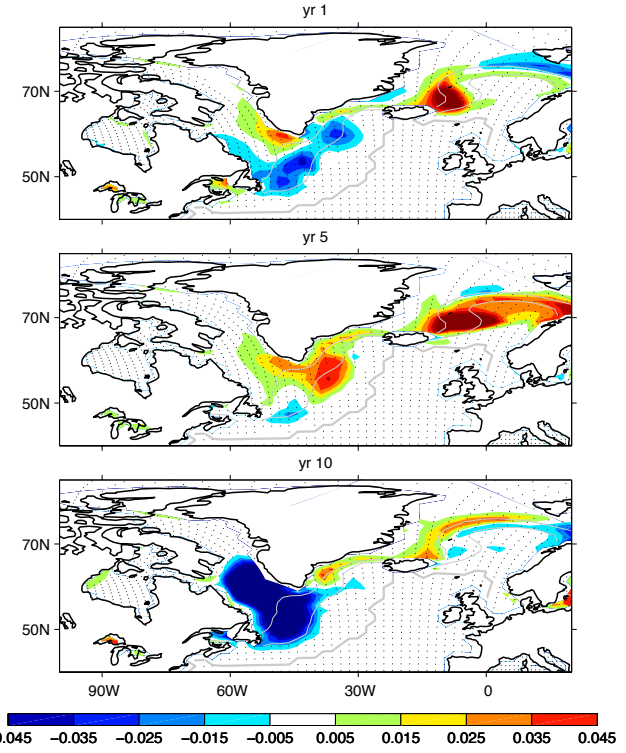

Fig. 13. composite of anomalous March sea ice cover during the year following the eruption (left), 5 years later (middle), and 10 years later (right) for the period after 1400 A.D. Grey lines show contours of the average sea ice cover in March of 0, 0.5 and 1.

of about 60° N up to four years after an eruption, which later intensifies and extends to subpolar latitudes as a result of a reduction in deep water formation, as discussed below.

Five years after the volcanic eruption, the SLP anomaly decreases (not shown). Nevertheless, as indicated above, a significant SLP anomaly appears again near year 10–12, under the form of the dipole in the mid to high latitudes bearing similarity with a negative phase of the NAO. This could reflect the SLP response to the AMOC intensification seen at year 2–4 (Fig. 8 upper right), since Gastineau and Frankignoul (2011) found a weak but significant response of the atmosphere (negative NAO phase) to enhanced AMOC in several climate models including the control simulation with IPSLCM4. In the latter, the SLP response was of similar magnitude and most clearly seen four years after an AMOC intensification. Here, the AMOC intensification indeed remains significant until lag 8 (not shown) Whether there is a link with the weak AMOC intensification seen about 20 years after the eruption cannot be asserted here but could be established in dedicated experiments. As mentioned above, the strong surface cooling rapidly deepens the mixed layer south of Iceland (Fig. 12, top panel) and in the subtropics (not shown). The intensification of deep convection favors the penetration of the cooling signal at depth seen in Fig. (6) at high northern latitudes and a weakly significant retreat of sea ice cover (Fig. 13, left panel). However, this response loses significance in the following years (Fig. 12, middle panel), and instead, deep convection is reduced both in the Nordic Seas and South of Iceland 4 years after an eruption (Fig. 12, bottom panel). This persists for about a decade after the eruption. In the Nordic Seas, the reduction of deep convection is due to a persistent sea ice capping of the area during winter, resulting from the strong surface cooling (Fig. 13). This anomaly appears about 1 year after the eruption, peaks after four years and, again, persists for roughly a decade. Such anomalous sea ice extension is consistent with the sea ice reconstruction off Iceland from Masse et al. (2008), showing abrupt events that coincide with the volcanic eruptions after 1300 A.D.

South of Iceland, the winter mixed layer shallowing in Fig. (12) (bottom) is due to a strong negative salinity anomaly (Fig. (14) top). The latter is largely due to anomalous Ekman transport (Fig. (14), bottom), while anomalous atmospheric freshwater fluxes play a lesser role (Fig. (14), middle), consistent with Mignot and Frankignoul (2003, 2004). Note that the anomalous surface freshwater flux

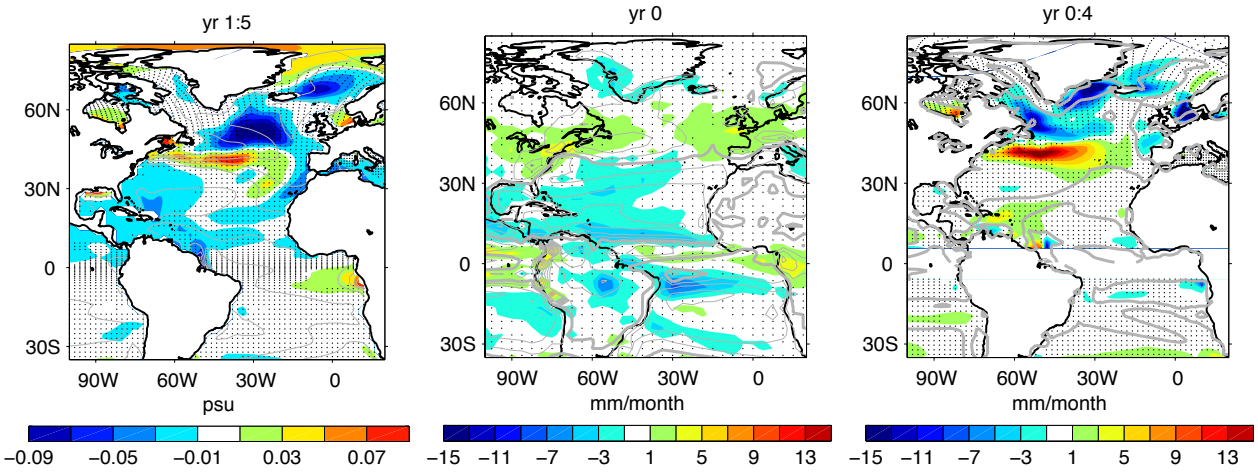

Fig. 14. Top: Composites of anomalous SSS averaged 1 to 5 years after the eruption. Grey lines show the annual mean SSS field in the model, with a contour interval of 2 psu. Middle: Composite of anomalous E-P during the year of the eruption. Bottom: composite of advection of mean salinity by anomalous Ekman currents (with a negative sign in order to be consistent with the E-P forcing term) averaged over the 4 years following the eruption. Values equatorward of 10° latitude are masked because undefined. All composite are computed for eruptions occurring later than 1400 A.D. For the two right panels, grey lines show the annual mean field in the model with a contour interval of 40mm/month. The zero contour is thicker. For all panels, dotted areas are not significant at the 5 % level.

caused by the volcanic eruptions are maximum during the year of the eruptions, and in the tropics (Fig. 14) , consistent with Trenberth and Dai (2007). The reduction of the northern trade winds (Fig. 8) is indeed associated to a northward shift in the inter-tropical convergence zone. As a result, precipitation is enhanced near 10° N and strongly reduced along the equator, including over the continents. In the northern deep tropics, evaporation is reduced, again because of reduced winds and SST. These anomalous surface freshwater fluxes induce the negative salinity anomaly in the northern subtropics in the years following the eruption.

6 Interannual to decadal response of the Atlantic Ocean to eruptions between 1100 and 1300

Figure (15) shows the response of the AMOC to the volcanic eruptions selected during the period of intense volcanic activity between 1100 and 1300. As during the later period, the in-phase response is essentially characterized by an anomalous upwelling around 30° N. The associated negative and positive cells south and north of this latitude have nevertheless a much weaker extension in depth (for the tropical one) and in latitude (for the northern one) than for the later period. Indeed, the anomalous sea level pressure induced during the year of an eruption occurring during the earlier period, shown in polar view in Fig. (16), is similar in the tropics and subtropics (not shown) but it has the opposite sign over the Canadian Archipelago and there is no strong high in the eastern North Atlantic. As a result, the anomalous wind stress curl is much weaker in the subpolar region, inducing a much weaker anomalous Ekman pumping and Ekman transport, and only little salt advection (not shown). The subpolar gyre is thus much less affected during the years following the eruption (not shown). Lacking the large subpolar freshening seen in the later period, the winter mixed layer remains anomalously deep in the subpolar region (Fig. (17) middle panel), even further south than deep convection locations, due to the surface cooling (Fig. 7), which might contribute to the broad and shallow AMOC intensification between 20° S and 45° N at years 2 to 4. It can be shown that the tropical part of this anomalous cell is associated with an equatorward shift of the subtropical gyre. On the other hand, deep convection is reduced in the Nordic Seas after a few years because of the sea ice capping discussed above. Note that in this period, the anomalous sea ice extension develops faster and it is stronger and more persistent (Fig. 18) than in the later period, consistent with the stronger cooling (Fig. 7). It is also interesting to note that the weak gyre response also contributes to maintain the oceanic surface cooling in the 1100–1300 A.D. period, since it does not induce the warm anomaly seen in the years following an eruption occurring after 1400 A.D. (Fig. 7). As a result, the negative AMOC anomaly seen over the ridges two to four years after an eruption is stronger and deeper than for the eruptions occurring after 1400 A.D. After a longer delay, when anomalous cooling and convection in the subpolar basin start to vanish, the shallowing of the winter mixed layer in the Nordic Seas seen at years 4–7 in Fig. (17) (bottom) persists and is likely responsible for the stronger negative AMOC weakening seen throughout the northern North Atlantic at least two decades after the eruptions (Fig. (15), bottom left). This behavior is consistent with

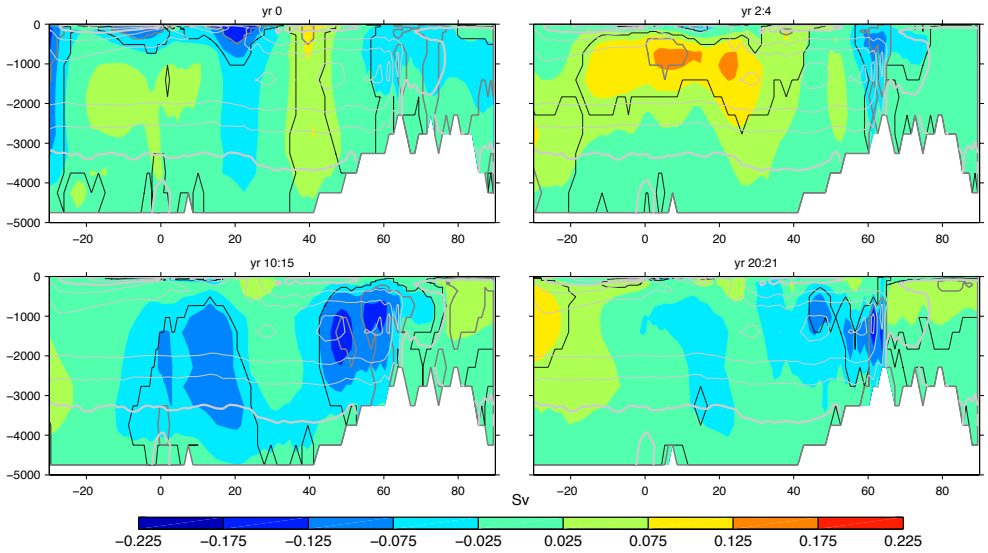

Fig. 15. As in Fig. 11 for the Atlantic meridional streamfunction during the period 1100–1300. Positive (negative) values correspond to a clockwise (counter-clockwise) circulation. Black and day grey contours mark significant areas at the 95 % and 80 % level, respectively, according to the Monte Carlo permutation test. Light grey contours show the annual mean Atlantic meridional circulation in the control simulation (contour interval is 3 Sv, thick contour corresponding to the zero contour.)

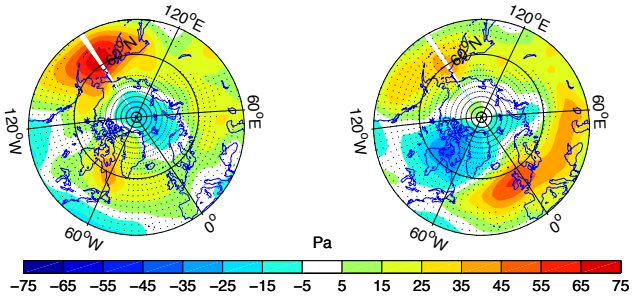

Fig. 16. composite of annual mean anomalous sea level pressure in phase with the volcanic eruptions of the period 1100–1300 A.D. (left) and with the volcanic eruptions post-1400 A.D. (right).

Zhong et al. (2010). That the AMOC weakening extends north of the ridges adds credit to the implied role of Nordic Seas convection and could explain why the AMOC behavior has become nearly opposite to that seen after 1400 A.D.

7 Conclusions and discussion

In this study, we have investigated the oceanic response to volcanic eruptions over the last thousand years, with a focus on the North Atlantic Ocean. We used a fully coupled AOGCM forced by a realistic chronology of volcanic eruptions, variations of the TSI and of the atmospheric greenhouse gases concentrations. Note that the TSI reconstruction chosen to force the model is relatively weak, and that some centennial features suggested by observations, such as temperature shifts between the medieval climate anomaly and the Little Ice Age, are not simulated in the model. In this sense, this simulation can be considered as a sensitivity simulation to the volcanic eruptions over the last millennium. Nevertheless, as far as the response of the ocean to intermittent and sudden volcanic events does not depend too strongly on the average temperature, this caveat does not invalidate our study. The analysis highlighted the multiple timescales of the response, including a fast tropical temperature adjustment to the strong volcanic-induced radiative forcing, dynamical adjustment in response to the associated atmospheric circulation modifications persisting roughly 5 years, and a subsequent adjustment of the AMOC in response to anomalous convection at high latitudes. The analysis also highlighted differences in the response during two distinct periods of the last millennium.

The global surface temperature response is maximum one to two years after a volcanic eruption. The anomaly penetrates at depth via subtropical oceanic ventilation as well as deep convection at high latitudes. It thus persists globally in the ocean for more than 20 years. During the year of the eruption, anomalous tropical cooling induces an anomalous high over the continents and a reduction of the trades in the Atlantic Ocean. The atmospheric response at mid to high latitudes depends on the eruptions. In this study, in order to investigate apparent discrepancy found in the literature regarding the AMOC response, we only separated eruptions occurring after 1400 from the ones occurring between 1100 and 1300. In the later period, the anomalous atmospheric

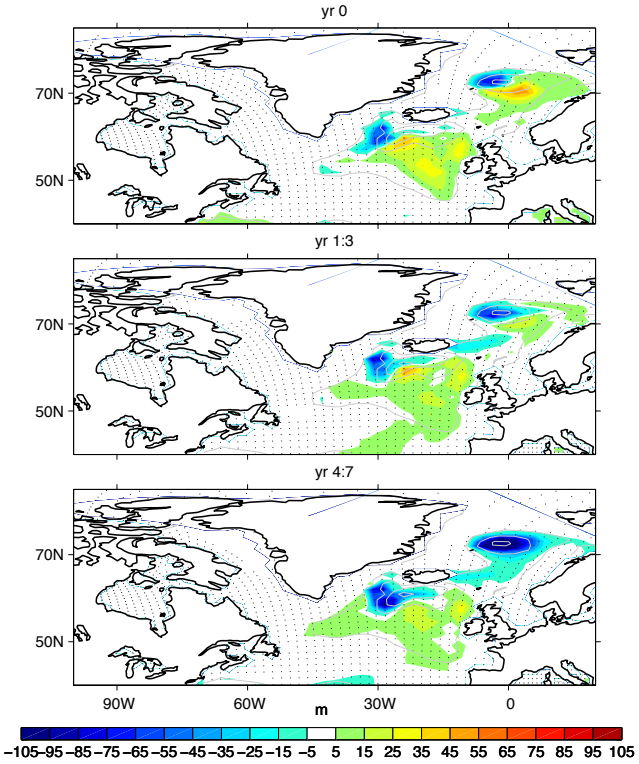

Fig. 17. Composites of anomalous March mixed layer depth in response to volcanic eruptions occurring during the period 1100–1300. The composite is shown for the year of the eruption (left), averaged over the following 3 years (middle), and averaged 4 to 7 years later (right). Grey lines show the annual mean mixed layer depth field in the model, with a contour interval of 500 m. Dotted areas are not significant at the 5 % level.

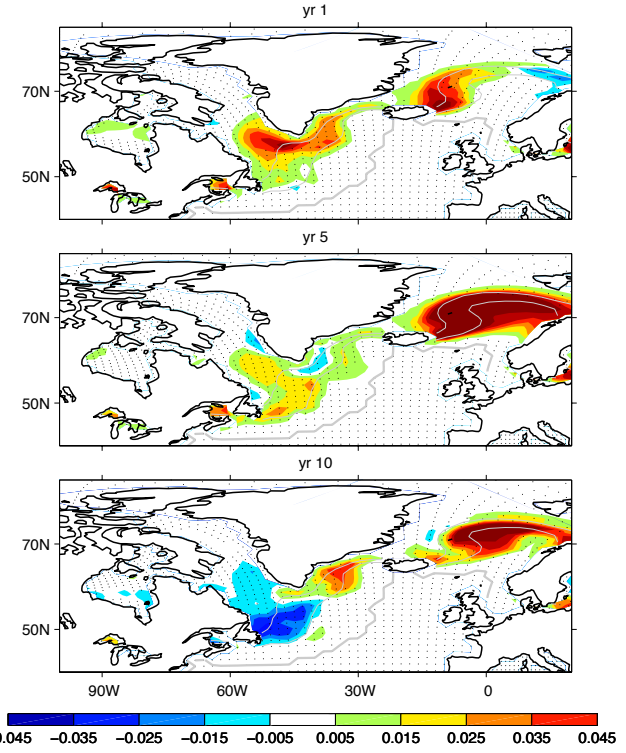

Fig. 18. Composites of anomalous March sea ice cover in response to volcanic eruptions occurring during the period 1100–1300. The composite is shown for the year following the eruption (left), 5 years later (middle), and 10 years later (right). Grey lines show contours of the average sea ice cover in March of 0, 0.5 and 1. Dotted areas are not significant at the 5 % level.

structure in response to an eruption induces strong wind stress curl anomalies over the North Atlantic Ocean, which lead to an important dynamical adjustment in the Atlantic Ocean at interannual timescales, namely one to five years after an eruption. This adjustment of the oceanic circulation is equivalent barotropic, with an upwelling around 30° N and a downwelling at 50° N and around the equator. The anomalous vertical oceanic circulation can reach the full depth of the ocean. During the following years, the atmospheric structure evolves inducing an anomalous acceleration of the AMOC in the subpolar basin. However, this anomaly does not persist more than a few years, because of reduced deep convection in the high northern latitudes under the effect of anomalous sea ice extension and surface freshening that develop a few years after the eruption. A weak reduction of the AMOC is thus detected a decade after the eruption. In the case of the eruptions occurring between 1100 and 1300, the anomalous SLP structure during the year of the eruption differs over the subpolar region from the one obtained during the later period. It induces much weaker wind stress curl anomalies over the Atlantic basin and thus a much weaker dynamical adjustment of the AMOC in the years following an eruption. On the other hand, the initial reduction of deep water formation is more persistent, as a result of a stronger surface cooling and more persistent sea ice cover anomalies, leading to a stronger negative anomaly of AMOC at high latitudes 2 to 4 years after an eruption, and a stronger reduction of the AMOC in the subpolar North Atlantic 10 to 15 years after the eruption.

As noted in the introduction, the oceanic response to volcanic eruptions is still largely unknown and recent studies based on climate models suggest either an AMOC enhancement or a reduction following volcanic eruptions of the last millennium. The present findings could possibly reconcile these previous studies, suggesting a strong sensitivity of the response to different volcanic eruptions. In particular, the AMOC intensification seen 5 to 10 years after the volcanic eruptions occurring after 1400 A.D. bears strong similarity with results of Ottera et al. (2010) using a different coupled climate model to investigate this period. On the other hand, the AMOC weakening in the northern North Atlantic and the large sea ice extension following the intense eruptions occurring between 1100 and 1300 can be compared to the response found by Zhong et al. (2010). Investigating the whole last

millennium, Zanchettin et al. (2011) noted a general AMOC intensification but note also a modulation of this response with the background state. The present analysis suggests that these different responses involve in fact similar mechanisms, namely an initial dynamical adjustment to anomalous winds and a subsequent thermohaline response to anomalous deep convection. However, the atmospheric response to the volcanic eruptions differ in the two periods and thus plays a large role in modulating the oceanic response. At least three factors could explain why the atmospheric response seems to change in time: the seasonality of the eruption, its intensity, and the cumulative effect in the case of successive eruptions. An analysis of these various effects requires specific experiments that are left for future studies. However, the results presented here suggest that the seasonality is a plausible explanation. Indeed, the eruptions during 1100–1300 occurred mostly during the cold season while those after 1400 occurred mostly during the warm season. Although cumulative effects may also play a role, they cannot explain why the short term response already differs in the two periods. Nonlinearities in the response could also be important, even though our results were not changed when the mega eruption of 1258 was omitted from the 100–1300 composite. Finally, since different responses of SLP and AMOC to eruptions pre and post 1400 occur as soon as the year of the eruption, the change in interannual variability pointed out in Fig. (2) (bottom panel) is probably not the cause.

Other features of the oceanic response to the eruptions can be compared to previous studies. The important role of sea ice dynamics was also noted by Stenchikov et al. (2009), Zhong et al. (2010) and Zanchettin et al. (2011). The response of the barotropic stream function bears also some interesting similarities with Zanchettin et al. (2011), including an initial response dominated by a shift of the gyres (or an inter gyre gyre in their framework) and a later response dominated by an intensification of the subpolar gyre. Generally, both studies highlight an initial dynamical response to atmospheric circulation and a subsequent decadal adjustment of the ocean. Comparison among these results also calls for a coordinated comparison of simulations of the last millennium.

The oceanic response is also likely to be affected by model biases and experiment design. In particular, the lack of deep convection in the Labrador Sea in the IPSLCM4 model is probably a major drawback. A better representation of the stratosphere is also needed to improve the representation of the effect of volcanic aerosols. Indeed, stratospheric dynamics and chemistry may significantly alter the modeled climatic impact of volcanic eruptions. This should be tested in the new version of the IPSL model including 39 atmospheric levels and an improved radiative module, currently under development, as well as in the forthcoming CMIP5 database.

Acknowledgements. The simulations used in this study have been run in the framework of ANR- ESCARSEL (2007–2011). The research leading to these results has received funding from the European Community's 7th framework program (FP7/2007–2013) under grant agreement No. GA212643 (THOR: "Thermohaline Overturning – at Risk", 2008–2012). Stimulating discussions with M.A. Sicre are gratefully acknowledged.

Edited by: U. Mikolajewicz

The publication of this article is financed by CNRS-INSU.

References

Ammann, C., Meehl, G., Washington, W., and Zender, C.: A monthly and latitudinally varying volcanic forcing dataset in simulations of 20th century climate, Geophys. Res. Lett, 30, 1657, doi:10.1029/2003GL016875, 2003.

Ammann, C., Joos, F., Schimel, D., Otto-Bliesner, B., and Tomas, R.: Solar influence on climate during the past millennium: Results from transient simulations with the NCAR climate system model, Proc. Nat. Acad. Sci. USA, 104, 3713–3718, doi:10.1073/pnas.0605064103, 2007.

Church, J., White, N. J., and Arblaster, J. M.: Significant decadal-scale impact of volcanic eruption and sea level and ocean heat content, Nature, 438, 74–77, doi:10.1038/nature04237, 2005.

Crowley, T.: Causes of climate change over the past 1000 years, Science, 289, 270–277, doi:10.1126/science.289.5477.270, 2000.

Fichefet, T. and Maqueda, M. A. M.: Sensitivity of a global sea ice model to the treatment of ice thermodynamics and dynamics, J. Geophys. Res., 102, 12609–12646, doi:10.1029/97JC00480, 1997.

Foukal, P., North, G., and Wigley, T.: A stellar view on solar variations and climate, Science, 306, 68–69, doi:10.1126/science.1101694, 2004.

Gao, C., Robock, A., and Ammann, C.: Volcanic forcing of climate over the last 1500 years: An improved ice-core based index for climate models, J. Geophys. Res., 113, D2311, doi:10.1029/2008JD010239, 2008.

Gastineau, G. and Frankignoul, C.: Cold-season atmospheric response to the natural variability of the Atlantic meridional overturning circulation, Clim. Dyn., in press, 2011.

Gleckler, P., Wigley, T. M. L., Santer, B. D., Gregory, J. M., AchutaRaoand, K., and Taylor, K. E.: Krakatoa's signature persists in the ocean, Nature, 429, 675, doi:10.1038/439675a, 2006.

Goosse, H. and Renssen, H.: Regional response of the climate system to solar forcing: the role of the ocean, Space Sci Rev., 125, 227–235, doi:10.1007/s1124-006-9059-0, 2006.

Goosse, H., Crowley, T., Zorita, E., Ammann, C., Renssen, H., and Driesschaert, E.: Modelling the climate of the last millen-

nium: What causes the differences between simulations?, Geophys. Res. Lett., 32, L06710, doi:10.1029/2005GL022368, 2005.

Gray, L., Beer, J., Geller, M., Haigh, J. D., Lockwood, M., Matthes, K., Cubasch, U., Fleitmann, D., Harrison, G., Hood, L., Luterbacher, J., Meehl, G. A., Shindell, D., van Geel, B., and White, W.: Solar influenced on climate, Rev. Geophys., 48, RG4001, doi:10.1029/2009RG000282, 2010.

Gray, S., Graumlich, L. J., Betancourt, J. L., and Pederson, G. T.: A tree-ring based reconstruction of the Atlantic Multidecadal Oscillation since 1567 A.D., J. Geophys. Res., 31, L12205, doi:10.1029/2004GL019932, 2004.

Grinsted, A., Moore, J. C., and Jevrejeva, S.: Application of the cross wavelet transform and wavelet coherence to geophysical time series, Nonlin. Processes Geophys., 11, 561–566, doi:10.5194/npg-11-561-2004, 2004.

Hofer, D., Raible, C. C., and Stocker, T. F.: Variations of the Atlantic meridional overturning circulation in control and transient simulations of the last millennium, Clim. Past, 7, 133–150, doi:10.5194/cp-7-133-2011, 2011.

Hourdin, F., Musat, I., Bony, S., Braconnot, P., Codron, F., Dufresne, J., Fairhead, L., Filiberti, M. A., Friedlingstein, P., Grandpeix, J. Y., Krinner, G., Levan, P., Li, Z., and Lott, F.: The LMDZ4 general circulation model: climate performance and sensitivity to parametrized physics with emphasis on tropical convection, Clim. Dyn., 27, 787–813, doi:10.1007/s00382-006-0158-0, 2006.

Jansen, E., Overpeck, J., Briffa, K. R., Duplessy, J.-C., Joos, F., Masson-Delmotte, V., Olago, B., Otto-Bliesner, B., Peliter, W. R., Rahmstorf, S., Ramesh, R., Raynaud, D., Rind, D., Solomina, O., Villalba, R., and Zhang, D.: Paleoclimate, in: Climate change 2007: the physical science basis. Contribution of working group I to the fourth assessment report of the intergouvernmental panel on climate change, edited by: Solomon, S., Qin, S., Manning, M., Chen, Z., Marquis, M., Averyt, K. B., Tignor, M., and Miller, H. L., Cambridge University Press, 433–497, 2007.

Jones, G. S., Gregory, J. M., Stott, P. A., Tett, S. F. B., and Thorpe, R. B.: An AOGCM simulation of the climate response to a volcanic super-eruption, Clim. Dyn., 25, 725–738, doi:10.1007/s00382-005-0066-8, 2005.

Jones, P. D., Osborn, T. J., and Briffa, K. R.: The evolution of climate over the last millennium, Science, 292, 662–667, doi:10.1126/science.1059126, 2001.

Knight, J., Allan, R., Folland, C., Vellinga, M., and Mann, M.: A signature of persistent natural thermohaline circulation cycles in observed climate, Geophys. Res. Lett., 32, L20708. doi:10.1029/2005GL024.233, 2005.

Krinner, G., Viovy, N., de Noblet-Ducoudre, N., Ogee, J., Polcher, J., Friedlingstein, P., Ciais, P., Sitch, S., and Prentice, I. C.: A dynamic global vegetation for studies of the coupled atmosphere-biosphere system, Glob. Biogeochem. Cy., 19, doi:10/1029/2003GB002199, 2005.

Kuroda, Y., Yamazaki, K., and Shibata, K.: Role of ozone in the solar cycle modulation of the North Atlantic Oscillation, J. Geophys. Res., 113, D14122, doi:10.1029/2007JD009336, 2008.

Laurian, A., Lazar, A., and Reverdin, G.: Generation Mechanism of Spiciness Anomalies: An OGCM Analysis in the North Atlantic Subtropical Gyre, J. Phys. Oceanogr., 39, 1003–1018, doi:10.1175/2008JPO3896.1, 2009.

Madec, G., Delecluse, P., Imbard, M., and Levy, M.: OPA 8. 1, ocean general circulation model reference manual, Notes du pole de modelisation, n. 11 Institut Pierre-Simon Laplace (IPSL), Paris, France, 1998.

Mann, M., Zhang, Z., Rutherford, S., Bradley, R., Hughes, M., Shindell, D., Ammann, C., Falugevi, G., and Ni, F.: Global Signatures and Dynamical Origins of the Little Ice Age and Medieval Climate Anomaly, Science, 326, 1256–1260, doi:10.1126/science.1177303, 2009.

Marti, O., Braconnot, P., Dufresne, J. L., Bellier, J., Benshila, R., Bony, S., Brockmann, P., Cadule, P., Caubel, A., Codron, F., de Noblet, N., Denvil, S., Fairhead, L., Fichefet, T., Foujols, M. A., Friedlingstein, P., Goosse, H., Grandpeix, J. Y., Guilyardi, E., Hourdin, F., Krinner, G., Lvy, C., Madec, G., Mignot, J., Musat, I., Swingedouw, D., and Talandier, C.: Key features of the IPSL ocean atmosphere model and its sensitivity to atmospheric resolution, Clim. Dyn., 34, 1–26, doi:10.1007/s00382-009-0640-6, 2010.

Masse, G., Rowland, S. J., Sicre, M.-A., Jacob, J., Jansen, E., and Belt: Abrupt climate changes for Iceland during the last millennium: Evidence from high resolution sea ice reconstructions, Earth Planet. Sc. Lett., 269, 564–568, doi:10.1016/j.epsl.2008.03.017, 2008.

Meehl, G., Arblaster, J., Branstator, G., and van Loon, H.: A coupled air-sea response mechanism to solar forcing in the Pacific region, J. Clim., 21, 2883–2897, doi:10.1175/2007JCLI1776.1, 2008.

Meehl, G., Arblaster, J., Matthes, K., Sassi, F., and van Loon, H.: Amplifying the Pacific Climate System Response to a Small 11-Year Solar Cycle Forcing, Science, 325, 1114–1118, doi:10.1126/science.1172872, 2009.

Mignot, J. and Frankignoul, C.: On the interannual variability of surface salinity in the Atlantic, Clim. Dyn., 20, 555–565, doi:10.1007/s00382-002-0294-0, 2003.

Mignot, J. and Frankignoul, C.: Interannual to interdecadal variability of sea surface salinity in the Atlantic and its link to the atmosphere in a coupled model, J. Geophys. Res., 109, C04005, doi:10.1029/2003JC002005, 2004.

Mignot, J. and Frankignoul, C.: On the variability of the Atlantic meridional overturning circulation, the North Atlantic Oscillation and the El Niño-Southern Oscillation in the Bergen Climate Model, J. Clim., 18, 2361–2375, doi:10.1175/JCLI3405.1, 2005.

Minnis, P., Harrison, E. F., Stowe, L. L., Gibson, G. G., Denn, F. M., Doelling, R., and Jr, Smith, W. L.: Radiative Climate Forcing by the Mount Pinatubo Eruption, Science, 259, 1411–1415, doi:10.1126/science.259.5100.1411, 1993.

Msadek, R. and Frankignoul, C.: Variability of the meridional overturning circulation and its influence onto the atmosphere in the IPSL climate model, Clim. Dyn., 33, 45–62, doi:10.1007/s00382-008-0452-0, 2009.

Myneni, R. B., Nemani, R. R., and Running, S. W.: Estimation of global leaf area index and absorbed par using radiative transfer models, Ieee T. Geosci. Remote., 35, 1380–1393, 1997.

Oman, L.: High latitude eruption cast shadow over the african monsoon and the flow of the Nile, Geophys. Res. Letters, 33, L18711, doi:10.1029/2006GL027665, 2006.

Ortega, P., Montoya, M., Gonzales-Rouco, F., Mignot, J., and Legutke, S.: Variability of the Atlantic meridional overturning circulation in the last millennium and two IPCC scenarios, Clim.

Dyn., in press, 2011.

Ottera, O. H., Bentsen, M., Drange, H., and Suo, L.: External forcing as a metronome for Atlantic multidecadal variability, Nature Geoscience, 3, 688–694, doi:10.1038/ngeo955, 2010.

Richter, T. O., Peeters, F., and van Weering, T.: Late Holocene (0–2.4 ka BP) surface water temperature and salinity variability, Feni Drift, NE Atlantic Ocean, Quaternary Sci. Rev., 28, 1941–1955, doi:10.1016/j.quascirev.2009.04.008, 2009.

Robock, A.: Volcanic eruptions and climate, Rev. Geophys., 38, 191–219, doi:10.1029/1998RG000054, 2000.

Robock, A. and Mao, J.: Winter warming from large volcanic eruptions, Geophys. Res. Lett., 19, 2405–2408, doi:10.1029/92GL02627, 1992.

Schmidt, G. A., Jungclaus, J. H., Ammann, C. M., Bard, E., Braconnot, P., Crowley, T. J., Delaygue, G., Joos, F., Krivova, N. A., Muscheler, R., Otto-Bliesner, B. L., Pongratz, J., Shindell, D. T., Solanki, S. K., Steinhilber, F., and Vieira, L. E. A.: Climate forcing reconstructions for use in PMIP simulations of the last millennium (v1.0), Geosci. Model Dev., 4, 33–45, doi:10.5194/gmd-4-33-2011, 2011.

Schneider, D. P., Ammann, C. M., Otto-Bliesner, B. L., and Kaufman, D. S.: Climate response to large, high latitude and low-latitude volcanic eruptions in the Community Climate System Model, J. Geophys. Res., 114, D05101, doi:10.1029/2008JD011222, 2009.

Servonnat, J., Yiou, P., Khodri, M., Swingedouw, D., and Denvil, S.: Influence of solar variability, CO_2 and orbital forcing between 1000 and 1850 AD in the IPSLCM4 model, Clim. Past, 6, 445–460, doi:10.5194/cp-6-445-2010, 2010.

Shapiro, A., Schmutz, W., Rozanov, E., Schoell, M., Haberreiter, M., Shapiro, A. V., and Nyeki, S.: A new approach to the long-term reconstruction of the solar irradiance leads to large historical solar forcing, Astronomy and Astrophysics, 529, 16173 pp., 2011.

Shindell, D., Schmidt, G. A., Miller, R. L., and Mann, M. E.: Volcanic and solar forcing of climate change during the preindustrial era, J. Clim., 16, 4094–4107, doi:10.1175/1520-0442, 2003.

Shindell, D., Schmidt, G. A., Mann, M. E., and Falugevi, G.: Dynamic winter climate response to large tropical volcanic eruptions since 1600, J. Geophys. Res., 109, D05104, doi:10.1029/2003JD004151, 2004.

Sicre, M., Jacob, J., Ezat, U., Rousse, S., Kissel, C., Yiou, P., Eriksson, J., Knudsen, K. L., Jansen, E., and Turon, J. L.: Decadal variability of sea surface temperatures off North Iceland over the last 2000 years, EPSL, 268, 137–142, doi:10.1016/j.epsl.2008.01.011, 2008.

Sicre, M., Hall, I., Mignot, J., Khodri, M., Ezat, U., Truong, M.-X., Eiriksson, J. J., and Knudsen, K. L.: Sea surface temperature variability in the subpolar Atlantic over the last two millennia, Paleoc., in press, 2011.

Solanki, S. K. and Krivova, N. A.: Solar variability of possible relevance for planetary climates, Space Sci. Rev., 125, 25–37, doi:10.1007/s11214-006-9044-7, 2006.

Stenchikov, G., Hamilton, K., Stouffer, R., Robock, A., Ramaswamy, V., Santer, B., and Graf, H.-F.: Arctic Oscillation response to volcanic eruptions in the IPCC AR4 climate models, J. Geophys. Res., 111, D07107, doi:10.1029/2005JD006286, 2004.

Stenchikov, G., Delworth, T. L., Ramswamy, V., Stouffer, R. J., Wittenberg, A., and Zeng, F.: Volcanic signals in oceans, J. Geophys. Res., 114, D16104, doi:10.1029/2008JD011673, 2009.

Stendel, M., Mogensen, I., and Christensen, J.: Influence of various forcings on global climate in historical times using a coupled atmosphere-ocean general circulation model, Clim. Dynam., 26, 1–15, doi:10.1007/s00382-005-0041-4, 2006.

Sutton, R. T. and Hodson, D. L. R.: Influence of the Ocean on North Atlantic Climate Variability: 1871-1999, J. Clim., 16, 3296–3313, doi:10.1175/1520-0442, 2003.

Sutton, R. T. and Hodson, D. L. R.: Atlantic Ocean Forcing of North American and European Summer Climate, Science, 309, 5731, 115–118, doi:10.1126/science.110949616, 2005.

Swingedouw, D., Braconnot, P., Delecluse, P., Guilyardi, E., and Marti, O.: The impact of global freshwater forcing on the thermohaline circulation: adjustment of North Atlantic convection sites in a CGCM, Clim. Dyn., 28, 291–305, doi:10.1007/s00382-006-0171-3, 2007.

Timmreck, C., Lorenz, S. J., Crowley, T. J., Kinne, S., Raddatz, T. J., Thomas, M. A., and Jungclaus, J. H.: Limited temperature response too the very large AD 1258 volcanic eruption, Geophys. Res. Letters, 36, L21708, doi:10.1029/2009GL040083, 2009.

Torrence, C. and Compo, G. P.: A practical guide to wavelet analysis, Bull. Am. Meteorol. Soc., 9, 61–78, 1998.

Trenberth, K. and Dai, A.: Effect of Mount Pinatubo volcanic eruption on the hydrological cycle as analog of geoengineering, Geophys. Res. Letters, 34, L15702, doi:10.1029/2007GL030524, 2007.

Valcke, S., Terray, L., and Piacentini, A.: Oasis 2.4, Ocean atmosphere sea ice soil: user's guide, Tech. Rep. TR/CMGC/00/10, CERFACS, Toulouse, France, 2000.

van der Schrier, G., Weber, S., and Drijfhout, S. S.: Sea level changes in the North Atlantic by solar forcing and internal variability, Clim. Dyn., 19, 435–447, doi:10.1007/s00382-002-0235-y, 2002.

Vieira, L. and Solanki, S.: Evolution of the solar magnetic flux on time scales of years to millennia, Annu. Rev. Astron. Astr., 509, arXiv/0911.4396, doi:10.1051/00046361/200913276, 2009.

Zanchettin, D., Timmreck, C., Graf, H.-F., Rubino, A., Lorenz, S., Lohmann, K., Kruger, K., and Jungclaus, J. H.: Bi-decadal variability excited in the coupled oceanatmosphere system by strong tropical volcanic eruptions, Clim. Dyn., in press, doi:10.1007/s00382-011-1167-1, 2011.

Zhong, Y., Miller, G. H., Otto-BLiesner, B. L., Holland, M. M., Bailey, D. A., Schneider, D. P., and Geirsdottir, A.: Centennial-scale climate change from decadally-paced explosive volcanism: a couled sea ice-ocean mechanism, Clim. Dyn., 37, 2373–2387, doi:10.1007/s00382-010-0967-z, 2011.

Zorita, E., von Storch, H., Gonzales-Rouco, F., Cubasch, U., Luterbacher, J., Legutke, S., Fischer-Bruns, I., and Schlese, U.: Climate evolution in the last five centuries simulatis by an ocean-atmosphere model: global temperatures, the North Atlantic Oscillation and the Late Maunder Minimum, Meterol. Z., 13, 271–289, doi:10.1127/0941-2894/2004/0013-0271, 2004.

On the formation of barrier layers and associated vertical temperature inversions: A focus on the northwestern tropical Atlantic

J. Mignot,[1] A. Lazar,[1] and M. Lacarra[1]

Received 6 July 2011; revised 26 November 2011; accepted 28 November 2011; published 3 February 2012.

[1] A unique barrier layer (BL) system in terms of persistence, extension, and associated subsurface temperature maximum is present seasonally in the northwestern tropical Atlantic. Based on climatological output of a general circulation ocean model, we show here that its development consists of two phases. In summer, the BL is relatively shallow and thin but subsurface temperature maxima are intense. The latter develop as a result of the specific seasonality of the freshwater discharge in this area, which limits the mixed layer to a very thin depth while the intense radiative heat flux penetrates significantly below, thereby heating the subsurface waters protected from air-sea interactions and inducing a barrier layer between the mixed layer and the ocean interior. In winter, the BL development is due to a surface decrease in salinity associated with the surface freshwater capping, which decouples the pycnocline, and hence the winter mixed layer, from the thermocline. The mechanism is ubiquitous in the sense that it is very similar to that of other areas at the same latitude, as well as at high latitudes in regions of seasonal surface freshening. Results are discussed in the light of a simple linear equation linking the BL development to time evolution of Sea Surface Temperature and Sea Surface Salinity stratification.

Citation: Mignot, J., A. Lazar, and M. Lacarra (2012), On the formation of barrier layers and associated vertical temperature inversions: A focus on the northwestern tropical Atlantic, *J. Geophys. Res.*, *117*, C02010, doi:10.1029/2011JC007435.

1. Introduction

[2] The northwestern tropical Atlantic was shown by *Mignot et al.* [2007, hereinafter MBLC07] to be a region with very thick and long lasting barrier layers (BLs). These BLs could furthermore be shown to be particularly persistent and impermeable on monthly timescales as defined by *Mignot et al.* [2009]. Their formation mechanism was studied by *Pailler et al.* [1999], *Masson and Delecluse* [2001], and *Ferry and Reverdin* [2004]. These authors highlighted in particular the influence of outflow from adjacent rivers. Indeed, two of the strongest rivers in the world (namely the Amazon and the Orenoque) outflow in this region, giving rise to a pronounced and specific Sea Surface Salinity (SSS) seasonal cycle. However, these previous studies largely ignored the deep and strong co-localized vertical temperature inversions that exceed 0.6°C [*de Boyer Montégut et al.*, 2007a, hereinafter BMLC07]. The latter are among the most vast, deep and strong of the tropical oceans. The climatic impact of temperature inversions has been illustrated by *Smyth et al.* [1996], *Vialard and Delecluse* [1998], and *Durand et al.* [2004] in the Pacific and in the Indian Ocean. Recently, *Balaguru* [2011] suggested a possible link between BLs and inversions in the tropical Atlantic and tropical cyclones.

[3] The BL system of the northwestern tropical Atlantic (Figure 1 and thick box in Figure 2) is located within the so-called Atlantic Warm Pool (AWP) that occupies the Gulf of Mexico, the Caribbean Sea, and the western tropical North Atlantic. Using atmospheric reanalysis and sensitivity experiments with an atmospheric general circulation model, *Wang et al.* [2006, 2008b] also showed the significant influence of the warm waters in the Atlantic Warm pool on western hemisphere summer rainfall and Atlantic hurricanes. The mechanism involves a modulation of the tropospheric vertical wind shear and thus of the moisture static stability of the overlying atmosphere. *Wang et al.* [2008a] also showed the link between the AWP's multidecadal variability and the larger scale Atlantic Multidecadal Oscillation (AMO) [*Knight et al.*, 2005] suggesting that the influence of the AMO on the tropical Atlantic cyclone activity, illustrated for example by *Enfield and Cid-Serrano* [2010], may operate through the mechanism of AWP-induced atmospheric changes. Furthermore, important interactions between this region and the tropical Pacific occur, in particular in terms of freshwater exchange [e.g., *Giannini et al.*, 2000; *Wang and Enfield*, 2003]. Finally, the BL system of the northwestern tropical Atlantic is located on the path of the surface branch of the Atlantic Meridional Overturning Circulation, so that its formation and seasonality could also be linked to remote oceanic conditions and influence the whole Atlantic climate

[1]UPMC/CNRS/IRD/MNHN IPSL-LOCEAN, Paris, France.

0148-0227/12/2011JC007435

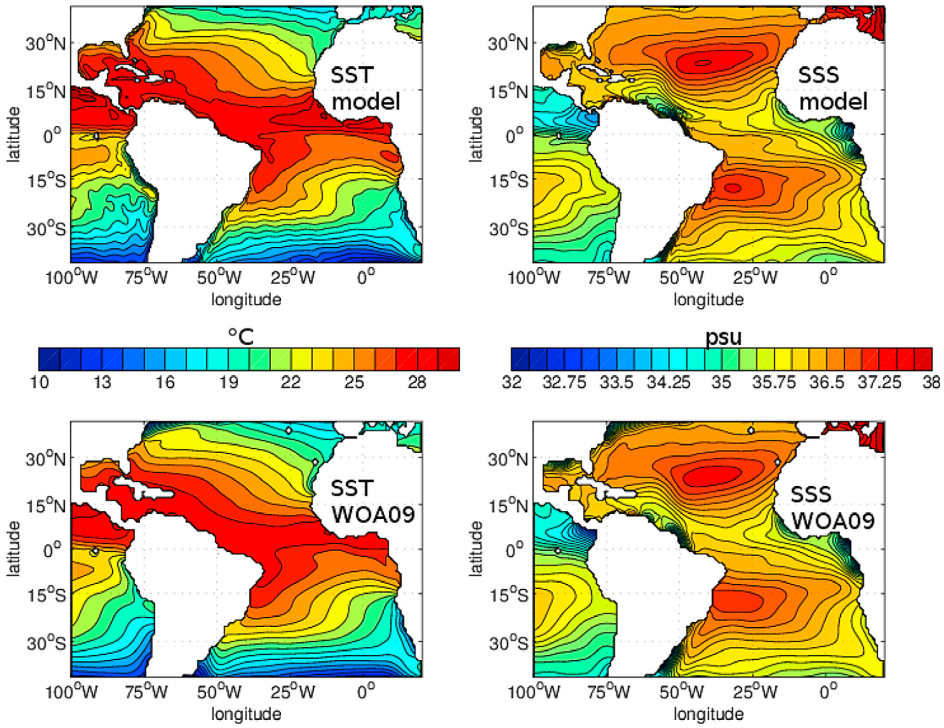

Figure 1. Annual mean (left) sea surface temperature (in °C) and (right) sea surface salinity (in psu) in (top) the simulation and (bottom) the WOA09 data set [*Locarnini et al.*, 2010; *Antonov et al.*, 2010].

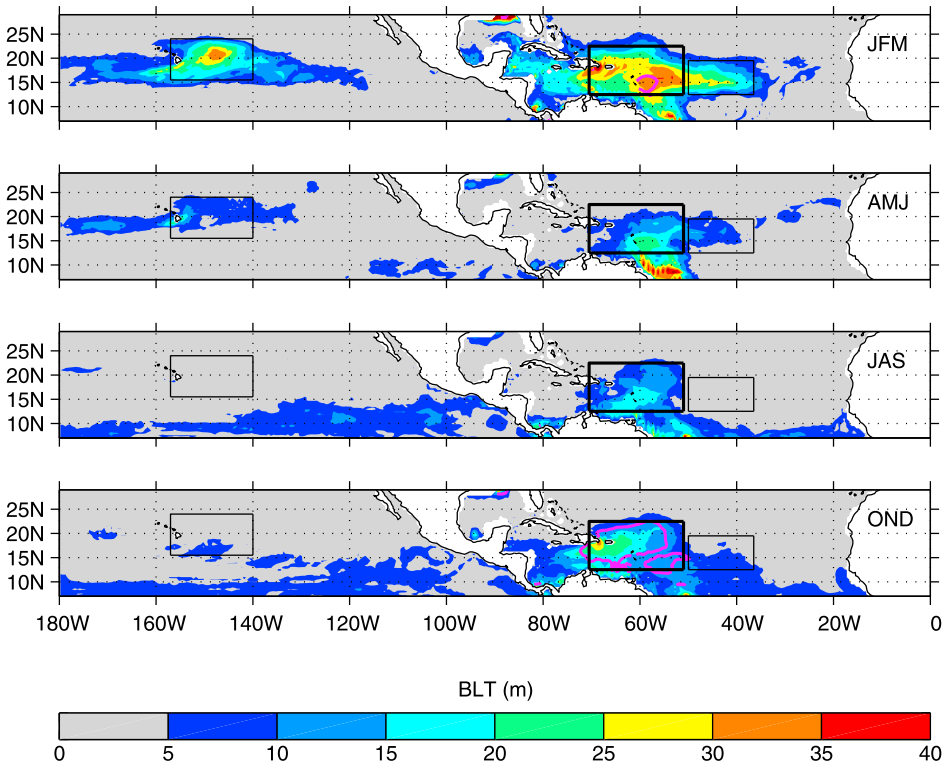

Figure 2. BL thickness (color scale) in the northern tropical Atlantic and east Pacific in the model. The magenta contours are subsurface temperature maximum greater than 0.6°C. The boxes highlight the BLs studied in the rest of the paper.

through oceanic conditions. This location is thus unique in terms of climatic variability and climatic impact.

[4] The studies of BMLC07 and MBLC07 also showed the presence of robust and thick BLs at similar latitudes in the center of each subtropical oceanic basin in winter. For the first time, these studies proposed a symmetry among subtropical oceanic basins in terms of BL climatology and formation processes. As compared to the BL system in the northwestern tropical Atlantic, BLs in the central subtropical basins appear later in the winter season and they are not associated with significant inversions of the vertical temperature gradient. This suggests that BL formation in the western tropical Atlantic may be specific to this region, although this is not well understood yet. In her recent study using sensitivity experiments with a coupled climate model, *Balaguru* [2011] suggested an important role of subsurface salinity for the formation of these BLs and of the surface salinity for the creation of the vertical temperature inversions.

[5] Our objective here is to gain a general understanding of the formation process of BLs and temperature inversions in tropical areas. In particular, a vertical temperature inversion requires a strong salinity stratification in order to keep the water column stable. How does the seasonality of the specific freshwater discharge and precipitation in this area participate in the formation of persistent BLs and strong subsurface temperature maxima? Is the latitudinal symmetry highlighted in MBLC07 still valid for this specific region? In order to address these issues, we propose to compare time series of the BL development in the northwestern tropical Atlantic to that of other subtropical BLs at similar latitudes. We deduce from this analysis that the development of the BL system in the northwestern tropical Atlantic happens in two steps, one due to the specificity of the region and the second similar other BL systems at similar latitudes. We also propose a prognostic equation for the BL development that is, under certain assumptions, applicable to all BL areas. We believe that such a model can be useful to modelers and observationalists to interpret or predict the presence or absence of BLs.

[6] In order to analyze in details the temperature and salinity budgets associated with BLs, we base our study on the outputs of a forced Ocean General Circulation Model (OGCM) The model and BL thickness computation are presented in section 2. The analysis of the BL system, its seasonality and its development mechanism are shown in section 3. In section 4, we derive a simple linear prognostic model for the BL development as a function of temperature and salinity stratifications, and we propose to use it as a framework to illustrate BL developments in the tropical band. Conclusions are given in section 5.

2. Model and Definitions

2.1. The Ocean Circulation Model

[7] We use the global Océan Parallèlisé (OPA) OGCM [*Madec et al.*, 1998]. OPA solves the primitive equations on an Arakawa C grid, with a second-order finite difference scheme. It assumes the Boussinesq and hydrostatic approximations, and the incompressibility hypothesis, and uses a free-surface formulation [*Roullet and Madec*, 2000]. The density is computed from potential temperature, salinity, and pressure using the *Jacket and McDougall* [1995] equation of state. In its global configuration ORCA05, the horizontal mesh is based on a 0.5° × 0.5° Mercator grid, and following *Murray* [1996], two numerical inland poles have been introduced in order to remove the North Pole singularity from the computational domain. The departure from the Mercator grid starts at 20°N and is constructed using a series of embedded ellipses based on the semianalytical method of *Madec and Imbard* [1996]. Realistic bottom topography and coastlines are derived from the study of *Smith and Sandwell* [1997], complemented by the 5′ Gridded Earth Topography (ETOPO5) dataset. The maximum depth of 5000 m is spanned by 30 z-levels ranging from 10 m thickness in the upper 120 m to 500 m thickness at the bottom. The ocean model is run with a time step of 2400 s.

[8] Lateral tracer mixing is done along isopycnals. Eddy-induced tracer advection is parameterized following *Gent and McWilliams* [1990] with coefficients decreased in the Tropics between 20°N and 20°S. Momentum is mixed along horizontal surfaces using coefficients varying with latitude, longitude, and depth. Vertical eddy diffusivity and viscosity coefficients are computed from a 1.5-level turbulent closure scheme based on a prognostic equation for the turbulent kinetic energy [*Blanke and Delecluse*, 1993]. Double diffusive mixing (i.e., salt fingering and diffusive layering) is computed following *Merryfield et al.* [1999]. Penetrative solar radiation corresponding to Type I water [*Jerlov*, 1968] is also used. This formulation will be detailed in section 3.2. This model configuration has been widely used for climatic studies, such as in the study by *de Boyer Montégut et al.* [2007b].

[9] The model run starts from an ocean at rest using the January temperature and salinity fields of the *Levitus* [1998] climatology. It is then run for a 3-yr period using a climatology of 1992–2000 forcing fields. In this study, we focus on climatological BL systems. This was our motivation for choosing this particular set up using a climatological forcing, thereby avoiding the effect of interannual variability and long-term trend. Such a forcing strategy has proven useful for investigating the mean seasonal cycle [e.g., *Durand et al.*, 2007]. Limitations inherent in using climatological values for relative humidity and cloudiness are discussed, for example by *de Boyer Montégut et al.* [2007b].

[10] The momentum surface boundary condition is given using the weekly European Remote Sensing Satellites-1 and -2 (ERS-1-2) wind stress interpolated daily with a cubic spline method [*Bentamy et al.*, 1996]. The insolation, longwave radiation and turbulent heat fluxes (and the evaporation) are computed from the semi-empirical or bulk formulae [*Timmermann et al.*, 2005], which relate the fluxes to the SST (computed by the model) and to meteorological parameters (10-m wind speed, surface air temperature and relative humidity, cloudiness). The daily 2-m air temperature is extracted from the National Centers for Environmental Prediction-National Center for Atmospheric Research (NCEP-NCAR) reanalysis [*Kalnay et al.*, 1996]. Monthly climatologies of relative humidity [*Trenberth et al.*, 1989] and cloudiness [*Berliand and Strokina*, 1980] are used. Precipitation data come from the Climate Prediction Center Merged Analysis of Precipitation (CMAP) product [*Xie and Arkins*, 1997]. The monthly values of river discharge [*United Nations Educational, Scientific and Cultural Organization* (*UNESCO*), 1996] are introduced into the model by

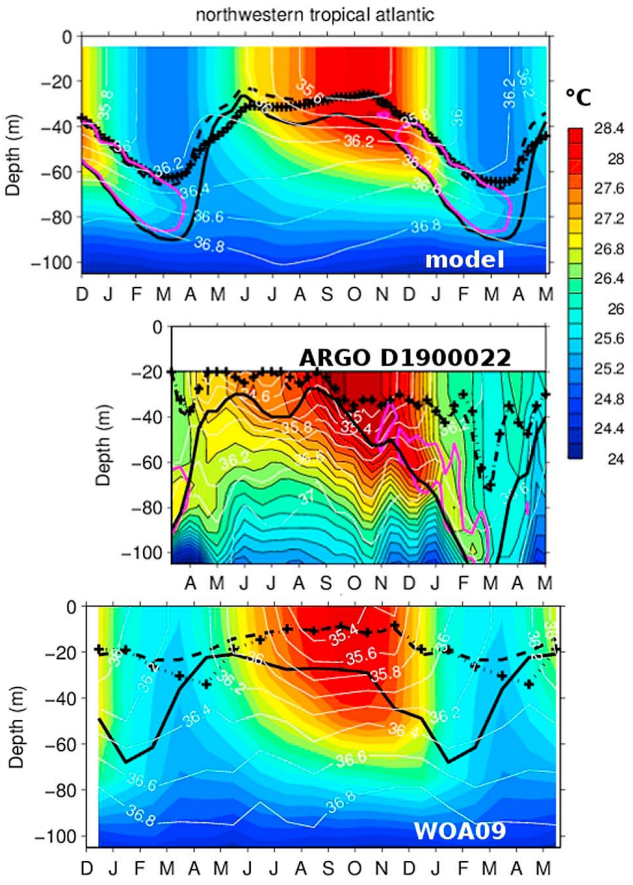

Figure 3. (top) Time evolution of temperature (colors, in °C) and salinity (white contours, in psu) from the surface to 100 m depth averaged over the thick box in the northwestern tropical Atlantic shown in Figure 2. The thick black lines shows the depth D_{T^*-02} (solid), the MLD (dashed) and the halocline depth $D_{S^*+\Delta S}$ with $\Delta S = 0.06$ psu diagnosed from the model data averaged over the same area (crosses). The magenta contour highlights vertical temperature inversions of 0.2° and more. (middle) Time evolution of temperature (colors) and salinity (white contours) from the surface to 100 m depth of the ARGO float D1900022 that traveled in the same area (between 55.5 and 60°W and 14 and 22°N between April 2002 and May 2003). A running mean over 3 points with equal weights has been applied to all time series. (bottom) Same as Figure 3 (top) using the monthly mean temperature and salinity fields from WOA09 [*Locarnini et al.*, 2010; *Antonov et al.*, 2010].

distributing the associated freshwater input as precipitation on the points surrounding the mouth of the rivers. The Amazon runoff is of particular relevance for the present study. Its seasonal variability is well reproduced by the model, as shown for example by *Masson and Delecluse* [2001]. It has a clear annual cycle, with a maximum in May, when it reaches 0.26 Sv, and a minimum in November of 0.13 Sv. A restoring term toward the *Levitus* [1998] SSS is applied to the freshwater budget, with a relaxation timescale of 2 months for a 50-m-thick layer. While there is no physical justification for this feedback term, as the atmosphere does not care about ocean surface salinity, it avoids SSS drift arising from the error in the prescribed freshwater budget.

[11] Available outputs are the temperature and salinity over all the model's vertical levels, as well as tendency terms based on the conservation equations for the temperature and salinity in the mixed layer. Oceanic output are available with 5-days resolution. We use the data from the last year of the model run. Figure 1 illustrates the annual mean SST and SSS fields as given by the model over the Atlantic area (Figure 1, top) and in the most recent version of the World Ocean Atlas (WOA09) [*Locarnini et al.*, 2010; *Antonov et al.*, 2010]. Note that the WOA09 climatology is given with a resolution of 1° only, so that fields appear smoother than in the model. Figure 1 shows that main features of the observed surface fields are quite well reproduced by the model. The SST maximum in the eastern equatorial Atlantic is slightly too warm in the model, and SSS maxima in the subtropics are slightly stronger than in the observations. The validity of this simulation for the BL process studied here will be done below through Figures 2 and 3, presented below.

2.2. Definitions

[12] Following previous barrier layer studies [e.g., *de Boyer Montégut et al.*, 2004], the barrier layer thickness (named simply BLT in the following) is defined here as the difference, when positive, between two depths:

$$BLT = D_\sigma - D_{T^*-02} \tag{1}$$

with $D_{T^*-02} < D_\sigma < 0$. D_{T^*-02} is the depth where the temperature has decreased by 0.2 °C as compared to the temperature at the reference depth of 10 m. The 0.2 °C threshold is based on the current precision of most common temperature sensors. D_σ is the depth where the potential density anomaly, here referred to as σ_θ (potential density $-$ 1000 kg/m^3), has increased from the reference depth by a threshold Δ_σ equivalent to the density difference for the same temperature change at constant salinity:

$$\Delta_\sigma = \sigma_\theta(T^* - 0.2, S^*, P_0) - \sigma_\theta(T^*, S^*, P_0) \tag{2}$$

with T^* and S^* are the temperature and salinity at the reference depth 10 m and P_0 is the pressure at the ocean surface. D_σ corresponds to the top of the pycnocline. Similarly, one can define the halocline depth as the depth where salinity has increased by a threshold ΔS from the reference depth. ΔS is defined such as to induce the same density change as $\Delta T = -0.2$°C. ΔS can thus be estimated from $\Delta S = \alpha_T/\beta_S \times \Delta T$ where α_T and β_S are typical values of the thermal expansion and saline contraction coefficients respectively . With $\alpha_T = 2500 \times 10^{-7}\ K^{-1}$ and $\beta_S = 0.75 \times 10^{-3} psu^{-1}$, we use the threshold $\Delta S = 0.06 psu$ to define the pycnocline.

[13] As shown by *de Boyer Montégut et al.* [2004], in the area of tropical barrier layers examined in the present work, D_{T^*-02} is climatologically deeper than D_σ, and D_σ is a good proxy for the mixed layer depth (MLD), in the sense of a layer where temperature, salinity and density are mixed and thus homogeneous. To the contrary, when D_σ is deeper than D_{T^*-02}, the absolute value of the right hand term in equation (1) gives the thickness of a layer called compensated layer (CL in the following), in reference to a stratification regime where upper halocline and thermocline

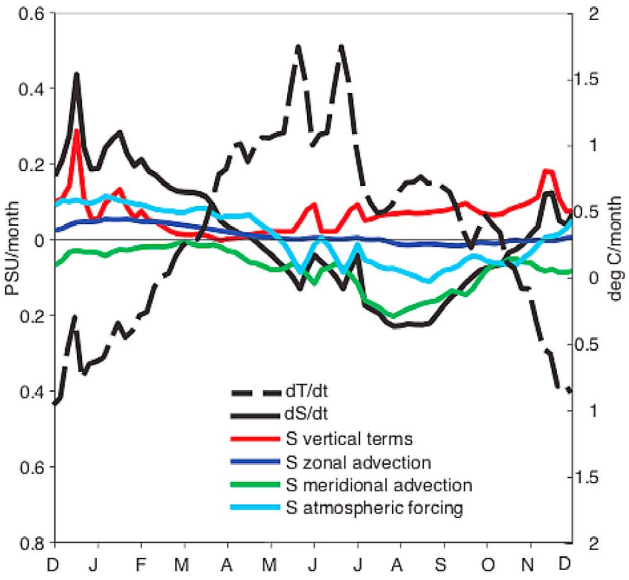

Figure 4. Time series of the mixed layer salinity (thick black line) and temperature (thick dashed line) tendencies computed online by the ocean model averaged over the box shown in Figure 2 with thick lines, in the northwestern tropical Atlantic. For the salinity, the decomposition of this tendency into four physical terms is also shown. The atmospheric forcing term, namely freshwater flux, is in light blue. The zonal advective term ($\vec{u}.\vec{\nabla}S$, where $\vec{u}$ is the zonal velocity) is in dark blue, the meridional advective term ($\vec{v}.\vec{\nabla}S$, where $\vec{v}$ is the meridional velocity) in green. In red, we show the sum of all vertical terms, namely vertical advection, vertical mixing and entrainment. All these terms are computed on-line in the model. The monthly averages that are shown are computed from the 5-days averages available as monthly outputs. The residual between all these terms and the total tendency is small (not shown).

are partially compensated in density. Then, D_σ is no longer a good proxy for the MLD, since it reaches below the top of the thermocline (see *de Boyer Montégut et al.* [2004] for climatological distribution and *Liu et al.* [2009] for interannual variations of the MLD).

[14] Given that in the classic view of a water column, potential temperature is supposed to decrease downward, so that temperature is almost constant above the depth D_{T^*-02}, the latter has been commonly identified in the literature as the Isothermal Layer Depth (ILD). In fact, the layer above D_{T^*-02} is often not isothermal. Instead it may shelter subsurface temperature maxima associated with strong vertical temperature gradients (see BMLC07 for global spatiotemporal distribution of subsurface temperature maxima). Assimilating this surface layer to an ILD overlooks these subsurface temperature inversions that may occur when compensating salinity stratification ensures hydrostatic stability. An important part of the following analysis is precisely dedicated to variations of temperature within this layer and in particular to warming at depth. Therefore, in the following, we prefer to refer to this depth using its definition (D_{T^*-02}) rather than use the misleading acronym ILD. In spite of this ambiguity, this depth, which can be considered as the top of the thermocline, has a clear and important physical definition: it corresponds to the depth below which waters are significantly colder than in surface. By construction, mixing through this interface cools surface waters. In contrast, mixing through the MLD can either warm or cool surface layers, depending on the temperature of waters just below (see Figure 1 of BMLC07 for illustrative hydrological profiles). Note that because subsurface temperature inversions may be present, it is important to consider a decrease of the temperature for the BL definition, whereas an absolute change is used for the temperature mixed layer definition. *Liu et al.* [2009] use an absolute criteria and, as a result, underestimate the BL thickness in cases of temperature inversions.

[15] The time derivative of equation (1) indicates that favorable conditions of BL development occur particularly when D_{T^*-02} becomes deeper, or deepens faster, than the MLD (D_σ). In a cooling season, these conditions are met if a sufficiently strong halocline (with upward decreasing salinity), or a surface salinity decrease, limits the MLD seasonal deepening. In section 4, we will derive equations that help to quantify this consideration and place it in a broader context.

[16] Finally, the temperature inversions are identified, as in BMLC07, by the depth of the subsurface maximum and the difference between this maximum and the temperature of the mixed layer. In this article, we restrict ourselves to temperature inversions located above the thermocline and specifically above D_{T^*-02}.

[17] The computations are done at each spatial grid point of the model, at the temporal resolution of the model output (5 days). Monthly climatologies are then computed as the median of the corresponding 5-day means.

3. Results

3.1. The BL in the Northwestern Tropical Atlantic

[18] Figure 2 shows the seasonal BL thickness in the northern tropical Atlantic and east Pacific basins as well as contours of subsurface temperature maxima. Thick BLs in the northwestern tropical Atlantic, north of the Amazon mouth and east of the Puerto Rico Islands are clearly seen, and are associated with strong vertical temperature maxima (thick box). They compare well with observations shown in MBLC07 (their Figures 1 and 4), although thicknesses are slightly smaller in the model. Vertical temperature inversions are stronger and deeper. This barrier layer system persists roughly all yearlong and reaches its maximum thickness in winter. Vertical temperature inversions are strongest in autumn. The seasonality, longitudinal location and temperature inversion distinguishes this system from BLs located around the same latitudes but in the center of the basins. In the central tropical Pacific and central tropical Atlantic, a thick BL is centered near 20°N and 15°N, respectively, from January to March (thin boxes), consistent with in-situ previous observations (MBLC07).

[19] The time series of modeled temperature and salinity averaged over the area limited by the thick box in Figure 2 and as a function of depth helps in gaining understanding of the evolution of this BL system (Figure 3, top): starting in June from a situation of basic stratification, the salinity stratification strengthens and a BL of about 10 m develops quickly. This formation is due to a quasi-constant mixed layer depth (dashed line in Figure 3 (top)) associated with an

initial deepening of D_{T^*-02} (solid line). Note that mathematically, for a simplified water column with negligible subsurface heat fluxes, D_{T^*-02} is, by construction, expected to shoal between June and October, since the surface temperature warms. This surprising deepening will be analyzed below by considering the effect of penetrating solar radiation. This phase lasts until mid-October, when SST stops warming. The second phase of the BL development starts in early November, when the mixed layer begins to cool and freshen. Both D_{T^*-02} and MLD increase, but at different rates. As a result, the BL deepens down to 80 m and thickens, reaching 20 m. Simultaneously, the temperature inversion appears and develops, occupying the whole BL. It rapidly reaches about 0.4°C. Around April, during the spring restratification, the BL and temperature inversion disappear within 1 to 2 months and both D_{T^*-02} and MLD rapidly shoal back to 40 m depth.

[20] As indicated above, the BL climatology in the model is highly comparable to observations from MBLC07. Nevertheless, before analyzing in detail the BL and temperature inversion evolutions, we can further validate this timing. For comparison, Figure 3 (middle) shows the temperature and salinity measured in the same area between April 2002 and May 2003 by the ARGO float D1900022. Beginning in early May 2002, there is a relatively thin BL around 20 m depth, which persists until August. This BL then deepens and thickens from September onward. A subsurface temperature maximum of 0.1 to 0.2°C is present in mid-June and of more than 0.4°C from October onward. During the autumn and winter, it weakens and deepens with the BL. The BL persists until March, when it was detected around 80 m depth in 2003 and 100 m depth in 2004. This behavior bears strong similarity with the BL development in the model (Figure 3, top). The main difference is that the freshening and the halocline shallowing happens much more quickly in the ARGO float. Furthermore, the minimum thickness observed in August is not seen in the model. However, note that the model results (Figure 3, top) have been spatially averaged over a relatively large area (see box in Figure 2), while Figure 3 (bottom) shows the measurements of a single ARGO float. When model data are averaged over a smaller box restricted to the area spanned by the ARGO float, the spring freshening in particular is much more abrupt and closer to the ARGO measurements (not shown). Furthermore, because the run only shows the climatological variations and the ARGO float takes measurements during a particular year, interannual variability of salinity or temperature, via advection or atmospheric forcing in particular, could also explain part of the discrepancy. Figure 3 (bottom) shows the time evolution and temperature and salinity over the northwestern tropical Atlantic box in the WOA09 [*Locarnini et al.*, 2010; *Antonov et al.*, 2010]. As indicated above, the spatial resolution of this data set is twice that of the model, and the data are only available at monthly time steps. It is thus not suited for a precise analysis of the BL development and we only show it in order to validate the seasonal cycle of temperature and salinity in the area. Indeed, this panel largely confirms the climatological persistence of the BL over the whole year, and the two distinct seasonal patterns: a BL at relatively constant depth in summer, and sudden deepening and thickening in winter.

[21] The overall good agreement between the model and observations gives confidence for using the model to more carefully examine the development of the BL and the subsurface temperature inversion. In particular, it confirms that the two seasons can be analyzed separately: the summer (and surface warming) season, lasting from June to mid-October, when the BL develops as a result of a deepening of D_{T^*-02} while MLD is near constant, and the inter season, from mid-October to early May, when both D_{T^*-02} and MLD deepen, the temperature inversion is much weaker and the BL is thicker.

3.2. The Summer BL

[22] As discussed above, BLs and temperature inversions depend upon the presence of both a salinity and temperature stratification. The model salinity budget in the mixed layer (Figure 4) indicates that the freshening that occurs from April to October is primarily due to meridional advection of freshwater. The dominant freshwater input is thus due to the advection from the equatorward salinity minimum sustained by the Amazon river outflow (maximum in May–June [*UNESCO*, 1996]), and the inter tropical convergence zone (ITCZ, located around 5 to 8°N in August–September). The Amazon outflow peaks to about 0.25 Sv in May, which converts to a trend of roughly 0.75psu/month at the mouth of the river. Observations from *Xie and Arkins* [1997] suggest that local precipitation amounts to about 4mm/day in this region in this season. This corresponds to a salinity trend of about 0.14 psu/month over a mixed layer of 30 m, which is consistent with the model atmospheric forcing term (light blue).

[23] In summer, the mixed layer is maintained at a quasi-constant depth (Figure 3) as a result of the competitive action between surface freshening and warming on the one hand, and vertical mixing due to wind stirring and vertical entrainment on the other hand. The causes, then, of the initial deepening of D_{T^*-02} in June are related to the more general question of what controls the temperature increase below the mixed layer. Since the mixed layer temperature increases during June, the only way D_{T^*-02} can deepen is in case of a faster warming below the MLD, as seen in Figure 3 between 30 m and D_{T^*-02}. The quasi-vertical isotherms visible there in the model, and to a lesser extent in the observations, suggest that the subsurface warming is due to residual vertical turbulence that extends the mixed layer water temperature down to below the mixed layer. However, as detailed below, we argue the penetrative solar radiation explains the evolution of the upper thermocline stratification.

[24] In the model, the solar radiation is allowed to penetrate through the top few meters of the ocean, as described in section 2. To achieve this, a formulation including extinction coefficients is assumed for the downward irradiance I following *Paulson and Simpson* [1977]:

$$I(z) = Q_{sr}\left(Re^{-z\xi 1} + (1-R)e^{-z\xi 2}\right) \quad (3)$$

where Q_{sr} is the penetrative part of the surface heat flux, $\xi 1$ and $\xi 2$ are two extinction length scales and R determines the relative contribution of the two terms. The default values used correspond to a Type I water in the work by *Jerlov* [1968] classification: $\xi 1 = 0.35\ m$, $\xi 2 = 23\ m$ and $R = 0.58$. The contribution of this penetrative radiative flux to the temperature tendency occurs through its vertical derivative following $H = 1/(\rho Cpdz) * (I(k) - I(k+1))$, where dz is the thickness of layer k. Figure 5 (colors) shows this

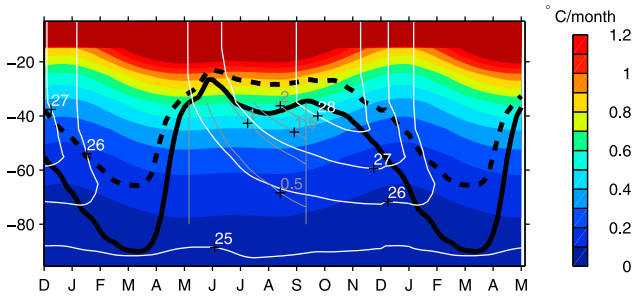

Figure 5. Time evolution of the vertical derivative of the solar penetrative heat flux, expressed in °C/*month* and averaged over the BL area in the northwestern Atlantic (box in Figure 2). For clarity, values above 1.2 °C/*month* and for depths above 15m were not plotted. The thick black lines show the depth D_{T^*-02} (solid), the MLD (dashed) respectively. White contours are temperature contours. The thin grey lines show the temperature change (in °C) due to the cumulative time integration of the penetrative heat flux (colors) from early May to September (vertical thin lines). See text for details.

contribution, which was computed offline as described above. In spring and summer, when the incoming solar flux is maximum, the penetrative flux can reach 0.8°C/*month* at the base of the MLD near 30 *m* and 0.5°C/*month* near 40 *m*. The subsurface warming due precisely to the penetrative heat flux can be quantified by the cumulative time integral of this flux. Thin grey contours in Figure 5 show this integration beginning in early May, when the temperature at 40 m depth is 25.9°C. The grey contours show that at 40 m depth, the penetrative heat flux has induced a warming of 1°C by mid-July, which is consistent with the warming of about 0.9°C seen in the model. This analysis demonstrates the dominant role of penetrative heat flux in subsurface warming, though subsurface mixing and diffusion may compensate at times.

[25] Between July and October, the penetrative flux is around 0.6°C/*month* just below the MLD, which is consistent with the simultaneous subsurface temperature increase from 27.0°C to 28.6°C (colors in Figure 3 (top)). This value exceeds the surface warming rate (less than 0.5°C/*month*; Figure 4, dashed line), so that as the vertical temperature evolves, the isotherms become more vertical and D_{T^*-02} deepens. Meanwhile, the surface advection of low salinity water prevents D_σ from deepening, so a BL forms. Note that the surface warming reaches a relative minimum value in July, further strengthening the relative importance of subsurface warming and favoring the deepening of D_{T^*-02}. In August, as this process persists, the isotherms bend, forming a modest temperature inversion (Figure 3, top) that is permitted by the pre-existing fresh water cap. In agreement with findings of *Vialard and Delecluse* [1998] in the Pacific warm pool, this suggests that the penetrative heat flux is responsible for the observed North Western tropical Atlantic BL and temperature inversion in spring and summer, when the surface freshening maintains a shallow MLD and prevents vertical mixing.

[26] Comparing the summertime dynamics of the northwestern tropical Atlantic to the summertime dynamics of the central Atlantic and Pacific (Figure 6) confirms that it is the specific phasing of the freshening and the maximum solar forcing that permits the summer BL described above to form in northwestern tropical Atlantic. In the central basins, in contrast, the surface warming is rather accompanied by surface salinification (Figure 6) (see also *Dessier and Donguy* [1994] and *Foltz and McPhaden* [2008] for a precise analysis of the SSS seasonal cycle in the Atlantic). As a result, during the summertime warming, the halocline shoals slightly, but remains coupled to the mixed layer depth, so a BL does not form.

3.3. The Winter BL

[27] As described above, at the beginning of winter, the BL development in the northwestern tropical Atlantic clearly enters a second phase (Figure 3) when it deepens and is accompanied by a mixed layer cooling. Figure 6 shows that this second phase occurs also at similar latitudes in the central Pacific (Figure 6, top) and the central Atlantic (Figure 6, bottom). In these two areas, there was no significant source of freshwater to create favorable conditions for a BL formation in summer. Instead, a strong surface freshening occurs in early winter due to the meridional advection of freshwater from the equator by seasonal Ekman transport, as detailed in MBLC07. In the central Atlantic box, the surface freshening occurs from late summer to winter (Figure 6, bottom). In summer, surface temperature is increasing so the freshening is not strong enough to sustain a significant BL. The wintertime freshening, observed in both

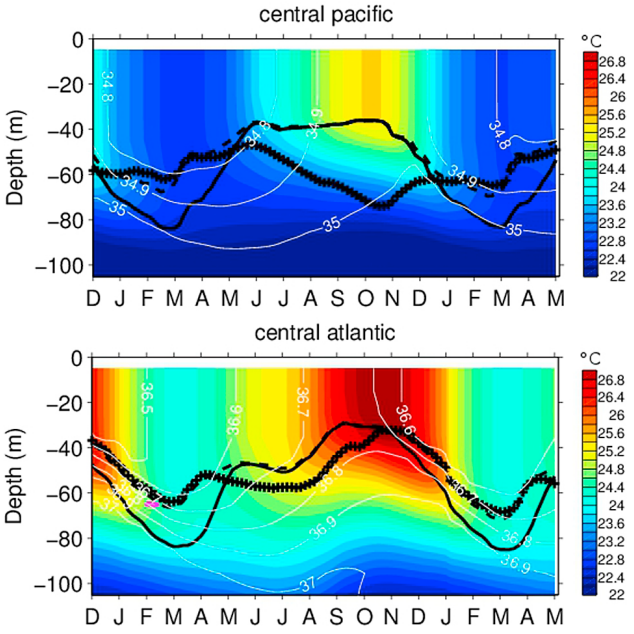

Figure 6. Time evolution of temperature (colors) and salinity (white contours) from the surface to 100 m depth averaged in the (top) central Pacific and (bottom) central Atlantic (see boxes in Figure 2). The thick black lines show the D_{T^*-02} (solid), the MLD (dashed) diagnosed from the model data averaged over the same area. The lines marked with crosses show the depth where salinity is changed by 0.06 psu as compared to the surface value.

the central and northwestern Atlantic, associated with the poleward freshwater advection (MBLC07) can induce a BL that deepens with time. MBLC07 suggested that the BL formation in this area is due to the different response of density (dominated by salinity) and temperature to winter forcing, and in particular to vertical mixing. The analysis of the time series in Figures 3 and 6 clarifies this view: the deepening of D_{T^*-02} is by definition associated with the surface temperature decrease. The deepening of the MLD is due to convective mixing forced by the surface cooling and salinification, as well as the intensification of vertical mixing through an input of momentum from the winds. Again, if salinity was vertically uniform, MLD would equal D_{T^*-02} and neither a BL nor a temperature inversion would appear. Here, the presence of a halocline with a downward gradient is a sufficient condition for a slower deepening of the D_σ, and the BL develops. In the other basins, the phenomenon is similar. A weak vertical temperature inversion (less than 0.1°C) is also associated with the BL due to the fact that the autumn thermocline waters are protected from air-sea interactions and thus cool at a slower rate than the surface waters. Finally, note that in all cases, even though the incoming solar radiative flux is weaker than in summer and the mixed layer is deeper, the penetrative heat flux still has the capacity to heat the layers below the mixed layer (Figure 5) and thus probably helps maintain warm waters below the mixed layer.

4. A Linear Model for the BL Evolution

4.1. A Linear Equation for the BL Evolution

[28] We propose here to derive a simple prognostic equation for the BL thickness (and for the compensated layer, CL, thickness), in order to express the tendency of these layers to form and vanish as a function of temperature and salinity. In the idealized case of a water column with negligible subsurface heat fluxes right below the mixed layer, in the vicinity of D_{T^*-02}, a temporal equation for D_{T^*-02} is:

$$\partial_t D_{T^*-02} = (\partial_z T)^{-1}|_{D_{T^*-02}} \times \partial_t SST, \tag{4}$$

where the vertical temperature gradient is computed at the depth D_{T^*-02}. Equation (4) shows that, for such an adiabatic evolution of the thermocline, and in particular with a standard upward temperature gradient in the thermocline ($\partial_z T < 0$), D_{T^*-02} shoals (respectively deepens) by construction when the SST warms up (respectively cools down). Note that this equation holds in the presence of a subsurface temperature inversion, as long as it is well formed and in a quasi-stationary state. Qualitatively, a relatively strong subsurface warming, as compared to the SST warming, can result in a deepening of the thermocline isotherms with negligible MLD change, leading to a BL thickening. This situation occurs particularly in the tropics in the summer season when $D_{T^*-0.2}$ is closest to the surface and exposed to significant solar penetrative radiations. Mathematically, a corresponding second term should then be added to equation (4).

[29] Following equation (4) and similarly neglecting subsurface buoyancy fluxes near D_σ, one can derive the following equation for the temporal evolution of the pycnocline depth,

$$\partial_t D_\sigma = (\partial_z \sigma)^{-1}|_{D_\sigma} \partial_t SS\sigma, \tag{5}$$

Where $SS\sigma$ refers to the sea surface density. It is then useful to linearize the equation of state according to:

$$\sigma = \rho_{ref}(-\alpha_T T + \beta_S S) \tag{6}$$

with α_T the thermal expansion coefficient of water (neglecting its pressure dependence) and β_S the haline contraction coefficient. Inserting the linearized σ in equation (5) and using equation (1), the time evolution of BLT can be written

$$\partial_t BLT = \frac{-\alpha_T \partial_t SST + \beta_S \partial_t SSS}{-\alpha_T \partial_z T + \beta_S \partial_z S} - \partial_t D_{T^*-02}, \tag{7}$$

where the vertical derivatives are taken at the pycnocline depth. This equation is not valid in the upper ocean where both temperature and salinity are well mixed.

[30] We now introduce the vertical density ratio $R_z = \frac{\alpha_T \partial_z T}{\beta_S \partial_z S}$. R_z is generally similar to R_l, the lateral density ratio [e.g., *Rudnick and Martin*, 2002], which varies significantly over the world oceans between -10 and 10 [*Chen*, 1995].

[31] Using equation (7) and the vertical density ratio, and neglecting the variations over depth of temperature and density vertical gradients, one finally gets

$$\partial_t BLT = \frac{1}{1 - R_z}\left(\frac{\partial_t SSS}{\partial_z S} - \frac{\partial_t SST}{\partial_z T}\right) \tag{8}$$

for $\partial_z S$ and $\partial_z T$ different from zero. Equation (8) is interesting because it indicates that for given vertical temperature and salinity gradients, the BL development depends linearly upon SSS and SST time derivatives. Note that the above hypotheses on temperature and density subsurface fluxes and density linearity imply that subsurface salinity fluxes are also negligible. This last hypothesis is more robust than the one for heat fluxes.

[32] In order to further clarify the role of salinity versus temperature stratification in the development of a BL, one can write a similar equation as equation (4) for $D_{S^*+\Delta S}$:

$$\partial_t D_{S^*+\Delta S} = (\partial_z S)^{-1}|_{D_{S^*+\Delta S}} \partial_t SSS. \tag{9}$$

Then, neglecting the vertical variation of the salinity vertical gradient, equation (7) becomes

$$\partial_t BLT = \frac{1}{1 - R_z}(\partial_t D_{S^*+\Delta S} - \partial_t D_{T^*-02}) \tag{10}$$

This equation indicates that the BL development depends on the evolution of the distance between the top of the thermocline and of the halocline respectively. Hence one can verify that a BL tends to develop if $D_{T^*-0.2}$ deepens faster than $D_{S^*+\Delta S}$, since the latter will limit the deepening trend of D_σ. Figure 7 shows a sketch of the main types of idealized stable vertical profiles of temperature and salinity below the MLD, as in the work by *Liu et al.* [2009]. Note that the latter study related these profiles to the Turner Angle, which is closely related to R_z. Here, it is simpler to relate the profiles directly to R_z as it is the latter that appears in equation (8). The simplest, and most common, case of vertical stratification in the upper ocean corresponds to an upward temperature gradient below the thermocline and a downward salinity gradient below the halocline. In this case, $R_z < 0$ at the base of the thermocline. For $R_z \ll -1$, the temperature gradient

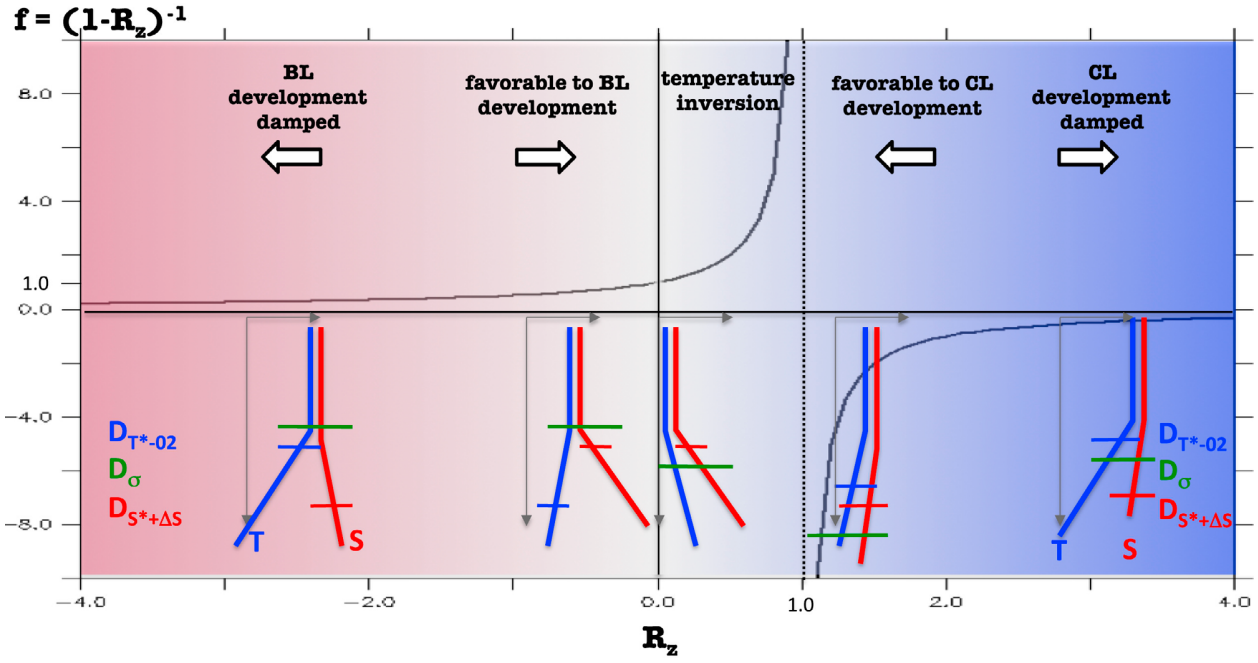

Figure 7. Schematic of the different stratification regimes described in section 4 and link to BL development conditions. The profile graphics illustrate typical temperature (in blue), salinity (in red) profiles as a function of R_z. Horizontal lines on the profiles sketch the D_{T^*-02} (in blue), $D_{S^*+\Delta S}$ (in red) and D_σ (in green) (see text for definitions). The background graphics shows the function $f = (1 - R_z)^{-1}$, which is the modulating factor in equations (8) and (10).

largely dominates the salinity in terms of its effect on the density gradient, and $1/(1 - R_z)$ tends toward zero and damps BL development in equation (10). In other words, D_σ varies almost like $D_{T^*-0.2}$, at the expense of BL development. For R_z close to zero and negative, the salinity gradient now dominates the temperature one, $1/(1 - R_z)$ is close to unity and BL varies in unity with changes in $D_{S^*+\Delta S} - D_{T^*-0.2}$. Such a profile corresponds mainly to weak temperature and strong salinity gradients. In this case, the BL develops essentially because $D_{T^*-0.2}$ deepens easily while D_σ varies almost like $D_{S^*+\Delta S}$, that is little since the halocline is strong (see equation (8)). For $0 < R_z <= 1$, a temperature inversion prevails and density is compensated by a salinity increase. However, equations (8) and (10) do not hold since D_{T^*-02} is not present in such an idealized profile. Another equation for the development of a CL should be derived, but this is beyond the scope of the present study. Note nevertheless that the temperature decreases at greater depth and a thick BL could be defined, as discussed by *de Boyer Montégut et al.* [2007a]. For $R_z >= 1$, the temperature profile is stable and compensated. Equation (10) functions as for the latter regime: $D_{T^*-0.2} > D_{S^*+\Delta S} > D_\sigma$ and $(1 - R_z)^{-1}$ reach high negative values, and a small deepening of $D_{T^*-0.2}$ is, as expected, highly favorable to the development of a CL. Finally, for R_z much larger than 1, profiles are not compensated and the density gradient is controlled by the temperature gradient. Equation (8) says that the changes in CL tends toward zero when R_z grows, in agreement with the lack of compensations. We illustrate below how this equation helps interpreting the tropical BL.

4.2. Interpretation of the Northwestern Tropical Atlantic BLs

[33] Figure 8 shows the values of R_z averaged over the northwestern tropical Atlantic (Figure 8, top) and in the central Atlantic and Pacific basins (Figures 8 (middle) and 8 (bottom), respectively). As discussed earlier, equation (4) is missing an important term of subsurface heat flux, and thus it doesn't explain the evolution of $D_{T^*-0.2}$ in summer in the North Atlantic Warm Pool. In terms of stratification regimes, nevertheless, Figure 8 shows that $-1 \ll R_z < 0$ during this season. The BL modulating factor is then close to unity, and equation (10) confirms that such a situation is favorable to the development of a BL (Figure 7), whose thickness is proportional to changes in the distance separating the top of the thermocline and halocline.

[34] In the central Pacific and Atlantic basins (Figures 8 (middle) and 8 (bottom)), on the contrary, in summer, $D_{S^*+\Delta S}$ is relatively deep (see crosses in Figure 6) while $D_{T^*-0.2}$. is stable or tends to shoal (solid black lines in Figure 6), due to intense surface warming. Hence R_z is strongly negative, and $1/(1 - R_z)$ is close to 0. According to equation (10), this limits BL formation. This is in agreement with the vanishing of the BL that exists in spring prior to the surface salinity decrease (e.g., Figure 3).

[35] In autumn, the rapid weakening of $\partial T/\partial z$ due to surface cooling reduces (in absolute values) R_z, which can eventually even become positive in case of a temperature inversion. Even though equation (4) does not hold in that case, one can see that the modulating factor in equation (10) approaches 1. BLT time variation depends essentially on the

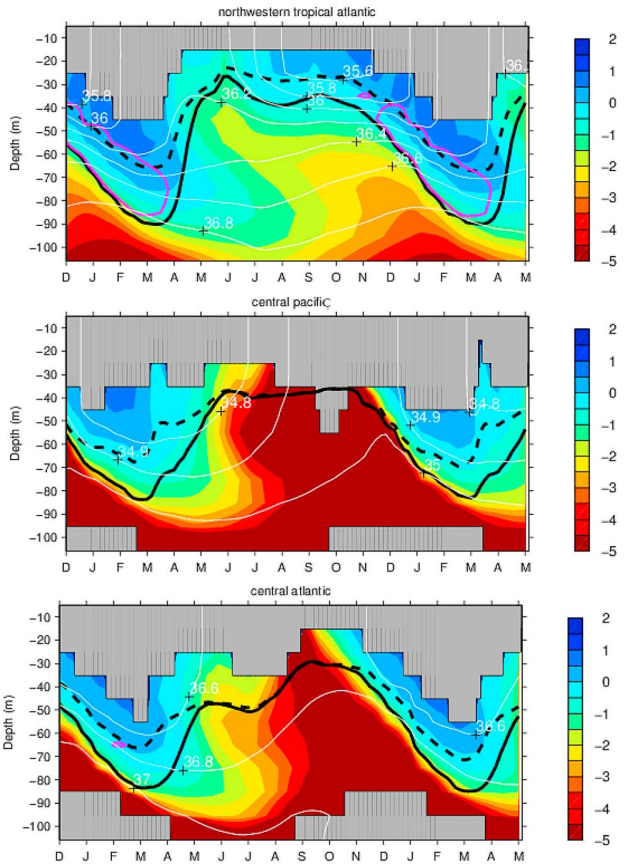

Figure 8. Vertical density ratio $R_z = \frac{\alpha_T \partial_z T}{\beta_S \partial_z S}$ averaged (top) over the present study area and over the (middle) central Pacific area and (bottom) central Atlantic area. Areas where $\partial_z S = 0$ are shown in grey. As in Figure 3, the thick black lines show the depth D_{T^*-02} (solid) and the MLD (dashed) diagnosed from the model data averaged over the same area.

change in distance between the tops of the halocline and the thermocline. $D_{T^*-0.2}$ deepens slightly faster than $D_{S^*+\Delta S}$, and consequently the BL thickens. This holds both in the western tropical Atlantic and in the central basins (Figure 8).

5. Conclusions

[36] We have investigated the formation mechanism of particularly thick and long lasting BLs located in the northwestern tropical Atlantic. The particular motivation was to understand their specific vertical thermal structure as compared to BLs located at the same latitude in the central Atlantic and in the central Pacific: subsurface temperature maxima of up to 1°C can be found in the northwestern tropical Atlantic. This is much more than in any other tropical area of the world, and it extends over a large region.

[37] We have shown that the seasonal cycle of BLs in the northwestern tropical Atlantic is composed of two phases. In spring and summer, intense freshwater input from the Amazon discharge and ITCZ precipitation induce a shallow and strongly marked salinity stratification that limits the deepening of the mixed layer. Meanwhile, some of the intense solar radiative flux penetrates below the mixed layer, inducing the development of unique subsurface temperature maxima and BLs. We argue that in the northwestern tropical Atlantic, the summer BL develops while the mixed layer is maintained at constant depth and the thermocline deepens although the surface temperature increases. In the center of the tropical basins, no major freshwater input such as the Amazon and the Orenoque can decouple the vertical stratification of temperature and salinity during this season and thus prevents a BL from forming during the summer.

[38] In winter, the surface temperature cools and the salinity stratification is maintained through the poleward transport of fresh equatorial mixed layers. The wind-induced mixing leads to a deepening of both the MLD and D_{T^*-02}, but because of the salinity stratification, the two deepen at different rates and a BL is maintained in-between. This second phase of BL development leads to a deeper and thicker BL than during the summer phase. Similar BL development is seen in the central Atlantic and central Pacific. In all three areas, it is associated with a relatively warm reservoir in the BL. The latter is much stronger in the northwestern tropical Atlantic since it results partly from the persistence of the one created in summer. The present analysis, which uses a consistent set of temperature and salinity vertical profiles from model outputs, gives confidence to the winter BL formation mechanism proposed by MBLC07.

[39] These results shade light on the presence of intense subsurface temperature maxima in the northwestern tropical Atlantic. They are indeed due to an early (in terms of seasonality) capping of surface mixing by freshwater input, while the mixed layer is sufficiently shallow to allow significant penetration of radiative heat flux. When the freshwater capping occurs in winter, as in the center of the basins, the mixed layer is already relatively deep and the BL simply occurs as a result of different deepening speed of MLD and D_{T^*-02}. This mechanism is largely consistent with results from model sensitivity experiment performed by *Balaguru* [2011], who also emphasized the importance of surface salinity in the creation of the strong vertical temperature inversions. As indicated in the introduction, previous studies have illustrated the climatic impact of temperature inversions in the Indian and Pacific Ocean. These studies dealt with subsurface temperature exceeding by 0.1 to 0.2°C the surface temperature. Here, the subsurface warm reservoir can exceed the surface temperature by almost 1°C. Its potential impact in terms of tropical cyclone predictability has already been suggested by *Balaguru* [2011]. In the future, we wish to assess the question of potential climatic impact of changes in seasonality and/or magnitude of the Amazon discharge. The mechanism that we purpose here would need to be confirmed by the other high resolution OGCMs, including those under inter-annual forcing.

[40] We have also derived a linear prognostic model for the BL and CL development as a function of temperature and salinity stratifications. We have illustrated that despite strong assumptions, it constitutes a good framework to discuss BL developments, and compare the behavior in different basins or seasons. The numerous possible improvements of this model, such as the inclusion of subsurface heat fluxes, are left for future studies.

[41] **Acknowledgments.** We would like to thank Nicolas Martin for help with the ARGO floats. The authors also acknowledge Christian Ethé

for the simulation. We also acknowledge Kyla Drushka and the editor for useful and constructive remarks that greatly helped to improve the manuscript.

References

Antonov, J. I., D. Seidov, T. P. Boyer, R. A. Locarnini, A. V. Mishonov, H. E. Garcia, O. K. Baranova, M. M. Zweng, and D. R. Johnson (2010), *World Ocean Atlas 2009*, vol. 2, *Salinity*, edited by S. Levitus, 184 pp., U.S. Govt. Print. Off., Washington, D. C.

Balaguru, K. (2011), Barrier layers of the Atlantic Warm pool: Formation mechanism and influence on weather and climate, PhD thesis, Tex. A&M Univ., College Station.

Bentamy, A., Y. Quilfen, F. Gohin, N. Grima, M. Lenaour, and J. Servain (1996), Determination and validation of average wind fields from ERS-1 scatterometer measurements, *Global Atmos. Ocean Syst.*, *4*, 1–29.

Berliand, M. E., and T. G. Strokina (1980), Global distribution of the total amount of clouds, technical report, 71 pp., Hydrometeorol. Publ. House, Saint Petersburg, Russia.

Blanke, B., and P. Delecluse (1993), Variability of the tropical Atlantic Ocean simulated by a general circulation model with two different mixed-layer physics, *J. Phys. Oceanogr.*, *23*, 1363–1388.

Chen, L. G. (1995), Mixed layer density ratio from the Levitus data, *J. Phys. Oceanogr.*, *25*(4), 691–701.

de Boyer Montégut, C., G. Madec, A. S. Fisher, A. Lazar, and D. Iudicone (2004), Mixed layer depth over the global ocean: An examination of profile data and a profile-based climatology, *J. Geophys. Res.*, *109*, C12003, doi:10.1029/2004JC002378.

de Boyer Montégut, C., J. Mignot, A. Lazar, and S. Cravatte (2007a), Control of salinity on the mixed layer depth in the world ocean. Part I: General description, *J. Geophys. Res.*, *112*, C06011, doi:10.1029/2006JC003953.

de Boyer Montégut, C., J. Vialard, S. S. C. Shenoi, D. Shankar, F. Durand, C. Ethé, and G. Madec (2007b), Simulated seasonal and interannual variability of mixed layer heat budget in the northern Indian Ocean, *J. Clim.*, *20*, 3249–3268.

Dessier, A., and J. R. Donguy (1994), The sea surface salinity in the tropical Atlantic between 10°S and 30°N—Seasonal and interannual variations (1977–1989), *Deep Sea Res. I*, *41*, 81–100.

Durand, F., S. R. Shetye, J. Vialard, D. Shankar, S. S. C. Shenoi, C. Ethe, and G. Madec (2004), Impact of temperature inversions on SST evolution in the South-Eastern Arabian Sea during the pre-summer monsoon season, *Geophys. Res. Lett.*, *31*, L01305, doi:10.1029/2003GL018906.

Durand, F., D. Shankar, C. de Boyer Montégut, S. S. C. Shenoi, B. Blanke, and G. Madec (2007), Modeling the barrier-layer formation in the South-Eastern Arabian Sea, *J. Clim.*, *20*, 2109–2120.

Enfield, D. B., and L. Cid-Serrano (2010), Secular and multidecadal warmings in the North Atlantic and their relationships with major hurricane activity, *Int. J. Climatol.*, *30*(2), 174–184.

Ferry, N., and G. Reverdin (2004), Sea surface salinity interannual variability in the western tropical Atlantic: An ocean general circulation model study, *J. Geophys. Res.*, *109*, C05026, doi:10.1029/2003JC002122.

Foltz, G. R., and M. J. McPhaden (2008), Seasonal mixed layer salinity balance of the tropical North Atlantic Ocean, *J. Geophys. Res.*, *113*, C02013, doi:10.1029/2007JC004178.

Gent, P. R., and J. C. McWilliams (1990), Isopycnal mixing in ocean circulation models, *J. Phys. Oceanogr.*, *20*, 150–151.

Giannini, A., Y. Kushnir, and M. C. Cane (2000), Interannual variability of Caribbean rainfall, ENSO, and the Atlantic Ocean, *J. Clim.*, *13*, 297–310.

Jacket, D. R., and T. J. McDougall (1995), Minimal adjustment of hydrographic data to achieve static stability, *J. Atmos. Oceanic Technol.*, *12*, 381–389.

Jerlov, N. G. (1968), *Optical Oceanography*, 194 pp., Elsevier, Amsterdam.

Kalnay, E., et al. (1996), The NCEP/NCAR 40-year reanalysis project, *Bull. Am. Meteorol. Soc.*, *77*, 437–471.

Knight, J. R., R. J. Allan, C. K. Folland, M. Vellinga, and M. E. Mann (2005), A signature of persistent natural thermohaline circulation cycles in observed climate, *Geophys. Res. Lett.*, *32*, L20708, doi:10.1029/2005GL024233.

Levitus, S. (1998), Climatological atlas of the world ocean, *Tech. Rep., 13*, NOAA, Rockville, Md.

Liu, H., S. A. Grodsky, and J. A. Carton (2009), Observed sub seasonal variability of oceanic barrier and compensated layers, *J. Clim.*, *22*(22), 6104–6119.

Locarnini, R. A., A. V. Mishonov, J. I. Antonov, T. P. Boyer, H. E. Garcia, O. K. Baranova, M. M. Zweng, and D. R. Johnson (2010), *World Ocean Atlas 2009*, vol. 1, *Temperature*, edited by S. Levitus, 184 pp., U.S. Govt. Print. Off., Washington, D. C.

Madec, G., and M. Imbard (1996), A global ocean mesh to overcome the North Pole singularity, *Clim. Dyn.*, *12*(6), 381–388.

Madec, G., P. Delecluse, M. Imbard, and M. Levy (1998), OPA 8.1: Ocean general circulation model reference manual, *Notes du Pole de Model.*, *11*, Inst. Pierre-Simon Laplace, Paris.

Masson, S., and P. Delecluse (2001), Influence of the Amazon River runoff on the tropical Atlantic, *Phys. Chem. Earth B*, *26*(2), 137–142.

Merryfield, W. J., G. Holloway, and A. E. Gargett (1999), A global ocean model with double-diffusive mixing, *J. Phys. Oceanogr.*, *29*(6), 1124–1142.

Mignot, J., C. de Boyer Montégut, A. Lazar, and S. Cravatte (2007), Control of salinity on the mixed layer depth in the world ocean: 2. Tropical areas, *J. Geophys. Res.*, *112*, C10010, doi:10.1029/2006JC003954.

Mignot, J., C. de Boyer Montégut, and M. Tomczak (2009), On the porosity of barrier layers, *Ocean Sci.*, *5*, 379–387.

Murray, R. J. (1996), Explicit generation of orthogonal grids for ocean models, *J. Comput. Phys.*, *126*, 251–273.

Pailler, K., B. Bourles, and Y. Gouriou (1999), The barrier layer in the western tropical Atlantic Ocean, *Geophys. Res. Lett.*, *26*, 2069–2072.

Paulson, C. A., and J. J. Simpson (1977), Irradiance measurements in the upper ocean, *J. Phys. Oceanogr.*, *7*, 952–956.

Roullet, G., and G. Madec (2000), Salt conservation, free surface and varying volume: A new formulation for ocean GCMs, *J. Geophys. Res.*, *105*, 23,927–23,942.

Rudnick, D. L., and J. P. Martin (2002), On the horizontal density ratio in the upper ocean, *Dyn. Atmos. Oceans*, *36*, 3–21.

Smith, W. H. F., and D. T. Sandwell (1997), Global sea floor topography from satellite altimetry and ship depth soundings, *Science*, *277*, 1956–1962.

Smyth, W. D., D. Hebert, and J. N. Moum (1996), Local ocean response to a multiphase westerly wind burst: 2. Thermal and freshwater responses, *J. Geophys. Res.*, *101*, 22,513–22,534.

Timmermann, R., H. Goosse, G. Madec, T. Fichefet, C. Ethe, and V. Duliere (2005), On the representation of high latitude processes in the ORCA-LIM global coupled sea ice–ocean model, *Ocean Modell.*, *8*, 175–201.

Trenberth, K. E., J. G. Olson, and W. G. Large (1989), A global ocean wind stress climatology based on the ECMWF analyses, technical report, 93 pp., Natl. Cent. for Atmos. Res., Boulder, Colo.

United Nations Educational, Scientific and Cultural Organization (UNESCO) (1996), Monthly and annual discharges recorded at various selected stations, technical report, 600 pp., Paris.

Vialard, J., and P. Delecluse (1998), An OGCM study for the TOGA decade. Part I: Role of salinity in the physics of the western Pacific fresh pool, *J. Phys. Oceanogr.*, *28*, 1071–1088.

Wang, C., and D. B. Enfield (2003), A further study of the influences of the tropical Western Hemisphere warm pool, *J. Clim.*, *16*, 1476–1493.

Wang, C., D. B. Enfield, S.-K. Lee, and C. W. Landsea (2006), Influences of the Atlantic warm pool on Western Hemisphere summer rainfall and Atlantic hurricanes, *J. Clim.*, *19*, 3011–3028.

Wang, C., S.-K. Lee, and D. B. Enfield (2008a), Atlantic Warm Pool acting as a link between Atlantic Multidecadal Oscillation and Atlantic tropical cyclone activity, *Geochem. Geophys. Geosyst.*, *9*, Q05V03, doi:10.1029/2007GC001809.

Wang, C., D. B. Enfield, and S.-K. Lee (2008b), Climate response to anomalously large and small Atlantic warm pools during the summer, *J. Clim.*, *21*, 2437–2450.

Xie, P., and P. A. Arkins (1997), A 17-year monthly analysis based on gauge observations, satellite estimates and numerical model outputs, *Bull. Am. Meteorol. Soc.*, *78*(11), 2539–2558.

M. Lacarra, A. Lazar, and J. Mignot, LOCEAN, UPMC Case 100, 4 place Jussieu, F-75252 Paris CEDEX 05, France. (juliette.mignot@locean-ipsl.upmc.fr)

Clim Dyn
DOI 10.1007/s00382-015-2898-1

Decadal prediction skill in the ocean with surface nudging in the IPSL-CM5A-LR climate model

Juliette Mignot[1,2,3] · Javier García-Serrano[3] · Didier Swingedouw[4] · Agathe Germe[3] · Sébastien Nguyen[3] · Pablo Ortega[3,5] · Eric Guilyardi[3,6] · Sulagna Ray[3,7]

Received: 31 December 2014 / Accepted: 28 October 2015

Abstract Two decadal prediction ensembles, based on the same climate model (IPSL-CM5A-LR) and the same surface nudging initialization strategy are analyzed and compared with a focus on upper-ocean variables in different regions of the globe. One ensemble consists of 3-member hindcasts launched every year since 1961 while the other ensemble benefits from 9 members but with start dates only every 5 years. Analysis includes anomaly correlation coefficients and root mean square errors computed against several reanalysis and gridded observational fields, as well as against the nudged simulation used to produce the hindcasts initial conditions. The last skill measure gives an upper limit of the predictability horizon one can expect in the forecast system, while the comparison with different datasets highlights uncertainty when assessing the actual skill. Results provide a potential prediction skill (verification against the nudged simulation) beyond the linear trend of the order of 10 years ahead at the global scale, but essentially associated with non-linear radiative forcings, in particular from volcanoes. At regional scale, we obtain 1 year in the tropical band, 10 years at mid-latitudes in the North Atlantic and North Pacific, and 5 years at tropical latitudes in the North Atlantic, for both sea surface temperature (SST) and upper-ocean heat content. Actual prediction skill (verified against observational or reanalysis data) is overall more limited and less robust. Even so, large actual skill is found in the extratropical North Atlantic for SST and in the tropical to subtropical North Pacific for upper-ocean heat content. Results are analyzed with respect to the specific dynamics of the model and the way it is influenced by the nudging. The interplay between initialization and internal modes of variability is also analyzed for sea surface salinity. The study illustrates the importance of two key ingredients both necessary for the success of future coordinated decadal prediction exercises, a high frequency of start dates is needed to achieve robust statistical significance, and a large ensemble size is required to increase the signal to noise ratio.

Keywords Decadal variability · Oceanic predictability · Surface nudging

✉ Juliette Mignot
juliette.mignot@locean-ipsl.upmc.fr

[1] Climate and Environmental Physics, Physics Institute, University of Bern, Bern, Switzerland

[2] Oeschger Center for Climate Change Research, University of Bern, Bern, Switzerland

[3] LOCEAN/IPSL (Sorbonne Universités UPMC-CNRS-IRD-MNHN), 4 place Jussieu, 75005 Paris, France

[4] Environnements et Paléoenvironnements Océaniques et Continentaux (EPOC), UMR CNRS 5805 EPOC - OASU - Université de Bordeaux, Allée Geoffroy Saint-Hilaire, 33615 Pessac, France

[5] Present Address: NCAS-Climate, Department of Meteorology, University of Reading, Reading RG6 6BB, UK

[6] NCAS-Climate, Department of Meteorology, University of Reading, Reading RG6 6BB, UK

[7] Present Address: Atmospheric and Oceanic Sciences Program, Princeton University, Princeton, NJ, USA

1 Introduction

Because of the potential socio-economic impacts, decadal climate prediction has developed as a novel topic over the last few years (Meehl et al. 2014) and given rise to great expectations. The goal of this exercise is to exploit the predictability of internally-generated climate variability together with that from the externally-forced component, as well as to enhance prediction skill by correcting the forced model

Published online: 01 December 2015

response. The 11th chapter of the Intergovernemental Panel on Climate Change (IPCC) fifth assessment report (Kirtman et al. 2013) describes the recent scientific achievements on this topic, but also emphasizes that several technical and scientific challenges remain. Although prediction skill arises mostly from external forcing (e.g. Doblas-Reyes et al. 2013), initialization of the slow components of the climate system has also provided added value for the first few years of the forecast, most notably in the North Atlantic (e.g. Hazeleger et al. 2013b; Corti et al. 2012; Kim et al. 2012; Oldenborgh et al. 2012; Swingedouw et al. 2013; García-Serrano et al. 2014). This is at least partly due to the initialization of the Atlantic Meridional Overturning Circulation (AMOC), which shows large inertia in climate models (e.g. Persechino et al. 2013). Over the North Pacific, some signs of improved prediction skill through initialization have been found associated with the Pacific Decadal Oscillation (PDO), (Mantua et al. 1997) or Interdecadal Pacific Oscillation (IPO) (Keenlyside et al. 2008; Meehl et al. 2010; Oldenborgh et al. 2012; Meehl and Teng 2012). Mochizuki et al. (2010) and Chikamoto et al. (2013) showed that models ability to follow the subsurface temperature evolution in the North Pacific increases thanks to initialization. Because of its potential effect on the atmosphere, SST has been the focus of most of these studies and is indeed commonly used as an indicator of the ocean's state in decadal prediction assessments. Nevertheless, subsurface fields are somewhat shielded from weather noise and might thus be expected to be more predictable than the surface fields (e.g. Branstator and Teng 2010), while they might still have the potential to affect the atmosphere on long time scales. Indeed, the oceanic heat content acts as a key indicator of climate perturbations on seasonal, interannual and longer time scales (e.g. Lozier et al. 2008), accounting for the total amount of heat variation, through storage and transport, that could potentially be available for the atmosphere. Using a statistical analysis of control simulations, Branstator and Teng (2012) showed that initialization has the potential to improve prediction skill of the upper 300 m temperature up to the first 5 years in the North Pacific and 9 years in the North Atlantic.

Initialization techniques are numerous (Kirtman et al. 2013), including assimilation of surface information only (e.g. Keenlyside et al. 2008; Merryfield et al. 2010; Swingedouw et al. 2013; Ray et al. 2015), restoring to 3-dimensional data (e.g. Voldoire et al. 2014; Bombardi et al. 2014), forcing of the ocean model with atmospheric observations (Matei et al. 2012; Yeager et al. 2012) and more sophisticated alternatives based on fully coupled data assimilation schemes (Zhang 2007; Sugiura et al. 2009; Karspeck et al. 2014). It is yet difficult to distinguish whether one specific method clearly yields enhanced skill, as few studies have focused on comparing different techniques with a single climate model. Noteworthy is the study of Matei et al. (2012), who found that hindcast experiments starting from reconstruction simulations forced with the observed evolution of the atmospheric state and associated heat flux over the ocean (including SST information although not explicitly) constitute a simple but skillful strategy for initialized climate predictions over the next decade, as compared to a 3-dimensional restoring towards ocean reanalysis. Bellucci et al. (2013) highlighted the strong differences in prediction skill obtained with forecast systems using different ocean data assimilation products. Using perfect model approaches, Dunstone and Smith (2010) and Zhang et al. (2010) found, as expected, an improvement in skill when subsurface information is used as part of the initialization. Nevertheless, given the uncertainty in ocean reanalysis below the surface (e.g. Ray et al. 2015), several studies also focused on prediction skill using only information from the sea surface (e.g. Keenlyside et al. 2008; Merryfield et al. 2010). In particular, Kumar et al. (2014) and Ray et al. (2015) showed that SST nudging is efficient in reconstructing the observed subsurface variability in the equatorial Pacific.

Given climate models usual biases notably in terms of mean state, another question that arises regarding the generation of initial conditions for predictions is the opportunity to use full field or anomaly initialization. In the first case, the coupled model is initialized with a state close to the real-world attractor and after initialization, drifts towards its own attractor. The second case limits this shock, but leads to question the link between mean state and variability. To put it differently, is it possible to properly reconstruct, and predict ENSO variability, for example, even if the warm pool is not correctly located in the model? Magnusson et al. (2012), Hazeleger et al. (2013a) and Smith et al. (2013) show that at decadal time scales, it is difficult to determine whether one of these two strategies is more skillful than the other.

This study aims at assessing prediction skill in the ocean with the IPSL-CM5A-LR climate model initialized via nudging towards observed SST anomalies. As described above, this set up lies on the side of relatively simple initialization techniques. Servonnat et al. (2014) investigated the performance of this technique for the reconstruction of subsurface variability in a perfect model configuration using the same climate model. Ray et al. (2015) carried similar analysis but under historical conditions and using observations, highlighting the current uncertainty in subsurface ocean variability. Swingedouw et al. (2013) showed the skill of the system in reproducing the Atlantic Meridional Overturning Circulation (AMOC) variability and Séférian et al. (2014) used it to demonstrate the relatively long forecasting capabilities of the primary production in the tropical Pacific as compared to SST. Here, we provide a more systematic investigation of ocean surface and subsurface predictability of the system. The model, experimental set-up and statistics are presented in Sect. 2. Global and tropical SST prediction skills are described in Sect. 3. Sections 4 and 5 concentrate on the prediction skill

in the North Atlantic and in the North Pacific respectively. Section 6 discusses issues on sea surface salinity (SSS). Conclusions are given in the final section.

2 Model and methods

2.1 The climate model

We use the Earth System Model IPSL-CM5A-LR (Dufresne et al. 2013), developed at the Institut Pierre Simon Laplace (IPSL). The atmospheric model is LMDZ5 (Hourdin et al. 2013), with a horizontal resolution of 1.875° × 3.75° and 39 vertical levels. The ocean model is NEMOv3.2 (Madec 2008), in ORCA2 configuration. This non-regular grid has a nominal resolution of 2°, refined in the Tropics and the subpolar North Atlantic. The ocean grid has 31 vertical levels. NEMOv3.2 also includes the sea-ice component LIM2 (Fichefet and Maqueda 1997) and the biogeochemical module PISCES (Aumont and Bopp 2006). The performances of the oceanic component in the coupled configuration are discussed in Mignot et al. (2013). The reader is referred to the special issue in Climate Dynamics (http://link.springer.com/journal/382/40/9/) for a collection of studies describing various aspects and components of the model as well as its performance for climatic studies. We emphasize here the contribution from Persechino et al. (2013) who investigated the model's potential predictability.

2.2 The decadal prediction system

The set of experiments considered here is summarized in Table 1. It first includes a 3-member ensemble of non-initialized historical simulations, all available on the CMIP5 database. They use prescribed external radiative forcing from the observed increase in greenhouse gases and aerosols concentrations, as well as the ozone changes and the land-use modifications. They also include estimates of solar irradiance and volcanic eruptions, represented as a decrease in the total solar irradiance. These simulations start from year 1850. Their initial conditions come from the 1000-year long control simulation under preindustrial conditions and are each separated by 10 years. Each of these simulations was integrated until end of 2005. From January 1st 2006, they were prolonged using external forcing corresponding to the RCP4.5 scenario, as described in Taylor et al. (2012). This ensemble of 3 members of historical + scenario simulations will be referred to as HIST in the following.

The second set of experiments under consideration is a 3-member ensemble of nudged simulations, so called as they include a nudging towards observed anomalous SST variations. Each nudged simulation (NUDG1, NUDG2 and NUDG3 in the following) was started on January 1st 1949 from one of the historical simulations, using strictly the same external forcing, and applying also a nudging, or restoring term. This term consists in an additional heat flux term Q imposed in the equation for the SST evolution and written as $Q = -\gamma\,(SST'_{mod} - SST'_{ERSST})$. SST'_{mod} stands for the modeled SST anomaly with respect to the climatological mean computed between 1949 and 2005 in the corresponding historical simulation. SST'_{ERSST} are the anomalous SST from the Reynolds et al. (2007) dataset with respect to the same climatological period. We use a restoring coefficient γ of 40 $\mathrm{Wm^{-2}K^{-1}}$, corresponding to a relaxing timescale of around 60 days over a mixed layer of 50 m depth. This rather weak value as compared to previous studies using surface nudging (Keenlyside et al. 2008; Dunstone and Smith 2010; Luo et al. 2005) typically represents the amplitude of air-sea thermal coupling (e.g. Frankignoul and Kestenare 2002) and was justified in previous papers (Swingedouw et al. 2013; Servonnat et al. 2014; Ray et al.

Table 1 Table summarizing the hind cast simulations used in this study. We specify in particular the initialization strategy, the number of members of the ensemble, the start dates frequency, the length (in years) of each hindcasts. The final columns gives some additional remarks for clarity

Initialization strategy	Ens. size	Start dates	Length (years)	Name	Remark
Non-initialized	3	Yearly (1961–2013)	10	HIST	Independent long-term historical simulations HIST1, HIST2, HIST3
Continuous surface nudging	3	Yearly (1961–2013)	10	NUDG	Independent long-term nudged simulations NUDG1, NUDG2, NUDG3
Surface nudging	3	Every 5 years (1961–2006)	10	DEC1	Launched from NUDG1
Surface nudging	3	Every 5 years (1961–2006)	10	DEC2	Launched from NUDG2
surface nudging	3	Yearly (1961–2013)	10	**DEC3**	Launched from NUDG3
Surface nudging	9	Every 5 years (1961–2006)	10	**DEC9**	From DEC1 + DEC2 + DEC3

2015). Efficiency of this nudging strategy in reconstructing subsurface variability is more specifically studied in Ray et al. (2015), and the reader is referred to Swingedouw et al. (2013) for a focus on the AMOC. Servonnat et al. (2014) investigate several aspects of surface nudging in a perfect model context. Note also that as indicated in the previous references, nudging is not applied when and where the model sea-ice cover exceeds 50 %.

A set of 3-member ensembles of runs at least 10 years long where the restoring constraint is no longer applied (while the external forcing from historical and scenario simulations is used) was then launched from each nudged simulation. These simulations make up our retrospective forecasts, or hindcasts. For NUDG1 and NUDG2, hindcasts were launched on January 1st 1961 and every 5 years afterwards until January 1st 2006, as recommended in the CMIP5 protocol (Taylor et al. 2012). These two sets of hindcasts, named DEC1 and DEC2 in the following, were both submitted to the CMIP5 near term database (e.g. García-Serrano et al. 2014). Hindcasts starting from NUDG3 were launched every year from January 1st 1961 until January 1st 2013. These series of hindcasts, named DEC3, was not submitted to the ESG, but is now part of the multi-model decadal forecast exchange project (http://www.metoffice.gov.uk/research/climate/seasonal-to-decadal/long-range/decadal-multimodel; Smith et al. 2012). For all ensembles, initial conditions of the individual members were obtained by applying at the first time step a perturbation to the SST field seen by the atmospheric component, chosen randomly at each grid point between −0.05 and 0.05 °C. Note that, strictly speaking, each group of 3 members in DEC9 also differ in terms of oceanic perturbation, since they originate from a different coupled simulation. Analysis of the impact of such differences in initial perturbations is beyond the scope of this paper and is not likely to have a strong effect (Du et al. 2012). Note also that as in other CMIP5-type hindcasts, external forcing is exactly the same as in historical and nudged simulations. This forcing thus includes volcanic eruptions, even though this forcing would in reality not be available at the start date of the forecast in an operational context.

In the following, we evaluate the forecasting skill of the system using two ensembles of initialized hindcasts: the ensemble DEC3, on the one hand, consisting of 3 members launched every year, and the ensemble named DEC9, on the other hand, resulting from the merging of DEC1, DEC2 and a subsample of DEC3, which consists thus in a 9-member ensemble of hindcasts launched every 5 years from January 1st 1961 to January 1st 2006. On top of these, we consider the ensemble of HIST simulations as a benchmark for multiyear prediction skill without initialization.

2.3 Verification datasets

In order to validate the prediction skill of the system, five different datasets are used. First, we consider ERSST, the SST field from Reynolds et al. (2007), which was used for the nudging. Performances are expected to be highest with this reference dataset, which, for our purposes, covers the period (1961–2013). This dataset is represented with the dark blue color in the figures. The HadISST dataset (Rayner 2003) taken as an alternate verification dataset gave very similar results as ERSST and is thus not shown. Secondly, we consider two ocean reanalyses, namely ORAS4 (Balmaseda et al. 2013, color code orange in the figure), available until 2011, and SODA2.2.4 (SODA hereafter, color code cyan in the figures) (Ja and Giese 2008; Giese and Ray 2011; Ray and Giese 2012), available until 2005. As described in Ray et al. (2015), for example, these two reanalyses are based on different ocean models, with different resolutions, different forcing datasets and different assimilation schemes, which may lead to substantial differences. They yield a consistent (significantly correlated at the 90 % confidence level) reconstruction of the oceanic variability mainly down to 200 m (Ray et al. 2015). We use them both in order to assess the prediction skill of the system but taking into account the uncertainty in data, in particular for ocean variables hard to constrain such as the AMOC. For the AMOC, we also consider the reconstruction proposed by Latif et al. (2006), using a dipole of SST between the Northern and Southern Atlantic (featured in yellow in the figures). Finally, for the subsurface temperature, integrated ocean heat content and for the salinity, we also use the EN3 set of objectively analyzed temperature and salinity profiles (color code purple) proposed by Ingleby and Huddleston (2007). This product is not optimized for SST, as it does not integrate specific surface data. All these datasets will be collectively referred to as DATA from now on in the text. Note however that these data sets are always considered individually in all computations, and not averaged out. Furthermore, for clarity of the figures, the ACC and RMSE skill scores computed for the HIST simulations with respect to each of these data sets are not identified individually with specific colors.

2.4 Data processing

As discussed for example in Oldenborgh et al. (2012), a large part of the skill in decadal temperature forecasts is due to the trend. In order to study the predictability of the variability around the trend, it is important to remove the effect of the trend as cleanly as possible. A good definition of the trend is nevertheless difficult to obtain, given the non-linearity of the forcing (see discussion in García-Serrano et al. 2014). Furthermore, estimates of local trends

are subject to large sampling variability because of the lower signal to noise ratio for smaller spatial scales. Therefore, we focus here on spatial averages over relatively large domains (typically, the North Atlantic Ocean between 30° and 60°N) in order to maximize the signal to noise ratio (Goddard et al. 2012).

The treatment of data is then done as follows. Firstly, all ensemble sets (HIST, NUDG3, DEC and DATA) are organized mimicking the hindcasts outputs, that is as a function of start dates (from 1961 to 2013 or 2006 depending on the DEC system under consideration) and lead times (from 1 to 10 years). Secondly, anomalies are computed. The reference period is estimated as the overlapping period between the observational records and the hindcasts, i.e. (1961–2005) if the SODA reanalysis is included. Results were also tested against the use of a longer reference period, namely 1961–2011. This implies excluding the SODA reanalysis, but main results were unchanged. We then consider, for each dataset, anomalies with respect to the linear trend. This trend is estimated separately for each forecast time over the reference period. The simulated trend is computed separately for each individual member and the same methodology is applied both for DEC3 and DEC9. Observational trend is also considered as forecast-time dependent. Note that this procedure includes a correction of a bias in the mean state as well as of the linear response to external forcings. We assume that the residual signal represents the unforced variability, but we know that this is just an assumption as the external forcing is not linear. Note that the IPSL-CM5A-LR coupled model has a climate sensitivity of 3.9 K for a doubling of CO_2 (Dufresne et al. 2013), which places it at the 4th out of 11 models of the CMIP5 ranked per decreasing climate sensitivity (Vial et al. 2013) and is stronger than the newest estimates of climate sensitivity around 3 K (Collins et al. 2014).

To ensure having the same number of verification years at each forecast time in DEC3, we consider the verification period (1966–2005) when the SODA dataset is included. Following the 4-year average approach this implies that the common verification period spans from 1966/1969 to 2002/2005,with a total of 37 values per forecast lead time. Results are also tested against the common verification period 1966/1969 to 2008/2011, when SODA is excluded. Except if discussed in the text, results are generally similar. Note that the use of such common verification framework yields the same number of degrees of freedom for all lead times for a single time series (e.g. García-Serrano et al. 2012); this enables a consistent comparison of forecast skills at different lead times. Furthermore, given that the non-initialized simulations are in fact a re-organization of the outputs from three long-term simulations (HIST1, HIST2, HIST3), the time series constructed for the different lead times are identical and thus the statistical metrics are constant. The same applies to the DATA time series following this approach. Note furthermore that this common verification framework was not used for DEC9 due to the few start dates available.

2.5 Forecast quality assessment

Multi-annual prediction skill is measured in terms of anomaly correlation coefficients (ACC) and root mean square errors (RMSE). ACC and RMSE are calculated based on the ensemble mean of the hindcasts. Both measures are computed for DEC and HIST respectively, against DATA, and for each lead time. Significance of the correlation is tested with a one-sided Student t test at the 90 % confidence level. The number of degrees of freedom takes into account the autocorrelation of each time series, as suggested in Bretherton et al. (1999). We also test the significance of the ACC difference between HIST and DEC. The purpose of this additional test is to evaluate the added-value of initialization for the prediction skill. Significance of the difference between the RMSE of initialized (DEC) versus non-initialized (HIST) ensembles is evaluated using a Fisher test. Note that a fair estimation of the continuous ranked probability score (Ferro 2014) was found to yield very similar conclusions as the RMSE. Given that the evaluation of probability distribution might be problematic in DEC9 which only counts 8 realizations, we decided to show only RMSE here.

All ACC and RMSE are also computed against the NUDG3 (simply named NUDG in the following) outputs, and significance is tested similarly. The point of evaluating prediction skill against both DATA and NUDG is to compare actual and potential predictability, respectively. Such assessment is particularly relevant when initial conditions have been constructed through nudging rather than directly taken from an independent dataset. In this case, indeed, the correlation and RMSE of hindcasts with respect to NUDG is expected to be higher than computed against DATA, as NUDG contains effectively the initial conditions from which the hindcasts were launched, and these can then be substantially different from the data (e.g. Ray et al. 2015). The forecasting skill against NUDG gives an idea of the upper limit of possible skill in the system, while the one computed against DATA measures the actual skill against a particular reconstruction of reality. The potential prediction skill defined here is inspired from Boer et al. (2013) but not fully equivalent: for Boer et al. (2013) potential forecast skill is analogous to actual forecast skill, but with the divergence of the forecast from the observed evolution being replaced by a measure of the divergence of model results from each other. Here, we rather use a different reference, namely the NUDG simulation. Note also that only one nudged simulation is used, and not the average of the

three. Indeed, the nudging only has a limited impact on the ocean subsurface, so that the three nudged simulations do slightly differ after a certain depth (Ray et al. 2015). As a result, averaging the three nudged simulations in these regions would risk to blur the reconstructed variability at depth. Note however that it would not change the results regarding the SST prediction skill.

We also compare the skill of the forecasts with the performance of a first order auto-regressive model (e.g. Ho et al. 2012). Initial conditions are taken from the last year before the beginning of the hindcasts, that is the last year with supposedly known conditions. The time constant involved in the auto-regressive model is estimated from the fit of the autocorrelation function of the considered time series taken in the long-term control run by a decreasing exponential (e.g. Mignot and Frankignoul 2003).

Finally, while the metrics presented above focus on the ensemble mean, it is also important to consider the dispersion of the hindcasts around this mean, in order to estimate their reliability. A forecast system is considered as reliable when the forecast probabilities of a certain variable match the observed ones. These questions have been extensively tackled for seasonal forecasts (e.g. Weisheimer et al. 2011; Batté and Déqué 2012), and much less for the decadal predictions (Corti et al. 2012; Ho et al. 2013). Here, since our analysis only uses one prediction system, the error primarily comes from uncertainty in initial conditions. In this respect, the spread of the set of predictions can be used as a measure of the prediction error. This ensemble spread is compared to the RMSE of the forecast ensembles with respect to DATA or NUDG. For a prediction to be reliable, or trustworthy, the time-mean ensemble spread about the ensemble mean should equal the time-mean RMSE of the ensemble mean forecast. The system is said overdispersed if the spread significantly exceeds the RMSE. In this case, the probabilistic forecasts are unreliable as the individual forecasts may produce too different results. On the contrary, if the spread is significantly smaller than the RMSE (system underdispersive), especially at short forecast ranges, it may indicate that the initial perturbation of the probabilistic forecast is too weak to realistically sample the uncertainty of the system. The system can then be characterized as overconfident, and it is in any case also poorly reliable. Note nevertheless that caution is required when assessing the reliability in DEC3, given the very low number of members.

3 Global and tropical SST prediction skill

3.1 Global SST prediction skill

Figure 1a shows the time series of detrended global-mean SST anomalies averaged over the forecast years 2–5 in the DEC3 ensemble mean and the corresponding non-initialized hindcasts HIST. Outputs from the NUDG simulation and ERSST are also shown. These time series highlight the decadal climate variability at global scale and the cooling signatures of the major volcanoes which have erupted over the last 50 years: Mt Agung in 1963, El Chichon in 1982 and Mt Pinatubo in 1991. Because of the strong negative radiative forcing of these volcanic eruptions, ACC of the hindcasts with both NUDG and the DATA is not significantly different from that obtained with the non-initialized hindcasts (Fig. 1b). The global mean SST indeed primarily responds to external forcing, and this figure illustrates the weak added value of initialization for predicting this climate quantity over the period considered here (which includes rather strong volcanic eruptions). Consistently with Mehta et al. (2013), volcanic eruptions are one of the important sources of decadal prediction skill for global SST. When computed against NUDG and ERSST (the dataset used for the nudging) ACC remains significant at all lead times. SODA and more clearly ORAS4 yield lower scores. This illustrates the uncertainty in available datasets, and how it hampers hindcast verification. Note that the AR1 predictive method started from DEC3 and computed with respect to NUDG is not skillful. This is consistent with an important role of external forcing, which may appear after the date when the hindcast was launched.

Figure 1e further illustrates the influence of non-linear external forcing in the DEC9 predictive system. Because hindcasts are launched every 5 years only in this set, their specific timing with respect to the volcanic eruptions listed above is very important. More precisely, one should note that the start dates used in DEC9 (following the CMIP5 protocol) are in phase or slightly leading the eruptions. As a result, for the forecast range 2–5 years for example, two start dates (1982–1985 and 1992–1995) are very strongly influenced by the eruptions [since the radiative impact typically lasts 3 years, (e.g. Robock 2000)]. This highly contrasts with the forecast range 4–7 years, which is, for each start date, only impacted by the last year of the volcanic radiative effect [see also Fig. 10 in Germe et al. (2014)]. As a result, the main source of predictability for global SST is partly lost for the forecast range 4–7 years and the correlation skill drops. Impact of the main volcanic eruptions in the last 60 years falls again in the time window of the predictions at lead times 6–9 years, thereby contributing to enhance the correlation skill again. Such specific sampling issue does not occur in DEC3 (Fig. 1b). A subsampling analysis of the start date frequency in DEC3 confirms that the drop of skill from forecast ranges 3–6 years until 5–8 years, followed by a recovery at the forecast range 6–9 years essentially comes from the specific choice of start dates every 5 years starting from 1961 (Fig. 2).

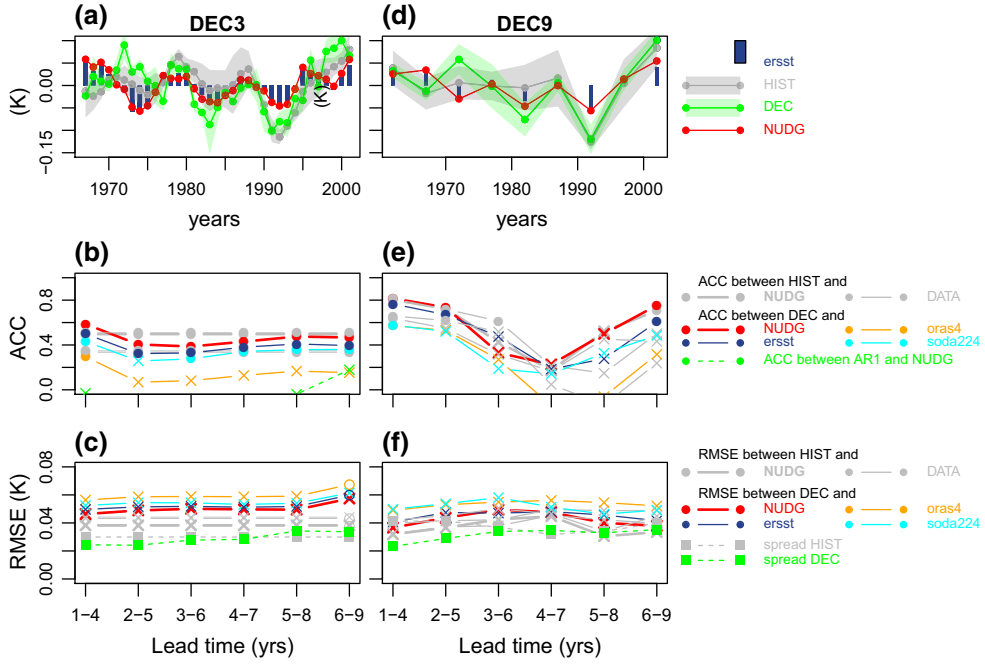

Fig. 1 **a** and **d** Time series of the detrended ensemble mean forecast anomalies averaged over the forecast years 2–5 [*green*, DEC3 (**a**), DEC9 (**b**)] and the accompanying non-initialized (*grey*) experiments of the global-mean sea surface temperature (SST). The *green* and *grey shadings* respectively show the spread of the forecasts. The *red line* shows the time series from the nudged experiment. The observational time series from the ERSST dataset are represented with *dark blue vertical bars*, where a 4-year running mean has been applied for consistency with the time averaging of the predictions. The time axis corresponds to the first year of the forecast period (i.e. year 2 of each forecast). **b** and **e** Correlation of the ensemble mean with the NUDG reference (*thick red* and *grey lines* respectively, for the DEC and HIST forecast ensembles), along the forecast time for 4-year averages. The figure also shows the correlation of DEC with ERSST (*dark blue*), ORAS4 (*orange*) and SODA (*light blue*) in *thin lines*, together with their counterparts for the HIST ensemble (*grey thin lines*', different data sets not identified with colors). Significant correlations according to a one-sided 90 % confidence level with a t-distribution are represented with a *circle*, non significant ones with a cross. The number of degrees of freedom has been computed taking into account the autocorrelation of the time series, which are different for each forecast time. A *filled circle* indicates significant correlations but not passing a two-sided *t* test for the differences between the DEC and HIST correlations. **c** and **f** RMSE of the ensemble mean along the forecast time for 4-year forecast averages are plotted with *solid lines*. *Circles* are used where the DEC skill is significantly better than the HIST skill with 90 % confidence using a two-sided *F* test. *Dashed lines* represent the ensemble spread estimated as the standard deviation of the anomalies around the multi-model ensemble mean. *Green line* is for the spread of the initialized hindcasts [DEC3 (**c**), DEC9 (**e**)], *grey dashed lines* for the non-initialized ones

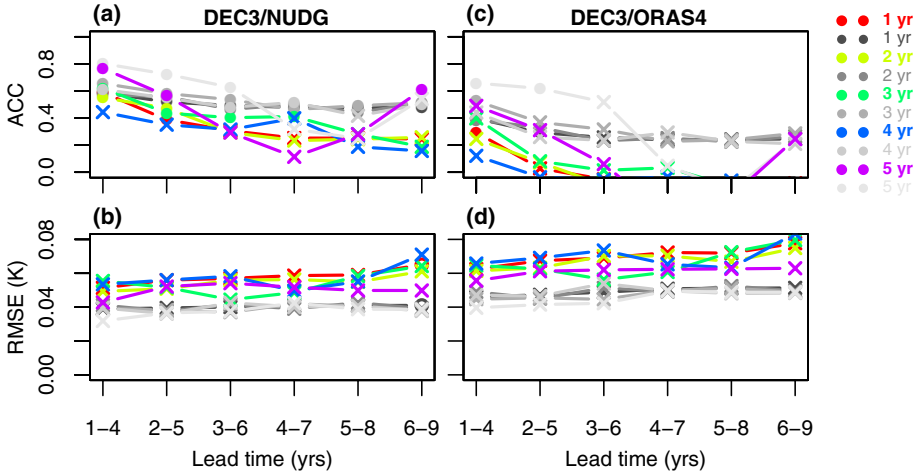

Fig. 2 **a** Potential ACC skill score of global mean SST with start dates taken with an interval of 1–5 years from 1961 to 2005 in DEC3. *Grey lines* show the corresponding skill for the HIST ensemble. **b** as **a** for the RMSE. **c** and **d** Same as **a** and **b** for the skill scores computed against ORAS4. Hindcasts launched between 1961 and 2005 were used here, but anomalies were not computed against a common verification period since this would be too restrictive for the longest start date intervals (see Sect. 2.4 for details)

Benefits of the system's initialization in bringing together the different members are yet visible from the fact that the spread of the initialized hindcasts is initially smaller than for non-initialized hindcasts (Fig 1c). Afterwards, it increases with forecast time, towards the level of the non-initialized hindcasts spread, illustrating the decreased influence of initialization with forecast time. Eventually, the spread of DEC3 is even slightly larger than that of HIST. Note however that differences are not significant. The spread of HIST hindcasts is slightly lower than the RMSE with respect to the NUDG simulation, suggesting that the potential non-initialized forecast system is overconfident (underdispersive). This feature is worse for the initialized system (Fig. 1c). This lack of reliability is reduced in the DEC9 system (Fig. 1f) for which the RMSE is reduced. We recall that DEC9 differs from DEC3 in terms of start dates frequency and ensemble size. Figure 2 shows that the reduction of the RMSE in DEC9 does not arise from a decrease in the start date frequency. It is thus due to the increase in the number of members which indeed is expected to yield a better estimate of RMSE through a more accurate estimation of the ensemble mean. Nevertheless, Fig. 2 also shows that a reduction of the start date frequency yields more noisy and therefore less robust statistics, which can lead to spurious results. The RMSE of DEC3 is larger than that of HIST, whatever the reference set (Fig. 1c). This feature is reduced in DEC9, probably as a result of the better estimation of the RMSE. Still, this result is relatively surprising, given the expected added value from initialization to correct part of the errors in the unforced model response and put the model in phase with the unforced variability, thereby decreasing the RMSE similarly for DEC3 and DEC9. These differences are nevertheless not significant, and this feature disappears for other regions investigated below.

Figure 3 shows the potential ACC skill score of the HIST and DEC3 ensembles computed grid-pointwise for detrended SST for the lead times 1, 2–5 and 6–9 years. The added-value of initialization for the first lead time is clearly illustrated on the top panel: for a lead time of 1 year, SST is skillfully predicted over all oceanic regions in the initialized hindcasts. For longer lead times, fewer regions remain skillfully predicted in the initialized runs. The subpolar North Atlantic, the extratropical North Pacific, the northern Indian Ocean and the western tropical Pacific, as well

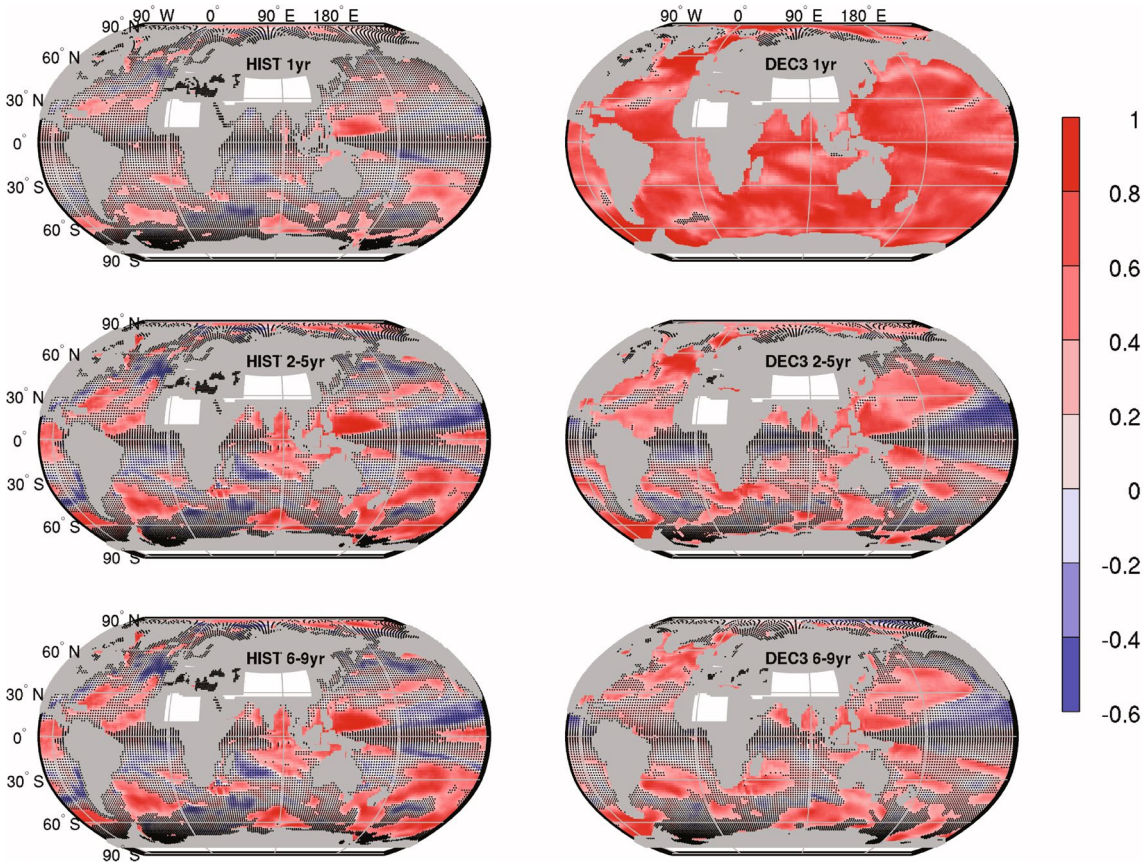

Fig. 3 Ensemble mean ACC of detrended SST in the HIST (*left*) and DEC3 (*right*) hindcasts against the NUDG simulation, for a lead time of 1 year (*top*), 2–5 years (*middle*) and 6–9 years (*bottom*). Non-significant correlations at the 90 % confidence level are marked with *black dots*

as localized areas of the Southern Ocean stand out. In the CCSM4 experimental decadal prediction system, Karspeck et al. (2014) found that the subpolar North Atlantic was the only region where the initialized predictions outperform the non-initialized ones. The maps shown here are a bit more encouraging, but they only show potential skill. Note that the maps computed against ERSST rather than NUDG are very similar (not shown). In the following, we focus on specific regions and discuss both the potential and actual prediction skill, including uncertainty arising from observational datasets.

3.2 Tropical SST prediction skill

In the tropical band, forecasting skill is investigated using individual forecast years, instead of multi-year averages. Both potential and actual SST predictions are skillful for the first lead time only (Fig. 4b). The non-initialized ensemble, on the other hand, is never significantly skillful (ACC is always negative), indicating that the prediction skill at 1 year lead time has been enabled by the initialization of the coupled model. For this first lead time, RMSE of DEC3 is smaller (but not significantly) than that of HIST, further highlighting the impact of initialization. This effect is lost for longer forecast ranges, with the spread of DEC3 reaching the level of HIST. All statistics (both actual and potential) thus nicely highlight a prediction skill of 1 year over the tropical band, thanks to the better initial conditions, an effect that is lost afterwards. Actual and potential ACC skills also loose significance after the first lead time, but the decrease is more gradual in DEC9, this may be due to sampling effects. Furthermore, DEC9 is roughly reliable for the first two lead times. As above, a subsampling analysis of the start dates frequency in DEC3 shows that these improvements of DEC9 performances over DEC3 comes from the increase in the number of members (not shown). However, for lead times longer than 3 years, the evolution of skills with the lead time in DEC9 is, again, very noisy. This ACC recovery at lead time 7 years in DEC9 (Fig. 4e) gives another illustration of possible spurious predictions and conclusions when too few start dates are used. Another sampling impact is noticeable in the RMSE of DEC9 with two peaks at lead time 4 and 9 years, separated by the start date frequency of 5 years (Fig. 4f).

Further analysis shows that skill at lead time 1 is also found when considering the tropical Atlantic or the tropical Pacific separately (Fig. 3 right). In the tropical Pacific, the skill of year 1 in this region is consistent with the literature: in theory, ENSO is believed to be predictable on the order of 1 or 2 years in advance because of the self-sustained nature of the tropical Pacific coupled ocean-atmosphere system (e.g. Neelin et al. 1998). In practice, however, this predictability is reduced because of the influence of stochastic atmospheric forcings, such as surface wind bursts in the western equatorial Pacific (e.g. Kleeman and Moore 1997; Perigaud and Cassou 2000; Fedorov et al. 2003). Thus, ENSO predictability is usually limited to a few months, reaching 2 years only in some specific studies (Luo

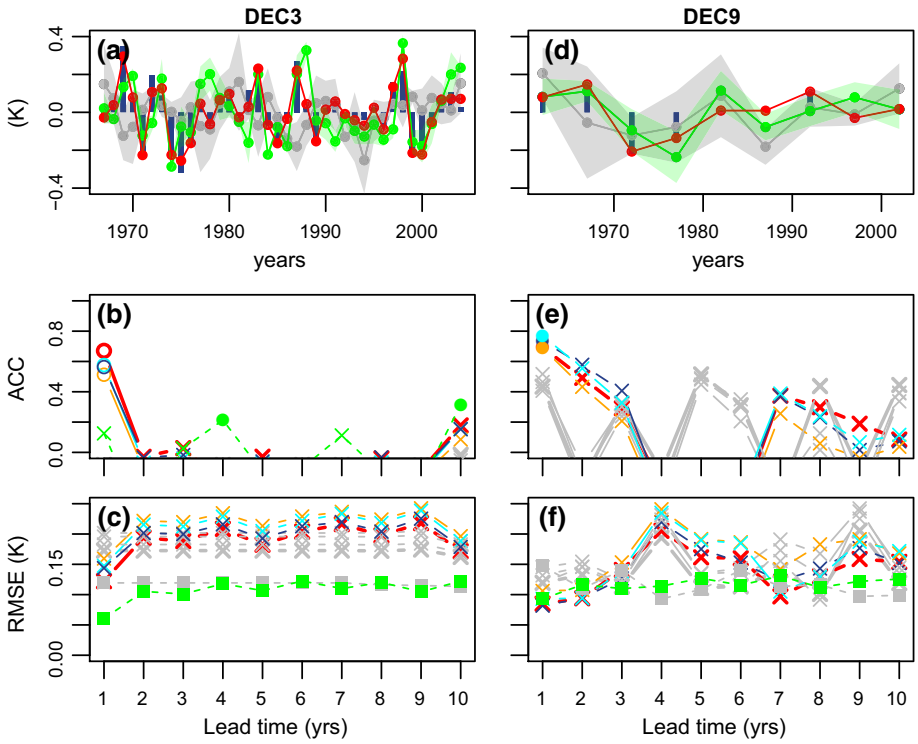

Fig. 4 Same as Fig. 1 for SST averaged over the region (20°S–20°N). In the *upper panels*, HIST and DEC time series are considered for a lead time of 1 year. In the *middle* and *bottom panels*, *note* that the forecast ranges are not 4-year averaged

et al. 2008; Volpi et al. 2013). This general result seems to hold for our specific forecast system.

4 Prediction skill in the North Atlantic Ocean

As indicated above, the North Atlantic Ocean is often found to be the most predictable region of the world's ocean when compared to non-initialized predictions (e.g. Hazeleger et al. 2013b; Corti et al. 2012; Kim et al. 2012; Oldenborgh et al. 2012; Doblas-Reyes et al. 2013). We focus first on the North Atlantic variability, by looking at the linearly detrended SST average over the Atlantic region (0°–60°N) (Fig. 5). Note that this index slightly differs from the canonical definition of Atlantic Multidecadal Oscillation (AMO, e.g Sutton and Hodson 2005) as it is not low pass filtered. It is only computed using a 4-year running mean, as forecast ranges of 4 years are considered. It is used here to characterize the Atlantic Multidecadal Variability (AMV). The variability in HIST is strongly dominated by the model's bidecadal variability described in Escudier et al. (2013) and Ortega et al. (2015b). This internal variability is partly phased by external forcings, as shown in Swingedouw et al. (2013, 2015). However, according to these studies, the Mt Agung eruption (1963) induces a phasing of the AMOC (see below) only 15 years later and thus of the North Atlantic SSTs after about 20 years, i.e. from the mid-1980s. This phasing can indeed be seen around the end of the period in Fig. 5a and is confirmed by a positive correlation between the North Atlantic SST from HIST and from ERSST for the period [1987–2005] (not shown). Before this, the variability in HIST is strong and completely un-phased with data.

Both potential and actual prediction skill are significant for all forecast ranges for DEC3, contrary to HIST (Fig. 5b). The statistical prediction based on an AR1 process is also significantly correlated with the NUDG, but only for the forecast range 1–4 years, which is consistent with previous findings showing that dynamical predictions out-perform statistical predictions based on persistence over large parts of North Atlantic for longer lead times (e.g. Ho et al. 2012). This suggests that the additional skill potentially coming from ocean dynamics, beyond the thermal inertia, is noticeable after about 1–4 years ahead (e.g. Matei et al. 2012). We also note that ACC computed against NUDG is generally slightly higher than the ones computed against DATA, in particular for shortest forecast ranges, and it shows a skill decrease with forecast time. The degradation in the North Atlantic SST multi-year skill is even more clearly seen in DEC9, and it has also been found in recent studies using start dates every 5 years, in particular with the ENSEMBLES decadal re-forecasts ensemble (Oldenborgh et al. 2012; García-Serrano and Doblas-Reyes 2012) and the CMIP5 ensemble (Kim et al. 2012). This is less obvious from yearly start dates, but it was reported in

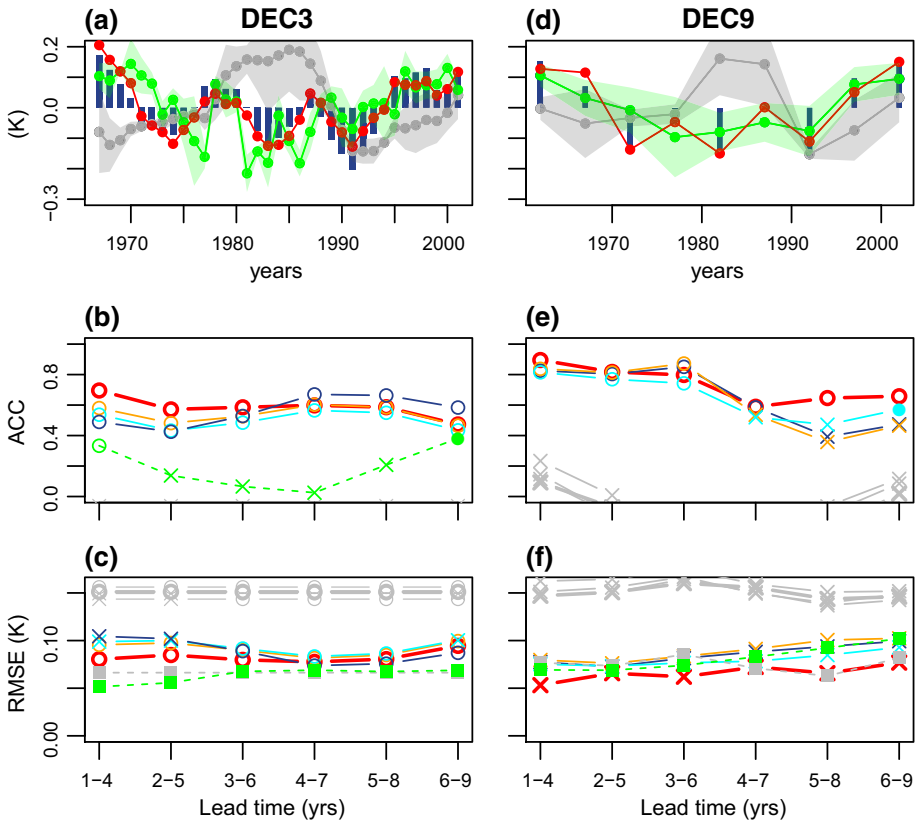

Fig. 5 Same as Fig. 1 for SST averaged over the region (0°–60°N) in the Atlantic

the DePreSys system by García-Serrano et al. (2012). In DEC9, significance of actual skill is lost at forecast ranges longer than 4–7 years.

As for ACC (Fig. 5b), RMSE of the initialized hindcasts (with respect to the NUDG simulation) is significantly smaller than for the non-initialized ones for all forecast ranges (Fig. 5c). The difference is no longer significant when RMSE is computed against all other datasets, except for ORAS4. This can indicate a weak impact of initialization or a weak signal to noise ratio. In DEC9, RMSE is reduced as compared to DEC3, but given the reduced degrees of freedom, it is not significantly different from that of HIST, even when assessed against NUDG (Fig. 5f). Furthermore, as above, while DEC3 is strongly overconfident (underdispersive), DEC9 is a more reliable prediction system thanks to the increased number of members.

Figure 6 compares the prediction skill of SST anomalies in the North Atlantic midlatitude (30°–60°N) and low-latitude (0°–30°N) regions respectively. As for the total North Atlantic SST variability, correlation with the NUDG simulation is significant at all lead times for the extratropical North Atlantic, both in DEC3 (Fig. 6b) and in DEC9 (not shown). Furthermore, the correlation skill score with NUDG is almost constant for all forecast ranges, as in Fig. 5. On the contrary, for the low-latitude part, the potential skill score is significant and significantly different from non-initialized hindcasts only until the forecast range 2–5 to 3–6 years in DEC3 (Fig. 6d and in DEC9, not shown). As discussed in García-Serrano et al. (2012), this finding illustrates that the added-value from initialization in the AMV skill during the second half of the hindcast is likely dominated by midlatitudes in the SST area average. The skill of the AR1 model is also very different in the two regions: while it is pretty skillful at midlatitudes, it does not provide any skillful information at lower latitudes. This suggests that the long prediction skill at midlatitudes is linked to the long persistence of SST anomalies. It is consistent with the observed autocorrelation functions shown for the two regions in García-Serrano et al. (2012). This difference between low and mid-latitudes skill as a function for short and long forecast ranges can be carried over to actual prediction skill in DEC3, although details in the significance of ACC depend on the dataset and forecast range that is considered for verification. On the contrary, ACC significance decays with forecast time at lower latitudes. The picture is consistent but more noisy in DEC9, in particular in the northern region (not shown).

Figure 7a, b shows the correlation maps of the observed SST averaged over the northern Atlantic (0°–60°N) with SST anomalies in observations and NUDG. All time series have been averaged over four consecutive years prior to computing the correlation. These maps compare the representation of the observed variability averaged over the

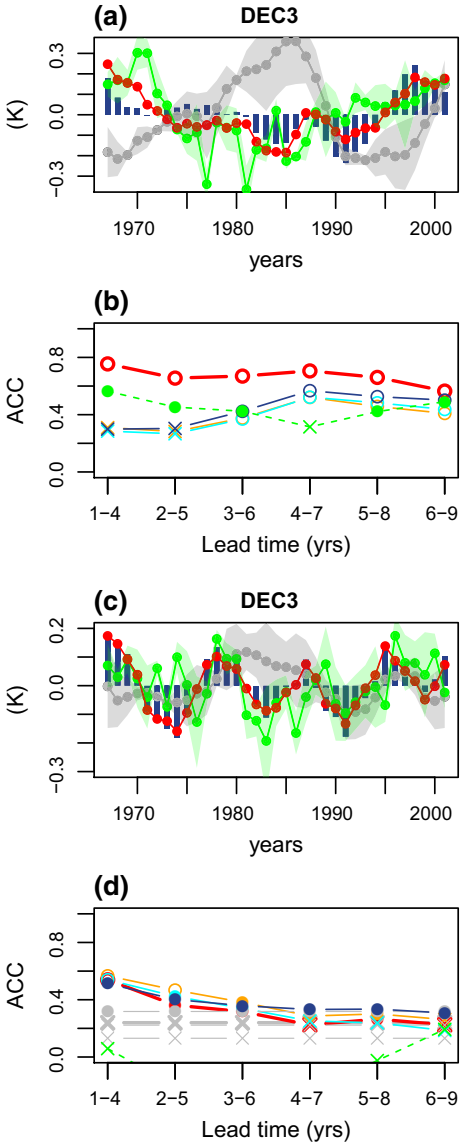

Fig. 6 Same as Fig. 1a, b for SST averaged over the mid latitudes (30°–60°N) (**a** and **b**) and low latitude (0°–30°N) (**c** and **d**) in the Atlantic

North Atlantic in the nudged simulation and in the observations. The patterns are both well significant over the whole North Atlantic, except primarily along the Gulf Stream path, similarly to what is found in other studies (e.g. Marini 2013). The pattern in the bottom panel (Fig. 7c) is different with observations and NUDG: in the non-initialized simulations (HIST), correlation against the AMV variability is only significant equatorward of 15°N and in the western subtropical part of the North Atlantic. This suggests that SST variability in the extratropical North Atlantic mainly relies on the internal variability rather than the response to radiative forcing Comparing Fig. 7b, c shows the nudging efficiency to bring North Atlantic variability

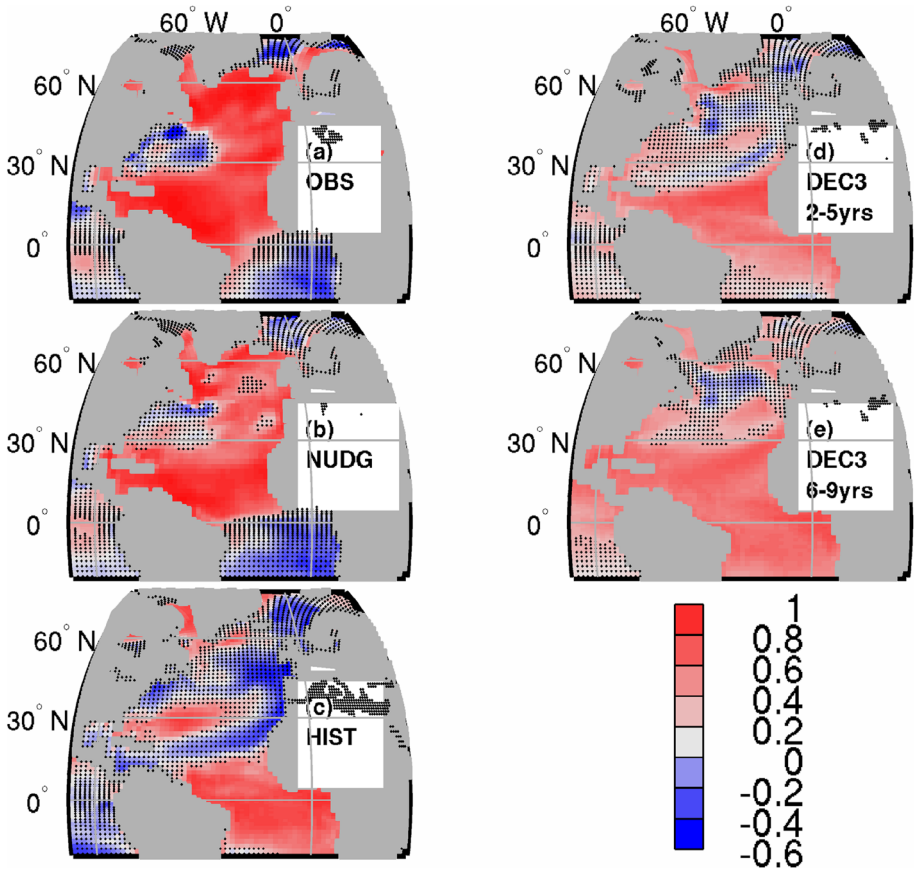

Fig. 7 Correlation of observed ERSST time series averaged between 0° and 60°N in the Atlantic against the SST field in **a** ERSST, **b**–**c** NUDG and HIST respectively, **d**, **e** DEC3 at forecast range 2–5 and 6–9 years respectively. All SST fields are linearly detrended and considered as averages over 4 consecutive years. Non-significant correlations at the 90 % level are marked with the *black dots*

close to observations. Nevertheless, at subpolar latitudes, the NUDG pattern shows non significant areas, unlike what is found in ERSST (Fig. 7a, b). These areas are quite small, but they indicate that locally, the nudging is not always sufficiently strong with respect to the model's deficiencies and internal variability to constrain the SST anomalies. As previous studies have suggested that this area is crucial for predictability in the north and tropical Atlantic (e.g. Dunstone et al. 2011), this may explain the lack of actual predictability in our model. Specific reasons for this poor constraining of SST in this region is probably linked to the strong internal variability of this area in the model Escudier et al. (2013), Ortega et al. (2015a) and/or a particular sensitivity to external radiative forcing as in other CMIP5 models (e.g. García-Serrano et al. 2014). The correlation of the predicted SST at forecast range 2–5 years with the observed North Atlantic variability (Fig. 7d) largely resembles the one found for HIST (panel c): it is hardly significant in the extratropical North Atlantic and the significant domain extends only slightly poleward as compared to HIST. In other words, the nudging works correctly in the North Atlantic but it yields a gain of predictability only between 15° and 30°N in the North Atlantic. It does not constrain sufficiently the subpolar SSTs. At the forecast range 6–9 years (Fig. 7e), though, areas of significant correlation in the northern and eastern subpolar Atlantic emerge. This is consistent with enhanced actual predictability seen in Fig. 6b. This cannot be due to external forcing in the model, as the structure in HIST is very different. Oceanic dynamics is a plausible explanation, as it may bring the DEC structure closer to the one of NUDG in spite of a lack of predictability in the subpolar North Atlantic. Predictability gained thanks to oceanic dynamics in the North Atlantic has already been invoked by previous studies (e.g. Matei et al. 2012). Another candidate is the effect of the initialization in correcting the model's response to external forcing, identified as one of the premises of decadal climate prediction (Meehl et al. 2014), and its persistence along the hindcast period (Fig. 6b). In IPSL-CM5-LR probably both effects are at play.

Given the impact of the AMOC on the North Atlantic temperatures (e.g. Knight et al. 2005), we also attempt to evaluate its prediction skill. The major limitation for this assessment is the poor consistency of reanalyses in terms of AMOC variability (Reichler et al. 2012; Pohlmann et al. 2013). As an illustration, the time series of the maximum of the AMOC at 48°N from the ORAS4 and SODA reanalyses have a correlation coefficient of 0.24 over the common period (1961–2012), and 0.25 at 26°N. Both values are significant at the 90 % level (1-sided) but explain only

6% of the covariance. Correlation for the absolute maximum in latitude is close to 0. Swingedouw et al. (2015) have evidenced the influence of the volcanic forcing on the timing of bi-decadal variability in the North Atlantic in data and simulations. In particular, volcanic eruptions were found to induce an acceleration of the AMOC with a delay of roughly 15 years after the eruption. Swingedouw et al. (2013) showed that the SST nudging still plays an important role, as they translate the role of atmospheric forcing such as the persistent NAO events in the 1980s and 1990s. This might explain the slightly delayed AMOC maximum around the end of the 1990s in NUDG as compared to HIST (Fig. 8a, b), but this effect is weaker in the present analysis than in Swingedouw et al. (2013) as only one realization of NUDG is used here.

Figure 8 shows that our system has no skill in predicting the AMOC reconstructed by either of these reanalyses. By contrast, potential predictability as measured using ACC is significant at all lead times (Fig. 8b), in agreement with the long AMOC internal predictability (Persechino et al. 2013). Although these values start higher than for the non-initialized hindcasts at the first two forecast ranges, the difference is not significant. The same conclusion holds for the RMSE although initialization has also helped to reduce the spread of the initialized hindcasts.

In order to better understand the impact of the initialization on the North Atlantic ocean and its predictability, we investigate the predictability of vertically averaged ocean heat content in DEC3 (Fig. 9). In the North Atlantic midlatitudes, there is practically no actual skill for the heat content integrated down to 300 m or below which is consistent with the lack of actual SST skill in the same region (Figs. 6b, 7d, e). The potential skill is significant for all forecast ranges. It is higher than the skill obtained for non-initialized hindcasts until the forecast range 2–5 years, but the difference is not significant. As for the AMOC, the ocean heat content is found to be strongly impacted by the model's internal variability, characterized by a 20 year time scale.

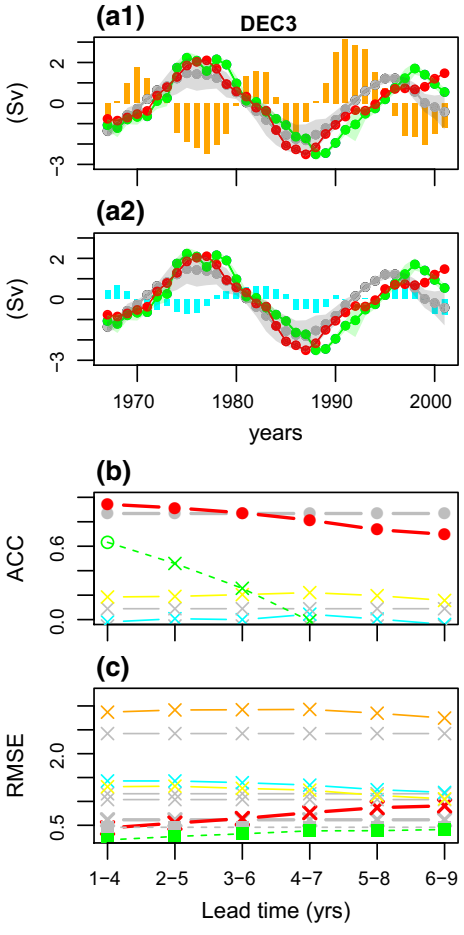

Fig. 8 Same as Fig. 1 for the AMOC maximum at 48°N verified against ORAS4 (**a1**) and SODA (**a2**). The *yellow line* on panel **b** and **c** shows the skill scores (ACC and RMSE) of the AMOC computed against the reconstruction proposed by Latif et al. (2006), using a dipole of SST between the Northern and Southern Atlantic

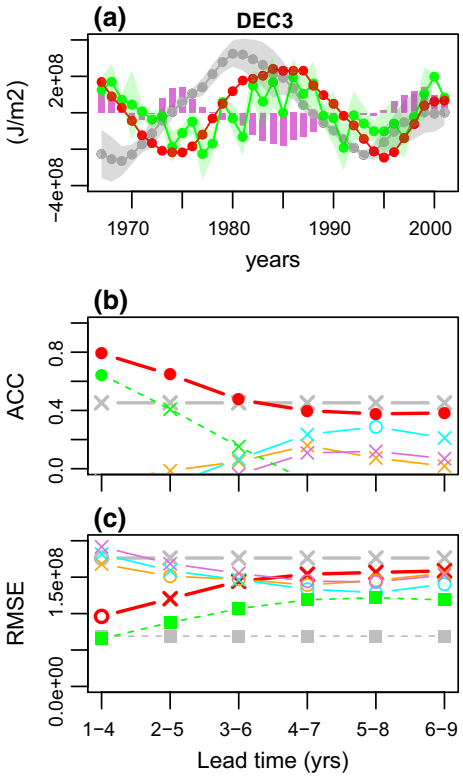

Fig. 9 Same as Fig. 1 for the oceanic heat content integrated down to 300 m and averaged over the North Atlantic sub polar region (30°–60°N). The *purple bars* in panel (**a**) and *purple lines* in panel (**b**) and (**c**) correspond to the heat content computed from the EN3 dataset

5 Prediction skill in the North Pacific Ocean

Prediction skill of the tropical Pacific was discussed in Sect. 3.2. The northern Pacific Ocean is usually one of the regions with the lowest actual skill in near-term temperature forecasting (Guemas et al. 2012; Kim et al. 2012; Branstator and Teng 2012; Bellucci et al. 2013), although hints of improved predictability in the North Pacific temperatures by initialization have been found by Mochizuki et al. (2010), Chikamoto et al. (2013) and Magnusson et al. (2012). After a trend analysis, Bellucci et al. (2014) suggest that the poor skill in the extra-tropical North Pacific reflects the inability of the models to correctly reproduce the observed ratio between forced and unforced variability in this region, where the warming trend only explains a small fraction of the total variability. Figure 3 nevertheless reveals potential prediction skill in our system in the North Pacific midlatitudes. One can identify three skilful regions in the North Pacific in our model, at lead-time 2–5 years (middle right panel): Firstly, a skilful region is found between 5° and 15°N in the western Pacific, which also appears in HIST, thereby suggesting that it is associated to external forcing. A second skilful region is found between 15° and 30°N in the western to central Pacific. This region is not skilful in HIST. Thus it has been positively affected by the initialization. It looses skill at lead time 6–9 years (Fig. 3 bottom right). Consistently, ACC for SST averaged over the low latitudes (0°–30°N) in the Pacific is only significant when computed against NUDG (potential predictability), and only over the forecast range 1–4 years (not shown). This is less than what was described for the tropical to subtropical North Atlantic above. As discussed previously, this is due to the dominant influence of ENSO in the Pacific, poorly predictable beyond 1 year, while the tropical Atlantic benefits from the influence of subpolar latitudes and cross-equatorial heat transport by the AMOC. Finally, the maps also show a skilful region between 30° and 45°N extending almost through the whole Pacific basin, which is still significantly correlated with NUDG at forecast range 6–9 years, while no skill is found in HIST. This region bears similarity with the skilful region highlighted in Kim et al. (2012, 2014), Doblas-Reyes et al. (2013). Figure 10 confirms that in our system, the potential skill averaged over the northern extratropical Pacific from 30° to 45°N is significant for all forecast ranges and significantly different from the skill obtained for non-initialized hindcasts. Interestingly, actual prediction skill is also significant for all lead times so that although scores are slightly lower, actual prediction skill practically equals potential skill in this region. Furthermore, the actual skill is at least as good as for the Atlantic (Figs. 5b, 6b). Note that the shape of the ACC evolution with increasing forecast ranges 1–4 years,

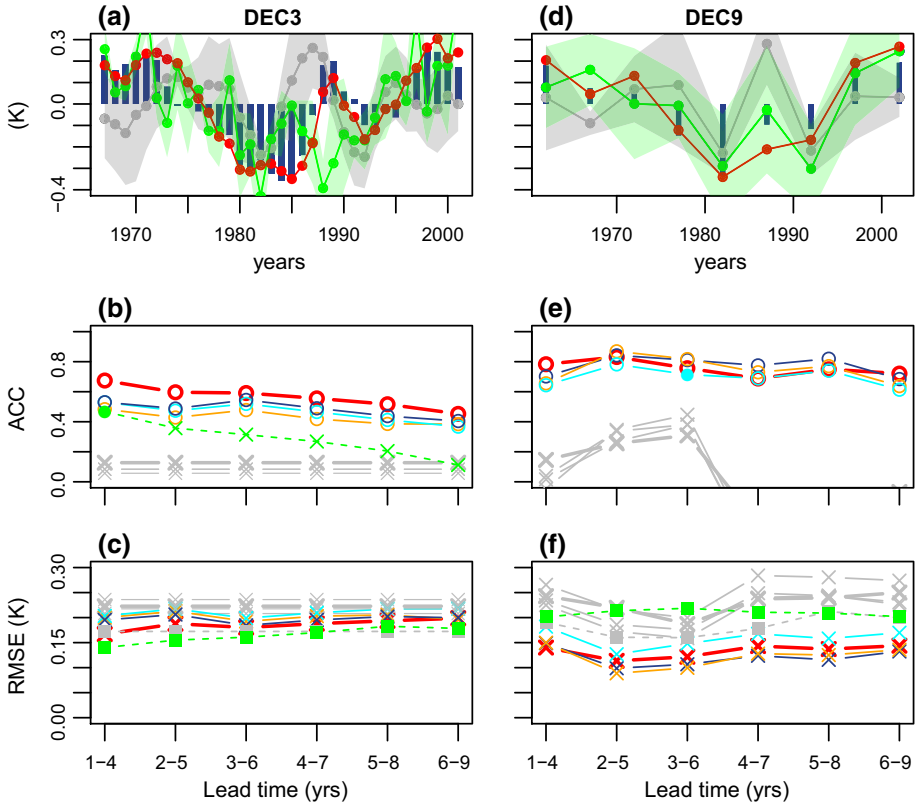

Fig. 10 Same as Fig. 1 for SST averaged over the region (30°–45°N) in the Pacific

as computed against NUDG and DATA contrasts with the skill of the statistical AR1 process. The latter yields a significant correlation only for the shortest forecast range, and it decreases quickly afterwards. This suggests a role of the oceanic circulation on this predictability beyond thermal inertia. RMSE of DEC3 is not significantly different from HIST, and neither is the spread (Fig. 10c). In general, DEC3 appears to be reliable, with the ensemble mean RSME matching the ensemble spread, while DEC9 can be rather considered as overdispersive.

The correlation between SST averaged over this region (30°–45°N) and the first empirical orthogonal function of annual mean SSTs between 20° and 75°N amounts to −0.94 (significant at the 95 % level, not shown) in the control simulation. This indicates that the SST average shown in Fig.10 can be taken as a measure of the negative phase of the Pacific Decadal Oscillation (PDO) in IPSL-CM5A-LR, in a manner similar to the definition in Mantua et al. (1997). Fig. 11 shows that in observations, SSTs averaged in the area also project on the typical PDO pattern (a), and that this is well represented in NUDG (b). However, the spatial pattern associated in the model with the observed variations of SST in the North Pacific (30°–45°N), Fig. 11c) is not a PDO-like pattern. It rather bears similarity with the second least damped mode of North Pacific SST variability found by Newman et al 2007. The predicted pattern related to the observed time series (d and e) captures some of the positive anomalies in the central North Pacific, but not in the latitude band between 30° and 45°N. Furthermore, the predicted pattern is positive in the whole subtropics, near the eastern coast and in the north. This also resembles the second least-damped mode of North Pacific SST variability found by Newman (2007), except for the tropical and eastern subtropical part. Newman (2007, 2013) suggested that the observed PDO represents the sum of several stochastic phenomena rather than a single physical process, and they showed that long term predictability in the North Pacific is primarily due to the second least-damped mode. The fact that the observed PDO time series projects onto this mode in the historical simulation may explain the relatively long predictability in the North Pacific found in the model. The North Pacific climate has experienced several climate shifts over the past decades, in particular in 1976/1977 (e.g. Trenberth and Hurrell 1994; Mantua et al. 1997; Deser et al. 2004; Yeh et al. 2011), in 1988/89 (Hare and Mantua 2000; Trenberth and Hurrell 1994) and in 1998/99 (Minobe 2000; Di Lorenzo et al. 2008; Ding et al. 2013). In the context of the PDO being represented by the sum of several stochastic processes, Newman (2007) explain that these shifts may only be predictable within the timescale of the most rapidly decorrelating noise, i.e. around 2 years. The ERSST curve in Fig. 10a shows how these shifts translate in terms of SST averaged of the North Pacific midlatitudes. The three transitions are reasonably reproduced in the NUDG simulation, and the 1976 and the 1998 ones are reasonably predicted 2–5 years in advance. This may again be explained by the

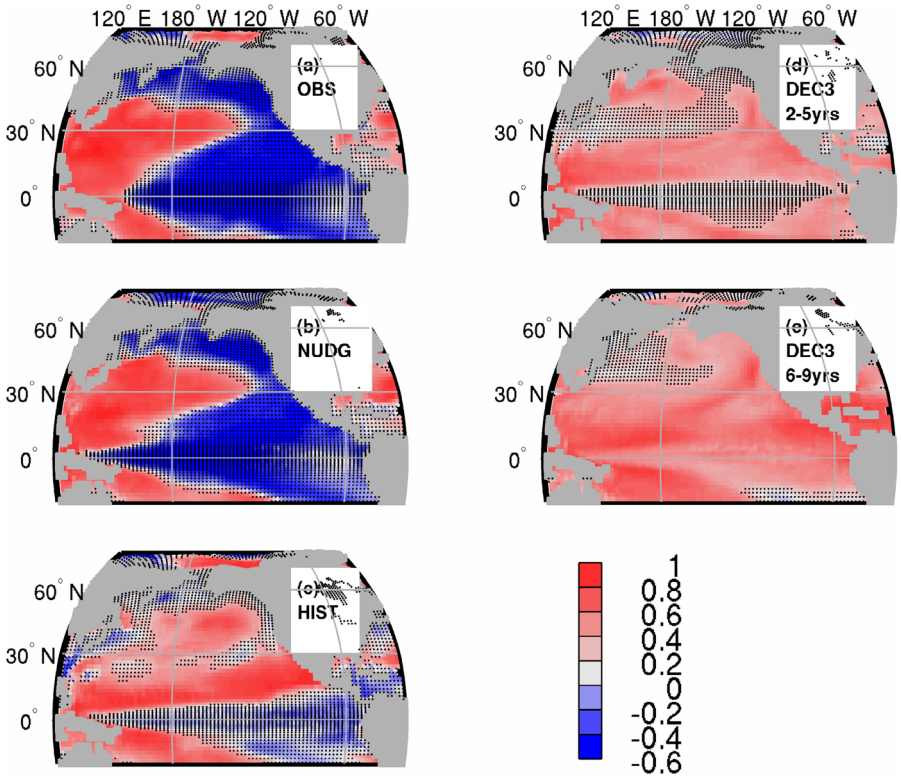

Fig. 11 Correlation of observed ERSST time series averaged between 30° and 45°N in the Pacific against the SST field in **a** ERSST, **b**, **c** NUDG and HIST respectively, **d**, **e** DEC3 at forecast range 2–5 and 6–9 years respectively. All SST fields are linearly detrended and considered as averages over 4 consecutive years. Non-significant correlations at the 90 % level are marked with the *black dots*

dominance in the model of one specific mechanism for the PDO, as opposed to what is found in Newman (2007). The late 1980's event is rather well predicted with a 1 year lead time (not shown), while it is missed with at a 2–5 years forecast range. Note also that in the model, SST average between 30° and 45° in the Pacific is strongly correlated with the SSTs in the North Atlantic low-latitudes (r = 0.45, significant at the 95 % level, not shown). Although this statistical link is not realistic [see for example Marini (2013)], it may also explain the relatively long predictive skill detected in the North Pacific in our model.

We turn now to the investigation of the OHC, a key variable for ocean memory and thus predictability. Ocean heat content integrated down to 300 m over the extratropical Pacific shows surprisingly good potential prediction skill, as compared to literature (Fig. 12). Initialized predictions are potentially skillful for all forecast ranges, and ACC measured against SODA (i.e. actual skill) is significant and significantly different from non-initialized hindcasts up to the forecast range of 5–8 years. For ORAS4 and EN3, ACC is in general significant as well, although not significantly different from the skill obtained in HIST. Time series for the forecast range 2–5 years (Fig. 12a) confirm the relatively good reconstruction of the ocean heat content variability in NUDG with respect to EN3. These performances are overall striking and good and contrast with the general idea that decadal predictability over the North Pacific is quite low. Nevertheless, Chikamoto et al. (2013) reported prediction skill over almost a decade for subsurface temperatures in the North Pacific, which is in agreement with our actual skill assessment. The potential predictability of our system suggests that even longer skillful forecasts might be achieved in the future. Interestingly, once again, the AR1 statistical model yields significant prediction skill for lead times 1–4 years, but the ACC drops rapidly as forecast times increases. This clearly suggests a role of ocean processes for the long predictability detected in ocean heat content in IPSL-CM5A-LR.

6 Results on salinity

In a perfect model framework, Servonnat et al. (2014) showed a good ability of SST nudging in reconstructing SSS variability in the tropics. It is therefore interesting to evaluate the prediction skill of this variable in the same region for our set of experiments (Fig. 13). Note however that given the lack of long-term satellite measurements, SSS reconstructions and reanalysis are subject to much higher uncertainty than temperature, so that actual

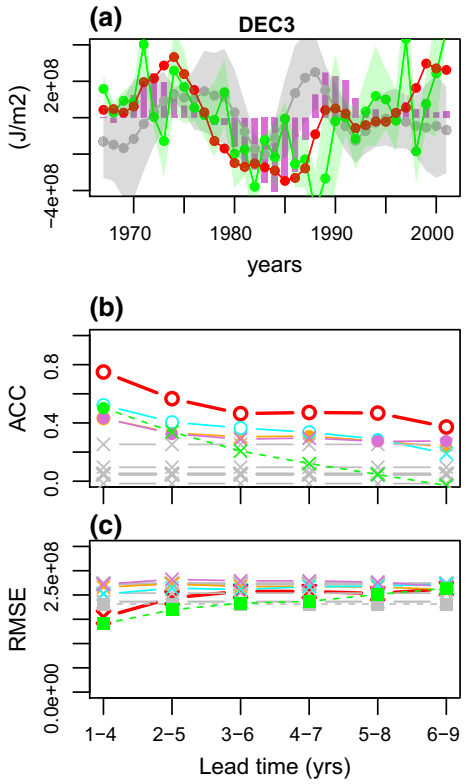

Fig. 12 Same as Fig. 9 averaged over the Pacific extratropical region (30°–45°N)

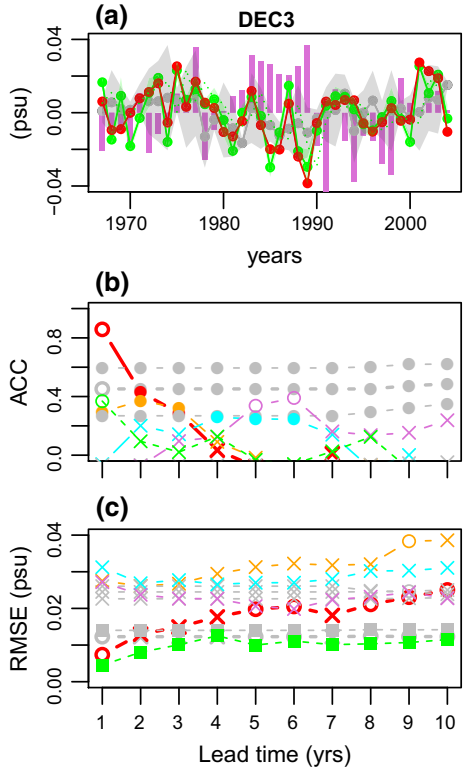

Fig. 13 Same as Fig. 4 (*left*), but for the SSS [average over the latitude band (20°S–20°N)]. The *purple bars* in panel (**a**) and *purple lines* in panel (**b**) and (**c**) are from EN3 dataset

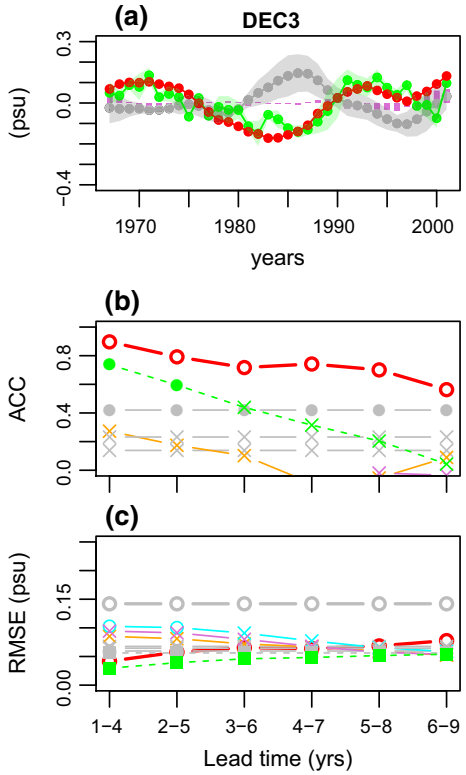

Fig. 14 Same as Fig. 1 for SSS averaged over the region (30°–60°N) in the Atlantic

prediction skill (or the lack of) has to be interpreted with care. Potential prediction skill of SSS over the tropical band (20°S–20°N) is significant for the first three forecast years, but both ACC and RMSE are significantly different in DEC3 and HIST only the first year. SSS has thus been impacted by the nudging in the Tropics, as described in (Servonnat et al. 2014) and given its relatively longer persistence than SST (e.g. Mignot and Frankignoul 2003), it is potentially predictable over relatively longer forecast ranges too. The AR1 model yields potential skill for 1-year lead time. In terms of actual prediction skill, ACC is low but significant only when computed against ORAS4. NUDG is indeed significantly correlated with ORAS4 at the 90 % confidence level ($r = 0.70$), suggesting that SSS has been reconstructed with some agreement as compared to ORAS4. Note that these results primarily come from the tropical Pacific, while potential skill is only significant for the first two lead times in the tropical Atlantic. Séférian et al. (2014) found similar results in the tropical Pacific for the nutrient primary productivity.

We now examine the prediction skill, both potential and actual, of the SSS in the North Atlantic (30°–60°N) (Fig. 14). As indicated by the weak correlation between NUDG and the DATA (Table 2, top), SSS has not been properly reconstructed in these regions as compared to reanalysis. SSS typical variability in all simulations is much stronger than in the DATA (Table 2, top, first column), probably as a result of the strong bi-decadal variability in this region in the model. Nevertheless, SSS has been influenced by the nudging, as correlations between HIST and NUDG are also very weak. Note that the same applies to SST (Fig. 6a). In the North Atlantic, the resulting SSS variability both in the NUDG and DEC3 time series is strongly

Table 2 Correlation between SSS time series in different regions in the reanalysis (ORAS4 and SODA respectively), and the HIST, NUDG and DEC3 time series computed from the model simulations as described in the text at the forecast range 2–5 years

Atlantic - [30°N-60°N]	std (psu)	EN3	ORAS4	SODA	HIST	NUDG	DEC3	SST
EN3 / ERSST	0.025	1	0.05	**0.77**	0.23	0.08	-0.27	0.35
ORAS4	0.028	-	1	0.17	0.14	0.10	0.17	-0.34
SODA	0.032	-	-	1	0.42	-0.20	-0.47	0.19
HIST	0.065	-	-	-	1	-0.57	-0.66	**0.80**
NUDG	0.094	-	-	-	-	1	**0.79**	**0.64**
DEC3	0.081	-	-	-	-	-	1	**0.69**
Pacific - [30°N-45°N]	std (psu)	EN3	ORAS4	SODA	HIST	NUDG	DEC3	SST
EN3 / ERSST	0.016	1	**0.72**	**0.60**	0.32	0.27	0.29	-0.10
ORAS4	0.027	-	1	**0.86**	0.36	0.26	0.32	0.06
SODA	0.019	-	-	1	0.23	0.14	0.14	0.44
HIST	0.016	-	-	-	1	0.24	-0.12	-0.02
NUDG	0.022	-	-	-	-	1	0.51	0.06
DEC3	0.022	-	-	-	-	-	1	0.42

The last column gives the correlation between the SSS and the SST time series for dataset separately. Significant correlation at the 90 % level with a two-sided student test have been highlighted in bold

correlated with the corresponding SST. It was also the case in the non-initialized runs HIST. This strong link between SST and SSS in the North Atlantic in this model has been extensively described in Escudier et al. (2013). The correlation of SST and SSS in the NUDG shows that SST nudging has strongly impacted the SSS through the 20-yr cycle. Significant skill score and correlation of the DEC3 time series of SST and SSS for the forecast range 2–5 years shows that this phasing in the NUDG carries on in the hindcasts and yields potential predictability for the SSS in the northern North Atlantic. Given the role of SSS anomalies for deep convection and the AMOC, this type of mechanism for SSS predictability is encouraging for AMOC predictability. Unfortunately, actual prediction skill is not significant. Nevertheless, since SSS is not properly constrained in this region in data and reanalysis, large uncertainties remain concerning large-scale SSS observation products. Reasons for these discrepancies are beyond the scope of the present study.

In the model, SSS and SST are not as tightly linked in the North Pacific as in the North Atlantic. Nevertheless, the salinity is also affected by the nudging, as seen from the weak correlations between HIST and NUDG time series (Table 2). The high (although not significant at the 90 % confidence level) correlation between NUDG and DEC3 can thus be attributed to the SSS internal persistence, with makes it potentially predictable in the model.

7 Conclusions

Two decadal prediction ensembles, based on hindcasts performed with the same model and the same simple initialization strategy have been analyzed. The initialization consists of surface nudging to ERSST anomalies, with a relatively weak nudging strength, namely $40\,W.m^{-2}.K^{-1}$. The first ensemble consists of 3 members of hindcasts launched every year between 1961 and 2013. The second ensemble consists of 9 members launched every 5 years between 1961 and 2006. The focus of this study has been on assessing multi-year prediction skill of the ocean in these two decadal prediction ensembles.

The first important outcome of this study is precisely the difficulty to assess the actual skill, because of data uncertainty. For SST, ACC and RMSE measured from one observational dataset (ERSST) and two reanalysis (ORAS4 and SODA) led in general to similar conclusions in terms of predictability horizon, but with different values for the ACC and the RMSE. For the salinity and the ocean heat content, EN3, ORAS4 and SODA could also lead to different predictability horizons. For the AMOC, the three reconstructions considered here were found to be very weakly correlated. Understanding the reasons for these particularities are beyond the scope of this study. We suggest nevertheless that forthcoming assessments of decadal predictions should be performed against several -at least more than one -datasets, as a measure of the uncertainty of the data.

A second major conclusion is the importance of increasing the number of members and start dates in decadal prediction systems. This idea is not new (e.g. Kirtman et al. 2013) and in the literature, the issue of the small size of ensembles has been overcome by using multi-model ensembles (e.g. Oldenborgh et al. 2012; Bellucci et al. 2014). We showed here that 3 members are usually not enough to estimate consistently the ensemble mean, and thus yield biased estimates of the RMSE. Increasing the ensemble size to 9 members helps in reducing this problem. It leads to overall more reliable predictions, as the ensemble mean is more accurately estimated, so that the RMSE is reduced and it becomes comparable to the spread. Probabilistic skill scores yield similar conclusions (not shown), although the estimation of a probability density function with 9 members could only be tested with a start date interval of 5 years (DEC9) and should be considered with care. Increasing the number of start dates also appeared crucial in order to obtain robust prediction skill scores. With only 8 or 9 start dates to verify against, prediction scores are very noisy and thus poorly trustworthy. The major influence of non-linear effects of external forcing as well as background decadal variability has been illustrated.

A third particularity of the present study as compared to previously published evaluations of decadal prediction systems is the parallel assessment of both potential and actual prediction skill. Computing skill scores against observations and reanalysis datasets is of course crucial for practical applications. From a technical point of view, this is also important in order to evaluate the efficiency of the initialization strategy. However, from a pure scientific point of view, potential prediction skill gives a robust insight in the maximum predictive horizon which can be expected for a particular forecast system, thereby suggesting possible mechanisms responsible for the predictability, and areas where specific efforts on measurement systems and/or model improvements should be made. In the case of DEC3, particularly long potential prediction skill has been found for the AMOC, the upper 300m ocean heat content and the SSS in the North Atlantic, and could be interpreted in terms of the internal mode variability of the IPSL-CM5A-LR model. Even if this does not translate in terms of actual skill it gives hope for future systems using more efficient initialization techniques, and provides physical explanation for predictive skill.

For linearly detrended SST, both potential and actual prediction skill is of the order of 10 years at the global scale, and this is essentially due to the non-linear response to external forcing. Regionally, the horizon of the potential skill is 1 year in the tropical band, 10 years at mid latitudes in the North

Atlantic and in the North Pacific and 5 years at low latitudes in the North Atlantic. These results are generally consistent with previously published single and multi-models analysis, even yielding longer predictability in the North Pacific midlatitudes. This is a particularly important result given the relatively simple initialization strategy used here, namely a weak nudging to observed SST anomalies. This score may come from the model's specific spatial pattern associated to the observed SST variability in the North Pacific, and/or spurious correlation between SST variability in the North Atlantic and North Pacific. Regarding the North Atlantic, we have shown that the nudging helps phasing the SST but in hindcast mode, it is not strong enough to constrain it with respect to the strong internal variability of the model. Few studies analyzed in detail the prediction skill of integrated ocean heat content in such systems. Here, we find surprisingly high actual skill for this variable in the extratropical North Pacific. Over the North Atlantic, it has no actual skill, and neither does the AMOC, but we also underlined very strong discrepancies among the different datasets for this variable, illustrating the difficulties to observe or reconstruct this large-scale feature. The particularly long prediction skill obtained in surface and subsurface over the extratropical North Pacific will deserve a dedicated future study.

Surface SST nudging also proved relatively efficient to induce significant potential predictability of sea surface salinity in the tropics for about 3 years, which is longer than the prediction skill on SST. In the extratropical North Atlantic, our analysis also showed distinctive behavior resulting from a dominant internal mode of variability at the 20-year timescale in our model. SST nudging indeed exerts a strong influence on SSS, which induces a strong phasing of this variable in the nudged simulation. This leads to a surprisingly long potential predictability of SSS in the extratropical North Atlantic. Comparison with other systems should be performed in order to better understand the robustness and the reasons for this result. Although the mechanism is encouraging, this effect did not induce significant actual skill for SSS. Given promising results regarding the realism of this 20-year timescale in the North Atlantic (e.g. Swingedouw et al. 2015), next steps on the path of investigating the performance of surface initialization will consist of testing SSS and surface wind stress initialization. Data uncertainty is presently a strong limitation regarding the use of SSS for decadal prediction initial conditions but hope may come from recent satellite missions.

Acknowledgments This work was supported by the EU project SPECS funded by the European Commissions Seventh Framework Research Program (FP7) under the Grant agreement 308378. J.G.-S. was supported by the FP7-funded NACLIM (ENV-308299) project. Computations were carried out at the CCRT-TGCC supercomputing centre. We are grateful to both reviewers for their constructive comments which helped improved the manuscript.

References

Aumont O, Bopp L (2006) Globalizing results from ocean in situ iron fertilization studies. Glob Biogeochem Cycles. doi:10.1029/2005GB002591

Balmaseda MA, Mogensen K, Weaver AT (2013) Evaluation of the ECMWF ocean reanalysis system ORAS4. Q J R Meteorol Soc 139(674):1132–1161. doi:10.1002/qj.2063

Batté L, Déqué M (2012) A stochastic method for improving seasonal predictions. Geophys Res Lett. doi:10.1029/2012GL051406

Bellucci A, Gualdi S, Masina S, Storto A, Scoccimarro E, Cagnazzo C, Fogli P, Manzini E, Navarra A (2013) Decadal climate predictions with a coupled OAGCM initialized with oceanic reanalyses. Clim Dyn 40(5–6):1483–1497. doi:10.1007/s00382-012-1468-z

Bellucci A, Haarsma R, Gualdi S, Athanasiadis PJ, Caian M, Cassou C, Fernandez E, Germe A, Jungclaus J, Kröger J, Matei D, Müller W, Pohlmann H,Salas y Melia D, Sanchez E, Smith D, Terray L, Wyser K, Yang S,(2014) An assessment of a multimodel ensemble of decadal climate predictions. Clim Dyn. doi:10.1007/s00382-014-2164-y

Boer GJ, Kharin VV, Merryfield WJ (2013) Decadal predictability and forecast skill. Clim Dyn 41(7–8):1817–1833. doi:10.1007/s00382-013-1705-0

Bombardi RJ, Zhu J, Marx L, Huang B, Chen H, Lu J, Krishnamurthy L, Krishnamurthy V, Colfescu I, Kinter JL, Kumar A, Hu ZZ, Moorthi S, Tripp P, Wu X, Schneider EK (2014) Evaluation of the CFSv2 CMIP5 decadal predictions. Clim Dyn. doi:10.1007/s00382-014-2360-9

Branstator G, Teng H (2010) Two limits of initial-value decadal predictability in a CGCM. J Clim 23:6292–6311. doi:10.1175/2010JCLI3678.1

Branstator G, Teng H (2012) Potential impact of initialization on decadal predictions as assessed for CMIP5 models. Geophys Res Lett. doi:10.1029/2012GL051974

Bretherton CS, Widmann M, Dymnikov VP, Wallace JM, Bladé I (1999) The effective number of spatial degrees of freedom of a time-varying field. J Clim 12(7):1990–2009. doi:10.1175/1520-0442(1999)012<1990:TENOSD>2.0.CO;2

Chikamoto Y, Kimoto M, Ishii M, Mochizuki T, Sakamoto TT, Tatebe H, Komuro Y, Watanabe M, Nozawa T, Shiogama H, Mori M, Yasunaka S, Imada Y (2013) An overview of decadal climate predictability in a multi-model ensemble by climate model MIROC. Clim Dyn 40(5–6):1201–1222. doi:10.1007/s00382-012-1351-y

Collins M, Knutti R, Dufresne JL, Fichefet T, Friedlingstein P, Gao X, Gutowski WJ, Johns T, Krinner G, Shongwe M, Tebaldi C, Weaver AJ, Wehner M (2014) Climate change 2013: the physical science basis. Contribution of working group I to the fifth assessment report of the intergovernmental panel on climate change. In: Stocker T, Qin D, Plattner GK, Tignor M, Allen S, Boschung J, Nauels A, Xia Y, Bex Y, Midgley VP (eds) Long-term climate change: projections, commitments and irreversibility. Cambridge University Press, Cambridge, New York

Corti S, Weisheimer A, Palmer TN, Doblas-Reyes FJ, Magnusson L (2012) Reliability of decadal predictions. Geophys Res Lett. doi:10.1029/2012GL053354

Deser C, Phillips AAS, Hurrell JWJ (2004) Pacific interdecadal climate variability: Linkages between the tropics and the North Pacific during boreal winter since 1900. J Clim 17(16):3109–3124. doi:10.1175/1520-0442(2004)017<3109:PICVLB>2.0.CO;2

Di Lorenzo E, Schneider N, Cobb KM, Franks PJS, Chhak K, Miller AJ, McWilliams JC, Bograd SJ, Arango H, Curchitser E, Powell TM, Rivière P (2008) North Pacific Gyre Oscillation

links ocean climate and ecosystem change. Geophys Res Lett 35(8):L08,607. doi:10.1029/2007GL032838

Ding H, Greatbatch RJ, Latif M, Park W, Gerdes R (2013) Hindcast of the 1976/77 and 1998/99 Climate Shifts in the Pacific. J Clim 26(19):7650–7661. doi:10.1175/JCLI-D-12-00626.1

Doblas-Reyes FJ, Andreu-Burillo I, Chikamoto Y, García-Serrano J, Guemas V, Kimoto M, Mochizuki T, Rodrigues LRL, van Oldenborgh GJ (2013) Initialized near-term regional climate change prediction. Nat Commun 4:1715. doi:10.1038/ncomms2704

Du H, Doblas-Reyes FJ, García-Serrano J, Guemas V, Soufflet Y, Wouters B (2012) Sensitivity of decadal predictions to the initial atmospheric and oceanic perturbations. Clim Dyn 39(7–8):2013–2023. doi:10.1007/s00382-011-1285-9

Dufresne JL, Ma Foujols, Denvil S, Caubel A, Marti O, Aumont O, Balkanski Y, Bekki S, Bellenger H, Benshila R, Bony S, Bopp L, Braconnot P, Brockmann P, Cadule P, Cheruy F, Codron F, Cozic A, Cugnet D, Noblet N, Duvel JP, Ethé C, Fairhead L, Fichefet T, Flavoni S, Friedlingstein P, Grandpeix JY, Guez L, Guilyardi E, Hauglustaine D, Hourdin F, Idelkadi A, Ghattas J, Joussaume S, Kageyama M, Krinner G, Labetoulle S, Lahellec A, Lefebvre MP, Lefevre F, Levy C, Li ZX, Lloyd J, Lott F, Madec G, Mancip M, Marchand M, Masson S, Meurdesoif Y, Mignot J, Musat I, Parouty S, Polcher J, Rio C, Schulz M, Swingedouw D, Szopa S, Talandier C, Terray P, Viovy N, Vuichard N (2013) Climate change projections using the IPSL-CM5 Earth System Model: from CMIP3 to CMIP5. Clim Dyn 40(9–10):2123–2165. doi:10.1007/s00382-012-1636-1

Dunstone NJ, Smith DM (2010) Impact of atmosphere and sub-surface ocean data on decadal climate prediction. Geophys Res Lett. doi:10.1029/2009GL041609

Dunstone NJ, Smith DM, Eade R (2011) Multi-year predictability of the tropical Atlantic atmosphere driven by the high latitude North Atlantic Ocean. Geophys Res Lett. doi:10.1029/2011GL047949

Escudier R, Mignot J, Swingedouw D (2013) A 20-year coupled ocean–sea ice–atmosphere variability mode in the North Atlantic in an AOGCM. Clim Dyn. doi:10.1007/s00382-012-1402-4

Fedorov AV, Harper SL, Philander SG, Winter B, Wittenberg A (2003) How predictable is El Niño? Bull Am Meteorol Soc 84(7):911–919. doi:10.1175/BAMS-84-7-911

Ferro CAT (2014) Fair scores for ensemble forecasts. Q J R Meteorol Soc 140(683):1917–1923. doi:10.1002/qj.2270

Fichefet T, Maqueda MAM (1997) Sensitivity of a global sea ice model to the treatment of ice thermodynamics and dynamics. J Geophys Res 102:12609–612646. doi:10.1029/97JC00480

Frankignoul C, Kestenare E (2002) The surface heat flux feedback. Part I: estimates from observations in the Atlantic and the North Pacific. Clim Dyn 19(8):633–647. doi:10.1007/s00382-002-0252-x

García-Serrano J, Doblas-Reyes FJ (2012) On the assessment of near-surface global temperature and North Atlantic multi-decadal variability in the ENSEMBLES decadal hindcast. Clim Dyn 39(7–8):2025–2040. doi:10.1007/s00382-012-1413-1

García-Serrano J, Doblas-Reyes FJ, Coehlo CAS (2012) Understanding Atlantic multi-decadal variability prediction skill. Geophys Res Lett. doi:10.1029/2012GL053283

García-Serrano J, Guemas V, Doblas-Reyes FJ (2014) Added-value from initialization in predictions of Atlantic multi-decadal variability. Clim Dyn. doi:10.1007/s00382-014-2370-7

Germe A, Chevallier M, Salas y, Mélia D, Sanchez-Gomez E, Cassou C (2014) Interannual predictability of Arctic sea ice in a global climate model: regional contrasts and temporal evolution. Clim Dyn 43(9–10):2519–2538. doi:10.1007/s00382-014-2071-2

Giese BS, Ray S (2011) El Niño variability in simple ocean data assimilation (SODA), 1871 2008. J Geophys Res 116(C2):C02,024. doi:10.1029/2010JC006695

Goddard L,Kumar a, Solomon a, Smith D, Boer G, Gonzalez P, Kharin V, Merryfield W, Deser C, Mason SJ, Kirtman BP, Msadek R, Sutton R, Hawkins E, Fricker T, Hegerl G, Ferro CaT, Stephenson DB, Meehl Ga, Stockdale T, Burgman R, Greene aM, Kushnir Y, Newman M, Carton J, Fukumori I, Delworth T (2012) A verification framework for interannual-to-decadal predictions experiments. Clim Dyn. doi:10.1007/s00382-012-1481-2

Guemas V, Doblas-Reyes FJ, Lienert F, Soufflet Y, Du H (2012) Identifying the causes of the poor decadal climate prediction skill over the North Pacific. J Geophys Res: Atmos. doi:10.1029/2012JD018004

Hare SR, Mantua NJ (2000) Empirical evidence for North Pacific regime shifts in 1977 and 1989. Prog Oceanogr 47(2–4):103–145. doi:10.1016/S0079-6611(00)00033-1

Hazeleger W, Guemas V, Wouters B, Corti S, Andreu-Burillo I, Doblas-Reyes FJ, Wyser K, Caian M (2013a) Multiyear climate predictions using two initialization strategies. Geophys Res Lett 40(9):1794–1798. doi:10.1002/grl.50355

Hazeleger W, Wouters B, van Oldenborgh GJ, Corti S, Palmer T, Smith D, Dunstone N, Kröger J, Pohlmann H, von Storch JS (2013b) Predicting multiyear North Atlantic Ocean variability. J Geophys Res: Oceans 118(3):1087–1098. doi:10.1002/jgrc.20117

Ho CK, Hawkins E, Shaffrey L, Underwood FM (2012) Statistical decadal predictions for sea surface temperatures: a benchmark for dynamical GCM predictions. Clim Dyn 41(3–4):917–935. doi:10.1007/s00382-012-1531-9

Ho CK, Hawkins E, Shaffrey L, Bröcker J, Hermanson L, Murphy JM, Smith DM, Eade R (2013) Examining reliability of seasonal to decadal sea surface temperature forecasts: the role of ensemble dispersion. Geophys Res Lett 40(21):5770–5775. doi:10.1002/2013GL057630

Hourdin F, Foujols MA, Codron F (2013) Impact of the LMDZ atmospheric grid configuration on the climate and sensitivity of the IPSL-CM5A coupled model. Clim Dyn 40(9–10):2167–2192. doi:10.1007/s00382-012-1411-3

Ingleby B, Huddleston M (2007) Quality control of ocean temperature and salinity profiles historical and real-time data. J Mar Syst 65(1–4):158–175. doi:10.1016/j.jmarsys.2005.11.019

Ja Carton, Giese BS (2008) A reanalysis of ocean climate using simple ocean data assimilation (SODA). Mon Weather Rev 136(8):2999–3017. doi:10.1175/2007MWR1978.1

Karspeck A, Yeager S, Danabasoglu G, Teng H (2014) An evaluation of experimental decadal predictions using CCSM4. Clim Dyn. doi:10.1007/s00382-014-2212-7

Keenlyside N, Latif M, Jungclaus J (2008) Advancing decadal-scale climate prediction in the North Atlantic sector. Nature 453:1–5. doi:10.1038/nature06921

Kim HM, Webster PJ, Curry JA (2012) Evaluation of short-term climate change prediction in multi-model CMIP5 decadal hindcasts. Geophys Res Lett. doi:10.1029/2012GL051644

Kim HM, Ham YG, Scaife Aa (2014) Improvement of Initialized Decadal Predictions over the North Pacific Ocean by Systematic Anomaly Pattern Correction. Journal of Climate p 140416111812004, doi:10.1175/JCLI-D-13-00519.1

Kirtman B, Power S, Adedoyin J, Boer G, Bojariu R, Camilloni I, Doblas-Reyes F, Fiore A, Kimoto M, Meehl G, Prather M, Sarr A, Schär C, Sutton R, van Oldenborgh G, Vecchi G, Wang H, Schär C, van Oldenborgh G (2013) Near-term Climate Change: Projections and Predictability. In: Stocker T, D Qin GK, Plattner M, Tignor S, Allen J, Boschung A, Nauels Y, Xia Y, Bex P, Midgley V (eds) Climate Change 2013: The Physical Science Basis. Contribution of Working Group I to the Fifth Assessment Report of the Intergovernmental Panel on Climate Change, Cambridge University Press, Cambridge, United Kingdom and New York, NY, USA, chap 11, pp 953–1028

Kleeman R, Moore AM (1997) A theory for the limitation of ENSO predictability due to stochastic atmospheric transients. J Atmos Sci 54(6):753–767. doi:10.1175/1520-0469(1997)054<0753:ATFTLO>2.0.CO;2

Knight JR, Allan RJ, Folland CK, Vellinga M, Mann ME (2005) A signature of persistent natural thermohaline circulation cycles in observed climate. Geophys Res Lett 32(20):L20,708. doi:10.1029/2005GL024233

Kumar A, Wang H, Xue Y, Wang W (2014) How much of monthly subsurface temperature variability in the equatorial Pacific can be recovered by the specification of sea surface temperatures? J Clim 27(4):1559–1577. doi:10.1175/JCLI-D-13-00258.1

Latif M, Böning C, Willebrand J (2006) Is the thermohaline circulation changing? J Clim 19:4631–4637. doi:10.1175/JCLI3876.1

Lozier MS, Leadbetter S, Williams RG, Roussenov V, Reed MSC, Moore NJ (2008) The spatial pattern and mechanisms of heat-content change in the North Atlantic. Science 319(5864):800–3. doi:10.1126/science.1146436

Luo J, Masson S, Behera S (2005) Seasonal climate predictability in a coupled OAGCM using a different approach for ensemble forecasts. J Clim 18:4474–4497. doi:10.1175/JCLI3526.1

Luo JJ, Masson S, Behera SK, Yamagata T (2008) Extended ENSO predictions using a fully coupled ocean–atmosphere model. J Clim 21(1):84–93. doi:10.1175/2007JCLI1412.1

Madec G (2008) NEMO ocean engine. Tech. Rep. 27, Institut Pierre Simon Laplace

Magnusson L, Alonso-Balmaseda M, Corti S, Molteni F, Stockdale T (2012) Evaluation of forecast strategies for seasonal and decadal forecasts in presence of systematic model errors. Clim Dyn 41(9–10):2393–2409. doi:10.1007/s00382-012-1599-2

Mantua NJ, Hare SR, Zhang Y, Wallace JM, Francis RC (1997) A Pacific interdecadal climate oscillation with impacts on Salmon production. Bull Am Meteorol Soc 78(6):1069–1079. doi:10.1175/1520-0477(1997)078<1069:APICOW>2.0.CO;2

Marini C, Frankignoul C (2013) An attempt to deconstruct the Atlantic Multidecadal Oscillation. Clim Dyn 3–4:607–625. doi:10.1007/s00382-013-1852-3

Matei D, Pohlmann H, Jungclaus J, Müller W, Haak H, Marotzke J (2012) Two tales of initializing decadal climate prediction experiments with the ECHAM5/MPI-OM model. J Clim 25(24):8502–8523. doi:10.1175/JCLI-D-11-00633.1

Meehl G, Teng H (2012) Case studies for initialized decadal hindcasts and predictions for the Pacific region. Geophys Res Lett. doi:10.1029/2012GL053423

Meehl G, Hu A, Tebaldi C (2010) Decadal prediction in the Pacific region. J Clim 23:2259–2973. doi:10.1175/2010JCLI3296.1

Meehl GA, Goddard L, Boer G, Burgman R, Branstator G, Cassou C, Corti S, Danabasoglu G, Doblas-Reyes F, Hawkins E, Karspeck A, Kimoto M, Kumar A, Matei D, Mignot J, Msadek R, Navarra A, Pohlmann H, Rienecker M, Rosati T, Schneider E, Smith D, Sutton R, Teng H, van Oldenborgh GJ, Vecchi G, Yeager S (2014) Decadal climate prediction: an update from the Trenches. Bull Am Meteorol Soc 95(2):243–267. doi:10.1175/BAMS-D-12-00241.1

Mehta VM, Wang H, Mendoza K (2013) Decadal predictability of tropical basin average and global average sea surface temperatures in CMIP5 experiments with the HadCM3, GFDL-CM2.1, NCAR-CCSM4, and MIROC5 global Earth System Models. Geophys Res Lett 40(11):2807–2812. doi:10.1002/grl.50236

Merryfield WJ, Lee W, Boer GJ, Kharin VV, Pal B, Scinocca JF, Flato GM (2010) The first coupled historical forecasting project (CHFP1). Atmos Ocean 48(4):263–283. doi:10.3137/AO1008.2010

Mignot J, Frankignoul C (2003) On the interannual variability of surface salinity in the Atlantic. Clim Dyn 20:555–565. doi:10.1007/s00382-002-0294-0

Mignot J, Swingedouw D, Deshayes J, Marti O, Talandier C, Séférian R, Lengaigne M, Madec G (2013) On the evolution of the oceanic component of the IPSL climate models from CMIP3 to CMIP5: A mean state comparison. Ocean Model 72:167–184. doi:10.1016/j.ocemod.2013.09.001

Minobe S (2000) Spatio-temporal structure of the pentadecadal variability over the North Pacific. Prog Oceanogr 47(2–4):381–408. doi:10.1016/S0079-6611(00)00042-2

Mochizuki T, Ishii M, Kimoto M, Chikamoto Y, Watanabe M, Nozawa T, Sakamoto TT, Shiogama H, Awaji T, Sugiura N, Toyoda T, Yasunaka S, Tatebe H, Mori M (2010) Pacific decadal oscillation hindcasts relevant to near-term climate prediction. Proc Nat Acad Sci USA 107(5):1833–1837. doi:10.1073/pnas.0906531107

Neelin JD, Battisti DS, Hirst AC, Jin FF, Wakata Y, Yamagata T, Zebiak SE (1998) ENSO theory. J Geophys Res 103(C7):14261. doi:10.1029/97JC03424

Newman M (2007) Interannual to decadal predictability of tropical and North Pacific sea surface temperatures. J Clim 20:2333–2356. doi:10.1175/JCLI4165.1

Newman M (2013) An empirical benchmark for decadal forecasts of global surface temperature anomalies. J Clim 26(14):5260–5269. doi:10.1175/JCLI-D-12-00590.1

van Oldenborgh GGJ, Doblas-Reyes FJF, Wouters B, Hazeleger W (2012) Decadal prediction skill in a multi-model ensemble. Clim Dyn 38(7–8):1263–1280. doi:10.1007/s00382-012-1313-4

Ortega P, Lehner F, Swingedouw D, Masson-Delmotte, Valerie Raible C, Casado M, Yiou P (2015a) A model-tested North Atlantic Oscillation reconstruction for the past millennium. Nature (in press)

Ortega P, Mignot J, Swingedouw D, Sévellec F, Guilyardi E (2015) Reconciling two alternative mechanisms behindbidecadal AMOC variability. Prog Oceanogr 137(A):237–249. doi:10.1016/j.pocean.2015.06.009

Perigaud CM, Cassou C (2000) Importance of oceanic decadal trends and westerly wind bursts for forecasting El Niño. Geophys Res Lett 27(3):389–392. doi:10.1029/1999GL010781

Persechino A, Mignot J, Swingedouw D (2013) Decadal predictability of the Atlantic meridional overturning circulation and climate in the IPSL-CM5A-LR model. Clim Dyn 40(9–10):2359–2380. doi:10.1007/s00382-012-1466-1

Pohlmann H, Smith DM, Ma Balmaseda, Keenlyside NS, Masina S, Matei D, Wa Müller, Rogel P (2013) Predictability of the mid-latitude Atlantic meridional overturning circulation in a multi-model system. Clim Dyn 41(3–4):775–785. doi:10.1007/s00382-013-1663-6

Ray S, Giese BS (2012) Historical changes in El Niño and La Niña characteristics in an ocean reanalysis. J Geophys Res 117(C11):C11,007. doi:10.1029/2012JC008031

Ray S, Swingedouw D, Mignot J, Guilyardi E (2015) Effect of surface restoring on subsurface variability in a climate model during 1949–2005. Clim Dyn 44(9–10):2333–2349. doi:10.1007/s00382-014-2358-3

Rayner NA (2003) Global analyses of sea surface temperature, sea ice, and night marine air temperature since the late nineteenth century. J Geophys Res 108(D14):4407. doi:10.1029/2002JD002670

Reichler T, Kim J, Manzini E, Kröger J (2012) A stratospheric connection to Atlantic climate variability. Nat Geosci 5(September):783–787. doi:10.1038/NGEO1586

Reynolds RW, Smith TM, Liu C, Chelton DB, Casey KS, Schlax MG (2007) Daily high-resolution-blended analyses for sea surface temperature. J Clim 20(22):5473–5496. doi:10.1175/2007JCLI1824.1

Robock A (2000) Volcanic eruptions and climate. Rev Geophys 38(1998):191–219. doi:10.1029/1998RG000054

Séférian R, Bopp L, Gehlen M, Swingedouw D, Mignot J, Guilyardi E, Servonnat J (2014) Multi-year prediction of Tropical Pacific Marine Productivity. PNAS 111(32):11646–11651. doi:10.1073/pnas.1315855111

Servonnat J, Mignot J, Guilyardi E, Swingedouw D, Séférian R, Labetoulle S (2014) Reconstructing the subsurface ocean decadal variability using surface nudging in a perfect model framework. Clim Dyn. doi:10.1007/s00382-014-2184-7

Smith DM, Aa Scaife, Boer GJ, Caian M, Doblas-Reyes FJ, Guemas V, Hawkins E, Hazeleger W, Hermanson L, Ho CK, Ishii M, Kharin V, Kimoto M, Kirtman B, Lean J, Matei D, Merryfield WJ, Wa Müller, Pohlmann H, Rosati A, Wouters B, Wyser K (2012) Real-time multi-model decadal climate predictions. Clim Dyn 41(11–12):2875–2888. doi:10.1007/s00382-012-1600-0

Smith DM, Eade R, Pohlmann H (2013) A comparison of full-field and anomaly initialization for seasonal to decadal climate prediction. Clim Dyn 41(11–12):3325–3338. doi:10.1007/s00382-013-1683-2

Sugiura N, Awaji T, Masuda S, Toyoda T, Igarashi H, Ishikawa Y, Ishii M, Kimoto M (2009) Potential for decadal predictability in the North Pacific region. Geophys Res Lett 36(20):L20,701. doi:10.1029/2009GL039787

Sutton RT, Hodson DLR (2005) Atlantic Ocean Forcing of North American and European Summer Climate. Science 309(5):115–118. doi:10.1126/science.110949616

Swingedouw D, Mignot J, Labetoulle S, Guilyardi E, Madec G (2013) Initialisation and predictability of the AMOC over the last 50 years in a climate model. Clim Dyn 40(9–10):2381–2399. doi:10.1007/s00382-012-1516-8

Swingedouw D, Ortega P, Mignot J, Guilyardi E, Masson-Delmotte V, Butler PG, Khodri M, Séférian R (2015) Bidecadal North Atlantic ocean circulation variability controlled by timing of volcanic eruptions. Nat Commun 6:6545. doi:10.1038/ncomms7545

Taylor KE, Stouffer RJ, Meehl GA (2012) An Overview of CMIP5 and the Experiment Design. Bull Am Meteorol Soc 93(4):485–498. doi:10.1175/BAMS-D-11-00094.1

Trenberth KE, Hurrell JW (1994) Decadal atmosphere-ocean variations in the Pacific. Clim Dyn 9(6):303–319. doi:10.1007/BF00204745

Vial J, Dufresne JL, Bony S (2013) On the interpretation of inter-model spread in CMIP5 climate sensitivity estimates. Clim Dyn 41(11–12):3339–3362. doi:10.1007/s00382-013-1725-9

Voldoire A, Claudon M, Caniaux G, Giordani H, Roehrig R (2014) Are atmospheric biases responsible for the tropical Atlantic SST biases in the CNRM-CM5 coupled model? Clim Dyn. doi:10.1007/s00382-013-2036-x

Volpi D, Doblas-Reyes FJ, García-Serrano J, Guemas V (2013) Dependence of the climate prediction skill on spatiotemporal scales: internal versus radiatively-forced contribution. Geophys Res Lett 40(12):3213–3219. doi:10.1002/grl.50557

Weisheimer A, Palmer TN, Doblas-Reyes FJ (2011) Assessment of representations of model uncertainty in monthly and seasonal forecast ensembles. Geophys Res Lett. doi:10.1029/2011GL048123

Yeager S, Karspeck A, Danabasoglu G, Tribbia J, Teng H (2012) A decadal prediction case study: late twentieth-century North Atlantic ocean heat content. J Clim 25(15):5173–5189. doi:10.1175/JCLI-D-11-00595.1

Yeh SW, Kang YJ, Noh Y, Miller AJ (2011) The North Pacific climate transitions of the winters of 1976/1977 and 1988/1989. J Clim 24(4):1170–1183. doi:10.1175/2010JCLI3325.1

Zhang R (2007) Anticorrelated multidecadal variations between surface and subsurface tropical North Atlantic. Geophys Res Lett 34(12):L12,713. doi:10.1029/2007GL030225

Zhang S, Rosati A, Delworth T (2010) The adequacy of observing systems in monitoring the Atlantic Meridional overturning circulation and North Atlantic climate. J Clim 23(19):5311–5324. doi:10.1175/2010JCLI3677.1

Bibliography

Ackerley, D., Booth, B. B. B., Knight, S. H. E., Highwood, E. J., Frame, D. J., Allen, M. R., and Rowell, D. P. 2011. Sensitivity of Twentieth-Century Sahel rainfall to sulfate aerosol and CO 2 forcing. *Journal of Climate*, 24(19):4999–5014. doi: 10.1175/JCLI-D-11-00019.1.

Alexander, M. and Penland, C. 1996. Variability in a mixed layer ocean model driven by stochastic atmospheric forcing. *Journal of Climate*, 9:2424–2442.

Anchukaitis, K. J., Buckley, B., Cook, E. R., Cook, B. I., D'Arrigo, R. D., and Ammann, C. M. 2010. Influence of volcanic eruptions on the climate of the Asian monsoon region. *Geophysical Research Letters*, 37(22):1–5. doi: 10.1029/2010GL044843.

Apaéstegui, J., Cruz, F. W., Sifeddine, A., Espinoza, J. C., Guyot, J. L., Khodri, M., Strikis, N., Santos, R. V., Cheng, H., Edwards, L., Carvalho, E., and Santini, W. 2014. Hydroclimate variability of the South American Monsoon System during the last 1600 yr inferred from speleothem isotope records of the north-eastern Andes foothills in Peru. *Climate of the Past Discussions*, 10(1):533–561. doi: 10.5194/cpd-10-533-2014.

Arzel, O., De Verdi??re, A. C., and Huck, T. 2007. On the origin of interdecadal oscillations in a coupled ocean-atmosphere model. *Tellus, Series A: Dynamic Meteorology and Oceanography*, 59(3): 367–383. doi: 10.1111/j.1600-0870.2007.00227.x.

Ba, J., Keenlyside, N. S., Latif, M., Park, W., Ding, H., Lohmann, K., Mignot, J., Menary, M., Otterå, O. H., Wouters, B., Salas y Melia, D., Oka, A., Bellucci, A., and Volodin, E. 2014. A multi-model comparison of Atlantic multidecadal variability. *Climate Dynamics*, 43(9-10):2333–2348. doi: 10.1007/s00382-014-2056-1.

Bacon, S. 1997. Circulation and Fluxes in the North Atlantic between Greenland and Ireland. *Journal of Physical Oceanography*, 27(7):1420–1435. doi: 10.1175/1520-0485(1997)027<1420:CAFITN>2.0.CO;2.

Bacon, S., Gould, W. J., and Jia, Y. 2003. Open-ocean convection in the Irminger Sea. *Geophysical Research Letters*, 30 (5)(1246).

Bader, J. and Latif, M. 2003. The impact of decadal-scale Indian Ocean sea surface temperature anomalies on Sahelian rainfall and the North Atlantic Oscillation. *Geophysical Research Letters*, 30 (22):1–4. doi: 10.1029/2003GL018426.

Baehr, J. and Piontek, R. 2014. Ensemble initialization of the oceanic component of a coupled model through bred vectors at seasonal-to-interannual timescales. *Geoscientific Model Development*, 7(1): 453–461. doi: 10.5194/gmd-7-453-2014.

Bakun, A. 1990. Global climate change and intensification of coastal ocean upwelling. *Science (New York, N.Y.)*, 247(4939):198–201. doi: 10.1126/science.247.4939.198.

Balaguru, K. *Barrier layers of the Atlantic Warm pool: formation mechanism and influence on weather and climate*. PhD thesis, Texas AM University, 2011.

Balmaseda, M. a., Smith, G. C., Haines, K., Anderson, D., Palmer, T. N., and Vidard, A. 2007. Historical reconstruction of the Atlantic Meridional Overturning Circulation from the ECMWF operational ocean reanalysis. *Geophysical Research Letters*, 34(23). doi: 10.1029/2007GL031645.

Balmaseda, M. A., Trenberth, K. E., and Källén, E. 2013. Distinctive climate signals in reanalysis of global ocean heat content. *Geophysical Research Letters*, 40(9):1754–1759. doi: 10.1002/grl.50382.

Bamber, J., van den Broeke, M., Ettema, J., Lenaerts, J., and Rignot, E. 2012. Recent large increases in freshwater fluxes from Greenland into the North Atlantic. *Geophysical Research Letters*, 39(19). doi: 10.1029/2012GL052552.

Barrier, N., Deshayes, J., Treguier, A.-M., and Cassou, C. 2015. Heat budget in the North Atlantic subpolar gyre: Impacts of atmospheric weather regimes on the 1995 warming event. *Progress in Oceanography*, 130:75–90. doi: 10.1016/j.pocean.2014.10.001.

Barton, E. D., Field, D. B., and Roy, C. 2013. Canary current upwelling: More or less? *Progress in Oceanography*, 116:167–178. doi: 10.1016/j.pocean.2013.07.007.

Belkin, I. M. 2004. Propagation of the "Great Salinity Anomaly" of the 1990s around the northern North Atlantic. *Geophysical Research Letters*, 31(8):L08306. doi: 10.1029/2003GL019334.

Belkin, I. M., Levitus, S., Antonov, J., and Malmberg, S.-A. 1998. "Great Salinity Anomalies" in the North Atlantic. *Progress in Oceanography*, 41(1):1–68. doi: 10.1016/S0079-6611(98)00015-9.

Bengtsson, L. 2010. The global atmospheric water cycle. *Environmental Research Letters*, 5(2):025202. doi: 10.1088/1748-9326/5/2/025202.

Bersch, M. 2002. North Atlantic Oscillation-induced changes of the upper layer circulation in the northern North Atlantic Ocean. *Journal of Geophysical Research: Oceans*, 107:C10, 3156.

Bersch, M., Yashayaev, I., and Koltermann, K. P. 2007. Recent changes of the thermohaline circulation in the subpolar North Atlantic. *Ocean Dynamics*, 57(3):223–235. doi: 10.1007/s10236-007-0104-7.

Bingham, R. J., Hughes, C. W., Roussenov, V., and Williams, R. G. 2007. Meridional coherence of the North Atlantic meridional overturning circulation. *Geophysical Research Letters*, 34(23). doi: 10.1029/2007GL031731.

Blaker, A. T., Hirschi, J. J.-M., McCarthy, G., Sinha, B., Taws, S., Marsh, R., Coward, A., and de Cuevas, B. 2014. Historical analogues of the recent extreme minima observed in the Atlantic meridional overturning circulation at 26Â°N. *Climate Dynamics*, 44(1-2):457–473. doi: 10.1007/s00382-014-2274-6.

Bombardi, R. J., Zhu, J., Marx, L., Huang, B., Chen, H., Lu, J., Krishnamurthy, L., Krishnamurthy, V., Colfescu, I., Kinter, J. L., Kumar, A., Hu, Z.-Z., Moorthi, S., Tripp, P., Wu, X., and Schneider, E. K. 2014. Evaluation of the CFSv2 CMIP5 decadal predictions. *Climate Dynamics*. doi: 10.1007/s00382-014-2360-9.

Bond, G., Heinrich, H., Broecker, W., Labeyrie, L., McManus, J., Andrews, J., Huon, S., Jantschik, R., Clasen, S., Simet, C., Tedesco, K., Klas, M., Bonani, G., and Ivy, S. 1992. Evidence for massive discharge of icebergs into the North Atlantic Ocean during the last glacial. *Nature*, 360:245–249.

Böning, C. W., Dieterich, C., and Barnier, B. 2001. Seasonal cycle of meridional heat transport in the subtropical North Atlantic: a model intercomparison in relation to observations near 25Â°N. *Progress in Oceanography*, 48(2-3):231–253. doi: 10.1016/S0079-6611(01)00006-4.

Böning, C. W., Scheinert, M., Dengg, J., Biastoch, A., and Funk, A. 2006. Decadal variability of subpolar gyre transport and its reverberation in the North Atlantic overturning. *Geophysical Research Letters*, 33(21):L21S01. doi: 10.1029/2006GL026906.

Born, A. and Mignot, J. 2012. Dynamics of decadal variability in the Atlantic subpolar gyre: A stochastically forced oscillator. *Climate Dynamics*, 39(1-2):461–474. doi: 10.1007/s00382-011-1180-4.

Born, A. and Stocker, T. F. 2014. Two Stable Equilibria of the Atlantic Subpolar Gyre. *Journal of Physical Oceanography*, 44(1):246–264. doi: 10.1175/JPO-D-13-073.1.

Born, A., Stocker, T. F., Raible, C. C., and Levermann, A. 2012. Is the Atlantic subpolar gyre bistable in comprehensive coupled climate models? *Climate Dynamics*, 40(11-12):2993–3007. doi: 10.1007/s00382-012-1525-7.

Born, A., Mignot, J., and Stocker, T. F. 2015. Multiple Equilibria as a Possible Mechanism for Decadal Variability in the North Atlantic Ocean. *Journal of Climate*, 28(22):8907–8922. doi: 10.1175/JCLI-D-14-00813.1.

Bourassa, A. E., Robock, A., Randel, W. J., Deshler, T., Rieger, L. D., Lloyd, N. D., Llewellyn, E. J., and Degenstein, D. A. 2012. Large Volcanic Aerosol Load in the Stratosphere Linked to Asian Monsoon Transport. *Science*, 337(6090):78–81. doi: 10.1126/science.1219371.

Boutin, J., Martin, N., Kolodziejczyk, N., and Reverdin, G. 2016. Interannual anomalies of SMOS sea surface salinity. *Remote Sensing of Environment*, 180:128–136. doi: 10.1016/j.rse.2016.02.053.

Bower, A. S., Lozier, M. S., Gary, S. F., and Böning, C. W. 2009. Interior pathways of the North Atlantic meridional overturning circulation. *Nature*, 459(7244):243–7. doi: 10.1038/nature07979.

Boyer, T. P., Levitus, S., Antonov, J. I., Locarnini, R. A., and Garcia, H. E. 2005. Linear trends in salinity for the World Ocean, 1955-1998. *Geophysical Research Letters*, 32:L01604, doi:10.1029/2004GL021791. doi: 10.1029/2004GL021791.

Brad Adams, J., Mann, M. E., and Ammann, C. M. 2003. Proxy evidence for an El Niño-like response to volcanic forcing. *Nature*, 426(6964):274–8. doi: 10.1038/nature02101.

Brambilla, E. and Talley, L. D. 2006. Surface drifter exchange between the North Atlantic subtropical and subpolar gyres. *Journal of Geophysical Research*, 111(C7):C07026. doi: 10.1029/2005JC003146.

Branstator, G. and Teng, H. 2010. Two Limits of Initial-Value Decadal Predictability in a CGCM. *Journal of Climate*, 23:6292–6311. doi: 10.1175/2010JCLI3678.1.

Branstator, G. and Teng, H. 2012. Potential impact of initialization on decadal predictions as assessed for CMIP5 models. *Geophysical Research Letters*, 39(12). doi: 10.1029/2012GL051974.

Branstator, G., Teng, H., Meehl, G. a., Kimoto, M., Knight, J. R., Latif, M., and Rosati, a. 2012. Systematic Estimates of Initial-Value Decadal Predictability for Six AOGCMs. *Journal of Climate*, 25(6):1827–1846. doi: 10.1175/JCLI-D-11-00227.1.

Bretherton, C. S., Widmann, M., Dymnikov, V. P., Wallace, J. M., and Bladé, I. 1999. The Effective Number of Spatial Degrees of Freedom of a Time-Varying Field. *Journal of Climate*, 12(7):1990–2009. doi: 10.1175/1520-0442(1999)012<1990:TENOSD>2.0.CO;2.

Breugem, W., Chang, P., Jang, C. J., Mignot, J., and Hazeleger, W. 2008. Barrier layers and tropical Atlantic SST biases in coupled GCMs. *Tellus A*, 60(5):885–897. doi: 10.1111/j.1600-0870.2008.00343.x.

Brodeau, L., Barnier, B., Treguier, A.-M., Penduff, T., and Gulev, S. 2010. An ERA40-based atmospheric forcing for global ocean circulation models. *Ocean Modelling*, 31(3-4):88–104. doi: 10.1016/j.ocemod.2009.10.005.

Broecker, W. 1991. The great ocean conveyor. *Oceanography*, 4:79–89.

Camara, I., Kolodziejczyk, N., Mignot, J., Lazar, A., and Thierno-Gaye, A. 2015. On the seasonal variations of salinity of the tropical Atlantic mixed layer. *Journal of Geophysical Research: Oceans*. doi: 10.1002/2015JC010865.

Cassou, C. and Mignot, J. 2013. Enjeux, méthodes et fondamentaux de prévisibilité et prévision décennale. *La Météorologie*, 81(Mai):23–30.

Chang, C.-Y., Chiang, J. C. H., Wehner, M., Friedman, A. R., and Ruedy, R. 2011. Sulfate Aerosol Control of Tropical Atlantic Climate over the Twentieth Century. *Journal of Climate*, 24(10):2540–2555. doi: 10.1175/2010JCLI4065.1.

Chanut, J., Barnier, B., Large, W., Debreu, L., Penduff, T., Molines, J. M., and Mathiot, P. 2008. Mesoscale Eddies in the Labrador Sea and Their Contribution to Convection and Restratification. *Journal of Physical Oceanography*, 38(8):1617–1643. doi: 10.1175/2008JPO3485.1.

Cheng, W., Chiang, J. C. H., and Zhang, D. 2013. Atlantic Meridional Overturning Circulation (AMOC) in CMIP5 Models: RCP and Historical Simulations. *Journal of Climate*, 26(18):7187–7197. doi: 10.1175/JCLI-D-12-00496.1.

Chidichimo, M. P., Kanzow, T., Cunningham, S. A., Johns, W. E., and Marotzke, J. 2010. The contribution of eastern-boundary density variations to the Atlantic meridional overturning circulation at 26.5Â° N. *Ocean Science*, 6(2):475–490. doi: 10.5194/os-6-475-2010.

Church, J. A. and Others. Change in sea level. In Houghton, J. T. and Others, editors, *Climate Change 2001: the scientific basis. Contribution of working group I to the Third Assessment Report of the Intergouvernmental Panel on Climate Change*, pages 640–693. Cambridge University Press, 2001.

Chylek, P., Folland, C. K., Dijkstra, H. A., Lesins, G., and Dubey, M. K. 2011. Ice-core data evidence for a prominent near 20 year time-scale of the Atlantic Multidecadal Oscillation. *Geophysical Research Letters*, 38(13):n/a–n/a. doi: 10.1029/2011GL047501.

Clarke, R. A. and Gascard, J.-C. 1983. The formation of Labrador Sea water. Part I: Large-scale processes. *Journal of Physical Oceanography*, 13:1764–1788.

Coindreau, O., Hourdin, F., Haeffelin, M., Mathieu, A., and Rio, C. 2007. Assessment of Physical Parameterizations Using a Global Climate Model with Stretchable Grid and Nudging. *Monthly Weather Review*, 135(4):1474–1489. doi: 10.1175/MWR3338.1.

Colin de Verdière, A. and Huck, T. 1999. Baroclinic Instability: An Oceanic Wavemaker for Interdecadal Variability. *Journal of Physical Oceanography*, 29(5):893–910. doi: 10.1175/1520-0485(1999)029<0893:BIAOWF>2.0.CO;2.

Collins, M., Botzet, M., and Carril, A. F. 2006. Interannual to decadal climate predictability in the North Atlantic: A multimodel-ensemble study. *Journal of Climate*, pages 1195–1203.

Counillon, F., Bethke, I., Keenlyside, N., Bentsen, M., Bertino, L., and Zheng, F. 2014. Seasonal-to-decadal predictions with the ensemble Kalman filter and the Norwegian Earth System Model: a twin experiment. *Tellus A*, 66. doi: 10.3402/tellusa.v66.21074.

Cowtan, K. and Way, R. G. 2014. Coverage bias in the HadCRUT4 temperature series and its impact on recent temperature trends. *Quarterly Journal of the Royal Meteorological Society*, 140(683): 1935–1944. doi: 10.1002/qj.2297.

Cropper, T. E., Hanna, E., and Bigg, G. R. 2014. Spatial and temporal seasonal trends in coastal upwelling off Northwest Africa, 1981-2012. *Deep Sea Research Part I*, 86:94–111.

Cunningham, S. A., Kanzow, T., Rayner, D., Baringer, M. O., Johns, W. E., Marotzke, J., Longworth, H. R., Grant, E. M., Hirschi, J. J.-M., Beal, L. M., Meinen, C. S., and Bryden, H. L. 2007. Temporal variability of the Atlantic Meridional Overturning Circulation at 26.5Â°N. *Science (New York, N.Y.)*, 317(5840):935–8. doi: 10.1126/science.1141304.

Curry, R. and Mauritzen, C. 2005. Dilution of the northern North Atlantic Ocean in recent decades. *Science (New York, N.Y.)*, 308(5729):1772–4. doi: 10.1126/science.1109477.

Curry, R., McCartney, M. S., and Joyce, T. M. 1998. Oceanic transport of subpolar climate signals to mid-depth subtropical waters. *Nature*, 391:575–577.

Curry, R., Dickson, B., and Yashayaev, I. 2003. A change in the freshwater balance of the Atlantic Ocean over the past four decades. *Nature*, 426:826–829.

Curry, R. G. and McCartney, M. S. 2001. Ocean Gyre Circulation Changes Associated with the North Atlantic Oscillation. *Journal of Physical Oceanography*, 31(12):3374–3400. doi: 10.1175/1520-0485(2001)031<3374:OGCCAW>2.0.CO;2.

Da-Allada, C. Y., Alory, G., du Penhoat, Y., Kestenare, E., Durand, F., and Hounkonnou, N. M. 2013. Seasonal mixed-layer salinity balance in the tropical Atlantic Ocean: Mean state and seasonal cycle. *Journal of Geophysical Research: Oceans*, 118(1):332–345. doi: 10.1029/2012JC008357.

D'Addezio, J. M. and Bingham, F. M. 2014. A subtropical North Atlantic regional atmospheric moisture budget. *Journal of Geophysical Research: Oceans*, 119(12):8731–8748. doi: 10.1002/2014JC010300.

Danabasoglu, G. 2008. On Multidecadal Variability of the Atlantic Meridional Overturning Circulation in the Community Climate System Model Version 3. *Journal of Climate*, 21(21):5524–5544. doi: 10.1175/2008JCLI2019.1.

Dansgaard, W., Johnsen, S. J., Clausen, H. B., Dahl-Jensen, D., Gundestrup, N. S., Hammer, C. U., Hvidberg, C. S., Steffensen, J. P., Sveinbjörnsdottir, A. E., Jouzel, J., and Bond, G. 1993. Evidence for general instability of past climate from a 250-kyr ice-core record. *Nature Letters*, 364(6434): 218–220. doi: 10.1038/364218a0.

de Boyer Montégut, C., Mignot, J., Lazar, A., and Cravatte, S. 2007. Control of salinity on the mixed layer depth in the world ocean. Part I: general description. *Journal of Geophysical Research : Oceans*, 112(C06011):1–12. doi: 10.1029/2006JC003953.

de Lavergne, C., Madec, G., Le Sommer, J., Nurser, A. J. G., and Naveira Garabato, A. C. 2016. The Impact of a Variable Mixing Efficiency on the Abyssal Overturning. *Journal of Physical Oceanography*, 46(2):663–681. doi: 10.1175/JPO-D-14-0259.1.

Delcroix, T., McPhaden, M. J., Dessier, A., and Gouriou, Y. 2005. Time and space scales for sea surface salinity in the tropical oceans. *Deep Sea Research Part I: Oceanographic Research Papers*, 52(5):787–813. doi: 10.1016/j.dsr.2004.11.012.

Delworth, T. L., Manabe, S., and Stouffer, R. J. 1993. interdecadal variations of the thermohaline circulation in a coupled ocean-atmosphere model. *Journal of Climate*, 6:1993–2011.

Delworth, T. L. and Greatbatch, R. J. 2000. Multidecadal thermohaline circulation variability driven by atmospheric surface flux forcing. *Journal of Climate*, 13:1481–1495.

Delworth, T. L. and Mann, M. E. 2000. Observed and simulated multidecadal variability in the Northern Hemisphere. *Climate Dynamics*, 16(9):661–676. doi: 10.1007/s003820000075.

Delworth, T. L. and Zeng, F. 2012. Multicentennial variability of the Atlantic meridional overturning circulation and its climatic influence in a 4000 year simulation of the GFDL CM2.1 climate model. *Geophysical Research Letters*, 39(13):n/a–n/a. doi: 10.1029/2012GL052107.

Dengler, M., Schott, F. A., Eden, C., Brandt, P., Fischer, J., and Zantopp, R. 2004. Break-up of the Atlantic deep western boundary current into eddies at 8 degrees S. *Nature*, 432(7020):1018–20. doi: 10.1038/nature03134.

Deshayes, J., Straneo, F., and Spall, M. A. 2009. Mechanisms of variability in a convective basin. *Journal of Marine Research*, 67(3):273–303. doi: 10.1357/002224009789954757.

Deshayes, J., Tréguier, A.-M., Barnier, B., Lecointre, A., Le Sommer, J., Molines, J.-M., Penduff, T., Bourdallé-Badie, R., Drillet, Y., Garric, G., Benshila, R., Madec, G., Biastoch, A., Böning, C. W., Scheinert, M., Coward, A. C., and Hirschi, J. J.-M. 2013. Oceanic hindcast simulations at high resolution suggest that the Atlantic MOC is bistable. *Geophysical Research Letters*, 40(12): 3069–3073. doi: 10.1002/grl.50534.

Deshayes, J., Curry, R., and Msadek, R. 2014. CMIP5 model inter-comparison of freshwater budget and circulation in the North Atlantic. *Journal of Climate*, 27(May):3298–3317. doi: http://dx.doi.org/10.1175/JCLI-D-12-00700.1.

Dessier, A. and Donguy, J. R. 1994. The sea surface salinity in the tropical Atlantic between 10Â°S and 30Â°N seasonal and interannual variations (1977-1989). *Deep Sea Research Part I*, 41(1): 81–100.

Dickson, B., Meincke, J., Malmberg, S.-A., and Lee, A. 1988. The "great salinity anomaly" in the northern North Atlantic 1968-1982. *Progress in Oceanography*, 20:103–151.

Dickson, B., Lazier, J. R. N., Meincke, J., and Rhines, P. B. 1996. Long-term coordinated changes in the convective activity of the North Atlantic. *Decadal Climate Variability*, 38:241–295.

Dickson, B., Yashayaev, I., Meincke, J., and Turrell, B. 2002. Rapid freshening of the deep North Atlantic Ocean over the past four decades. *Nature*, 416:832–837.

Ding, Y., Carton, J. A., Chepurin, G. A., Stenchikov, G., Robock, A., Sentman, L. T., and Krasting, J. P. 2014. Ocean response to volcanic eruptions in Coupled Model Intercomparison Project 5 simulations. *Journal of Geophysical Research: Oceans*, 119(9):5622–5637. doi: 10.1002/2013JC009780.

Divine, D. V. and Dick, C. 2006. Historical variability of sea ice edge position in the Nordic Seas. *Journal of Geophysical Research*, 111(C1):C01001. doi: 10.1029/2004JC002851.

Doblas-Reyes, F. J., Andreu-Burillo, I., Chikamoto, Y., García-Serrano, J., Guemas, V., Kimoto, M., Mochizuki, T., Rodrigues, L. D., and van Oldenborgh, G. J. 2013. Initialized near-term regional climate change prediction. *Nature communications*, 4:1715. doi: 10.1038/ncomms2704.

Dong, B. and Sutton, R. 2015. Dominant role of greenhouse-gas forcing in the recovery of Sahel rainfall. *Nature Climate Change*, (June):1–5. doi: 10.1038/nclimate2664.

Dong, S., Baringer, M., Goni, G., and Garzoli, S. 2011. Importance of the assimilation of Argo float measurements on the Meridional Overturning Circulation in the South Atlantic. *Geophysical Research Letters*, 38(L18603). doi: 10.1029/2011GL048982.

Dong, S., Baringer, M. O., Goni, G. J., Meinen, C. S., and Garzoli, S. L. 2014. Seasonal variations in the South Atlantic Meridional Overturning Circulation from observations and numerical models. *Geophysical Research Letters*, 41:4611–4618. doi: 10.1002/2014GL060428.

Driscoll, S., Bozzo, A., Gray, L. J., Robock, A., and Stenchikov, G. 2012. Coupled Model Intercomparison Project 5 (CMIP5) simulations of climate following volcanic eruptions. *Journal of Geophysical Research: Atmospheres*, 117(D17):n/a–n/a. doi: 10.1029/2012JD017607.

Du, H., Doblas-Reyes, F. J., García-Serrano, J., Guemas, V., Soufflet, Y., and Wouters, B. 2012. Sensitivity of decadal predictions to the initial atmospheric and oceanic perturbations. *Climate Dynamics*, 39(7-8):2013–2023. doi: 10.1007/s00382-011-1285-9.

Dufresne, J.-L., Foujols, M.-a., Denvil, S., Caubel, A., Marti, O., Aumont, O., Balkanski, Y., Bekki, S., Bellenger, H., Benshila, R., Bony, S., Bopp, L., Braconnot, P., Brockmann, P., Cadule, P., Cheruy, F., Codron, F., Cozic, A., Cugnet, D., Noblet, N., Duvel, J.-P., Ethé, C., Fairhead, L., Fichefet, T., Flavoni, S., Friedlingstein, P., Grandpeix, J.-Y., Guez, L., Guilyardi, E., Hauglustaine, D., Hourdin, F., Idelkadi, A., Ghattas, J., Joussaume, S., Kageyama, M., Krinner, G., Labetoulle, S., Lahellec, A., Lefebvre, M.-P., Lefevre, F., Levy, C., Li, Z. X., Lloyd, J., Lott, F., Madec, G., Mancip, M., Marchand, M., Masson, S., Meurdesoif, Y., Mignot, J., Musat, I., Parouty, S., Polcher, J., Rio, C., Schulz, M., Swingedouw, D., Szopa, S., Talandier, C., Terray, P., Viovy, N., and Vuichard, N. 2013. Climate change projections using the IPSL-CM5 Earth System Model: from CMIP3 to CMIP5. *Climate Dynamics*, 40(9-10):2123–2165. doi: 10.1007/s00382-012-1636-1.

Dunstone, N. J. and Smith, D. M. 2010. Impact of atmosphere and sub-surface ocean data on decadal climate prediction. *Geophysical Research Letters*, 37(2). doi: 10.1029/2009GL041609.

Dunstone, N. J., Smith, D. M., and Eade, R. 2011. Multi-year predictability of the tropical Atlantic atmosphere driven by the high latitude North Atlantic Ocean. *Geophysical Research Letters*, 38(14). doi: 10.1029/2011GL047949.

Durack, P. J. and Wijffels, S. E. 2010. Fifty-Year trends in global ocean salinities and their relationship to broad-scale warming. *Journal of Climate*, 23(16):4342–4362. doi: 10.1175/2010JCLI3377.1.

Durack, P. J., Wijffels, S. E., and Matear, R. J. 2012. Ocean salinities reveal strong global water cycle intensification during 1950 to 2000. *Science*, 336(6080):455–8. doi: 10.1126/science.1212222.

Durand, F., Alory, G., Dussin, R., and Reul, N. 2013. SMOS reveals the signature of Indian Ocean Dipole events. *Ocean Dynamics*, 63(11-12):1203–1212. doi: 10.1007/s10236-013-0660-y.

Eden, C. and Jung, T. 2001. North Atlantic Interdecadal Variability: Oceanic Response to the North Atlantic Oscillation (1865-1997). *Journal of Climate*, 14(5):676–691. doi: 10.1175/1520-0442(2001)014<0676:NAIVOR>2.0.CO;2.

Eden, C. and Willebrand, J. 2001. Mechanisms of interannual to decadal variability of the North Atlantic circulation. *Journal of Climate*, 14(1994):2266–2280. doi: 10.1175/1520-0442(2001)014<2266:MOITDV>2.0.CO;2.

England, M. H., McGregor, S., Spence, P., Meehl, G. A., Timmermann, A., Cai, W., Gupta, A. S., McPhaden, M. J., Purich, A., and Santoso, A. 2014. Recent intensification of wind-driven circulation in the Pacific and the ongoing warming hiatus. *Nature Climate Change*, 4(3):222–227. doi: 10.1038/nclimate2106.

Escudier, R., Mignot, J., and Swingedouw, D. 2013. A 20-year coupled ocean-sea ice-atmosphere variability mode in the North Atlantic in an AOGCM. *Climate Dynamics*. doi: 10.1007/s00382-012-1402-4.

Evan, A. T., Vimont, D. J., Heidinger, A. K., Kossin, J. P., and Bennartz, R. 2009. The role of aerosols in the evolution of tropical North Atlantic Ocean temperature anomalies. *Science (New York, N.Y.)*, 324(5928):778–81. doi: 10.1126/science.1167404.

Fanning, A. F. and Weaver, A. J. 1997. Temporal-geographical meltwater influences on the North Atlantic Conveyor: Implications for the Younger Dryas. *Paleoceanography*, 12:307–320.

Feng, Q. Y. and Dijkstra, H. 2014. Are North Atlantic multidecadal SST anomalies westward propagating? *Geophysical Research Letters*, 41(2):541–546. doi: 10.1002/2013GL058687.

Ferry, N., Parent, L., Garric, G., Bricaud, C., Testut, C.-E., Le Galloudec, O., Lellouche, J. M., Drévillon, M., Greiner, E., Barnier, B., Molines, J.-M., Jourdain, N., Guinehut, S., Cabanes, C., and Zawadzki, L. 2012. GLORYS2V1 global ocean reanalysis of the altimetric era (1993-2009) at meso scale. *Mercator Ocean Quaterly Newsletter*, 44:28.

Fichefet, T., Poncin, C., Goosse, H., Huybrechts, P., Janssens, I., and Le Treut, H. 2003. Implications of changes in freshwater flux from the Greenland ice sheet for the climate of the 21st century. *Geophysical Research Letters*, 30(17):n/a–n/a. doi: 10.1029/2003GL017826.

Fischer, J., Schott, F. A., and Dengler, M. 2004. Boundary Circulation at the Exit of the Labrador Sea. *Journal of Physical Oceanography*, 34(7):1548–1570. doi: 10.1175/1520-0485(2004)034<1548:BCATEO>2.0.CO;2.

Fischer, J., Visbeck, M., Zantopp, R., and Nunes, N. 2010. Interannual to decadal variability of outflow from the Labrador Sea. *Geophysical Research Letters*, 37(24):n/a–n/a. doi: 10.1029/2010GL045321.

Flatau, M. K., Talley, L., and Niiler, P. P. 2003. The North Atlantic Oscillation, surface current velocities, and SST changes in the subpolar North Atlantic. *Journal of Climate*, 16(14):2355–2369. doi: 10.1175/2787.1.

Flückiger, J., Knutti, R., and White, J. W. C. 2006. Oceanic processes as potential trigger and amplifying mechanisms for Heinrich events. *Paleoceanography*, 21(2). doi: 10.1029/2005PA001204.

Folland, C. K., Palmer, T., and Parker, D. 1986. Sahel rainfall and worldwide sea temperatures 1901-85. *Nature*, 320:602–607.

Foltz, G. R. and McPhaden, M. J. 2008. Seasonal mixed layer salinity balance of the tropical North Atlantic Ocean. *Journal of Geophysical Research*, 113:C02013. doi: 10.1029/2007JC004178.

Foltz, G. R. and McPhaden, M. J. M. 2009. Impact of Barrier Layer Thickness on SST in the Central Tropical North Atlantic. *Journal of Climate*, 22(October):285–299. doi: 10.1175/2008JCLI2308.1.

Font, J., Boutin, J., Reul, N., Spurgeon, P., Ballabrera-Poy, J., Chuprin, A., Gabarró, C., Gourrion, J., Guimbard, S., Hénocq, C., Lavender, S., Martin, N., Martínez, J., McCulloch, M., Meirold-Mautner, I., Mugerin, C., Petitcolin, F., Portabella, M., Sabia, R., Talone, M., Tenerelli, J., Turiel, A., Vergely, J.-L., Waldteufel, P., Yin, X., Zine, S., and Delwart, S. 2013. SMOS first data analysis for sea surface salinity determination. *International Journal of Remote Sensing*, 34(9-10):3654–3670. doi: 10.1080/01431161.2012.716541.

Fox-Kemper, B., Ferrari, R., and Hallberg, R. 2008. Parameterization of Mixed Layer Eddies. Part I: Theory and Diagnosis. *Journal of Physical Oceanography*, 38(6):1145–1165. doi: 10.1175/2007JPO3792.1.

Frankcombe, L. M., Dijkstra, H. A., and von der Heydt, A. 2008. Sub-surface signatures of the Atlantic Multidecadal Oscillation. *Geophysical Research Letters*, 35(19):L19602. doi: 10.1029/2008GL034989.

Frankcombe, L. M., Dijkstra, H. A., and von der Heydt, A. 2009. Noise-Induced Multidecadal Variability in the North Atlantic: Excitation of Normal Modes. *Journal of Physical Oceanography*, 39 (1):220–233. doi: 10.1175/2008JPO3951.1.

Frankcombe, L. M., von der Heydt, A., and Dijkstra, H. A. 2010. North Atlantic Multidecadal Climate Variability: An Investigation of Dominant Time Scales and Processes. *J. Clim.*, 23:3626–3638.

Frankignoul, C. and Kestenare, E. 2002. The surface heat flux feedback. Part I: estimates from observations in the Atlantic and the North Pacific. *Climate Dynamics*, 19(8):633–647. doi: 10.1007/s00382-002-0252-x.

Frankignoul, C. 1985. Sea surface temperature anomalies, planetary waves and air-sea feedback in the middle latitudes. *Review of Geophysics*, 23:357–390.

Frankignoul, C. and Hasselmann, K. 1977. Stochastic climate models, Part 2: application to sea surface temperature anomalies and thermo-cline variability. *Tellus*, 29(1977):289–305.

Frankignoul, C., Kestenare, E., and Mignot, J. 2002. The surface heat flux feedback. Part II: Direct and indirect estimates in the ECHAM4/OPA8 coupled GCM. *Clim. Dyn.*, 19:633–647. doi: 10.1007/s00382-002-0253-9.

Furevik, T., Bentsen, M., and Drange, H. 2003. Description and evaluation of the Bergen climate model: ARPEGE coupled with MICOM. *Climate Dynamics*, pages 27–51. doi: 10.1007/s00382-003-0317-5.

Gaetani, M. and Mohino, E. 2013. Decadal prediction of the sahelian precipitation in CMIP5 simulations. *Journal of Climate*, 26(19):7708–7719. doi: 10.1175/JCLI-D-12-00635.1.

Gaillard, F., Autret, E., Thierry, V., Galaup, P., Coatanoan, C., and Loubrieu, T. 2009. Quality Control of Large Argo Datasets. *Journal of Atmospheric and Oceanic Technology*, 26(2):337–351. doi: 10.1175/2008JTECHO552.1.

Ganopolski, A. and Rahmstorf, S. 2001. Rapid changes of glacial climate simulated in a coupled climate model. *Nature*, 409:153–158.

Gelderloos, R., Straneo, F., and Katsman, C. a. 2012. Mechanisms behind the Temporary Shutdown of Deep Convection in the Labrador Sea: Lessons from the Great Salinity Anomaly Years 1968 - 71. *Journal of Climate*, 25(19):6743–6755. doi: 10.1175/JCLI-D-11-00549.1.

Germe, A., Chevallier, M., Salas y Mélia, D., Sanchez-Gomez, E., and Cassou, C. 2014. Interannual predictability of Arctic sea ice in a global climate model: regional contrasts and temporal evolution. *Climate Dynamics*, 43(9-10):2519–2538. doi: 10.1007/s00382-014-2071-2.

Germe, A., Sévellec, F., Mignot, J., Swingedouw, D., and Nguyen, S. 2016. On the robustness of near term climate predictability regarding initial state uncertainties. *Climate Dynamics*. doi: 10.1007/s00382-016-3078-7.

Giannini, A., Saravanan, R., and Chang, P. 2003. Oceanic forcing of Sahel rainfall on interannual to interdecadal time scales. *Science (New York, N.Y.)*, 302(5647):1027–30. doi: 10.1126/science.1089357.

Gierz, P., Lohmann, G., and Wei, W. 2015. Response of Atlantic overturning to future warming in a coupled atmosphere-ocean-ice sheet model. *Geophysical Research Letters*, 42(16):6811–6818. doi: 10.1002/2015GL065276.

Giese, B. S. and Ray, S. 2011. El Niño variability in simple ocean data assimilation (SODA), 1871 2008. *Journal of Geophysical Research*, 116(C2):C02024. doi: 10.1029/2010JC006695.

Godfrey, J. S. and Lindstrom, E. 1989. The heat budget of the equatorial western {P}acific surface mixed layer. *J. Geophys. Res.*, 94:8007–8017.

Goelzer, H., Mignot, J., Levermann, A., and Rahmstorf, S. 2006. Tropical versus high latitude freshwater influence on the thermohaline circulation. *Clim. Dyn.*, 27:715–725. doi: 10.1007/s00382-006-0161-5.

Goldenberg, S. B., Landsea, C. W., Mestas-Nunez, A. M., and Gray, W. M. 2001. The Recent Increase in Atlantic Hurricane Activity: Causes and Implications. *Science*, 293(5529):474–479. doi: 10.1126/science.1060040.

Gray, S. T. 2004. A tree-ring based reconstruction of the Atlantic Multidecadal Oscillation since 1567 A.D. *Geophysical Research Letters*, 31(12):L12205. doi: 10.1029/2004GL019932.

Greatbatch, R. J., Fanning, A. F., Goulding, A. D., and Levitus, S. 1991. A diagnosis of interpentadal circulation changes in the North Atlantic. *Journal of Geophysical Research*, 96(C12):22009. doi: 10.1029/91JC02423.

Griffies, S. M. 1997. Predictability of North Atlantic Multidecadal Climate Variability. *Science*, 275 (5297):181–184. doi: 10.1126/science.275.5297.181.

Griffies, S. M., Biastoch, A., Böning, C., Bryan, F., Danabasoglu, G., Chassignet, E. P., England, M. H., Gerdes, R., Haak, H., Hallberg, R. W., Hazeleger, W., Jungclaus, J., Large, W. G., Madec, G., Pirani, A., Samuels, B. L., Scheinert, M., Gupta, A. S., Severijns, C. a., Simmons, H. L., Treguier, A. M., Winton, M., Yeager, S., and Yin, J. 2009. Coordinated Ocean-ice Reference Experiments (COREs). *Ocean Modelling*, 26(1-2):1–46. doi: 10.1016/j.ocemod.2008.08.007.

Grodsky, S. A., Carton, J. A., Nigam, S., and Okumura, Y. M. 2012. Tropical Atlantic Biases in CCSM4. *Journal of Climate*, 25(11):3684–3701. doi: 10.1175/JCLI-D-11-00315.1.

Grodsky, S. A., Carton, J. A., and Bryan, F. O. 2014. A curious local surface salinity maximum in the northwestern tropical Atlantic. *Journal of Geophysical Research: Oceans*, 119(September 2013): 484–495. doi: 10.1002/2013JC009450.

Gulev, S. K., Barnier, B., Knochel, H., Molines, J.-M., and Cottet, M. 2003. Water Mass Transformation in the North Atlantic and Its Impact on the Meridional Circulation: Insights from an Ocean Model Forced by NCEP-NCAR Reanalysis Surface Fluxes. *Journal of Climate*, 16(19):3085–3110. doi: 10.1175/1520-0442(2003)016<3085:WMTITN>2.0.CO;2.

Haarsma, R. J. 2005. Sahel rainfall variability and response to greenhouse warming. *Geophysical Research Letters*, 32(17):L17702. doi: 10.1029/2005GL023232.

Hagos, S. M. and Cook, K. H. 2008. Ocean warming and late-twentieth-century Sahel drought and recovery. *Journal of Climate*, 21(15):3797–3814. doi: 10.1175/2008JCLI2055.1.

Häkkinen, S. 2001. Variability in sea surface height: A qualitative measure for the meridional overturning in the North Atlantic. *Journal of Geophysical Research: Oceans*, 106(C7):13,837–13,848.

Hakkinen, S. and Rhines, P. B. 2004. Surface salinity variability in the northern North Atlantic during recent decades. *Science*, 304 (5670):555–559. doi: 10.1126/science.1094917.

Häkkinen, S., Rhines, P. B., and Worthen, D. L. 2011. Atmospheric blocking and Atlantic multidecadal ocean variability. *Science (New York, N.Y.)*, 334(6056):655–9. doi: 10.1126/science.1205683.

Hall, A. and Manabe, S. 1997. Can local linear stochastic theory explain sea surface temperature and salinity variability? *Clim. Dyn.*, 13:167–180.

Ham, Y.-G., Rienecker, M. M., Suarez, M. J., Vikhliaev, Y., Zhao, B., Marshak, J., Vernieres, G., and Schubert, S. D. 2014. Decadal prediction skill in the GEOS-5 forecast system. *Climate Dynamics*, 42(1-2):1–20. doi: 10.1007/s00382-013-1858-x.

Hamlington, B. D., Leben, R. R., Nerem, R. S., Han, W., and Kim, K.-Y. 2011. Reconstructing sea level using cyclostationary empirical orthogonal functions. *Journal of Geophysical Research*, 116 (C12):C12015. doi: 10.1029/2011JC007529.

Hasselmann, K. 1976. Stochastic climate models Part I. Theory. *Tellus*, 28(6):473–485. doi: 10.1111/j.2153-3490.1976.tb00696.x.

Hasson, A., Delcroix, T., Boutin, J., Dussin, R., and Ballabrera-Poy, J. 2014. Analyzing the 2010-2011 La Niña signature in the tropical Pacific sea surface salinity using in situ data, SMOS observations, and a numerical simulation. *Journal of Geophysical Research: Oceans*, 119(6):3855–3867. doi: 10.1002/2013JC009388.

Hastenrath, S. 1990. Decadal-scale changes of the circulation in the tropical atlantic sector associated with Sahel drought. *International Journal of Climatology*, 10(5):459–472. doi: 10.1002/joc.3370100504.

Hátún, H., Sandø, A. B., Drange, H., Hansen, B., and Valdimarsson, H. 2005. Influence of the Atlantic subpolar gyre on the thermohaline circulation. *Science (New York, N.Y.)*, 309(5742):1841–4. doi: 10.1126/science.1114777.

Hawkins, E. and Sutton, R. T. 2007. Variability of the Atlantic thermohaline circulation described by three-dimensional empirical orthogonal functions. *Climate Dyn.*, 29:745–762.

Hawkins, E. and Sutton, R. T. 2008. Potential predictability of rapid changes in the Atlantic meridional overturning circulation. *Geophysical Research Letters*, 35(11):L11603. doi: 10.1029/2008GL034059.

Hawkins, E. and Sutton, R. T. 2011. Estimating climatically relevant singular vectors for decadal predictions of the Atlantic Ocean. *Journal of Climate*, 24(1):109–123. doi: 10.1175/2010JCLI3579.1.

Hawkins, E., Dong, B., Robson, J., Sutton, R. T., and Smith, D. 2014. The Interpretation and Use of Biases in Decadal Climate Predictions. *Journal of Climate*, 27(8):2931–2947. doi: 10.1175/JCLI-D-13-00473.1.

Haywood, J. M., Jones, A., Bellouin, N., and Stephenson, D. 2013. Asymmetric forcing from stratospheric aerosols impacts Sahelian rainfall. *Nature Climate Change*, 3(7):660–665. doi: 10.1038/nclimate1857.

Hazeleger, W., Guemas, V., Wouters, B., Corti, S., Andreu-Burillo, I., Doblas-Reyes, F. J., Wyser, K., and Caian, M. 2013a. Multiyear climate predictions using two initialization strategies. *Geophysical Research Letters*, 40(9):1794–1798. doi: 10.1002/grl.50355.

Hazeleger, W., Wouters, B., van Oldenborgh, G. J., Corti, S., Palmer, T., Smith, D. M., Dunstone, N., Kröger, J., Pohlmann, H., and von Storch, J.-S. 2013b. Predicting multiyear North Atlantic Ocean variability. *Journal of Geophysical Research: Oceans*, 118(3):1087–1098. doi: 10.1002/jgrc.20117.

Heimbach, P., Wunsch, C., Ponte, R. M., Forget, G., Hill, C., and Utke, J. 2011. Timescales and regions of the sensitivity of Atlantic meridional volume and heat transport: Toward observing system design. *Deep Sea Research Part II: Topical Studies in Oceanography*, 58(17-18):1858–1879. doi: 10.1016/j.dsr2.2010.10.065.

Held, I. M., Soden, B. J., Oceanic, N., and Science, A. 2006. Robust Responses of the Hydrological Cycle to Global Warming. *Journal of Climate*, 19(21):5686–5699. doi: 10.1175/JCLI3990.1.

Helm, K. P., Bindoff, N. L., and Church, J. A. 2010. Changes in the global hydrological-cycle inferred from ocean salinity. *Geophysical Research Letters*, 37(18):n/a–n/a. doi: 10.1029/2010GL044222.

Herbaut, C. and Houssais, M.-N. 2009. Response of the eastern North Atlantic subpolar gyre to the North Atlantic Oscillation. *Geophysical Research Letters*, 36(17):L17607. doi: 10.1029/2009GL039090.

Hermanson, L. and Sutton, R. T. 2010. Case studies in interannual to decadal climate predictability. *Climate Dynamics*, 35(7-8):1169–1189. doi: 10.1007/s00382-009-0672-y.

Hernandez, O., Boutin, J., Kolodziejczyk, N., Reverdin, G., Martin, N., Gaillard, F., Reul, N., and Vergely, J.-L. 2014. SMOS salinity in the subtropical North Atlantic salinity maximum: 1. Comparison with Aquarius and in situ salinity. *Journal of Geophysical Research: Oceans*, 119(12):8878–8896. doi: 10.1002/2013JC009610.

Hodson, D. L. R. and Sutton, R. T. 2012. The impact of resolution on the adjustment and decadal variability of the Atlantic meridional overturning circulation in a coupled climate model. *Climate Dynamics*, 39(12):3057–3073. doi: 10.1007/s00382-012-1309-0.

Hoerling, M., Hurrell, J. W., Eischeid, J., and Phillips, A. S. 2006. Detection and attribution of twentieth-century northern and southern African rainfall change. *Journal of Climate*, 19:3989–4008.

Hofer, D., Raible, C. C., F., S. T., and Stocker, T. F. 2010. Variations of the Atlantic meridional overturning circulation in control and transient simulations of the last millennium. *Climate of the Past Discussions*, 7:1267–1309. doi: 10.5194/cpd-6-1267-2010.

Holliday, N. P., Hughes, S. L., Bacon, S., Beszczynska-Möller, A., Hansen, B., Lavín, A., Loeng, H., Mork, K. A., Østerhus, S., Sherwin, T. J., and Walczowski, W. 2008. Reversal of the 1960s to 1990s freshening trend in the northeast North Atlantic and Nordic Seas. *Geophysical Research Letters*, 35 (3):L03614. doi: 10.1029/2007GL032675.

Hosoda, S., Suga, T., Shikama, N., and Mizuno, K. 2009. Global surface layer salinity change detected by Argo and its implication for hydrological cycle intensification. *Journal of Oceanography*, 65(4): 579–586. doi: 10.1007/s10872-009-0049-1.

Huck, T., Colin de Verdière, A., and Weaver, A. J. 1999. Interdecadal Variability of the Thermohaline Circulation in Box-Ocean Models Forced by Fixed Surface Fluxes. *Journal of Physical Oceanography*, 29(5):865–892. doi: 10.1175/1520-0485(1999)029<0865:IVOTTC>2.0.CO;2.

Huck, T., Colin de Verdière, A., Estrade, P., and Schopp, R. 2008. Low-frequency variations of the large-scale ocean circulation and heat transport in the North Atlantic from 1955-1998 in situ temperature and salinity data. *Geophysical Research Letters*, 35(23):L23613. doi: 10.1029/2008GL035635.

Iles, C. E. and Hegerl, G. C. 2014. The global precipitation response to volcanic eruptions in the CMIP5 models. *Environmental Research Letters*, 9(10):104012. doi: 10.1088/1748-9326/9/10/104012.

Iwi, A. M., Hermanson, L., Haines, K., and Sutton, R. T. 2012. Mechanisms Linking Volcanic Aerosols to the Atlantic Meridional Overturning Circulation. *Journal of Climate*, 25(8):3039–3051. doi: 10.1175/2011JCLI4067.1.

Jackson, L. C., Kahana, R., Graham, T., Ringer, M. A., Woollings, T., Mecking, J. V., and Wood, R. A. 2015. Global and European climate impacts of a slowdown of the AMOC in a high resolution GCM. *Climate Dynamics*, pages 1–18. doi: 10.1007/s00382-015-2540-2.

Janicot, S., Trzaska, S., and Poccard, I. 2001. Summer Sahel-ENSO teleconnection and decadal time scale SST variations. *Climate Dynamics*, 18(3-4):303–320. doi: 10.1007/s003820100172.

Johns, W. E. and Baringer, M. O. 2011. Continuous, array-based estmates of Atlantic ocean heat transport at 26.5Â°N. *Journal of Climate*, 24(10):2429–2449. doi: 10.1175/2010JCLI3997.1.

Joly, M., Voldoire, A., Douville, H., Terray, P., and Royer, J. 2007. African monsoon teleconnections with tropical SSTs: validation and evolution in a set of IPCC4 simulations. *Climate Dynamics*, 29: 1–20. doi: 10.1007/s00382-006-0215-8.

Jungclaus, J. H. and Keenlyside, N. S. 2006. Ocean circulation and tropical variability in the coupled model ECHAM5/MPI-OM. *Journal of Climate*, 19:3952–3972.

Jungclaus, J. H., Haak, H., Latif, M., Mikolajewicz, U., Junglcaus, J., Haak, H., Latif, M., and Mikolajewicz, U. 2005. Arctic-North Atlantic interactions and multidecadal variability of the meridional overturning circulation. *J. Clim.*, 18(19):4013–4019. doi: 10.1175/JCLI3462.1.

Kageyama, M., Mignot, J., Swingedouw, D., Marzin, C., Alkama, R., and Marti, O. 2009. Glacial climate sensitivity to different states of the Atlantic Meridional Overturning Circulation: results from the IPSL model. *Climate of the Past*, 5(3):551–570. doi: 10.5194/cp-5-551-2009.

Kalnay, E. and Others. 1996. The NCEP/NCAR 40-year reanalysis project. *Bull. Amer. Meteor. Soc.*, 77:437–471.

Kanzow, T., Send, U., Zenk, W., Chave, A. D., and Rhein, M. 2006. Monitoring the integrated deep meridional flow in the tropical North Atlantic: Long-term performance of a geostrophic array. *Deep Sea Research Part I: Oceanographic Research Papers*, 53(3):528–546. doi: 10.1016/j.dsr.2005.12.007.

Kanzow, T., Cunningham, S. A., Rayner, D., Hirschi, J. J.-M., Johns, W. E., Baringer, M. O., Bryden, H. L., Beal, L. M., Meinen, C. S., and Marotzke, J. 2007. Observed flow compensation associated with the MOC at 26.5 degrees N in the Atlantic. *Science (New York, N.Y.)*, 317(5840):938–41. doi: 10.1126/science.1141293.

Kanzow, T., Cunningham, S. A., Johns, W. E., Hirschi, J. J.-M., Marotzke, J., Baringer, M. O., Meinen, C. S., Chidichimo, M. P., Atkinson, C., Beal, L. M., Bryden, H. L., and Collins, J. 2010. Seasonal Variability of the Atlantic Meridional Overturning Circulation at 26.5Â°N. *Journal of Climate*, 23(21):5678–5698. doi: 10.1175/2010JCLI3389.1.

Karl, T. R., Arguez, A., Huang, B., Lawrimore, J. H., McMahon, J. R., Menne, M. J., Peterson, T. C., Vose, R. S., and Zhang, H.-M. 2015. CLIMATE CHANGE. Possible artifacts of data biases in the recent global surface warming hiatus. *Science*, 348(6242):1469–1472. doi: 10.1126/science.aaa5632.

Karspeck, A. R., Yeager, S. G., Danabasoglu, G., and Teng, H. 2014. An evaluation of experimental decadal predictions using CCSM4. *Climate Dynamics*, pages 1–17. doi: 10.1007/s00382-014-2212-7.

Karspeck, A. R., Stammer, D., Köhl, A., Danabasoglu, G., Balmaseda, M. A., Smith, D. M., Fujii, Y., Zhang, S., Giese, B. S., Tsujino, H., and Rosati, A. J. 2015. Comparison of the Atlantic meridional overturning circulation between 1960 and 2007 in six ocean reanalysis products. *Climate Dynamics*. doi: 10.1007/s00382-015-2787-7.

Keenlyside, N. S., Latif Mojib, M., and Jungclaus, J. H. 2008. Advancing decadal-scale climate prediction in the North Atlantic sector. *Nature*, 453(May):1–5. doi: 10.1038/nature06921.

Khodri, M., Izumo, T., Vialard, J., Cassou, C., Lengaigne, M., Mignot, J., Guilyardi, E., Lebas, N., Ruprich-Robert, Y., Robock, A., and McPhaden, M. J. M. 2016. How tropical explosive volcanic eruptions trigger El Niño events. *Nature Communications*, submitted.

Kirtman, B. P., Bitz, C., Bryan, F., Collins, W., Dennis, J., Hearn, N., Kinter, J. L., Loft, R., Rousset, C., Siqueira, L., Stan, C., Tomas, R., and Vertenstein, M. 2012. Impact of ocean model resolution on CCSM climate simulations. *Climate Dynamics*, 39(6):1303–1328. doi: 10.1007/s00382-012-1500-3.

Kirtman, B., Power, S. B., Adedoyin, J. A., Boer, G. J., Bojariu, R., Camilloni, I., Doblas-Reyes, F. J., Fiore, A., Kimoto, M., Meehl, G., Prather, M. J., Sarr, A., Schär, C., Sutton, R. T., van Oldenborgh, G. J., Vecchi, G. A., Wang, H. J., and Schär, C. Near-term Climate Change: Projections and Predictability. In Stocker, T., D. Qin, G.-K., Plattner, M., Tignor, S., Allen, J., Boschung, A., Nauels, Y., Xia, Y., Bex, P., and Midgley, V., editors, *Climate Change 2013: The Physical Science Basis. Contribution of Working Group I to the Fifth Assessment Report of the Intergovernmental Panel on Climate Change*, chapter 11, pages 953–1028. Cambridge University Press, Cambridge, United Kingdom and New York, NY, USA, 2013.

Knight, J. R., Allan, R. J., Folland, C. K., Vellinga, M., and Mann, M. E. 2005. A signature of persistent natural thermohaline circulation cycles in observed climate. *Geophysical Research Letters*, 32(20):1–4. doi: 10.1029/2005GL024233.

Knight, J. R., Folland, C. K., and Scaife, A. a. 2006. Climate impacts of the Atlantic Multidecadal Oscillation. *Geophysical Research Letters*, 33(17):L17706. doi: 10.1029/2006GL026242.

Knutti, R., Flueckiger, J., Stocker, T. F., and Timmernmann, A. 2004. Strong hemispheric coupling of glacial climate through freshwater discharge and ocean circulation. *Nature*, 430:851–856.

Kolodziejczyk, N., Reverdin, G., and Lazar, A. 2014. Interannual Variability of the Mixed Layer Winter Convection and Spice Injection in the Eastern Subtropical North Atlantic. *Journal of Physical Oceanography*, 45(2):504–525. doi: 10.1175/JPO-D-14-0042.1.

Kolodziejczyk, N., Hernandez, O., Boutin, J., and Reverdin, G. 2015. SMOS salinity in the subtropical North Atlantic salinity maximum: 2. Two-dimensional horizontal thermohaline variability. *Journal of Geophysical Research: Oceans*, 120(2):972–987. doi: 10.1002/2014JC010103.

Koltermann, K. P., Skov, A. V., Tereschenkov, V. P., Dobroliubov, S. A., Lorbacher, K., and Sy, A. 1999. Decadal changes in the thermohaline circulation of North Atlantic. *Deep Sea Res. II*, 46: 109–138.

Kosaka, Y. and Xie, S.-P. 2013. Recent global-warming hiatus tied to equatorial Pacific surface cooling. *Nature*, 501(7467):403–7. doi: 10.1038/nature12534.

Kuhlbrodt, T., Griesel, A., Montoya, M., Levermann, A., Hofmann, M., and Rahmstorf, S. 2007. On the driving processes of the Atlantic meridional overturning circulation. *Reviews of Geophysics*, 45 (2004):RG2001. doi: 10.1029/2004RG000166.

Kumar, A., Wang, H., Xue, Y., and Wang, W. 2014. How Much of Monthly Subsurface Temperature Variability in the Equatorial Pacific Can Be Recovered by the Specification of Sea Surface Temperatures? *Journal of Climate*, 27(4):1559–1577. doi: 10.1175/JCLI-D-13-00258.1.

Kwon, Y.-O. and Frankignoul, C. 2012. Stochastically-driven multidecadal variability of the Atlantic meridional overturning circulation in CCSM3. *Climate Dynamics*. doi: 10.1007/s00382-011-1040-2.

Kwon, Y.-O. and Frankignoul, C. 2014. Mechanisms of Multidecadal Atlantic Meridional Overturning Circulation Variability Diagnosed in Depth versus Density Space. *Journal of Climate*, 27(24):9359–9376. doi: 10.1175/JCLI-D-14-00228.1.

Lamb, H. H. 1970. Volcanic Dust in the Atmosphere; with a Chronology and Assessment of Its Meteorological Significance. *Philosophical Transactions of the Royal Society A: Mathematical, Physical and Engineering Sciences*, 266(1178):425–533. doi: 10.1098/rsta.1970.0010.

Langehaug, H. R., Rhines, P. B., Eldevik, T., Mignot, J., and Lohmann, K. 2012. Water mass transformation and the North Atlantic Current in three multicentury climate model simulations. *Journal of Geophysical Research*, 117(C11):C11001. doi: 10.1029/2012JC008021.

Latif, M., Roeckner, E., Botzet, M., Esch, M., Haak, H., Hagemann, S., Jungclaus, J. H., Legutke, S., Marsland, S. J., Mikolajewicz, U., and Mitchell, J. 2004. Reconstructing, Monitoring, and Predicting Multidecadal-Scale Changes in the North Atlantic Thermohaline Circu-

lation with Sea Surface Temperature. *Journal of Climate*, 17(7):1605–1614. doi: 10.1175/1520-0442(2004)017<1605:RMAPMC>2.0.CO;2.

Laurian, A., Lazar, A., Reverdin, G., Rodgers, K., and Terray, P. 2006. Poleward propagation of spiciness anomalies in the North Atlantic Ocean. *Geophysical Research Letters*, 33:L13603.

Laurian, A., Lazar, A., and Reverdin, G. 2009. Generation Mechanism of Spiciness Anomalies: An OGCM Analysis in the North Atlantic Subtropical Gyre. *Journal of Physical Oceanography*, 39(4): 1003–1018. doi: 10.1175/2008JPO3896.1.

Lazier, J. R. N., Pickart, R. S., and Rhines, P. B. Deep convection. In Siedler, G., Church, J., and Gould, J., editors, *Ocean circulation and climate*, pages 387–400. Academic Press, 2001.

Lehner, F., Born, A., Raible, C. C., and Stocker, T. F. 2013. Amplified Inception of European Little Ice Age by Sea Ice-Ocean-Atmosphere Feedbacks. *Journal of Climate*, 26(19):7586–7602. doi: 10.1175/JCLI-D-12-00690.1.

Lehner, F., Raible, C. C., Keller, K., Joos, F., and Mignot, J. 2015. Climate and carbon cycle dynamics in a continuous 850-2100 CE simulation with CESM1. *Earth System Dynamics*, 16:9580. doi: 10.5194/esdd-6-351-2015.

Levermann, A. and Born, A. 2007. Bistability of the Atlantic subpolar gyre in a coarse-resolution climate model. *Geophysical Research Letters*, 34(24):L24605. doi: 10.1029/2007GL031732.

Li, J., Sun, C., and Jin, F.-F. 2013. NAO implicated as a predictor of Northern Hemisphere mean temperature multidecadal variability. *Geophysical Research Letters*, 40(20):5497–5502. doi: 10.1002/2013GL057877.

Li, L., Schmitt, R. W., Ummenhofer, C. C., and Karnauskas, K. B. 2016. North Atlantic salinity as a predictor of Sahel rainfall. *Science Advances*, 2(May). doi: 10.1126/sciadv.1501588.

Liu, H., Grodsky, S. A., and Carton, J. A. 2009. Observed sub seasonal variability of oceanic barrier and compensated layers. *Journal of Climate*, 22(22):6104–6119. doi: 10.1175/2009JCLI2974.1.

Liu, X., Köhl, A., Stammer, D., Masuda, S., Ishikawa, Y., and Mochizuki, T. 2016. Impact of inconsistency between the climate model and its initial conditions on climate prediction. *Climate Dynamics*. doi: 10.1007/s00382-016-3194-4.

Lozier, M. S. 2010. Deconstructing the conveyor belt. *Science*, pages 1507–1511.

Lozier, M. S., Leadbetter, S., Williams, R. G., Roussenov, V., Reed, M. S. C., and Moore, N. J. 2008. The spatial pattern and mechanisms of heat-content change in the North Atlantic. *Science (New York, N.Y.)*, 319(5864):800–803. doi: 10.1126/science.1146436.

Lu, J. and Delworth, T. L. 2005. Oceanic forcing of the late 20th century Sahel drought. *Geophysical Research Letters*, 32(22):L22706. doi: 10.1029/2005GL023316.

Lukas, R. and Lindstrom, E. 1991. The mixed layer of the western equatorial Pacific Ocean. *Journal of Geophysical Research: Oceans*, 96:3343–3357.

Lumpkin, R. and Garraffo, Z. 2005. Evaluating the Decomposition of Tropical Atlantic Drifter Observations. *Journal of Atmospheric and Oceanic Technology*, 22(9):1403–1415. doi: 10.1175/JTECH1793.1.

Luo, J., Masson, S., and Behera, S. 2005. Seasonal climate predictability in a coupled OAGCM using a different approach for ensemble forecasts. *Journal of climate*, 18:4474–4497. doi: 10.1175/JCLI3526.1.

Magnusson, L., Alonso-Balmaseda, M., Corti, S., Molteni, F., and Stockdale, T. 2012. Evaluation of forecast strategies for seasonal and decadal forecasts in presence of systematic model errors. *Climate Dynamics*, 41(9-10):2393–2409. doi: 10.1007/s00382-012-1599-2.

Maher, N., McGregor, S., England, M. H., and Sen Gupta, A. 2015. Effects of volcanism on tropical variability. *Geophysical Research Letters*, pages n/a–n/a. doi: 10.1002/2015GL064751.

Manabe, S. and Stouffer, R. J. 1995. Simulation of abrupt climate change induced by freshwater input to the North Atlantic Ocean. *Nature*, 378:165–167.

Manabe, S. and Stouffer, R. J. 1997. Coupled ocean-atmosphere model response to freshwater input: Comparison to Younger Dryas event. *Paleoceanography*, 12:321–336.

Marini, C. and Frankignoul, C. 2013. An attempt to deconstruct the Atlantic Multidecadal Oscillation. *Climate Dynamics*, 2013(3-4):607–625. doi: 10.1007/s00382-013-1852-3.

Marini, C., Frankignoul, C., and Mignot, J. 2011. Links between the Southern Annular Mode and the Atlantic Meridional Overturning Circulation in a Climate Model. *Journal of Climate*, 24(3): 624–640. doi: 10.1175/2010JCLI3576.1.

Marshall, J., Johnson, H. L., and Goodman, P. J. 2001. A study of the interaction of the North Atlantic Oscillation with ocean circulation. *Journal of Climate*, 14:1399–1421.

Marti, O., Braconnot, P., Dufresne, J.-L., Bellier, J., Benshila, R., Bony, S., Brockmann, P., Cadule, P., Caubel, A., Codron, F., de Noblet-Ducoudre, N., Denvil, S., Fairhead, L., Fichefet, T., Foujols, M.-A., Friedlingstein, P., Goosse, H., Grandpeix, J.-Y., Guilyardi, E., Hourdin, F., Idelkadi, A., Kageyama, M., Krinner, G., Lévy, C., Madec, G., Mignot, J., Musat, I., Swingedouw, D., and Talandier, C. 2010. Key features of the IPSL ocean atmosphere model and its sensitivity to atmospheric resolution. *Climate dynamics*, 34:1–26. doi: 10.1007/s00382-009-0640-6.

Marzeion, B., Levermann, A., and Mignot, J. 2007. The Role of Stratification-Dependent Mixing for the Stability of the Atlantic Overturning in a Global Climate Model. *Journal of Physical Oceanography*, 37(11):2672–2681. doi: 10.1175/2007JPO3641.1.

Marzocchi, A., Hirschi, J. J.-M., Holliday, N. P., Cunningham, S. A., Blaker, A. T., and Coward, A. C. 2015. The North Atlantic subpolar circulation in an eddy-resolving global ocean model. *Journal of Marine Systems*, 142:126–143. doi: 10.1016/j.jmarsys.2014.10.007.

Masson, S., Luo, J.-J., Madec, G., Vialard, J., Durand, F., Gualdi, S., Guilyardi, E., Behera, S. K., Delecluse, P., Navarra, A., and Yamagata, P. 2005. Impact of barrier layer on winter-spring variability of the southeastern {A}rabian {S}ea. *Geophysical Research Letters*, 32(L07703): doi:10.1029/2004GL021980.

Matei, D., Pohlmann, H., Jungclaus, J., Müller, W., Haak, H., and Marotzke, J. 2012. Two Tales of Initializing Decadal Climate Prediction Experiments with the ECHAM5/MPI-OM Model. *Journal of Climate*, 25(24):8502–8523. doi: 10.1175/JCLI-D-11-00633.1.

Mauritzen, C. and Hakkinen, S. 1999. On the relationship between dense water formation and the Meridional Overturning Cell in the North Atlantic Ocean. *Deep-Sea Res. I*, 46:877–894.

McCarthy, G. D., King, B. A., Cipollini, P., McDonagh, E. L., Blundell, J. R., and Biastoch, A. 2012. On the sub-decadal variability of South Atlantic Antarctic Intermediate Water. *Geophysical Research Letters*, 39(10):n/a–n/a. doi: 10.1029/2012GL051270.

McCarthy, G. D., Smeed, D. A., Johns, W. E., Frajka-Williams, E., Moat, B., Rayner, D., Baringer, M. O., Meinen, C. S., Collins, J., and Bryden, H. L. 2015. Measuring the Atlantic Meridional Overturning Circulation at 26Â°N. *Progress in Oceanography*, 130(September):91–111. doi: 10.1016/j.pocean.2014.10.006.

McGregor, H. V., Dima, M., Fischer, H. W., and Mulitza, S. 2007. Rapid 20th-century increase in coastal upwelling off northwest Africa. *Science (New York, N.Y.)*, 315(5812):637–9. doi: 10.1126/science.1134839.

McGregor, H. V., Evans, M. N., Goosse, H., Leduc, G., Martrat, B., Addison, J. A., Mortyn, P. G., Oppo, D. W., Seidenkrantz, M.-S., Sicre, M.-A., Phipps, S. J., Selvaraj, K., Thirumalai, K., Filipsson, H. L., and Ersek, V. 2015. Robust global ocean cooling trend for the pre-industrial Common Era. *Nature Geoscience*, 8(9):671–677. doi: 10.1038/ngeo2510.

McGregor, S., Timmermann, A., and Timm, O. 2010. A unified proxy for ENSO and PDO variability since 1650. *Climate of the Past*, 6:1–17.

McManus, J., Francois, R., Gherardi, J.-M., Keigwin, L. D., and Brown-Leger, S. 2004. Collapse and rapid resumption of Atlantic meridional circulation linked to deglacial climate changes. *Nature*, 428: 834–837.

Meehl, G. A., Goddard, L., Boer, G., Burgman, R., Branstator, G., Cassou, C., Corti, S., Danabasoglu, G., Doblas-Reyes, F., Hawkins, E., Karspeck, A., Kimoto, M., Kumar, A., Matei, D., Mignot, J., Msadek, R., Navarra, A., Pohlmann, H., Rienecker, M., Rosati, T., Schneider, E., Smith, D., Sutton, R., Teng, H., van Oldenborgh, G. J., Vecchi, G., and Yeager, S. 2014. Decadal Climate Prediction:

An Update from the Trenches. *Bulletin of the American Meteorological Society*, 95(2):243–267. doi: 10.1175/BAMS-D-12-00241.1.

Mellor, G. L., Mechoso, C. R., and Keto, E. 1982. A diagnostic calculation of the general circulation of the atlantic ocean. *Deep Sea Research Part A. Oceanographic Research Papers*, 29 Upper-l(10): 1171–1192. doi: 10.1016/0198-0149(82)90088-7.

Menary, M. B., Park, W., Lohmann, K., Vellinga, M., Palmer, M. D., Latif, M., and Jungclaus, J. H. 2011. A multimodel comparison of centennial Atlantic meridional overturning circulation variability. *Climate Dynamics*, 38(11-12):2377–2388. doi: 10.1007/s00382-011-1172-4.

Menary, M. B., Hodson, D. L. R., Robson, J. I., Sutton, R. T., and Wood, R. A. 2015. A Mechanism of Internal Decadal Atlantic Ocean Variability in a High-Resolution Coupled Climate Model. *Journal of Climate*, 28(19):7764–7785. doi: 10.1175/JCLI-D-15-0106.1.

Mercier, H., Lherminier, P., and Sarafanov, A. 2015. Variability of the meridional overturning circulation at the Greenland - Portugal OVIDE section from 1993 to 2010. *Progress in Oceanography*, pages 1–12.

Merryfield, W. J., Lee, W., Boer, G. J., Kharin, V. V., Pal, B., Scinocca, J. F., and Flato, G. M. 2010. The first coupled historical forecasting project (CHFP1). *Atmosphere-Ocean*, 48(4):263–283. doi: 10.3137/AO1008.2010.

Mignot, J. and Frankignoul, C. 2004. Interannual to interdecadal variability of sea surface salinity in the Atlantic and its link to the atmosphere in a coupled model. *Journal of Geophysical Research C: Oceans*, 109(4):C04005. doi: 10.1029/2003JC002005.

Mignot, J., Ganopolski, A., and Levermann, A. 2006. Atlantic subsurface temperatures: response to a shut-down of the overturning circulation and consequences for its recovery. *Journal of Climate*, 20: 4884–4898. doi: 10.1175/JCLI4280.1.

Mignot, J. and Frankignoul, C. 2005. The variability of the Atlantic meridional overturning circulation, the North Atlantic Oscillation, and the El Ninõ-Southern Oscillation in the Bergen climate model. *Journal of climate*, 18:2361–2375. doi: 10.1175/JCLI3405.1.

Mignot, J. and Frankignoul, C. 2010. local and remote impacts of a tropical Atlantic salinity anomaly. *Climate Dynamics*, 35:1133–1147. doi: 10.1007/s00382-009-0621-9.

Mignot, J. and Frankignoul, C. 2003. On the interannual variability of surface salinity in the Atlantic. *Climate Dynamics*, 20(May 2002):555–565. doi: 10.1007/s00382-002-0294-0.

Mignot, J., de Boyer Montégut, C., Lazar, A., and Cravatte, S. 2007. Control of salinity on the mixed layer depth in the world ocean: 2. Tropical areas. *Journal of Geophysical Research : Oceans*, 112 (January 2000):1–12. doi: 10.1029/2006JC003954.

Mignot, J., Khodri, M., Frankignoul, C., and Servonnat, J. 2011. Volcanic impact on the Atlantic Ocean over the last millennium. *Climate of the Past*, 7(4):1439–1455. doi: 10.5194/cp-7-1439-2011.

Mignot, J., Lazar, A., and Lacarra, M. 2012. On the formation of barrier layers and associated vertical temperature inversions: A focus on the northwestern tropical Atlantic. *Journal of Geophysical Research*, 117(C2):C02010. doi: 10.1029/2011JC007435.

Mignot, J., García-Serrano, J., Swingedouw, D., Germe, A., Nguyen, S., Guilyardi, E., and Ray, S. 2015. Decadal prediction skill in the ocean with surface nudging in the IPSL-CM5A-LR climate model. *Climate Dynamics*. doi: 10.1007/s00382-015-2898-1.

Moffa-Sanchez, P., Born, A., and Hall, I. R. 2014. Solar forcing of North Atlantic surface temperature and salinity over the past millennium. *Nature Geoscience*, n(n):6–9. doi: 10.1038/NGEO2094S.

Mohino, E., Janicot, S., and Bader, J. 2011. Sahel rainfall and decadal to multi-decadal sea surface temperature variability. *Climate Dynamics*, 37(3):419–440. doi: 10.1007/s00382-010-0867-2.

Montoya, M., Griesel, A., Levermann, A., Mignot, J., Hofmann, M., Ganopolski, A., and Rahmstorf, S. 2005. The Earth System Model of intermediate complexity CLIMBER-3α. Part I: description and performance for present-day conditions. *Climate Dynamics*, 25:237–263. doi: 10.1007/s00382-005-0044-1.

Mote, P. W. 2002. Coastal upwelling in a warmer future. *Geophysical Research Letters*, 29(23):2138. doi: 10.1029/2002GL016086.

Msadek, R. and Frankignoul, C. 2008. Atlantic multidecadal oceanic variability and its influence on the atmosphere in a climate model. *Climate Dynamics*, 33(1):45–62. doi: 10.1007/s00382-008-0452-0.

Msadek, R., Dixon, K. W., Delworth, T. L., and Hurlin, W. J. 2010. Assessing the predictability of the Atlantic meridional overturning circulation and associated fingerprints. *Geophysical Research Letters*, 37(19). doi: 10.1029/2010GL044517.

Msadek, R., Johns, W. E., Yeager, S. G., Danabasoglu, G., Delworth, T. L., and Rosati, A. 2013. The Atlantic Meridional Heat Transport at 26.5Â°N and Its Relationship with the MOC in the RAPID Array and the GFDL and NCAR Coupled Models. *Journal of Climate*, 26(12):4335–4356. doi: 10.1175/JCLI-D-12-00081.1.

Msadek, R., Delworth, T. L., Rosati, A. J., Anderson, W. G., Vecchi, G. A., Chang, Y.-S., Dixon, K. W., Gudgel, R. G., Stern, W. F., Wittenberg, A. T., Yang, X., Zeng, F., Zhang, R., and Zhang, S. 2014. Predicting a Decadal Shift in North Atlantic Climate Variability Using the GFDL Forecast System. *Journal of Climate*, 27(17):6472–6496. doi: 10.1175/JCLI-D-13-00476.1.

Muir, L. C. and Fedorov, A. V. 2016. Evidence of the AMOC interdecadal mode related to westward propagation of temperature anomalies in CMIP5 models. *Climate Dynamics*. doi: 10.1007/s00382-016-3157-9.

Müller, W. A., Pohlmann, H., Sienz, F., and Smith, D. M. 2014. Decadal climate predictions for the period 1901-2010 with a coupled climate model. *Geophysical Research Letters*, 41(6):2100–2107. doi: 10.1002/2014GL059259.

Munoz, E., Kirtman, B., and Weijer, W. 2011. Varied representation of the Atlantic Meridional Overturning across multidecadal ocean reanalyses. *Deep-Sea Research Part II: Topical Studies in Oceanography*, 58(17-18):1848–1857. doi: 10.1016/j.dsr2.2010.10.064.

Myers, P. G., Fanning, A. F., Weaver, A. J., Meyers, P. G., Fanning, A. F., and Weaver, A. J. 1996. JEBAR, bottom pressure torque and Gulf Stream separation. *Journal Of Physical Oceanography*, 26(5):671–683. doi: 10.1175/1520-0485(1996)026<0671:JBPTAG>2.0.CO;2.

Narayan, N., Paul, A., Mulitza, S., and Schulz, M. 2010. Trends in coastal upwelling intensity during the late 20th century. *Ocean Science*, 6(3):815–823. doi: 10.5194/os-6-815-2010.

Nieves, V., Willis, J. K., and Patzert, W. C. 2015. GLOBAL WARMING. Recent hiatus caused by decadal shift in Indo-Pacific heating. *Science (New York, N.Y.)*, 349(6247):532–5. doi: 10.1126/science.aaa4521.

Nilsson, J. and Walin, G. 2001. Freshwater forcing as a booster of thermohaline circulation. *Tellus*, 53A:629–641.

Nilsson, J., Broström, G., and Walin, G. 2003. The Thermohaline Circulation and Vertical Mixing: Does Weaker Density Stratification Give Stronger Overturning? *Journal of Physical Oceanography*, 33(12):2781–2795. doi: 10.1175/1520-0485(2003)033<2781:TTCAVM>2.0.CO;2.

Nurser, A. J. G., Marsh, R., and Williams, R. G. 1999. Diagnosing Water Mass Formation from Air-Sea Fluxes and Surface Mixing. *Journal of Physical Oceanography*, 29(7):1468–1487. doi: 10.1175/1520-0485(1999)029<1468:DWMFFA>2.0.CO;2.

Ohba, M., Shiogama, H., Yokohata, T., and Watanabe, M. 2013. Impact of strong tropical volcanic eruptions on enso simulated in a coupled gcm. *Journal of Climate*, 26(14):5169–5182. doi: 10.1175/JCLI-D-12-00471.1.

Oman, L., Robock, A., Stenchikov, G. L., and Thordarson, T. 2006. High-latitude eruptions cast shadow over the African monsoon and the flow of the Nile. *Geophysical Research Letters*, 33(18): 1–5. doi: 10.1029/2006GL027665.

Omrani, H., Drobinski, P., and Dubos, T. 2012. Investigation of indiscriminate nudging and predictability in a nested quasi-geostrophic model. *Quarterly Journal of the Royal Meteorological Society*, 138 (662):158–169. doi: 10.1002/qj.907.

Ortega, P., Hawkins, E., and Sutton, R. 2011a. Processes governing the predictability of the Atlantic meridional overturning circulation in a coupled GCM. *Climate Dynamics*, 37(9-10):1771–1782. doi: 10.1007/s00382-011-1025-1.

Ortega, P., Montoya, M., González-Rouco, F., Mignot, J., and Legutke, S. 2011b. Variability of the Atlantic meridional overturning circulation in the last millennium and two IPCC scenarios. *Climate Dynamics*, 38(9-10):1925–1947. doi: 10.1007/s00382-011-1081-6.

Ortega, P., Mignot, J., Swingedouw, D., Sévellec, F., and Guilyardi, E. 2015. Reconciling two alternative mechanisms behind bi-decadal variability in the North Atlantic. *Progress in Oceanography*, 137:237–249. doi: 10.1016/j.pocean.2015.06.009.

Otterå, O., Bentsen, M., Drange, H., Suo, L., and Ottera, O. H. 2010. External forcing as a metronome for Atlantic multidecadal variability. *Nature Geoscience*, 3(688):688–694. doi: 10.1038/ngeo955.

Palmer, T. N. 1986. Influence of the Atlantic, Pacific and Indian Oceans on Sahel rainfall. *Nature*, 322(6076):251–253. doi: 10.1038/322251a0.

Park, J.-Y., Bader, J., and Matei, D. 2015. Northern-hemispheric differential warming is the key to understanding the discrepancies in the projected Sahel rainfall. *Nature Communications*, 6:5985. doi: 10.1038/ncomms6985.

Pausata, F. S. R., Chafik, L., Caballero, R., and Battisti, D. S. 2015. Impacts of high-latitude volcanic eruptions on ENSO and AMOC. *Proceedings of the National Academy of Sciences*, 112(45): 201509153. doi: 10.1073/pnas.1509153112.

Penduff, T., Barnier, B., and de Verdiere, A. C. 2000. Self-adapting open boundaries for a sigma coordinate model of the eastern North Atlantic. *J. Geophys. Res.*, 105(C5):11279–11297. doi: 10.1029/1999JC900335.

Persechino, A., Mignot, J., and Swingedouw, D. 2013. Decadal predictability of the Atlantic meridional overturning circulation and climate in the IPSL-CM5A-LR model. *Climate dynamics*, 40(9-10):2359–2380. doi: 10.1007/s00382-012-1466-1.

Peterson, B. and Holmes, R. 2002. Increasing river discharge to the Arctic Ocean. *Science*, 298 (5601): 2171–2173.

Peterson, B. J., McClelland, J., Curry, R., Holmes, R. M., Walsh, J. E., and Aagaard, K. 2006. Trajectory shifts in the Arctic and subarctic freshwater cycle. *Science (New York, N.Y.)*, 313(5790): 1061–6. doi: 10.1126/science.1122593.

Pickart, R. S., Straneo, F., and Moore, G. W. K. 2003a. Is the Labrador Sea Water formed in the Irminger basin? *Deep Sea Res. I*, 50:23–52.

Pickart, R. S. and Spall, M. a. 2007. Impact of Labrador Sea Convection on the North Atlantic Meridional Overturning Circulation. *Journal of Physical Oceanography*, 37(9):2207–2227. doi: 10.1175/JPO3178.1.

Pickart, R. S., Torres, D. J., and Clarke, R. A. 2002. Hydrography of the Labrador Sea during Active Convection. *J. Phys. Oceanogr.*, 32(2):428–457. doi: 10.1175/1520-0485(2002)032<0428:HOTLSD>2.0.CO;2.

Pickart, R., Spall, M., and Ribergaard, M. 2003b. Deep convection in the Irminger Sea forced by the Greenland tip jet. *Nature*, 424:152–156.

Pierce, D. W., Gleckler, P. J., Barnett, T. P., Santer, B. D., and Durack, P. J. 2012. The fingerprint of human-induced changes in the ocean's salinity and temperature fields. *Geophysical Research Letters*, 39(21):n/a–n/a. doi: 10.1029/2012GL053389.

Pohlmann, H. and Jungclaus, J. 2009. Initializing decadal climate predictions with the GECCO oceanic synthesis: Effects on the North Atlantic. *Journal of Climate*.

Pohlmann, H., Botzet, M., Latif, M., Roesch, A., Wild, M., and Tschuck, P. 2004. Estimating the Decadal Predictability of a Coupled AOGCM. *Journal of Climate*, 17(22):4463–4472. doi: 10.1175/3209.1.

Pohlmann, H., Smith, D. M., Balmaseda, M. a., Keenlyside, N. S., Masina, S., Matei, D., Müller, W. a., and Rogel, P. 2013. Predictability of the mid-latitude Atlantic meridional overturning circulation in a multi-model system. *Climate Dynamics*, 41(3-4):775–785. doi: 10.1007/s00382-013-1663-6.

Qiu, B. and Huang, R. X. 1995. Ventilation of the North Atlantic and North Pacific: Subduction Versus Obduction. *Journal of Physical Oceanography*, 25(10):2374–2390. doi: 10.1175/1520-0485(1995)025<2374:VOTNAA>2.0.CO;2.

Qu, T., Gao, S., and Fukumori, I. 2013. Formation of salinity maximum water and its contribution to the overturning circulation in the North Atlantic as revealed by a global general circulation model. *Journal of Geophysical Research: Oceans*, 118(4):1982–1994. doi: 10.1002/jgrc.20152.

Qu, T., Zhang, L., and Schneider, N. 2016. North Atlantic subtropical underwater and its year to year variability during the Argo period. *Journal of physical oceanography*, in press.

Rahmstorf, S. 1996. On the freshwater forcing and transport of the {A}tlantic thermohaline circulation. *Clim. Dyn.*, 12:799–811.

Rahmstorf, S., Crucifix, M., Ganopolski, A., Goosse, H., Kamenkovich, I., Knutti, R., Lohmann, G., Marsh, B., Mysak, L., Wang, Z., and Weaver, A. 2005. Thermohaline circulation hysteresis: a model intercomparison. *Geophys. Res. Letters*, 32(L23605).

Rahmstorf, S., Box, J. E., Feulner, G., Mann, M. E., Robinson, A., Rutherford, S., and Schaffernicht, E. J. 2015. Exceptional twentieth-century slowdown in Atlantic Ocean overturning circulation. *Nature Climate Change*, 5(5):475–480. doi: 10.1038/nclimate2554.

Rasmussen, T. L. and Thomsen, E. 2004. The role of the {N}orth {A}tlantic {D}rift in the millennial timescale glacial climate fluctuations. *Palaeogeography, Palaeoclimatology, Palaeoecology*, 210:101–116. doi: 10.1016/j.palaeo.2004.04.005.

Ray, S., Swingedouw, D., Mignot, J., and Guilyardi, E. 2015. Effect of surface restoring on subsurface variability in a climate model during 1949-2005. *Climate Dynamics*, 44(9-10):2333–2349. doi: 10.1007/s00382-014-2358-3.

Read, J. F. 2001. CONVEX-91: Water masses and circulation of the Northeast Atlantic subpolar gyre. *Progress in Oceanography*, 48(4):461–510. doi: 10.1016/S0079-6611(01)00011-8.

Reul, N., Chapron, B., Lee, T., Donlon, C., Boutin, J., and Alory, G. 2014. Sea surface salinity structure of the meandering Gulf Stream revealed by SMOS sensor. *Geophysical Research Letters*, 41(9):3141–3148. doi: 10.1002/2014GL059215.

Reverdin, G. 2010. North Atlantic Subpolar Gyre Surface Variability (1895-2009). *Journal of Climate*, 23(17):4571–4584. doi: 10.1175/2010JCLI3493.1.

Reverdin, G., Cayan, D., and Kushnir, Y. 1997. Decadal variability of hydrography in the upper northern North Atlantic in 1948-1990. *Journal of Geophysical ...*, 102 (C4):8505–8531.

Reverdin, G., Kestenare, E., Frankignoul, C., and Delcroix, T. 2007. Surface salinity in the Atlantic Ocean (30Â°S-50Â°N). *Progress in Oceanography*, 73(3-4):311–340. doi: 10.1016/j.pocean.2006.11.004.

Rhein, M., Kieke, D., Hüttl-Kabus, S., Roessler, A., Mertens, C., Meissner, R., Klein, B., Böning, C. W., and Yashayaev, I. 2011. Deep water formation, the subpolar gyre, and the meridional overturning circulation in the subpolar North Atlantic. *Deep-Sea Research Part II: Topical Studies in Oceanography*, 58(17-18):1819–1832. doi: 10.1016/j.dsr2.2010.10.061.

Rhein, M., Kieke, D., and Steinfeldt, R. 2015. Advection of North Atlantic Deep Water from the Labrador Sea to the southern hemisphere. *Journal of Geophysical Research*, 120:2471–2487. doi: 10.1002/2014JC010605.Received.

Ridley, J. K., Huybrechts, P., Gregory, J. M., and Lowe, J. A. 2005. Elimination of the Greenland Ice Sheet in a High CO 2 Climate. *Journal of Climate*, 18(17):3409–3427. doi: 10.1175/JCLI3482.1.

Rind, D., Russell, G., Schmidt, G., Sheth, S., Collins, D., DeMenocal, P., and Teller, J. 2001. Effects of glacial meltwater in the GISS coupled atmosphere-ocean model 2. A bipolar seesaw in Atlantic Deep Water production. *J. Geophys. Res.*, 106:27,327–355,365.

Robock, A. 2000. Volcanic eruptions and climate. *Rev. Geophys.*, 38(1998):191–219. doi: 10.1029/1998RG000054.

Robson, J., Sutton, R., and Smith, D. 2014. Decadal predictions of the cooling and freshening of the North Atlantic in the 1960s and the role of ocean circulation. *Climate Dynamics*, 42(9-10): 2353–2365. doi: 10.1007/s00382-014-2115-7.

Robson, J., Ortega, P., and Sutton, R. 2015. A recent reversal of climatic trends in the North Atlantic. *Nature Geoscience*, pages 1–15. doi: 10.1038/ngeo2727.

Rodríguez-Fonseca, B., Janicot, S., Mohino, E., Losada, T., Bader, J., Caminade, C., Chauvin, F., Fontaine, B., García-Serrano, J., Gervois, S., Joly, M., Polo, I., Ruti, P., Roucou, P., and Voldoire, A. 2011. Interannual and decadal SST-forced responses of the West African monsoon. *Atmospheric Science Letters*, 12(1):67–74. doi: 10.1002/asl.308.

Romanova, V. and Hense, A. 2015. Anomaly transform methods based on total energy and ocean heat content norms for generating ocean dynamic disturbances for ensemble climate forecasts. *Climate Dynamics*. doi: 10.1007/s00382-015-2567-4.

Rowell, B. D. P., Folland, C. K., Maskell, K., Ward, M. N., Rowell, D. P., Folland, C. K., Maskell, K., and Ward, M. N. 1995. Variability of summer rainfall over tropical north Africa (1906-92): Observations and modelling. *Quarterly Journal of the Royal Meteorological Society*, 121(66):669–704. doi: 10.1002/qj.49712152311.

Rowell, D. P. 2003. The Impact of Mediterranean SSTs on the Sahelian Rainfall Season. *Journal of Climate*, 16(5):849–862. doi: 10.1175/1520-0442(2003)016<0849:TIOMSO>2.0.CO;2.

Rühlemann, C., Mulitza, S., and Lohmann, G. 2004. Intermediate depth warming in the tropical Atlantic related to weakened thermohaline circulation: Combining paleoclimate data and modeling results for the last. *Paleoceanography*, 19(PA1025, doi:10.1029/2003PA000948).

Ruiz-Barradas, A., Nigam, S., and Kavvada, A. 2013. AMO's structure and climate footprint in observations and IPCC AR5 climate simulations. *Climate Dynamics*, 41(5-6):3301–3315. doi: 10.1007/s00382-013-1712-1.

Sanchez-Gomez, E., Cassou, C., Ruprich-Robert, Y., Fernandez, E., and Terray, L. 2015. Drift dynamics in a coupled model initialized for decadal forecasts. *Climate Dynamics*, pages 1–22. doi: 10.1007/s00382-015-2678-y.

Santer, B. D., Bonfils, C., Painter, J. F., Zelinka, M. D., Mears, C., Solomon, S., Schmidt, G. a., Fyfe, J. C., Cole, J. N. S., Nazarenko, L., Taylor, K. E., and Wentz, F. J. 2014. Volcanic contribution to decadal changes in tropospheric temperature. *Nature Geoscience*, 7(3):185–189. doi: 10.1038/NGEO2098.

Santer, B. D., Solomon, S., Bonfils, C., Zelinka, M. D., Painter, J. F., Beltran, F., Fyfe, J. C., Johannesson, G., Mears, C., Ridley, D. a., Vernier, J.-p., and Wentz, F. J. 2015. Observed multivariable signals of late 20th and early 21st century volcanic activity. *Geophysical Research Letters*, 42:500–509. doi: 10.1002/2014GL062366.

Sarafanov, A., Falina, A., Sokov, A., and Demidov, A. 2008. Intense warming and salinification of intermediate waters of southern origin in the eastern subpolar North Atlantic in the 1990s to mid-2000s. *Journal of Geophysical Research*, 113(C12):C12022. doi: 10.1029/2008JC004975.

Sato, K., Suga, T., and Hanawa, K. 2006. Barrier layers in the subtropical gyres of the world's oceans. *Geophysical Research Letters*, 33(8):L08603. doi: 10.1029/2005GL025631.

Schaller, N., Kay, A. L., Lamb, R., Massey, N. R., van Oldenborgh, G. J., Otto, F. E. L., Sparrow, S. N., Vautard, R., Yiou, P., Ashpole, I., Bowery, A., Crooks, S. M., Haustein, K., Huntingford, C., Ingram, W. J., Jones, R. G., Legg, T., Miller, J., Skeggs, J., Wallom, D., Weisheimer, A., Wilson, S., Stott, P. A., and Allen, M. R. 2016. Human influence on climate in the 2014 southern England winter floods and their impacts. *Nature Climate Change*, advance on. doi: 10.1038/nclimate2927.

Schiller, A., Mikolajewicz, U., and Voss, R. 1997. The stability of the North Atlantic thermohaline circulation in a coupled ocean-atmosphere general circulation model. *Climate Dynamics*, 13:325–347.

Schott, F., Visbeck, M., and Fischer, J. 1993. Observations of vertical currents and convection in the central Greenland Sea during the winter of 1988-1989. *Journal of Geophysical Research*, 98 (C8):14 401–14 421.

Séférian, R., Bopp, L., Gehlen, M., Swingedouw, D., Mignot, J., Guilyardi, E., and Servonnat, J. 2014. Multi-year prediction of Tropical Pacific Marine Productivity. *PNAS*, 111(32):11646–11651. doi: 10.1073/pnas.1315855111.

Send, U., Lankhorst, M., and Kanzow, T. 2011. Observation of decadal change in the Atlantic meridional overturning circulation using 10 years of continuous transport data. *Geophysical Research Letters*, 38(24):n/a–n/a. doi: 10.1029/2011GL049801.

Servonnat, J., Yiou, P., Khodri, M., Swingedouw, D., and Denvil, S. 2010. Influence of solar variability, {CO2} and orbital forcing during the last millennium in the {IPSLCM4} model. *Clim. Past*, 6:445–460. doi: 10.5194/cp-6-445-2010.

Servonnat, J., Mignot, J., Guilyardi, E., Swingedouw, D., Séférian, R., and Labetoulle, S. 2014. Reconstructing the subsurface ocean decadal variability using surface nudging in a perfect model framework. *Climate Dynamics*. doi: 10.1007/s00382-014-2184-7.

Sévellec, F. and Fedorov, A. V. 2013. The Leading, Interdecadal Eigenmode of the Atlantic Meridional Overturning Circulation in a Realistic Ocean Model. *Journal of Climate*, 26(7):2160–2183. doi: 10.1175/JCLI-D-11-00023.1.

Sévellec, F. and Huck, T. 2015. Geostrophic closure of the zonally-averaged Atlantic Meridional Overturning Circulation. *Journal of Physical Oceanography*, page 151030091929009. doi: 10.1175/JPO-D-14-0148.1.

Sévellec, F., Huck, T., Ben Jelloul, M., and Vialard, J. 2009. Nonnormal Multidecadal Response of the Thermohaline Circulation Induced by Optimal Surface Salinity Perturbations. *Journal of Physical Oceanography*, 39(4):852–872. doi: 10.1175/2008JPO3998.1.

Shi, L., Alves, O., Wedd, R., Balmaseda, M. A., Chang, Y., Chepurin, G., Ferry, N., Fujii, Y., Gaillard, F., Good, S. A., Guinehut, S., Haines, K., Hernandez, F., Lee, T., Palmer, M., Peterson, K., Masuda, S., Storto, A., Toyoda, T., Valdivieso, M., Vernieres, G., Wang, X., and Yin, Y. 2015. An assessment of upper ocean salinity content from the Ocean Reanalyses Inter-comparison Project (ORA-IP). *Climate Dynamics*. doi: 10.1007/s00382-015-2868-7.

Sicre, M.-A., Khodri, M., Mignot, J., Eiríksson, J., Knudsen, K.-L., Ezat, U., Closset, I., Nogues, P., and Massé, G. 2013. Sea surface temperature and sea ice variability in the subpolar North Atlantic from explosive volcanism of the late thirteenth century. *Geophysical Research Letters*, 40 (20):5526–5530. doi: 10.1002/2013GL057282.

Sicre, M.-A., Jacob, J., Ezat, U., and Rousse, S. 2008. Decadal variability of sea surface temperatures off North Iceland over the last 2000 years. *Earth and Planetary Science Letters*, 268:137–142. doi: 10.1016/j.epsl.2008.01.011.

Singh, A., Delcroix, T., and Cravatte, S. 2011. Contrasting the flavors of El Niño-Southern Oscillation using sea surface salinity observations. *Journal of Geophysical Research*, 116(C6):C06016. doi: 10.1029/2010JC006862.

Sinha, B., Topliss, B., Blaker, A. T., and Hirschi, J.-M. 2013. A numerical model study of the effects of interannual time scale wave propagation on the predictability of the Atlantic meridional overturning circulation. *Journal of Geophysical Research: Oceans*, 118(1):131–146. doi: 10.1029/2012JC008334.

Skliris, N., Marsh, R., Josey, S. A., Good, S. A., Liu, C., and Allan, R. P. 2014. Salinity changes in the World Ocean since 1950 in relation to changing surface freshwater fluxes. *Climate Dynamics*, 43 (3-4):709–736. doi: 10.1007/s00382-014-2131-7.

Smeed, D. A., McCarthy, G. D., Cunningham, S. A., Frajka-Williams, E., Rayner, D., Johns, W. E., Meinen, C. S., Baringer, M. O., Moat, B. I., Duchez, A., and Bryden, H. L. 2014. Observed decline of the Atlantic meridional overturning circulation 2004-2012. *Ocean Science*, 10(1):29–38. doi: 10.5194/os-10-29-2014.

Smith, D. M., Cusack, S., Colman, A. W., Folland, C. K., Harris, G. R., and Murphy, J. M. 2007. Improved surface temperature prediction for the coming decade from a global climate model. *Science (New York, N.Y.)*, 317(5839):796–9. doi: 10.1126/science.1139540.

Smith, D. M., Eade, R., and Pohlmann, H. 2013. A comparison of full-field and anomaly initialization for seasonal to decadal climate prediction. *Climate Dynamics*, 41(11-12):3325–3338. doi: 10.1007/s00382-013-1683-2.

Smith, R. S., Sutton, R., and Gregory, J. M. 2014. The impact of salinity perturbations on the future uptake of heat by the Atlantic Ocean. *Geophysical Research Letters*, pages n/a–n/a. doi: 10.1002/2014GL062169.

Smith, T. M., Reynolds, R. W., Peterson, T. C., and Lawrimore, J. 2008. Improvements to NOAA's historical merged land-ocean surface temperature analysis (1880-2006). *Journal of Climate*, 21(10): 2283–2296. doi: 10.1175/2007JCLI2100.1.

Spall, M. A. 1993. Variability of sea surface salinity in stochastically forced systems. *Clim. Dyn.*, 8: 151–160.

Spence, P., Saenko, O. A., Sijp, W., and England, M. 2012. The Role of Bottom Pressure Torques on the Interior Pathways of North Atlantic Deep Water. *Journal of Physical Oceanography*, 42(1): 110–125. doi: 10.1175/2011JPO4584.1.

Stan, C. and Kirtman, B. P. 2008. The Influence of Atmospheric Noise and Uncertainty in Ocean Initial Conditions on the Limit of Predictability in a Coupled GCM. *Journal of Climate*, 21(14): 3487–3503. doi: 10.1175/2007JCLI2071.1.

Stenchikov, G., Delworth, T. L., Ramaswamy, V., Ramswamy, V., Stouffer, R. J., Wittenberg, A., and Zeng, F. 2009. volcanic signals in oceans. *Journal of Geophysical Research*, 114:D16104. doi: 10.1029/2008JD011673.

Stockdale, T. N., Anderson, D. L. T., Alves, J. O. S., and Balmaseda, M. A. 1998. Global seasonal rainfall forecasts using a coupled ocean-atmosphere model. *Nature*, 392(6674):370–373. doi: 10.1038/32861.

Stocker, T. F. and Wright, D. G. 1991. Rapid transitions of the ocean's deep circlation induced by changes in surface water fluxes. *Nature*, 351:729–732.

Stocker, T. F. 2015. The silent services of the world ocean. *Science*, 350(6262):764–766. doi: 10.1126/science.aac8720.

Stott, P. A., Sutton, R. T., and Smith, D. M. 2008. Detection and attribution of Atlantic salinity changes. *Geophysical Research Letters*, 35(21):L21702. doi: 10.1029/2008GL035874.

Stouffer, R. J., Yin, J., Gregory, J. M. J. M., Dixon, K. W., Spelman, M. J., Hurlin, W., Weaver, a. J., Eby, M., Flato, G. M., Hasumi, H., Hu, A., Jungclaus, J. H., Kamenkovich, I. V., Levermann, A., Montoya, M., Murakami, S., Nawrath, S., Oka, A., Peltier, W. R., Robitaille, D. Y., Sokolov, A. P., Vettoretti, G., Weber, S. L., and Weber, N. 2006. Investigating the causes of the response of the thermohaline circulation to past and future climate changes. *Journal of Climate*, 19(8):1365–1387. doi: 10.1175/JCLI3689.1.

Straneo, F. 2006. On the Connection between Dense Water Formation, Overturning, and Poleward Heat Transport in a Convective Basin. *Journal of Physical Oceanography*, 36(9):1822–1840. doi: 10.1175/JPO2932.1.

Sugiura, N., Awaji, T., Masuda, S., Toyoda, T., Igarashi, H., Ishikawa, Y., Ishii, M., and Kimoto, M. 2009. Potential for decadal predictability in the North Pacific region. *Geophysical Research Letters*, 36(20):L20701. doi: 10.1029/2009GL039787.

Sundby, S. and Drinkwater, K. 2007. On the mechanisms behind salinity anomaly signals of the northern North Atlantic. *Progress in Oceanography*, 73:190–202. doi: 10.1029/2003GL019334.

Sutton, R. T. and Hodson, D. L. R. 2005. Atlantic Ocean Forcing of North American and European Summer Climate. *Science*, 309. no. 5(2005):115–118. doi: 10.1126/science.110949616.

Swingedouw, D., Braconnot, P., Delecluse, P., Guilyardi, E., and Marti, O. 2006. The impact of global freshwater forcing on the thermohaline circulation: adjustment of North Atlantic convection sites in a CGCM. *Climate Dynamics*, 28(2-3):291–305. doi: 10.1007/s00382-006-0171-3.

Swingedouw, D., Mignot, J., Braconnot, P., Mosquet, E., Kageyama, M., and Alkama, R. 2009. Impact of freshwater release in the North Atlantic under different climate conditions in an OAGCM. *Climate Dynamics*, 22:6377–6403. doi: 10.1175/2009JCLI3028.1.

Swingedouw, D., Mignot, J., Labetoulle, S., Guilyardi, E., and Madec, G. 2013a. Initialisation and predictability of the AMOC over the last 50 years in a climate model. *Climate Dynamics*, 40(9-10): 2381–2399. doi: 10.1007/s00382-012-1516-8.

Swingedouw, D., Rodehacke, C. B., Behrens, E., Menary, M., Olsen, S. M., Gao, Y., Mikolajewicz, U., Mignot, J., and Biastoch, A. 2013b. Decadal fingerprints of freshwater discharge around Greenland in a multi-model ensemble. *Climate Dynamics*, 41(3-4):695–720. doi: 10.1007/s00382-012-1479-9.

Swingedouw, D., Rodehacke, C. B., Olsen, S. M., Menary, M., Gao, Y., Mikolajewicz, U., and Mignot, J. 2014. On the reduced sensitivity of the Atlantic overturning to Greenland ice sheet melting in projections: a multi-model assessment. *Climate Dynamics*. doi: 10.1007/s00382-014-2270-x.

Swingedouw, D., Ortega, P., Mignot, J., Guilyardi, E., Masson-Delmotte, V., Butler, P. G., Khodri, M., and Séférian, R. 2015. Bidecadal North Atlantic ocean circulation variability controlled by timing of volcanic eruptions. *Nature communications*, 6:6545. doi: 10.1038/ncomms7545.

Sylla, A. *Analyse des biais climatiques de l'Atlantique tropical dans une famille de simuations basées sur les modèles de l'IPSL*. Master2, Université Cheikh Anta Diop, 2015.

Talandier, C., Deshayes, J., Treguier, A.-M., Capet, X., Benshila, R., Debreu, L., Dussin, R., Molines, J.-M., and Madec, G. 2014. Improvements of simulated Western North Atlantic current system and impacts on the AMOC. *Ocean Modelling*, 76:1–19. doi: 10.1016/j.ocemod.2013.12.007.

te Raa, L. A. and Dijkstra, H. A. 2002. Instability of the thermohaline ocean circulation on interdecadal timescales. *J. Phys. Oceanogr.*, 32:138–160.

Terray, L., Corre, L., Cravatte, S., Delcroix, T., Reverdin, G., and Ribes, A. 2012. Near-Surface Salinity as Nature's Rain Gauge to Detect Human Influence on the Tropical Water Cycle. *Journal of Climate*, 25:958–977.

Tett, S. F. B., Sherwin, T. J., Shravat, A., and Browne, O. 2014. How Much Has the North Atlantic Ocean Overturning Circulation Changed in the Last 50 Years? *Journal of Climate*, 27(16):6325–6342. doi: 10.1175/JCLI-D-12-00095.1.

Thierry, V., de Boisséson, E., and Mercier, H. 2008. Interannual variability of the Subpolar Mode Water properties over the Reykjanes Ridge during 1990-2006. *Journal of Geophysical Research*, 113 (C4):C04016. doi: 10.1029/2007JC004443.

Thoma, M., Gerdes, R., Greatbatch, R. J., and Ding, H. 2015. Partially coupled spin-up of the MPI-ESM: Implementation and first results. *Geoscientific Model Development*, 8(1):51–68. doi: 10.5194/gmd-8-51-2015.

Thomas, M. D., Tréguier, A.-M., Blanke, B., Deshayes, J., and Voldoire, A. 2015. A Lagrangian Method to Isolate the Impacts of Mixed Layer Subduction on the Meridional Overturning Circulation in a Numerical Model. *Journal of Climate*, 28(19):7503–7517. doi: 10.1175/JCLI-D-14-00631.1.

Tierney, J. E., Abram, N. J., Anchukaitis, K. J., Evans, M. N., Giry, C., Kilbourne, K. H., Saenger, C. P., Wu, H. C., and Zinke, J. 2015. Tropical sea surface temperatures for the past four centuries reconstructed from coral archives. *Paleoceanography*, 30(3):226–252. doi: 10.1002/2014PA002717.

Timmermann, A., Latif, M., Voss, R., and Grötzner, A. 1998. North Atlantic interdecadal variability: a coupled air-sea mode. *Journal of Climate*, 11:1906–1932.

Toole, J., Curry, R., Joyce, T., McCartney, M., and Peña-Molino, B. 2011. Transport of the North Atlantic Deep Western Boundary Current about 39Â°N, 70Â°W: 2004-2008. *Deep Sea Research Part II: Topical Studies in Oceanography*, 58(17-18):1768–1780. doi: 10.1016/j.dsr2.2010.10.058.

Tréguier, A. M., Theetten, S., Chassignet, E., Penduff, T., Smith, R., Talley, L., Beismann, J. O., and Böning, C. 2005. Salinity distribution and circulation of the North Atlantic subpolar gyre in high resolution models. *Journal of Physical Oceanography*, 35(May2005):757–774.

Trenberth, K. E. and Fasullo, J. T. 2013. An apparent hiatus in global warming? *Earth's Future*, 1 (1):19–32. doi: 10.1002/2013EF000165.

Trenberth, K. E., Fasullo, J. T., Branstator, G., and Phillips, A. S. 2014. Seasonal aspects of the recent pause in surfaceÂ warming. *Nature Climate Change*, 4(October). doi: 10.1038/nclimate2341.

Tulloch, R. and Marshall, J. 2012. Exploring Mechanisms of Variability and Predictability of Atlantic Meridional Overturning Circulation in Two Coupled Climate Models. *Journal of Climate*, 25(12): 4067–4080. doi: 10.1175/JCLI-D-11-00460.1.

Tulloch, R., Marshall, J., and Smith, K. S. 2009. Interpretation of the propagation of surface altimetric observations in terms of planetary waves and geostrophic turbulence. *Journal of Geophysical Research*, 114(C2):C02005. doi: 10.1029/2008JC005055.

Tung, K.-K. and Zhou, J. 2010. The Pacific's Response to Surface Heating in 130 Yr of SST: La Niña-like or El Niño-like? *Journal of the Atmospheric Sciences*, 67(8):2649–2657. doi: 10.1175/2010JAS3510.1.

Tzortzi, E., Josey, S. A., Srokosz, M., and Gommenginger, C. 2013. Tropical Atlantic salinity variability: New insights from SMOS. *Geophysical Research Letters*, 40(10):2143–2147. doi: 10.1002/grl.50225.

Vannière, B., Guilyardi, E., Toniazzo, T., Madec, G., and Woolnough, S. 2014. A systematic approach to identify the sources of tropical SST errors in coupled models using the adjustment of initialised experiments. *Climate Dynamics*, 43(7-8):2261–2282. doi: 10.1007/s00382-014-2051-6.

Vautard, R. and Yiou, P. 2009. Control of recent European surface climate change by atmospheric flow. *Geophysical Research Letters*, 36(22):L22702. doi: 10.1029/2009GL040480.

Vellinga, M. and Wu, P. 2004. Low latitude Freshwater Influence on Centennial Variability of the Atlantic Thermohaline Circulation. *Journal of Climate*, 17 (23):4498–4511.

Vianna, M. L. and Menezes, V. V. 2013. Bidecadal sea level modes in the North and South Atlantic Oceans. *Geophysical Research Letters*, 40(22):5926–5931. doi: 10.1002/2013GL058162.

Vinogradova, N. T. and Ponte, R. M. 2013. Clarifying the link between surface salinity and freshwater fluxes on monthly to interannual time scales. *Journal of Geophysical Research: Oceans*, 118(6): 3190–3201. doi: 10.1002/jgrc.20200.

Voldoire, a., Sanchez-Gomez, E., Salas y Mélia, D., Decharme, B., Cassou, C., Sénési, S., Valcke, S., Beau, I., Alias, a., Chevallier, M., Déqué, M., Deshayes, J., Douville, H., Fernandez, E., Madec, G., Maisonnave, E., Moine, M.-P., Planton, S., Saint-Martin, D., Szopa, S., Tyteca, S., Alkama, R., Belamari, S., Braun, a., Coquart, L., and Chauvin, F. 2012. The CNRM-CM5.1 global climate model: description and basic evaluation. *Climate Dynamics*, 40(9-10):2091–2121. doi: 10.1007/s00382-011-1259-y.

Voldoire, A., Claudon, M., Caniaux, G., Giordani, H., and Roehrig, R. 2014. Are atmospheric biases responsible for the tropical Atlantic SST biases in the CNRM-CM5 coupled model? *Climate Dynamics*. doi: 10.1007/s00382-013-2036-x.

Walin, G. 1982. On the relation between sea-surface heat flow and thermal circulation in the ocean. *Tellus*, 34(2):187–195. doi: 10.1111/j.2153-3490.1982.tb01806.x.

Wang, C. and Zhang, L. 2013. Multidecadal ocean temperature and salinity variability in the tropical north atlantic: Linking with the AMO, AMOC, and subtropical cell. *Journal of Climate*, 26(16): 6137–6162. doi: 10.1175/JCLI-D-12-00721.1.

Wang, D., Gouhier, T. C., Menge, B. A., and Ganguly, A. R. 2015. Intensification and spatial homogenization of coastal upwelling under climate change. *Nature*, 518(7539):390–394. doi: 10.1038/nature14235.

Wang, W., Köhl, A., and Stammer, D. 2010. Estimates of global ocean volume transports during 1960 through 2001. *Geophysical Research Letters*, 37(15):n/a–n/a. doi: 10.1029/2010GL043949.

Wang, X., Wang, Q., Sidorenko, D., Danilov, S., Schröter, J., and Jung, T. 2012. Long-term ocean simulations in FESOM: evaluation and application in studying the impact of Greenland Ice Sheet melting. *Ocean Dynamics*, 62(10-12):1471–1486. doi: 10.1007/s10236-012-0572-2.

Ward, M. N. 1998. Diagnosis and short-lead time prediction of summer rainfall in tropical North Africa at interannual and multidecadal timescales. *Journal of Climate*, 11(12):3167–3191. doi: 10.1175/1520-0442(1998)011<3167:DASLTP>2.0.CO;2.

Watanabe, M., Shiogama, H., Tatebe, H., Hayashi, M., Ishii, M., and Kimoto, M. 2014. Contribution of natural decadal variability to global warming acceleration and hiatus. *Nature Climate Change*, 4 (10):893–897. doi: 10.1038/nclimate2355.

Wegmann, M., Brönnimann, S., Bhend, J., Franke, J., Folini, D., Wild, M., and Luterbacher, J. 2014. Volcanic influence on European summer precipitation through monsoons: Possible Cause for "years without summer". *Journal of Climate*, 27(10):3683–3691. doi: 10.1175/JCLI-D-13-00524.1.

Welander, P. 1986. Thermohaline effects in the ocean circulation and related simple models. *Large-scale transport processes in oceans and atmosphere*, pages 163–200. doi: 10.1007/978-94-009-4768-9.

Wen, N., Frankignoul, C., and Gastineau, G. 2015. Active AMOC-NAO coupling in the IPSL-CM5A-MR climate model. *Climate Dynamics*. doi: 10.1007/s00382-015-2953-y.

Winton, M. 1997. The effect of cold climate upon {N}orth {A}tlantic {D}eep {W}ater formation in a simple ocean-atmosphere model. *J. Clim.*, 10:37–51.

Wu, P. and Wood, R. 2008. Convection induced long term freshening of the subpolar North Atlantic Ocean. *Climate Dynamics*, 31(7-8):941–956. doi: 10.1007/s00382-008-0370-1.

Xie, P. and Arkins, P. A. 1997. A 17-year monthly analysis based on gauge observations, satellite estimates and numerical model outputs. *Bull. Am. Meteorol. Soc.*, 78(11):2539–2558.

Xu, Z., Li, M., Patricola, C. M., and Chang, P. 2013. Oceanic origin of southeast tropical Atlantic biases. *Climate Dynamics*, 43(11):2915–2930. doi: 10.1007/s00382-013-1901-y.

Yashayaev, I. 2007. Changing freshwater content: Insights from the subpolar North Atlantic and new oceanographic challenges. *Progress in Oceanography*, 73(3-4):203–209. doi: 10.1016/j.pocean.2007.04.014.

Yeager, S. and Danabasoglu, G. 2014. The Origins of Late-Twentieth-Century Variations in the Large-Scale North Atlantic Circulation. *Journal of Climate*, 27(9):3222–3247. doi: 10.1175/JCLI-D-13-00125.1.

Yeager, S., Karspeck, A., Danabasoglu, G., Tribbia, J., and Teng, H. 2012. A Decadal Prediction Case Study: Late Twentieth-Century North Atlantic Ocean Heat Content. *Journal of Climate*, 25(15): 5173–5189. doi: 10.1175/JCLI-D-11-00595.1.

Yoshimori, M., Raible, C., Stocker, T., and Renold, M. 2009. Simulated decadal oscillations of the Atlantic meridional overturning circulation in a cold climate state. *Climate Dynamics*, 34(1):101–121. doi: 10.1007/s00382-009-0540-9.

Yu, L., Gao, Y., and Otterå, O. H. 2015. The sensitivity of the Atlantic meridional overturning circulation to enhanced freshwater discharge along the entire , eastern and western coast of Greenland. *Climate Dynamics*. doi: 10.1007/s00382-015-2651-9.

Yu, L. 2011. A global relationship between the ocean water cycle and near-surface salinity. *Journal of Geophysical Research*, 116(C10):C10025. doi: 10.1029/2010JC006937.

Zanchettin, D., Rubino, a., Matei, D., Bothe, O., and Jungclaus, J. H. 2012a. Multidecadal-to-centennial SST variability in the MPI-ESM simulation ensemble for the last millennium. *Climate Dynamics*, 40(5-6):1301–1318. doi: 10.1007/s00382-012-1361-9.

Zanchettin, D., Timmreck, C., Graf, H.-F., Rubino, A., Lorenz, S., Lohmann, K., Kruger, K., Jungclaus, J. H., and Krüger, K. 2012b. Bi-decadal variability excited in the coupled ocean-atmosphere

system by strong tropical volcanic eruptions. *Clim. Dyn.*, 39(1-2):419–444. doi: 10.1007/s00382-011-1167-1.

Zeng, N. 2003. Atmospheric science. Drought in the Sahel. *Science (New York, N.Y.)*, 302(5647): 999–1000. doi: 10.1126/science.1090849.

Zhang, L. and Wang, C. 2013. Multidecadal North Atlantic sea surface temperature and Atlantic meridional overturning circulation variability in CMIP5 historical simulations. *Journal of Geophysical Research: Oceans*, 118(10):5772–5791. doi: 10.1002/jgrc.20390.

Zhang, L., Wang, C., and Wu, L. 2011. Low-frequency modulation of the Atlantic warm pool by the Atlantic multidecadal oscillation. *Climate Dynamics*, 39(7-8):1661–1671. doi: 10.1007/s00382-011-1257-0.

Zhang, R. 2007. Anticorrelated multidecadal variations between surface and subsurface tropical North Atlantic. *Geophysical Research Letters*, 34(12):L12713. doi: 10.1029/2007GL030225.

Zhang, R. 2010. Latitudinal dependence of Atlantic meridional overturning circulation (AMOC) variations. *Geophysical Research Letters*, 37(16):n/a–n/a. doi: 10.1029/2010GL044474.

Zhang, R. and Delworth, T. L. 2006. Impact of Atlantic multidecadal oscillations on India/Sahel rainfall and Atlantic hurricanes. *Geophysical Research Letters*, 33(17):L17712. doi: 10.1029/2006GL026267.

Zhang, S., Rosati, A., and Delworth, T. 2010. The Adequacy of Observing Systems in Monitoring the Atlantic Meridional Overturning Circulation and North Atlantic Climate. *Journal of Climate*, 23 (19):5311–5324. doi: 10.1175/2010JCLI3677.1.